Click on a title to access the first page of the contribution

Contents

Preface

This issue contains the Proceedings of the Workshop on the Critical Stability of Few-Body Quantum Systems, held at Erice, Sicily (Italy) from October 10 to 18, 2008.

This was the fifth Workshop on this subject, after Trento (1997), Les Houches (2001), Trento (2003) and Dresden (2005). As for these previous workshops, emphasis was put on the interdisciplinary character, with participants coming from theoretical chemistry, atomic, nuclear and particle physics, and mathematical physics and some of the topics touching few-body correlations in large systems, or applications to astrophysics.

To avoid too spread a variety of subjects, we suggested contributions on the following topics:

- Exotic hadrons,
- Antiproton physics,
- Light nuclei and hypernuclei,
- New methods in nuclear physics,
- Efimov states,
- Resonances, scattering on composite targets,
- Rigorous results, in particular for Coulomb systems,
- Traps,
- Atomic clusters
- Few-body correlations in large systems,
- Applications to Astrophysics.

The Workshop was organised in the framework of the School of Critical Stability, whose Director, André Martin, gave an introducing lecture, presenting the Ettore Majorana Centre of Erice, its history and its ongoing activities.

We had nearly fifty participants, coming from India, Brazil, United States and for most of them, from nearby or remote European countries.

As for the three previous workshops, (Few-Body Syst. 31 (2002) 71-266; 34 (2004) 1-208; 38:55-219,2006), the proceedings are published as a special issue of Few-Body Systems, this ensuring a widespread diffusion. We thank the editors and staff members for their help.

This Workshop benefited from the generous support of the European Science Foundation (ESF), the Institut National de Physique Nucléaire et de Physique des Particules (IN2P3), the Istituto Nazionale di Fisica Nucleare (INFN) and the Ettore Majorana Foundation and Centre for Scientific Culture (CCSEM).

Special thanks are due to Pr. A. Zichichi for the hospitality provide to us at Erice, and to Mrs. Fiorella Ruggiu for her efficient handling of the local organisation.

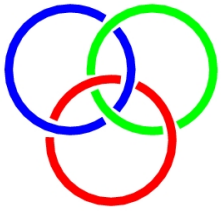

Aksel S. Jensen[1],
Alejandro Kievsky[2],
Jean-Marc Richard[3],
Laurent Wiesenfeld[4],

[1]Department of Physics and Astronomy, Aarhus University, 8000 Aarhus C, Denmark
[2]Istituto Nazionale di Fisica Nucleare, Largo Pontecorvo 2, 56127 Pisa, Italy
[3]LPSC, CNRS-IN2P3, Université Joseph Fourier and INPG, Grenoble, France
[4]LAOG, Université Joseph Fourier, Grenoble, France


André Martin
Erice 2008

Few-Body Systems 0, 2–6 (2009)

Few-Body Systems

Welcome address: Critical Stability of Quantum Few-Body Systems

André Martin

Theory Division, CERN, CH 1211 Genève 23

In the name of Professor Antonino Zichichi, I would like to welcome you at the Ettore Majorana Foundation and Centre for Scientific Culture, here, in Erice, for this workshop on Critical Stability of Quantum Few-Body Systems.

Since many of you are coming here for the first time, I would like to say a few words on Professor Antonino Zichichi and the founding of the Centre; Ettore Majorana; How I myself got interested in "Critical Stability".

Antonino Zichichi and the Centre

Antonino Zichichi was born in Trapani, the city by the sea that you can see from here. When he was young he used to go up to Erice on week-ends with friends. Antonino Zichichi is a great experimental physicist in the field of sub-nuclear physics. He has performed experiments at CERN, Frascati (near Rome) and DESY in Hamburg. I shall only present a subset of his experiments, and I shall not follow the chronological order.

- He was a member of a team of 6 physicists who measured for the first time, at CERN, the anomalous magnetic moment of the muon, checking the prediction of Schwinger (improved later by many others).
- In inelastic collisions he has discovered the "leading particle effect" and the "effective energy".
- He has invented a method to discover heavy leptons, heavier than the electron and the muon. He has performed an experiment at Adone, the Frascati electron-positron collider. This experiment gave a negative result because the energy of Adone was too low. However, later, at the SLAC collider, which had higher energy, in California, Martin Perl, using the same method, discovered the τ lepton, and eventually received the Nobel Prize for this discovery.

Now come two important experiments involving antiparticles:

- The PAPEP experiment, which is the observation of the annihilation of a proton with an antiproton producing an electron-positron pair. This experiment was extremely difficult because one had to fight against a tremendous background.

- He was able to observe, for the first time, at CERN, what he called the production of "anti-matter", in the form of anti-deuterons, i.e. a bound state of an antiproton and an antineutron. Previously only "elementary" antiparticles had been observed (I speak of particles which can be isolated, which excludes quarks), antiprotons, antineutrons, positrons, positive muons. The new thing was that he had observed *composite systems*. Many years later, at CERN, physicists have been able to manufacture anti-hydrogen, made of an antiproton and a positron (see Dan Brown "Angels and Demons").

Perhaps this explains the particular ties and admiration of Antonino Zichichi for P.A.M. Dirac. Paul Adrien Maurice Dirac was a British theoretician of French–Swiss origin. When I asked him here, in Erice, in 1982, if it was correct that his ancestors were coming from Saint-Maurice, in Valais, Switzerland, he answered "actually my great grand father was coming from Poitou and fled to Switzerland to avoid being recruited in Napoléon's army. There were people more famous than me, coming from Poitou, like Mr. Cadillac". Well, Dirac tried and succeeded to find a relativistic equation for the electron, explaining the spin of the electron, its magnetic moment and the fine structure of hydrogen. However, he fell on a major difficulty: His equation seemed to have *negative energy* solutions which were unacceptable. He solved the problem and predicted the existence of *antiparticles* with *positive* energy.

In your folders you will find texts by Antonino Zichichi explaining that in his eyes, Dirac was may be greater than Einstein. It is true indeed that for what concerns special relativity, Einstein was very courageous and made a big step, but he picked ripe fruits, prepared by Maxwell, Poincaré, Lorentz, and Minkowski, while what Dirac discovered was completely *unexpected*, and *extremely important*. Quantum electrodynamics, and later the electroweak theory and QCD (the so-called standard model) rest very heavily on the existence of antiparticles.

The big bang model works because there exists *particles* and *antiparticles*, because "In the beginning... the light shineth in the darkness" (John, I, 1-5). Now, why is our Universe dominated by *particles*, protons, neutrons, electrons, etc., and not *antiparticles*? Andrei Sakharov proposed that this is due to CP violation, seen first in K decays and now in B decays.

Last week, Kobayashi and Maskawa were given half of the Nobel prize for explaining CP violation by postulating the existence of 3 families of quarks and leptons (it has indeed been observed that there are 3 and only 3 families), leading to an irreducibly complex mixing matrix for charged currents in weak interactions, which explains CP violation. I cannot resist showing you (below, left) a picture of the recipient of the second half of the 2008 Nobel Prize, Yoshiro Nambu, taken in Erice in 1972.

I shall now discuss the public role of A.Z., limiting myself to a few points, once more not in chronological order:

- A.Z. is a great populariser of science, which, he insists on that, is a part of culture. Almost every Italian loves his TV programmes.
- When he was president of INFN (Istituto Nationale per la Fisica Nucleare), he played a major role. In particular he created the Gran-Sasso Un-

derground Laboratory, where very important experiments have been made and are being made now, for instance one on neutrino mixing using neutrinos coming from CERN through the terrestrial crust.

- He convinced pope John-Paul II to rehabilitate Galileo Galilei.
- In 1963 he created here, in Erice, the Ettore Majorana Foundation and Centre for Scientific Culture. Notice the word "culture". Initially, there was only *one* school, the "School of Subnuclear Physics". Participants were lodged in the cottages of "La Pineta" and the lectures were taking place in a relatively small lecture hall in San Lorenzo. Now there have been about 200 schools and workshops on different subjects taking place taking place (you have the list on the side of your folders), and more than 50 every year. The Centre also became bigger. After the acquisition of San Rocco, which became the centre of the "centre", San Francesco was added and later the Paul Dirac lecture hall was constructed behind the facade of the San Domenico church, in ruins. Below (right) is a picture of the opening ceremony in 1963. Antonino Zichichi stands between the great theoretician Victor Weisskpof, left, former director of CERN, recipient of the Wolf Prize and Sidney Drell, right, an excellent theoretician from SLAC, who played later a considerable role in the problem of arms control.

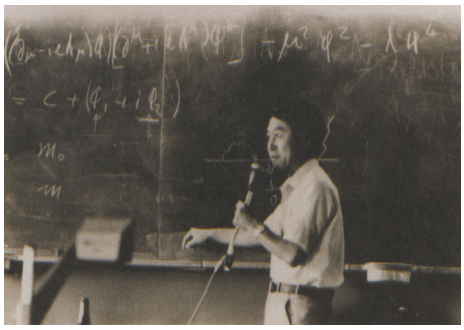

Among the many workshops, I would like to single out the one on "world emergencies" which I had the privilege to attend last year. At the time of the cold war there were meetings between American and Russian experts on disarmament. Now the subjects are climatic change, energy saving, aids, Alzheimer's disease.

I would like also to come back on the school of subnuclear physics. The 2008 session was devoted to the memory of the American theoretician from Harvard Sidney Coleman, who died recently. Sidney has been lecturing many times in Erice. His lectures were fantastic and he received the prize of the best lecturer. Yet he violated a sacred rule because, in spite of the posters that you see everywhere and the sheets in your folders, Sidney smoked everywhere. I am a witness that once his cigarette was finished while he was lecturing in San Rocco dressed in his impeccable white suit . He stopped and said "Nino, can you ask one of your slaves to bring me some cigarettes". Sure enough he got his cigarettes and continued lecturing. So any rule has exceptions!

About Ettore Majorana

Ettore Majorana was a Sicilian theoretical physicist born in Catania in 1906. In Rome, after a short time studying engineering, he moved to physics and joined the Fermi group. He turned out to be a GENIUS (this is the word of Fermi!). He has a relatively short list of publications in the field of atomic, molecular, and nuclear physics because once he had found something he did not care to publish it. Some of his most outstanding contributions are the Majorana neutrino which is its own antiparticle and allows neutrino-less double beta decay, and particles of arbitrary spins including what one would call now "Regge trajectories". I cannot resist telling you a story that I heard from the great Gian-Carlo Wick. In 1931 Frédéric and Irène Joliot-Curie discovered a mysterious penetrating neutral radiation produced in the bombarding of Beryllium by alpha particles. When their communication to the French Academy of Science arrived in Rome, Majorana exclaimed "idiots! they have not seen that it is the neutron" (in Italian"Stronzi, non hanno visto che è il neutrone"). However he did not publish anything about this, and the world had to wait for the experiment of Chadwick, in 1932, to know that the neutron existed.

After Rome Ettore Majorana visited the group of Niels Bohr in Copenhagen and the group of Heisenberg in Leipzig. After his return to Rome he got a professorship in Naples.

In 1938 he took a boat from Naples to Palermo, was seen in Palermo and then was supposed to return to Naples, but was never seen again. Did he commit suicide or had just decided to disappear from the world?

- In favour of the suicide thesis is the fact that before leaving Naples he had written to a friend that he was going to put an end to his life, not to be sad, not to wear black dresses. He had a rather strange character, was very shy, with a tendency to depression.
- in favour of the disappearance, is the fact that from Palermo he wrote to the same friend that he had changed his mind, but that he would not return to physics. Also the fact that before leaving Naples he took all his money from the bank, and finally that he was a very religious man. Then, where did he disappear? some people claim that he fled to Argentina, but this seems extremely unlikely. The evidence is very weak. He may just have disappeared somewhere in Sicily, in a convent for instance. This is quite possible when you see Mafia chiefs disappearing without being found during 30 years. In France there is the example of the great mathematician Alexander Groethendick who disappeared some years ago and is very likely still alive. Now assuming that Majorana disappeared, why? The thesis of the great Sicilian writer, Leonardo Sciaccia is that he was so clever that he knew already the terrible consequences of the work on nuclear physics. This does not seem very likely since nobody in Rome had thought of fission reactions ("I missed fission" said once Fermi to Jack Steinberger). Yet fission was to be discovered one year later.

Fermi was so desperate of the disappearance of Majorana that he asked Mussolini to undertake intensive investigations to find him. As we know they were

unsuccessful. Witnesses say that in Los Alamos, building the bomb, Fermi, faced with a difficult problem, kept saying "If Ettore was here he would find the solution".

For more about Ettore Majorana and the Erice centre, I recommend you to read the book by Antonino Zichichi: "Ettore Majorana, his genius and his long lasting legacy".

Finally, I come to:

Critical binding and I

I believe that my interest in critical binding started from my contacts with the Vienna school of theoretical physics, Walter Thirring, Harald Grosse and others.

In 1976, Thirring, Glaser, Grosse and I proved that the system proton-electron- negative muon is *not bound*.

I was also much interested by the work of Hill who showed that the negative hydrogen ion has one and only one bound state with natural parity, and also by the work of Grosse and Pittner who showed that the same is true for unnatural parity states. I was also impressed by Hill's theorem that all systems (A^+, B^-, B^-) are bound.

In 1991-1992 with Jean-Marc Richard first, and then T.T. Wu, we undertook a systematic study of systems of 3 unit-charge particles interacting by pure Coulomb forces, using only very general properties such as convexity, and also the typically French invention to represent any of these 3-body systems by a point in a triangle.

In 2000 again with T.T. Wu but also A. Krikeb, we studied 3 body systems, but, this time, with arbitrary charges. In particular we gave the first rigorous proof that the system $(\alpha, \mathrm{p}, \mu^-)$ is *unstable*. Yet, Semen Gerstein has shown that $(\alpha^-, \mathrm{p}, \mu^-)$, $(\alpha, \mathrm{d}, \mu^-)$ and $(\alpha, \mathrm{t}, \mu^-)$ are *metastable* with increasing lifetimes. I have the impression that this subject is not treated in this workshop. Yet this is crucial for catalysed fusion.

Finally, I acted as go-between between Jean-Marc Richard and Jurg Frölich. Jurg noticed that there was no rigorous proof that the hydrogen molecule was stable. The only "proofs" were using the Born-Oppenheimer approximation. Jurg and his student had a very complicated method of proof, but Jean-Marc proposed a super-simple proof based on the fact that many years ago, Hylleraas and Øre proved that the $(\mathrm{e}^+, \mathrm{e}^-, \mathrm{e}^+, \mathrm{e}^-)$ system is stable (except for annihilation!), and also on convexity. Later, Jean-Marc and his friends "proved" that all systems (A^+, A^+, B^-, C^-) are stable. The quotations marks mean that even though they used analytic methods in their variational approach, they made their calculations for discrete values of the masses.

To finish, I would like to wish you a very successful workshop. Here again I acted like a go-between, between Antonino Zichichi and the true organisers, Jean-Marc Richard, co-director of the school, Aksel Jensen, Alessandro Kievski and Laurent Wiesenfeld, the conveners. To them, to Antonino Zichichi who made this workshop possible, and Fiorella Ruggiu for her very efficient help, I address my deepest thanks.

Few-Body Systems 0, 1–8 (2009)

Few-Body Systems

A Personal Journey Through Hadronic Exotica*

Kamal K. Seth**

Department of Physics and Astronomy, Northwestern University, Evanston, IL 60208, USA

Abstract. The search for exotic hadrons has been forever fascinating and challenging. A review of many such searches, successful and unsuccessful, in which the author has been involved, is presented.

1 Introduction

Exotica and **Erotica** differ only in one letter. They are equally addictive. Like all addictions, they have consequences. They consume a lot of the resources. They make you often do things you should not do. **BUT**, they are exciting, and they give you a great surge of adrenaline.

I have to confess that over the years I have fallen for exotica, and often. So, let me take you on a personal journey through exotica.

So, what is Exotic? Exotic has to be unexpected. Exotic has to have the nature of the "forbidden fruit". Exotic in hadronic physics often begins with provocative suggestions by theorists, which drives experimentalists to search for it, often at **exotic cost** (think Higgs). At other times, it begins with an unexpected experimental observation for which theorists come up with exotic explanations (think J/ψ). I want to tell the story of the hadronic exotica, necessarily from a personal point of view.

2 Chasing Exotica in Nuclear Physics

I began my career as a nuclear physicist. So, my first run in with exotica was in the search for **exotic nuclei**. Nuclei are exotic if they are very rich in neutrons, i.e., have an exceptionally large value of $(N-Z)/A.$, or if they are just very heavy, $A \gg 240$. In the 1970's, there were no easy ways of making a nucleus which was very rich in neutrons, like ^{18}C with 6 protons and 12 neutrons. And so we went for it by the very exotic pion double charge exchange (DCX) reaction (π^+, π^-). We

*Article based on the presentation by K.K. Seth at the Fifth Workshop on Critical Stability, Erice, Sicily, Received December 12, 2009; Accepted January 8, 2009.

** *E-mail address:* kseth@northwestern.edu

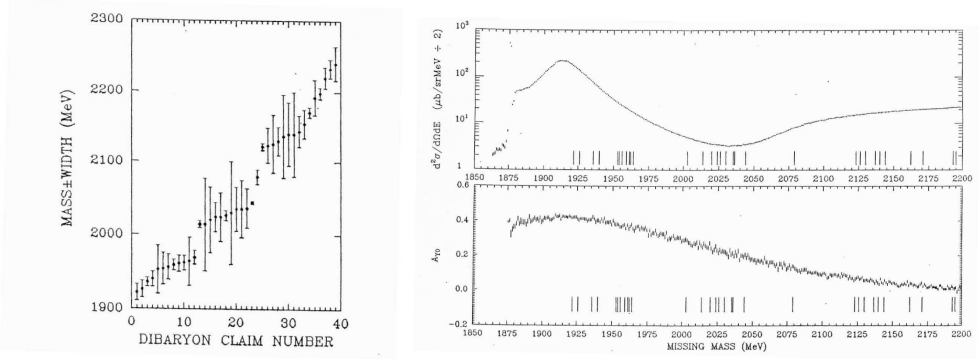

Figure 1. (Left) Claims for dibaryons. The ordinate shows calimed mass (points) and widths (error bars). (Right) $\boldsymbol{p}+d \to p'+X$ at $T_p = 800$ MeV, $\Theta = 15°$: Vertical lines mark the masses of the dibaryons claimed. (Upper panel) Differential cross sections. (Lower panel) Analyzing powers.

discovered ^{18}C by the reaction $^{18}\mathrm{O}(\pi^-,\pi^+)^{18}\mathrm{C}$ [1]. That was exciting. As I said before, exotica is addictive. So, after ^{18}C we went for ^{9}He, 2 protons+7 neutrons, $(N-Z)/A = 5/9$, by means of the reaction $^{9}\mathrm{Be}(\pi^-,\pi^+)^{9}\mathrm{He}$ [2]. We found it, and Bethe called it **"a drop of neutron star"**. How much more exotic can you get? Well, how about ^{6}H by $^{6}\mathrm{Li}(\pi^-,\pi^+)^{6}\mathrm{H}$. We tried and failed to find it, bound or unbound [3].

So, running after exotica can lead to disappointments.

The other end of exotic nuclei is the **superheavy nuclei**. I have never worked in this field. But Berkeley, Dubna, and GSI have crossed swords in claims about who has the heaviest of the superheavy. After some embarrassing incidents, the current winner is $^{294}\mathrm{X}_{114}$ with 114 protons and 180 neutrons [4]. That is exotic!

3 Chasing Exotica in Quark Physics

Quarks carry color, and **only color-neutral hadrons, $q\bar{q}$ mesons or qqq, baryons exist** in nature. In the quark bag model [5] hadrons with other color-neutral combinations, such as $(qqq)(qqq)$ **dibaryons**, or $qq\bar{q}\bar{q}$ **four-quark** state can exist. de Swart and colleagues calculated the masses of scores of dibaryons [6] and started a stampede for the search of dibaryons.

Lots of people started looking for dibaryons in their old experiments, analyzing old bubble chamber pictures and claiming observation of scores of dibaryons. As many as 40 dibaryon states were claimed in the mass range $1900 - 2300$ MeV (Fig. 1). We thought we could become famous by pinning these dibaryons down since we had orders of magnitude greater luminosity and energy resolution available at the Los Alamos Meson Factory. Instead of becoming **famous** for discovering dibaryons, we became **infamous** for killing all of them. No Dibaryons anywhere in Fig. 2.

4 Pentaquark

But that is not the end of this story. If not two baryons making a dibaryon, how about a baryon+a meson, or a color-neutral pentaquark? It surfaced a few years ago by the claim by Nakano et al. of a narrow peak, called Θ^+, with a mass of $M(\Theta^+) = 1540 \pm 10$ MeV, $\Gamma(\Theta^+) < 25$ MeV, in the invariant mass of K^+n in the reaction $\boldsymbol{\gamma n \rightarrow K^-(K^+n)}$ [7]. If true, it would have strangeness +1 and at least five quarks/antiquarks. The object was so exotic that a stampede of **confirming** claims flooded the literature. An equal number of non-observations were reported. If you go to Google, you find 99,800 entries for pentaquark (before this symposium), and it will be difficult to decide whether the pentaquark is alive or not.

In a high-statistics repeat of their own measurement, JLab found that their own earlier observation of Θ^+ was false and no evidence for the existence of the pentaquark exists [8]. However, rumor has it that Nakano et al. claim that they still see the pentaquark in a high-statistics remeasurement.

So, once claimed, an exotic is difficult to kill! I end with a quote from PDG08 summarizing the saga of the pentaquark: *"The whole story — the discoveries themselves, the tidal wave of papers by theorists and phenomenologists that followed, and the eventual* ***'undiscovery'*** *— is a curious episode in the history of science."*

5 Glueballs and Hybrids

Since glue carries color, it is possible to have hadrons build of pure glue, called glueballs $|gg\rangle$, and hybrid mesons containing glue, $|q\bar{q}g\rangle$. These have been predicted since the inception of QCD [9].

Glueballs have generally the same J^{PC} as $q\bar{q}$ mesons, and they mix with them. It is therefore essentially impossible to find a pure glueball. Nevertheless, brave searches and claims and counter–claims have been made. The summary of the situation is that pieces of the $J^{PC} = 0^{++}$ glueball are mixed into at least three well–known isoscalar mesons, $f_0(1370, 1500, 1710)$ and the pure exotic, $|gg, 0^{++}\rangle$ has been lost. A tensor $J^{PC} = 2^{++}$ glueball has had equally disappointing fate. It has surfaced many times, but I believe it was firmly put to rest by us in a $p\bar{p}$ measurement at LEAR (CERN) [10].

Hybrids $|q\bar{q}g\rangle$ have an advantage over glueballs. They can have $J^{PC} = 1^{-+}, 2^{+-}, \ldots$ which are not permitted for $q\bar{q}$ mesons. Such objects are manifestly exotic. In our π^-p experiment (E852) at BNL we claimed to have discovered at least three 1^{-+} mesons $\pi_1(1400, 1600, 2000)$, and a 2^{+-} meson $h_2(1900)$ [11]. I have to admit that while these hadrons are definitely not $q\bar{q}$ mesons, they also admit the possibility of being four–quark states, and not hybrids. In either case they are exotic.

6 The H Dibaryon

The *uuddss* H dibaryon was predicted by Jaffe [12], but it became so exotic that it was even considered a candidate for dark matter. Stubborn searches for the H

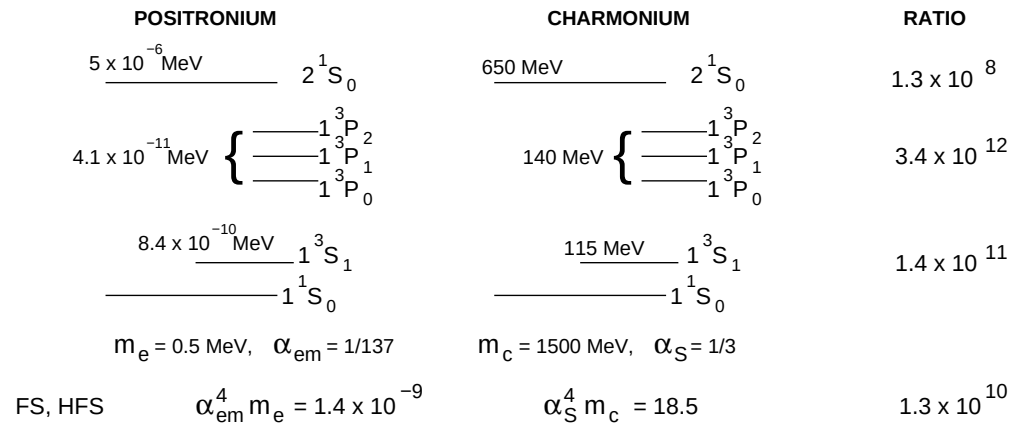

Figure 2. Comparing Positronium (e^+e^-) and Charmonium ($c\bar{c}$) spectra.

were made for years at Brookhaven and KEK. The u, d quark dibaryons died a long time ago, but the H dibaryon lived longer. By now, however, by common consensus it is also considered dead. For a detailed history see [13].

7 Exotica in QCD

In Dec. 1974, a large narrow peak was disocvered at $\sim$ 3.1 GeV mass at Brookhaven and SLAC [14] in e^+e^- formation and $\mu^+\mu^-$ decay. It was the $\boldsymbol{J/\psi}$ which launched the era of modern Quantum Chromodynamics (QCD). It is amusing to note that barely four weeks later **eight papers** by theoretical physicists (including four Nobel laureates) appeared in the Jan. 6, 1974 issue of Physical Review Letters [15], offering explanations of what J/ψ might be. Several of them were truely exotic explanations, like J/ψ was a bound state of a baryon/antibaryon, or two spin–one mesons, or it was a member of a $15 \oplus 1$ dimensional representation of SU(4). **Tells you that nobody is immune to the seduction of exotica.**

I have been talking too much about the exotics which failed to materialize. Let me now, for awhile, focus on exciting physics which is **not exotica, but excitica** (my construct for something very exciting).

8 QCD versus QED

The QCD potential which arises due to the exchange of a massless vector **photon** is $\boldsymbol{V(r) \propto \alpha_{em}/r}$. The QCD potential due to the exchange of a massless vector **gluon** is $\boldsymbol{V(r) \propto \alpha_{strong}/r}$. Because free quarks do not exist, in QCD there is an additional confinement term proportional to $\boldsymbol{r}$.

With such close analogy to QED, it is interesting to compare the QCD spectrum of charmonium with the QCD spectrum of positronium, with masses and interactions miles apart. The similarity is nothing short of fantastic. **Nature repeats herself!** with energy scales different by a factor $\boldsymbol{\sim 10^{10}}$.

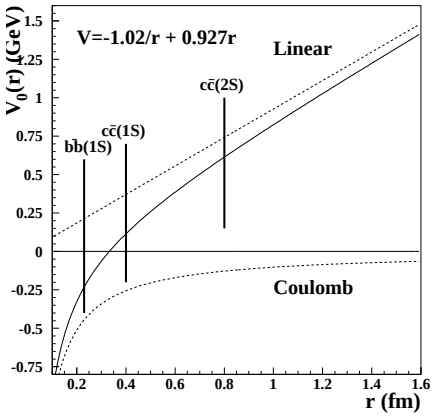

Figure 3. The $S-$wave bound states of charmonium and bottomonium as a function of the radius of the $q\bar{q}$ potential.

9 Hyperfine Interaction in QCD

The Coulombic ($\propto 1/r$) part of the QCD interaction gives rise to the usual spin dependence in the potential, with spin-orbit, tensor, and spin-spin components, in addition to the central part. Of these three, arguably the most important is the spin-spin interaction. For example, the ground state masses of $q\bar{q}$ mesons are:

$$M(q_1\bar{q}_2) = m_1(q_1) + m_2(q_2) + A_{hf}\left[\frac{\boldsymbol{s}_1 \cdot \boldsymbol{s}_2}{m_1 m_2}\right]$$

In order to determine the hyperfine interaction, A_{hf}, it is necessary to measure the **hyperfine splitting** between the spin–singlet and spin–triplet states. This means identifying and measuring the massses of ${}^3L_J$ and ${}^1L_J$ states. The masses of **spin–triplet** ${}^3L_J$ states, ${}^3S_1$ and ${}^3P_J$ states are well-determined because either they are directly populated in e^+e^- annihilation ($\left|{}^3S_1\right\rangle$) or they are reached by strong E1 transitions from the $\left|{}^3S_1\right\rangle$ states ($\left|{}^3S_1\right\rangle \rightarrow \gamma_{E1}\left|{}^3P_J\right\rangle$). The **spin–singlet** states ${}^1L_{J=L}$ can not be directly formed, and radiative transitions to them from spin–triplet states are either forbidden or weak M1. The net result is that our knowledge of the spin–singlet states, and therefore of the hyperfine interaction, has been very poor in the past. Very recently this has changed.

For heavy quark systems, $c\bar{c}$ charmonium, and $b\bar{b}$ bottomonium, we would like to know how the hyperfine interaction changes as we move from the Coulomb dominated region of the $q\bar{q}$ potential to the confinement dominated region. We would like to study the change in the hyperfine interaction

1. between $c\bar{c}(1S)$ and $c\bar{c}(2S)$
2. between $c\bar{c}(1S)$ and $b\bar{b}(1S)$
3. between $c\bar{c}(1S)$ and $c\bar{c}(1P)$

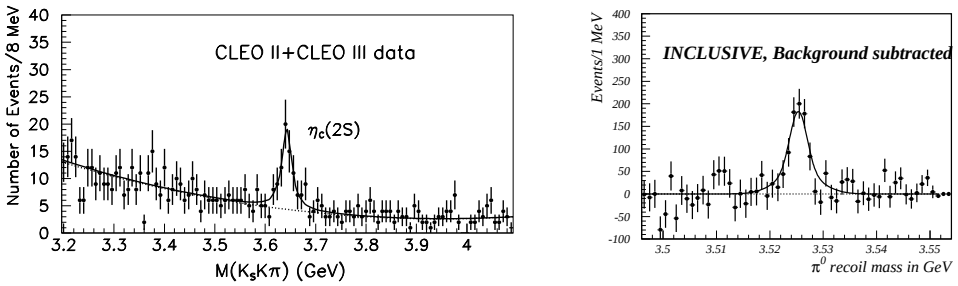

Figure 4. Identification of charmonium spin–singlet states: (left) $\eta_c'(2^1S_0)$ produced in $\gamma\gamma$ fusion, (right) $h_c(1^1P_1)$ produced in $\psi' \to \pi^0 h_c$.

Until recently, the only hyperfine splitting known was for the charmonium $1S$ states (see Fig. 3)

$$\Delta M_{hf}(1S) \equiv M(J/\psi(1S)) - M(\eta_c(1S)) = 116.7 \pm 1.2 \text{ MeV}$$

$\boldsymbol{\eta_c'(1^1S_0)}$**,** $\boldsymbol{h_c(1^1P_1)}$**, and** $\boldsymbol{\eta_b(1^1S_0)}$ were not even identified. In the last five years, all this has changed due to the measurements at Belle, BaBar, and CLEO. The results are:

$$\Delta M_{hf}(2S)_{c\bar{c}} \equiv M(\psi'(2S)) - M(\eta_c'(2S)) = +43.2 \pm 3.4 \text{ MeV (CLEO [16])}$$
$$\Delta M_{hf}(1P)_{c\bar{c}} \equiv M(\langle\chi_{cJ}(1P)\rangle) - M(h_c(1P)) = +0.02 \pm 0.23 \text{ MeV (CLEO [17])}$$

Even more recently BaBar has claimed the identification $\eta_b(^1S_0)$ with the result

$$\Delta M_{hf}(1S)_{b\bar{b}} \equiv M(\Upsilon(1S)) - M(\eta_b(1S)) = +71.4^{+4.1}_{-3.5} \text{ MeV (BaBar [18])}$$

An overall understanding of these hyperfine splittings is going to be a challenge to the theorists.

10 CHARMONIUM EXOTICS: The Unexpected States Above the $D\overline{D}$ Threshold

I now return to the domain of Exotica. Recently, a number of new states have been claimed in the mass region 3800–4700 MeV, above the $D\overline{D}$ breakup of charmonium at 3730 MeV. Three years ago, all that was known above $D\overline{D}$ was four vector states $\psi(3770,\ 4040,\ 4160,$ and $4415)$ observed as enhancements in the ratio, $R = \sigma(hh)/\sigma(\mu^+\mu^-)$. However, the great excitement, often called the **renaissance** in hadron spectroscopy, has come from the recent discovery of a whole host of unexpected states by the meson factory detectors, Belle and BaBar.

The new states are called **"charmonium-like states"**, not because they naturally fit into the spectrum of charmonium states, but because they seem to always decay into final states containing a charm quark and an anti-charm

quark. There are at least eleven of them around. The alphabet soup is getting thick with reports of X(3872), Y(4260), Y(4361), Y(4660), X(3940), Y(3940), Z(3940), X(4160), $Z^{\pm}(4430)$, $Z_1^{\pm}(4051)$ and $Z_2^{\pm}(4248)$. Except for the first two, X(3872) and Y(4260), which have been observed in measurements at several laboratories, the remaining nine come exclusively from Belle. They have not been reported by BaBar with similar capabilities, and in two cases, Y(4325) and the $Z^{\pm}$, they have been contradiected by BaBar. Reminds you of the old dibaryon story. I do not want to express my skepticism any further, but tell you only about the two certain exotics, X(3872) and Y(4260).

10.1 X(3872) and the molecular model

This narrow state with $M(\mathrm{X}) = \mathbf{3872.2 \pm 0.8}$ MeV, and $\Gamma(\mathrm{X}) = 1.34 \pm 0.64$ MeV, has been observed by Belle, BaBar, CDF, DØ, and it definitely exists. [PDG08] CDF angular correlation studies show that its $J^{PC} = 1^{++}$ or 2^{-+}. X(3872) does not easily fit in the charmonium spectrum. Since its mass is very close to $M(D) + M(D^*)$, the most popular conjecture is that it is a weakly **bound molecule** of D and D^*. If so, our recent precision measurement of D^0 mass at CLEO gives $M(D^0 D^{0*}) = \mathbf{3871.81 \pm 0.36}$ MeV. This corresponds to X(3872) being **unbound** by 0.4 ± 0.8 MeV. If X(3872) were even bound by ~ 0.4 MeV, the branching fraction for the molecule's breakup into $D\overline{D}\pi$ is predicted to be factor 400 smaller than observed. These observations raise serious doubts about the molecular model for X(3872).

Stop the presses: CDF now reports [19] $M(\mathrm{X}) = 3871.46 \pm 0.19$ MeV. So we now have X(3872) bound by 0.35 ± 0.41 MeV. The problem of the almost-bound/unbound nature of X(3872) is getting more and more sharply defined, and it is getting to be more and more exotic.

10.2 Y(4260) and the strange Vector

The Y(4260) has been observed in ISR production by BaBar, CLEO and Belle, and in direct production by CLEO. Y(4260) is clearly **a vector** with $J^{PC} = 1^{--}$. All known charmonium vectors are seen prominently as huge enhancements i hadronic decays, usually measured as the ratio $R = \sigma(h^+h^-)/\sigma(\mu^+\mu^-)$. But this vector is a very strange one, since it sits at a very deep minimum in R, with

$$M(\mathrm{Y}(4260)) = 4263^{+8}_{-9}\ \mathrm{MeV}, \quad \Gamma(\mathrm{Y}(4260)) = 95 \pm 14\ \mathrm{MeV} \qquad (\mathrm{PDG08})$$

So it is not likely to be a charmonium vector, which are all spoken for, anyway. So what is Y(4260)?

It is suggested that Y(4260) is a $c\bar{c}g$ charmonium hybrid. If so, there ought to be 0^{-+} and 1^{-+} hybrids companions nearby. Where are they? It is a real experimental challenge to clarify this situation before taking any theoretical conjecture seriously.

11 Epilogue

The sum total of the experiences in this journey through hadronic **exotica** is that the journey is certainly worth it. It is unquestionably exciting. But the road

is full of pitfalls and disappointments.

Only the brave should enter!

They should be proud of their successes, and humble enough to admit their failures.

References

1. H. Nann et al., Phys. Rev. Lett. **41**, 1589 (1978).
2. K. K. Seth et al., Phys. Rev. Lett. **58**, 1936 (1987).
3. B. Parker et al., Phys. Lett. **B 251**, 483 (1999).
4. Yu. Ts. Oganessian et al. Phys. Rev. **C 74**, 044602 (2006).
5. A. Chodos, R. L. Jaffe, et al. Phys. Rev. **D 9**, 3471 (1974).
6. P. J. Mulders, A. T. Aerts and J. J. de Swart, Phys. Rev. **D 19**, 2635 (1979); Phys. Rev. **D 21**, 1370 (1980); Phys. Rev. **D 21**, 2653 (1981).
7. T. Nakano et al. Phys. Rev. Lett. **91**, 012002 (2003).
8. B. McKinnon et al., Phys. Rev. Lett. **96**, 212001 (2006).
9. H. Fritzsch and M. Gell–Mann, in Proc. XVI Int. Conf. on HEP, Fermilab, Vol. 2, 1972, p. 135.
10. C. Amsler et al., Phys. Lett. **B 520**, 175 (2001).
11. See for example, G. S. Adams et al., J. Phys. (Conf.) **9**, 136 (2005).
12. R. L. Jaffe, Phys. Rev. Lett. **38**, 195 (1977); Phys. Rev. Lett. **38**, 617E (1977).
13. A. L. Tralfner, Ph. D. dissertation, UC Berkeley, 2006; also Phys. Rev. **C 77**, 044908 (2008).
14. J. J. Aubert et al., Phys. Rev. Lett. **33**, 1404 (1974); J. E. Augustin et al. Phys. Rev. Lett. **33**, 1406 (1974).
15. Various authors, Phys. Rev. Lett. **34**, 36-56 (1975).
16. D. M. Asner et al., Phys. Rev. Lett. **92**, 142001 (2004).
17. J. L. Rosner et al., Phys. Rev. Lett. **95**, 102003 (2005); S. Dobbs et al., Phys. Rev. Lett. **101**, 182003 (2008).
18. B. Aubert et al., Phys. Rev. Lett. **101**, 071801 (2008).
19. T. Kuhr, presented at QWG2008,
    also http://www-cdf.fnal.gov/physics/new/bottom/080724.blessed-X-Mass/;
    Belle Collaboration, arXiv:0809.1224.

Few-Body Systems 0, 1–4 (2009)

Few-Body Systems

Two-nucleon ϕ-meson clusters*

V. B. Belyaev[1], W. Sandhas[2], and I. I. Shlyk[1]

[1] Joint Institute for Nuclear Research, BLTP, Dubna, 141980, Russia
[2] Physikalisches Institut, Universitat Bonn, D-53115 Bonn, Germany

Abstract. On the basis of Faddeev equations the binding energies of the systems ϕnn, ϕnp and ϕpp are calculated. The results indicate the possibility of new few - nucleon meson clusters.

As it was intensively discussed recently [1-7] there are indications on the strong attraction of mesons with one strange quark K^- ($\overline{K}$) to the few-nucleon nuclei.Along this line it is interesting to look at the interaction of a meson with two strange quarks like the ϕ-meson with light nuclei. Already existing theoretical investigations of the ϕ-meson interaction show rather strong attraction between a ϕ-meson and a nucleon. Indeed, the calculation of the $\phi - N$ interaction within the quark model [8], and on the basis of a totally different phenomenological model [9] based on the dominant role of $s\overline{s}$ configuration in the ϕ-meson structure, predicts considerable $\phi - N$ attraction with a binding energy of about 9 MeV for the ϕN system.

Such a strong attraction in reality might be not very surprising if one agrees with physical arguments, that strong K^-N attraction appeared due to the influence of subthreshold resonances Λ_{1405} and Σ_{1385}.

Indeed, let us compare the mass of the state $\phi + N$ with masses of two subthreshold states $K + \Lambda_{1405}$ and $K + \Sigma_{1385}$. It turned out, that distances of above subthreshold states from threshold $\phi + N$ state are the same order of magnitude as in K^-N case, which means that as in K^-N system one can expect strong influence of Λ_{1405} and Σ_{1385} and strong attraction also in the ϕN system.

Bearing in mind this sort of strong attraction in the ϕN system, it is interesting to consider the possibility of bound states of a ϕ-meson with few nucleons, in particular with two neutrons or two protons. This is in fact a question concerning the existence of new nuclear clusters. In what follows we calculate the binding energies of the three-body systems ϕnn, ϕnp and ϕpp.

As in [9] a Yukawa type potential is chosen for the $\phi - N$ interaction :

$$V_{\phi N}(r) = -\alpha\, e^{-\mu\, r}/r \tag{1}$$

*Article based on the presentation by V. B. Belyaev at the Fifth Workshop on Critical Stability, Erice, Sicily, Received November 11, 2008 Accepted January 8, 2009.

with $\alpha = 1.25$ and $\mu = 600$ MeV. This potential is rather deep and narrow and supports binding in the ϕN system with binding energies $E_{\phi n} = -9.47$ and $E_{\phi p} = -9.40$ MeV.

For the np triplet s-wave interaction the potential MTIII [10] has been used. Our singlet s-wave interaction is based on the potential MTI [10] with the slight modification of having now a parameter $\lambda_A = 2.617$. This value is chosen in order to reproduce the experimental value of the nn-scattering length $a_{nn} = -18.5$ fm [11]. One can see that in the three-body systems ϕNN there are two scales of distances, related to the different ranges of the $N-N$ and $\phi-N$ interactions. This may produce a delicate interplay between a narrow attraction area of the $\phi-N$ interaction and repulsive parts of the MT-potentials, as it was emphasized in [12]. Apart from that, different ranges of the interaction can provide the cluster formation in the systems under consideration.

Let us start to describe a three particle system $\phi + 2N$. Our calculations are based on Faddeev equations [13] in differential form [14] written down for the 3-body systems ϕNN.

First, the Faddeev components of the wave function are expanded into partial waves:

$$\Psi_\alpha(\boldsymbol{\eta}_\alpha, \boldsymbol{\xi}_\alpha) = \sum_{LM\,l\,\lambda} \frac{1}{\eta_\alpha\,\xi_\alpha}\, U^L_{\alpha\,l\lambda}(\eta_\alpha,\, \xi_\alpha)\, Y^{LM}_{l\lambda}(\hat{\eta}_\alpha, \hat{\xi}_\alpha) \tag{2}$$

and only the lowest partial waves ($L = l = \lambda = 0$) are taken into account. Here $\eta_\alpha = |\boldsymbol{\eta}_\alpha|$, $\xi_\alpha = |\boldsymbol{\xi}_\alpha|$, $\hat{\eta}_\alpha = \boldsymbol{\eta}_\alpha / |\boldsymbol{\eta}_\alpha|$, $\hat{\xi}_\alpha = \boldsymbol{\xi}_\alpha / |\boldsymbol{\xi}_\alpha|$, $Y^{LM}_{l\lambda}$ are the bispherical harmonics. The Jacobi coordinates $\boldsymbol{\eta}_\alpha, \boldsymbol{\xi}_\alpha$ are as usual:

$$\boldsymbol{r}_i - \boldsymbol{r}_j = \frac{\boldsymbol{\eta}_\alpha}{a_\alpha}\,, \qquad \frac{m_i\,\boldsymbol{r}_i + m_j\,\boldsymbol{r}_j}{m_i + m_j} - \boldsymbol{r}_k = \frac{\boldsymbol{\xi}_\alpha}{b_\alpha} \tag{3}$$

where $\boldsymbol{r}_i$, m_i denote the radius-vector and the mass of particle i, the total mass is $M = m_1 + m_2 + m_3$,

$$a_\alpha = \sqrt{\frac{m_i\,m_j}{(m_i + m_j)\,M}}\,, \qquad b_\alpha = \sqrt{\frac{m_k(m_i + m_j)}{M^2}}\,, \tag{4}$$

and indices α take on following values: $\alpha = 3$ for $(ij)k = (12)3$, $\alpha = 1$ for $(ij)k = (23)1$, $\alpha = 2$ for $(ij)k = (31)2$.

Since there are two identical particles in the system (we take $m_N = m_n$ for ϕnp system) the following two coupled-differential Faddeev equations survive:

$$\left[\widehat{D} + V_i\left(\frac{\rho\cos\varphi}{a_i}\right) - E\right]\, U_i(\rho,\varphi) = -\,V_i\left(\frac{\rho\cos\varphi}{a_i}\right) \sum_{\alpha'\neq i} \frac{1}{\sin(2\gamma_{\alpha'_i})} \int_{c-}^{c+} U_{\alpha'}(\rho,\, \varphi')\,\mathrm{d}\varphi \tag{5}$$

for $i = 1, 2$ and $U_3 \equiv U_2$ where polar coordinates $\rho = \sqrt{\eta_\alpha^2 + \xi_\alpha^2}$, $\tan\varphi_\alpha =$

ξ_α/η_α are introduced and

$$
\begin{aligned}
& V_1 = V_{NN}\ , \quad V_2 = V_{\phi N}\ , \quad \widehat{D} = -\frac{\hbar^2}{2M}\left(\frac{\partial^2}{\partial\rho^2}\ +\ \frac{1}{\rho}\frac{\partial}{\partial\rho}\ +\ \frac{1}{\rho^2}\frac{\partial^2}{\partial\varphi^2}\right) \\
& c+ = \min\left\{\left|\varphi+\gamma_{\alpha'\alpha}\right|\ ,\ \pi\ -\ \left(\varphi+\gamma_{\alpha'\alpha}\right)\right\}\ , \quad c- = \left|\varphi-\gamma_{\alpha'\alpha}\right| \\
& \gamma_{ij} = \arcsin s_{ij}\ , \quad s_{\,ij} = \sqrt{\frac{m_k M}{(m_i+m_k)\,(m_j\ +\ m_k)}}\ ,
\end{aligned}
\tag{6}
$$

where i, j, k is an even permutation of $1, 2, 3$ and the indices correspond to 1 for the ϕ-meson, and 2 and 3 for the nucleons.

The two-dimensional system of Faddeev equations (5) has been solved by discretization of variables hyperradius ρ and hyperangle φ with N and M mesh points respectively. Stable results for three digits of binding energies were reached at $N = 110$, $M = 210$ and $L(\rho$ variable cutoff$) = 9$ fm.

As a result the binding energy of the system ϕnn with value $E_{\phi nn} = -21.8$ MeV has been obtained and value $E_{\phi np} = -37.9$ MeV for the binding of ϕnp system with np pair in triplet state. It should be noticed, that for this binding energy in ϕnp system both main ϕ-meson decay channels on K-mesons are closed. Let us comment last value of energy, which appeared rather large. From naive reasons in the configuration $\phi + d$ one would expect binding of order $2 \times E_{\phi N} + E_d$, which is much smaller than calculated value. However due to the strong attraction in ϕN - subsystem ($E_{\phi N} \sim -9$ MeV) one can expect, that in 3-particle ϕnp system, the configuration $\phi + d$ is rather suppressed. From that follows, that in the above system there is no strong cancellation between potential and kinetic energies of nucleons, like in deuteron and strong attractive triplet $N-N$ potential ($V_t \sim 100$ MeV) show his full value.

The dependence of the binding energy of ϕnn system on the parameter α of $\phi - N$ interaction is investigated. It is shown on the Figure 1, that excited states appear in this system.

As can be seen from the results, the binding in 3-particle systems like ϕNN is possible even at weaker $\phi - N$ attraction as compare to the potential (1) with parameters given in work [9].

In conclusion, it is interesting to consider clusters with number of neutrons more than two, for example four-body system $\phi+3n$. To take the first step to this problem, folding model to describe ϕnn cluster has been used. In the description of cluster ϕnn model wave function was taken, which however reproduce binding energy calculated above. Folding potential for the system $(\phi nn) + n$ is calculated. Here, the third neutron is considered in p-wave with respect to the cluster ϕnn. The potential, in which p-wave centrifugal barrier is taken into account, is shown on the Figure 1. It appeared, that there is no bound state in this potential. However, as we know from exact four-body calculations of $\eta_c + 3n$ system [15] folding model greatly underestimate the real binding of the system.

Acknowledgement. The work was supported financially by the Deutsche Forschungsgemeinschaft (DFG grant no 436 RUS 113/761/0-2) and the Heisenberg-Landau Program 2008.

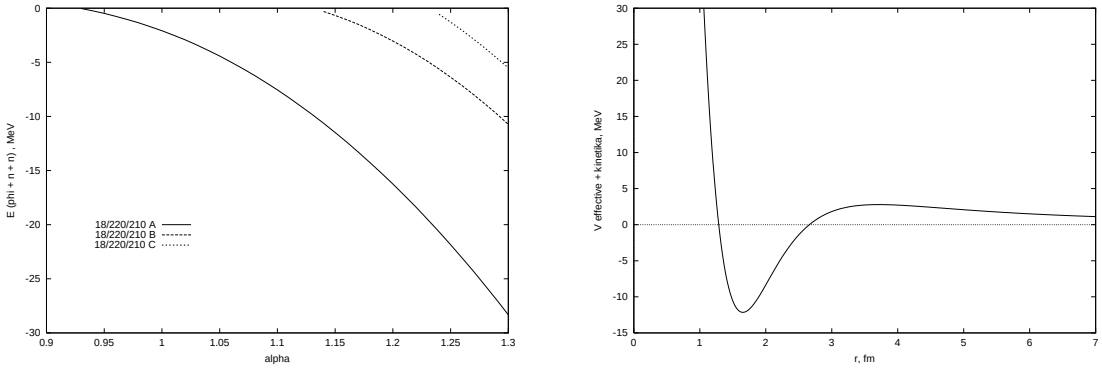

Figure 1. Left: The dependence of the binding energy of ϕnn system on the parameter α of $\phi - N$ interaction. Right: Folding potential with p-wave centrifugal barrier for the four-body system $(\phi nn) + n$.

References

1. Doté, A., Hyodo, T., Weise, W.: ArXiv: nucl-th/0802.0238 (2008)
2. Yamazaki, T., Akaishi, Y.: Phys. Lett. B 535, 70 (2002)
3. Agnello, M., et al.: Phys. Rev. Lett. 94, 212303 (2005)
4. Magas, V. K., Oset, E., Ramos, A., Toki, H.: Phys. Rev. C74, 025206 (2006)
5. Yamazaki, T., Akaishi, Y.: Phys. Rev. C76, 045201 (2007)
6. Shevchenko, N. V., Gal, A., Mares, J.: Phys. Rev. Lett. 98, 082301 (2007)
7. Shevchenko, N. V., Gal, A., Mareš, J., Révai, J.: Phys. Rev. C76, 044004 (2007)
8. Huang, F., Zhang, Z. Y., Yu, Y. W.: ArXiv: nucl-th/0601003 (2006)
9. Gao, H., Lee, T.-S. H., Marinov, V.: Phys. Rev. C63, 022201 (2001)
10. Malfliet, R. A., Tjon, J. A.: Nucl. Phys. A127, 161-168 (1969)
11. Howell, C. R., et al.: Phys. Lett. B444, 252-259 (1998)
12. Belyaev, V. B., Sandhas, W., Shlyk, I. I.: ArXiv: nucl-th/0707.4615 (2007)
13. Faddeev, L. D.: Zh. Eksp. Teor. Fiz., 39, 1459 (1960) (Sov. Phys. JETP, 12, 1014, 1961)
14. Pupyshev, V. V.: Theor. Math. Phys., 81:1, 1072-1077 (1989)
15. Belyaev, V. B., Shevchenko, N. V., Fix, A., Sandhas, W.: Nucl. Phys. A780, 100-111 (2006)

Few-Body Systems 0, 1–4 (2009)

Few-Body Systems

The kaon–few-nucleon levels and lifetimes calculated by a variational method*

S. Wycech [1] **, A.M. Green[2] ***

[1] Sołtan Institute for Nuclear Studies, Hoża 69, 00-681, Warsaw, Poland
[2] Helsinki Institute of Physics, P.O. Box 64, FIN-00014, Helsinki, Finland

Abstract. The search for nuclear states of $\overline{\mathrm{K}}$ mesons is presented and the main uncertainties: off-shell extrapolation of meson-nucleon scattering amplitudes, behavior of hadronic resonances in nuclei and extrapolation to high density nuclear regions are discussed. A two step method to perform variational calculations in the $\overline{\mathrm{K}}$–few-nucleon systems is suggested.

1 Introduction

Low energy $\overline{\mathrm{K}}$ mesons are attracted by nuclei. This attraction, well tested in kaonic atoms, has been attributed to coupling of the $\overline{\mathrm{K}}\mathrm{N}$ system to the $\Lambda(1405)$ baryon. More generally the system of interest consists of three channels $\overline{\mathrm{K}}\mathrm{N}$, $\Sigma\pi, \Lambda\pi$ coupled in the isospin $0, 1$ states. The scattering and reactions are usually described in terms of the $\hat{K}$ matrix related to the scattering matrix $\hat{T}$ by

$$\hat{T} = \hat{K} - \hat{K} i \hat{Q} \hat{T}, \tag{1}$$

where $\hat{Q}$ is a diagonal matrix of the c.m. channel momenta. Phenomenological $\hat{K}$-matrix elements are fitted to the $\overline{\mathrm{K}}\mathrm{N}$ elastic and inelastic scattering as well as to the $\Sigma\pi$ scattering data. An additional consistency condition has been formulated in terms of dispersion relations [1, 2]. The solutions in the dominant isospin 0 state yield attractive and large elastic $\hat{K}_{KN,KN}$ elements. These give rise to a singularity of $\hat{T}$ in the complex energy plane which is interpreted as the $\Lambda(1405)$ being a $\overline{\mathrm{K}}\mathrm{N}$ quasi-bound state. The position of the $\Lambda(1405)$ pole is not well fixed, and different sets of $\hat{K}$ locate it in the region of 1405-1417 MeV, while the width stays in the region of 35–50 MeV. In recent years other solutions for $\hat{K}$ based on SU(3) chiral models have been used [3]. These generate two singularities,

*Article based on the presentation by S. Wycech at the Fifth Workshop on Critical Stability, Erice, Sicily, Received November 30, 2008; Accepted January 8, 2009.
** *E-mail :* wycech@fuw.edu.pl
*** *E-mail :* anthony.green@helsinki.fi

one representing the $\overline{\rm K}$N quasi-bound state of energy about 1425 MeV and a broad resonance in the $\Sigma\pi$ channel. At this moment the selection of a proper model on the basis of two body states is not easy. The $\overline{\rm K}$-few-N quasi-bound states may be helpful in this respect. On the experimental side there exists one measurement that indicates the existence of a K^-pp state bound by ≈ 115MeV and ≈ 67 MeV wide [4]. The experimental search has become very active after Akaishi and Yamazaki showed that such bound states may exist in few nucleon systems [5].

The $\overline{\rm K}$-few-N states offer a new physics that is interesting in two aspects:

- The binding is generated by exciting nucleons to $\Lambda(1405)$ (and $\Sigma(1385)$).
- The bound states may involve very high nuclear densities.

2 Variational method

The variational method presented here allows one to find a satisfactory description of the $\overline{\rm K}$-N and N-N correlations at short distances. It consists of two steps:

(I) The meson wave function $\chi_K(\mathbf{x},\ \mathbf{x}_i)$ and complex energy $E(x_i)$ are found for a system of $\overline{\rm K}$ interacting with nucleons fixed at positions x_i.

(II) Next, the nucleon degrees of freedom are allowed to vary and the trial $\overline{\rm K}$-few-N wave function is used in the form $\Psi = \chi_K(\mathbf{x},\ \mathbf{x}_i)\chi_N(\mathbf{x}_i)$. The total Hamiltonian involves the meson and nucleon kinetic energies, NN and $\overline{\rm K}$N interactions. The minimal energy is found by varying parameters which enter χ_N and the AV18 NN potential is used [6]. The stability of these systems is given by the width determined as the average $\Gamma/2 = \langle\Psi|{\rm Im}[E(x_i)]|\Psi\rangle$.

The second step is standard, but the first one is not. It is presented here in some detail for the $\overline{\rm K}$NN system with a simplified one channel S wave interaction. Consider the scattering of a light meson bound on two identical fixed nucleons. The meson wave function χ_K is given by the solution of the multiple scattering equation

$$\chi_K(\mathbf{x},\mathbf{x}_1,\mathbf{x}_2) = \Sigma_i \int d\mathbf{y}\, \frac{\exp[i\,p\mid \mathbf{x}-\mathbf{y}\mid]}{4\pi\mid \mathbf{x}-\mathbf{y}\mid}\ 2\mu_{KN} V_{KN}(\mathbf{y},\mathbf{x}_i)\ \chi_K(\mathbf{y},\mathbf{x}_1,\mathbf{x}_2). \quad (2)$$

One looks for solutions of Eq. (2) which determine the complex momentum eigenvalue $p(x_i)$. It gives the energy and width of the quasi-bound system for given nucleon positions x_i. The potential is chosen in a separable form $V_{KN}(\mathbf{x}-\mathbf{x_i},\mathbf{x}'-\mathbf{x_i} = \lambda\ \upsilon(\mathbf{x}-\mathbf{x_i})\ \upsilon(\mathbf{x}'-\mathbf{x_i})$, with the Yamaguchi form-factor υ with inverse range κ and a *complex* strength λ. Equation (2) becomes a matrix equation for wave amplitudes ψ_i defined at each scatterer i by

$$\psi_i = \lambda \int d\mathbf{x}\, \upsilon(\mathbf{x}-\mathbf{x}_i)\, \chi_K(\mathbf{x},\mathbf{x}_1,\mathbf{x}_2). \quad (3)$$

To find equations for ψ_i one introduces matrix elements of the propagator

$$G_{i,j} = \int d\mathbf{y}d\mathbf{x}\ \upsilon(\mathbf{x}-\mathbf{x}_i)\ \frac{\exp(i\,k\mid \mathbf{xy}\mid)}{4\pi\mid \mathbf{x}-\mathbf{x}\mid}\ \upsilon(\mathbf{y}-\mathbf{x}_j). \quad (4)$$

The diagonal value, $G_{i,i} \equiv G_o$, determines the meson nucleon scattering matrix t by the well known relation $t(E) = (1+\lambda\ G_o)^{-1}\ \lambda$ which yields the full off-shell scattering amplitude $f(k,E,k') = \upsilon(k)\ t(E)\ \upsilon(k')$. Equation (2) can be

expressed in terms of scattering amplitudes t_i at each nucleon i and propagators describing the passage from the nucleon i to the other nucleon j. One arrives at a standard set of equations

$$\psi_i + \sum_{j \neq i} t_j \, G_{i,j} \, \psi_j = 0. \tag{5}$$

With two amplitudes ψ_i these reduce to

$$\psi_1 + t \; G \; \psi_2 = 0, \qquad \psi_2 + t \; G \; \psi_1 = 0, \tag{6}$$

where $G = G_{1,2}$. When the determinant $D = 1 - (t \; G)^2$ is put to zero, the binding "momenta" $p(r)$ may be obtained numerically. The solution of interest corresponding to $1 + tG = 0$ is symmetric, $\psi_2 = \psi_1$, and describes the meson in the S state with respect to the NN center of mass. It exists for all inter-nucleon distances *provided* there exists a singularity in $t(E)$ below the $\overline{\mathrm{K}}$N threshold as happens in the $\Lambda(1405)$ case. In some energy region $t = \gamma^2/(E - E^*)$, where $E^* = E_o - i\Gamma_o/2$ is the complex binding energy of $\Lambda(1405)$. The eigenvalue $p(r)$ is given by the condition $1 + tG = 0$, which now takes the form $E = E^* - \gamma^2 G(r,p)$. The solution $E \equiv E_B(r) - i\Gamma(r)/2$ depends on the N-N separation r. As Re$[G(r,p)]$ close to the resonance is positive, the binding of $\overline{\mathrm{K}}$ to fixed NN pair is stronger than the binding of $\overline{\mathrm{K}}$ to a nucleon, $|E_B(r)| > |E_o|$. Asymptotically for $r \to \infty$ one obtains $G \to 0$ and $E(r) \to E^*$, *i.e.*, the $\overline{\mathrm{K}}$ meson becomes bound to one of the nucleons. The lifetime of $\overline{\mathrm{K}}$NN becomes equal to the lifetime of $\Lambda(1405)$. Hence, the separation energy is understood here as the energy needed to split $\overline{\mathrm{K}}$-N-N $\to \Lambda(1405)$-N.

Eigenvalues corresponding to unstable quasi-bound states are obtained in the second quadrant of the complex $p(r) = p_R + ip_I$ plane. The propagator

$$tG = f(p) \; [\exp(-p_I r) \exp(ip_R r) - \exp(-\kappa r) \; (1 + r\frac{\kappa^2 - p^2}{2\kappa})]/r \tag{7}$$

is exponentially damped at large distances as required by the asymptotic form of the bound state wave function χ_K. This shape of $G(r)$ describes the $\overline{\mathrm{K}}$-N correlations. At small r, *i.e.*, at high nuclear densities p_I increases and the correlation range becomes smaller.

The difference between the binding at a given separation r and its asymptotic value generates a potential $V_K(r)$, which contracts the nucleons to a smaller radius. It is defined as Re$[V_K(r)] = E_B(r) - E_B(\infty)$ and generates the bound states. On the other hand some part of the binding is hidden in $E_B(\infty)$ that is in the structure of $\Lambda(1405)$.

2.1 Results

The outlined method was used to study the $\overline{\mathrm{K}}$NN, $\overline{\mathrm{K}}$NNN and $\overline{\mathrm{K}}$NNNN systems [8]. The input was based on the $\hat{K}$ matrix from ref. [2] and eq.(5) was generalized to include S + P wave interactions (the $\Sigma(1385)$ excitations) and the multiple scattering in $\overline{\mathrm{K}}$N and $\Sigma\pi$ channels. Some results are given in the tables. These show a dramatic dependence of the binding on the $\Lambda(1405)$ parameters which reflect uncertainties of the $\overline{\mathrm{K}}$N amplitudes at 100-200 MeV below the

threshold. The $\Sigma(1385)$ makes a weak impact in the S wave states. However, it may generate P wave branches of the spectra, in particular a bound K^-nn state [8].

Table 1. Binding energies and widths [MeV] of the $\overline{\mathrm{K}}\mathrm{NN}$, $I_{tot} = 1/2$, $I_{NN} = 1$ space-symmetric states [8]. The results on the left are based on parameters of ref.[2] extended off-shell by a separable model [$M_\Lambda = 1409$ MeV]. The results on the right are obtained with M_Λ shifted to 1405 MeV and with equally good fit to the data. The first column specifies the channels explicitly involved in the multiple scattering and meson-nucleon partial waves. R_{rms} is the radius mean squared of the N-N separation [fm]. The numbers in the second line of the right sector are very close to the Faddeev solution obtained with a similar input [7].

	E_B	Γ	R_{rms}	E_B	Γ	R_{rms}
$\overline{\mathrm{K}}\mathrm{N}$; S	35.5	37	2.4	50	51	2.05
$\overline{\mathrm{K}}\mathrm{N}$,$\Sigma\pi$; S	43	47	2.1	71	85	1.8
$\overline{\mathrm{K}}\mathrm{N}$; S, P	50	36	3.3	65	43	2.1
$\overline{\mathrm{K}}\mathrm{N}$,$\Sigma\pi$; S, P	56.5	39	2.3	78	60	1.9

Table 2. Binding energies and widths [MeV] of the $\overline{\mathrm{K}}\mathrm{NNNN}$, space-symmetric, $S_{tot} = 0$, $I_{tot} = 1/2$ states. The widths do not include non-mesonic decays. See caption to Table 1.

	E_B	Γ	E_B	Γ
S	121	25	170	10
$S + P$	136	20	172	10

Acknowledgement. This work is supported by the KBN grant 1P0 3B 04229 and the EU Contract No. MRTN-CT-2006-035482, "FLAVIAnet".

References

1. Martin, A. D.: Nucl. Phys. **B94**, 413 (1975)
2. Martin, B. R.: Nucl. Phys. **B184**, 33 (1981)
3. Hyodo, T., Weise, W.: Phys. Rev. **C77**, 035204 (2008)
   Oset, E., Ramos, A., Bennhold, C.: Phys. Lett. **B527**, 99 (2002)
   Borasoy, B., Meissner, U. G., Nissler, R.: Phys. Rev. **C74**, 055201 (2006)
4. Agnello, M., for FINUDA Collab.: Phys. Rev. Lett. **94**, 212303 (2005)
5. Akaishi, Y., Yamazaki T.: Phys. Rev. **C65**, 044005 (2002)
6. Wiringa, R.B., et al.: Phys. Rev. **C51**, 38 (1995)
7. Shevchenko, N. V., Gal, A., Mares, J.: Phys. Rev. Lett. **98**, 082301 (2007)
8. Wycech, S., Green, A. M.: arXiv:0808.3329[nucl-th] submitted to Phys. ReV. **C**; Int. J. Mod. Phys. **A22**, 629 (2007)

Few-Body Systems 0, 1–6 (2009)

Few-Body Systems

Four-quark stability*

J. Vijande[1], A. Valcarce[2], J.-M. Richard[3], N. Barnea[4]

[1] Departamento de Física Atómica, Molecular y Nuclear, Universidad de Valencia (UV) and IFIC (UV-CSIC), Valencia, Spain.

[2] Departamento de Física Fundamental, Universidad de Salamanca, E-37008 Salamanca, Spain

[3] Laboratoire de Physique Subatomique et Cosmologie, Université Joseph Fourier–INPG–IN2P3-CNRS 53, avenue des Martyrs, 38026 Grenoble, France

[4] The Racah Institute of Physics, The Hebrew University, 91904, Jerusalem, Israel

Abstract. The physics of charm has become one of the best laboratories exposing the limitations of the naive constituent quark model and also giving hints into a more mature description of meson spectroscopy, beyond the simple quark–antiquark configurations. In this talk we review some recent studies of multiquark components in the charm sector and discuss in particular exotic and non-exotic four-quark systems, both with pairwise and many-body forces.

More than thirty years after the so-called November revolution [1], heavy hadron spectroscopy remains a challenge. The formerly comfortable world of heavy mesons is shaken by new results [2]. This started in 2003 with the discovery of the $D^*_{s0}(2317)$ and $D_{s1}(2460)$ mesons in the open-charm sector. These positive-parity states have masses lighter than expected from quark models, and also smaller widths. Out of the many proposed explanations, the unquenching of the naive quark model has been successful [3]. When a $(q\bar{q})$ pair occurs in a P-wave but can couple to hadron pairs in S-wave, the latter configuration distorts the $(q\bar{q})$ picture. Therefore, the 0^+ and 1^+ $(c\bar{s})$ states predicted above the $DK(D^*K)$ thresholds couple to the continuum. This mixes meson–meson components in the wave function, an idea advocated long ago to explain the spectrum and properties of light-scalar mesons [4].

This possibility of $(c\bar{s}n\bar{n})$ (n stands for a light quark) components in D^*_s has open the discussion about the presence of compact $(c\bar{c}n\bar{n})$ four-quark states in the charmonium spectroscopy. Some states recently found in the hidden-charm sector may fit in the simple quark-model description as $(c\bar{c})$ pairs (e.g., $X(3940)$, $Y(3940)$, and $Z(3940)$ as radially excited χ_{c0}, χ_{c1}, and χ_{c2}), but others appear to be more elusive, in particular $X(3872)$, $Z(4430)^+$, and $Y(4260)$. The debate on the nature of these states is open, with special emphasis on the $X(3872)$. Since it

*Article based on the presentations by J. Vijande and J.-M. Richard at the Fifth Workshop on Critical Stability, Erice, Sicily, Received February 2, 2009; Accepted February 9, 2009.

was first reported by Belle in 2003 [5], it has gradually become the flagship of the new armada of states whose properties make their identification as traditional ($c\bar{c}$) states unlikely. An average mass of 3871.2 ± 0.5 MeV and a narrow width of less than 2.3 MeV have been reported for the $X(3872)$. Note the vicinity of this state to the $D^0\overline{D}^{*0}$ threshold, $M(D^0\,\overline{D}^{*0}) = 3871.2 \pm 1.2$ MeV. With respect to the $X(3872)$ quantum numbers, although some caution is still required until better statistic is obtained [6], an isoscalar $J^{PC} = 1^{++}$ state seems to be the best candidate to describe the properties of the $X(3872)$.

Another hot sector, at least for theorists, includes the $(cc\bar{n}\bar{n})$ states, which are manifestly exotic with charm 2 and baryon number 0. Should they lie below the threshold for dissociation into two ordinary hadrons, they would be narrow and show up clearly in the experimental spectrum. There are already estimates of the production rates indicating they could be produced and detected at present (and future) experimental facilities [7]. The stability of such $(QQ\bar{q}\bar{q})$ states has been discussed since the early 80s [8], and there is a consensus that stability is reached when the mass ratio $M(Q)/m(q)$ becomes large enough. See, e.g., [9] for Refs. This effect is also found in QCD sum rules [10]. This improved binding when M/m increases is due to the same mechanism by which the hydrogen molecule (p, p, e^-, e^-) is much more bound than the positronium molecule (e^+, e^+, e^-, e^-). What matters is not the Coulomb character of the potential, but its property to remain identical when the masses change. In quark physics, this property is named *flavour independence*. It is reasonably well satisfied, with departures mainly due to spin-dependent corrections.

The question is whether stability is already possible for $(cc\bar{n}\bar{n})$ or requires heavier quarks. In Ref. [9], a marginal binding was found for a specific potential for which earlier studies found no binding. This illustrates how difficult are such four-body calculations.

In another recent investigation, the four-body Schrödinger equation has been solved accurately using the hyperspherical harmonic (HH) formalism [11], with two standard quark models containing a linear confinement supplemented by a Fermi–Breit one-gluon exchange interaction (BCN), and also boson exchanges between the light quarks (CQC). The model parameters were tuned in the meson and baryon spectra. The results are given in Table 1, indicating the quantum numbers of the state studied, the maximum value of the grand angular momentum used in the HH expansion, $K_{\rm m}$, and the energy difference between the mass of the four-quark state, E_{4q}, and that of the lowest two-meson threshold calculated with the same potential model, Δ_E. For the $(cc\bar{n}\bar{n})$ system we have also calculated the radius of the four-quark state, R_{4q}, and its ratio to the sum of the radii of the lowest two-meson threshold, Δ_R.

Besides trying to unravel the possible existence of bound $(cc\bar{n}\bar{n})$ and $(c\bar{c}n\bar{n})$ states one should aspire to understand whether it is possible to differentiate between compact and molecular states. A molecular state may be understood as a four-quark state containing a single physical two-meson component, i.e., a unique singlet-singlet component in the colour wave function with well-defined spin and isospin quantum numbers. One could expect these states not being deeply bound and therefore having a size of the order of the two-meson system,

Table 1. $(c\bar{c}n\bar{n})$ (left) and $(cc\bar{n}\bar{n})$ (right) results.

$(c\bar{c}n\bar{n})$	CQC		BCN	
$J^{PC}(K_{\rm m})$	E_{4q}	Δ_E	E_{4q}	Δ_E
0^{++} (24)	3779	+34	3249	+75
0^{+-} (22)	4224	+64	3778	+140
1^{++} (20)	3786	+41	3808	+153
1^{+-} (22)	3728	+45	3319	+86
2^{++} (26)	3774	+29	3897	+23
2^{+-} (28)	4214	+54	4328	+32
1^{-+} (19)	3829	+84	3331	+157
1^{--} (19)	3969	+97	3732	+94
0^{-+} (17)	3839	+94	3760	+105
0^{--} (17)	3791	+108	3405	+172
2^{-+} (21)	3820	+75	3929	+55
2^{--} (21)	4054	+52	4092	+52

$(cc\bar{n}\bar{n})$	CQC			
$IJ^P(K_{\rm m})$	E_{4q}	Δ_E	R_{4q}	Δ_R
$0\,0^+$ (28)	4441	+15	0.624	>1
$0\,1^+$ (24)	3861	−76	0.367	0.808
$0\,2^+$ (30)	4526	+27	0.987	>1
$0\,0^-$ (21)	3996	+59	0.739	>1
$0\,1^-$ (21)	3938	+66	0.726	>1
$0\,2^-$ (21)	4052	+50	0.817	>1
$1\,0^+$ (28)	3905	+50	0.817	>1
$1\,1^+$ (24)	3972	+33	0.752	>1
$1\,2^+$ (30)	4025	+22	0.879	>1
$1\,0^-$ (21)	4004	+67	0.814	>1
$1\,1^-$ (21)	4427	+1	0.516	0.876
$1\,2^-$ (21)	4461	−38	0.465	0.766

i.e., $\Delta_R \sim 1$. Opposite to that, a compact state may be characterized by its involved structure on the colour space, its wave function containing different singlet-singlet components with non negligible probabilities. One would expect such states would be smaller than typical two-meson systems, i.e., $\Delta_R < 1$. Let us notice that while $\Delta_R > 1$ but finite would correspond to a meson-meson molecule $\Delta_R \stackrel{K\to\infty}{\longrightarrow} \infty$ would represent an unbound threshold.

As can be seen in Table 1 (left), in the case of the $(c\bar{c}n\bar{n})$ there appear no bound states for any set of quantum numbers, including the suggested assignment for the $X(3872)$. Independently of the quark–quark interaction and the quantum numbers considered, the system evolves to a well separated two-meson state. This is clearly seen in the energy, approaching the threshold made of two free mesons, and also in the probabilities of the different colour components of the wave function and in the radius [11]. Thus, in any manner one can claim for the existence of a bound state for the $(c\bar{c}n\bar{n})$ system.

A completely different behaviour is observed in Table 1 (right). Here, there are some particular quantum numbers where the energy is quickly stabilized below the theoretical threshold. Of particular interest is the 1^+ $cc\bar{n}\bar{n}$ state, whose existence was predicted more than twenty years ago [12]. There is a remarkable agreement on the existence of an isoscalar $J^P = 1^+$ $cc\bar{n}\bar{n}$ bound state using both BCN and CQC models, if not in its properties. For the CQC model the predicted binding energy is large, $-$ 76 MeV, $\Delta_R < 1$, and a very involved structure of its wave function (the DD^* component of its wave function only accounts for the 50% of the total probability) what would fit into compact state. Opposite to that, the BCN model predicts a rather small binding, -7 MeV, and Δ_R is larger than 1, although finite. This state would naturally correspond to a meson-meson molecule.

Concerning the other two states that are below threshold in Table 1 a more careful analysis is required. Two-meson thresholds must be determined assuming quantum number conservation within exactly the same scheme used in the four–

quark calculation. Dealing with strongly interacting particles, the two-meson states should have well defined total angular momentum, parity, and a properly symmetrized wave function if two identical mesons are considered (coupled scheme). When noncentral forces are not taken into account, orbital angular momentum and total spin are also good quantum numbers (uncoupled scheme). We would like to emphasize that although we use central forces in our calculation the coupled scheme is the relevant one for observations, since a small non-central component in the potential is enough to produce a sizeable effect on the width of a state. These state are below the thresholds given by the uncoupled scheme but above the ones given within the coupled scheme what discard these quantum numbers as promising candidates for being observed experimentally.

Binding increases for larger M/m, but in the $(bb\bar{n}\bar{n})$ sector, there is no proliferation of bound states. We have studied all ground states of $(bb\bar{n}\bar{n})$ using the same interacting potentials as in the double-charm case. Only four bound states have been found, with quantum numbers $J^P(I) = 1^+(0)$, $0^+(0)$, $3^-(1)$, and $1^-(0)$. The first three ones correspond to compact states.

Now, one could question the validity of the potential models used in these estimates, or more precisely, of the extrapolation from mesons to baryons, and then to multiquark states. For the short-range terms, in particular one-gluon exchange, the additive rule

$$V = -\frac{3}{16}\sum_{i<j}\tilde{\lambda}_i^{(c)}.\tilde{\lambda}_j^{(c)}\, v(r_{ij}) \ , \tag{1}$$

is justified. Here $v(r)$ is the quark–antiquark potential governing mesons, and $\tilde{\lambda}_i^{(c)}$ is the colour generator. This is the non-Abelian version of the $1/r \to \sum q_i q_j/r_{ij}$ rule in atomic physics.

The confining part, however, is hardly of pairwise character. Several authors have proposed that the linearly rising potential σr of mesons (σ is the string tension) is generalised as

$$V = \sigma \min(d_1 + d_2 + d_3) \ , \tag{2}$$

where d_i is the distance from the i^{th} quark to a junction whose location is optimised, exactly as in the famous problem of Fermat and Torricelli. Unfortunately, the potential (2) differs little from the empirical ansatz (1) which here reduces to $\sigma(r_{12} + r_{23} + r_{31})/2$. Hence baryon spectroscopy cannot probe the three-body character of confinement.

In the case of two quarks and two antiquarks, the confining potential reads

$$V_4 = \min(V_f,\, V_s) \ , \tag{3}$$

given by the minimum of a flip-flop potential V_f and a Steiner-tree potential V_s, sometimes named "butterfly" (see Fig. 1). In V_f, each gluon flux goes from a quark to an antiquark. The second term corresponds to a minimal Steiner tree, with four terminals and two Steiner points. It is remarkable that this potential, which is supported by lattice QCD [13] is more attractive than the additive ansatz. This is illustrated in Ref. [14], where the four-body problem is solved

Figure 1. String model for four quarks: flip-flop (left) and Steiner-tree (right), an alternative configuration that is favoured when the quarks (full disks) are well separated from the antiquarks (open circles).

Table 2. Four–quark variational energy E_4 of $QQ\overline{q}\overline{q}$ for the different confinement models (V_f stands for the flip-flop interaction, V_s for the Steiner-tree potential, and $V_4 = \min(V_f, V_s)$), compared to its threshold, and variational energy E_4' of $Q\overline{Q}q\overline{q}$ with the flip-flop model V_f, compared to its threshold T_4' as a function of the mass ratio.

M/m	E_4			T_4	E_4'	T_4'
	V_f	V_s	V_4		V_f	
1	4.644	5.886	4.639	4.676	4.644	4.676
2	4.211	5.300	4.206	4.248	4.313	4.194
3	4.037	5.031	4.032	4.086	4.193	3.959
4	3.941	4.868	3.936	3.998	4.117	3.811
5	3.880	4.754	3.873	3.942	4.060	3.705

with this confining term alone without short-range corrections. The results are displayed in Table 2. This four-body calculation is rather involved, as the potential at each point is obtained by a minimisation over several parameters. See Ref. [14] for technical details about the models and the numerical techniques used.

The results for the configurations $(QQ\bar{q}\bar{q})$ and $(Q\overline{Q}q\bar{q})$ are shown in Table 2 as function of the heavy-to-light mass ratio. Clearly, as M/m increases, a deeper binding is obtained for the flavour-exotic $(QQ\bar{q}\bar{q})$ system. For the hidden-flavour $(Q\overline{Q}q\bar{q})$, however, the stability deteriorates, becoming unbound for $M/m \gtrsim 1.2$.

More recently, the stability in this model has been demonstrated rigorously in the limit of very large M/m. The first step is to show that

$$V_4/\sigma \leq \frac{\sqrt{3}}{2}\left(|\boldsymbol{x}| + |\boldsymbol{y}|\right) + |\boldsymbol{z}| \ , \tag{4}$$

in terms of the Jacobi variables, $\boldsymbol{x} = \boldsymbol{r}_2 - \boldsymbol{r}_1$, $\boldsymbol{y} = \boldsymbol{r}_4 - \boldsymbol{r}_3$ and $\boldsymbol{z} = (\boldsymbol{r}_3 + \boldsymbol{r}_4 - \boldsymbol{r}_1 + \boldsymbol{r}_2)/2$, so that the Hamiltonian describing the relative motion is bounded by

$$H_b = \frac{\boldsymbol{p}_x^2}{M} + \sigma\frac{\sqrt{3}}{2}|\boldsymbol{x}| + \frac{\boldsymbol{p}_y^2}{m} + \sigma\frac{\sqrt{3}}{2}|\boldsymbol{y}| + \frac{\boldsymbol{p}_z^2}{4\mu} + \sigma|\boldsymbol{z}| \ , \tag{5}$$

(μ is the quark–antiquark reduced mass), which is *exactly solvable* for its ground state and gives binding for large M/m. Details will be published shortly [15].

To conclude, let us stress again the important difference between the two physical systems which have been considered. While for the $(c\bar{c}n\bar{n})$, there are two allowed physical *decay channels*, $(c\bar{c}) + (n\bar{n})$ and $(c\bar{n}) + (\bar{c}n)$, for the $(cc\bar{n}\bar{n})$ only one physical system contains the possible final states, $(c\bar{n})+(c\bar{n})$. Therefore,

a $(c\bar{c}n\bar{n})$ four-quark state will hardly present bound states, because the system will reorder itself to become the lightest two-meson state, either $(c\bar{c}) + (n\bar{n})$ or $(c\bar{n})+(\bar{c}n)$. In other words, if the attraction is provided by the interaction between particles i and j, it does also contribute to the asymptotic two-meson state. This does not happen for the $(cc\bar{n}\bar{n})$ if the interaction between, for example, the two quarks is strongly attractive. In this case there is no asymptotic two-meson state including such attraction, and therefore the system might bind.

Once all possible $(cc\bar{n}\bar{n})$, $(bb\bar{n}\bar{n})$ and $(c\bar{c}n\bar{n})$ quantum numbers have been exhausted very few alternatives remain. If additional bound four-quark states or higher configuration are experimentally found, then other mechanisms should be at work, for instance based on diquarks [4, 16, 17].

Acknowledgement. This work has been partially funded by the Spanish Ministerio de Educación y Ciencia and EU FEDER under Contract No. FPA2007-65748, by Junta de Castilla y León under Contract No. SA016A17, and by the Spanish Consolider-Ingenio 2010 Program CPAN (CSD2007-00042).

References

1. J.D. Bjorken, The November Revolution: A Theorist Reminisces, in: A Collection of Summary Talks in High Energy Physics (ed. J.D. Bjorken), p. 229 (World Scientific, New York, 2003).
2. J.L. Rosner, J. Phys. Conf. Ser. **69**, 012002 (2007).
3. J. Vijande, F. Fernández, and A. Valcarce, Phys. Rev. D. **73**, 034002 (2006).
4. R.L. Jaffe, Phys. Rept. **409**, 1 (2005).
5. Belle Collaboration, S.-K. Choi *et al*, Phys. Rev. Lett. **91**, 262001 (2003).
6. K.K. Seth, AIP Conf. Proc. **814**, 13 (2006).
7. A. del Fabbro, D. Janc, M. Rosina, and D. Treleani, Phys. Rev. D **71**, 014008 (2005).
8. J. P. Ader, J. M. Richard, and P. Taxil, Phys. Rev. D **25**, 2370 (1982); J. L. Ballot and J. M. Richard, Phys. Lett. B **123**, 449 (1983).
9. D. Janc and M. Rosina, Few Body Syst. **35** (2004) 175.
10. F. S. Navarra, M. Nielsen and S. H. Lee, Phys. Lett. B **649** (2007) 166.
11. J. Vijande, E. Weissman, N. Barnea, and A. Valcarce, Phys. Rev. D **76**, 094022 (2007).
12. S. Zouzou, B. Silvestre-Brac, C. Gignoux, and J.-M. Richard, Z. Phys. C **30**, 457 (1986).
13. F. Okiharu, H. Suganuma and T. T. Takahashi, Phys. Rev. **D72**, 014505 (2005), [hep-lat/0412012].
14. J. Vijande, A. Valcarce, and J.-M. Richard, Phys. Rev. D **76**, 114013 (2007).
15. Cafer Ay, J. Hyam Rubinstein, and J.-M. Richard, arXiv:0901.3022 [math-ph].
16. L. Maiani *et al*, Phys. Rev. Lett. **93**, 212002 (2004).
17. C. Alexandrou, Ph. de Forcrand, and B. Lucini, Phys. Rev. Lett. **97**, 222002 (2006).

Few-Body Systems 0, 1–6 (2009)

Few-Body Systems

Few-Body Approaches and Problems in Hypernuclei*

Avraham Gal

Racah Institute of Physics, The Hebrew University, Jerusalem 91904, Israel

Abstract.

It takes two nucleons to bind a Λ hyperon, and perhaps as many as three nucleons to bind two Λ hyperons. Here I review few-body calculations which consider the onset of binding in multi-strange hypernuclei, including Ξ hyperons once the free-space strong-interaction conversion $\Xi N \to \Lambda\Lambda$ becomes Pauli forbidden in a Λ-abundant matter. Quasibound states of $\overline{K}$ mesons in few-nucleon systems are also briefly discussed.

1 Introduction

The experimental information on hyperon interactions, with few exceptions, is limited to single-Λ hypernuclei. Little is known on strangeness $S = -2$ hypernuclei. The missing information is vital for extrapolating into strange hadronic matter, for both finite systems and in bulk, and into neutron stars [1, 2]. Studying the onset of nuclear binding for hyperons, in particular, is one of the most sensitive means of deducing the strength of hyperon–nucleon and hyperon–hyperon interactions. The onset of binding for $\Lambda\Lambda$ and $\Lambda\Xi$ hypernuclei was reviewed at the XVIIIth European Conference on Few-Body Problems in Physics [3]. This review provides the starting point for the present discussion that hinges on few-body hypernuclear systems. In addition to Λ and Ξ hyperons, I will briefly discuss also Σ hyperons and $\overline{K}$ mesons.

2 Λ hyperons

2.1 s-shell Λ and $\Lambda\Lambda$ hypernuclei

Complete few-body calculations of the s-shell hypernuclei, for systems of nucleons and Λ hyperons, with full account of coupled-channel effects due to the primary $\Lambda N - \Sigma N$ and $\Lambda\Lambda - \Xi N$ mixings, were reported by Nemura et al. [4] using

*Article based on the presentation by A. Gal at the Fifth Workshop on Critical Stability, Erice, Sicily, Received December 12, 2008; Accepted January 9, 2009.

stochastic variational methods and phenomenological potentials based partly on meson exchange models. The calculated spectra are shown in Fig. 1. In addition to the well established single-Λ hypernuclei ${}^{3}_{\Lambda}$H, ${}^{4}_{\Lambda}$H $-$ ${}^{4}_{\Lambda}$He and ${}^{5}_{\Lambda}$He, bound states are predicted for ${}^{4}_{\Lambda\Lambda}$H and ${}^{5}_{\Lambda\Lambda}$H - ${}^{5}_{\Lambda\Lambda}$He by fitting to ${}^{6}_{\Lambda\Lambda}$He, the only $\Lambda\Lambda$ hypernucleus established uniquely by experiment [5]. The calculated $B_{\Lambda\Lambda}({}^{4}_{\Lambda\Lambda}\mathrm{H})$ is minute; given the uncertainties in the input and in the calculations, this system could still prove unbound [6]. Note that the experimental evidence [7] for ${}^{4}_{\Lambda\Lambda}$H has been challenged recently [8]. For ${}^{5}_{\Lambda\Lambda}$H and ${}^{5}_{\Lambda\Lambda}$He it is found that the primary $\Lambda N - \Sigma N$ and the secondary $\Xi N - \Lambda\Sigma$ couplings enhance the primary $\Lambda\Lambda - \Xi N$ mixing so that a fairly large Ξ probability is obtained, even for a relatively weak $\Lambda\Lambda - \Xi N$ coupling potential.

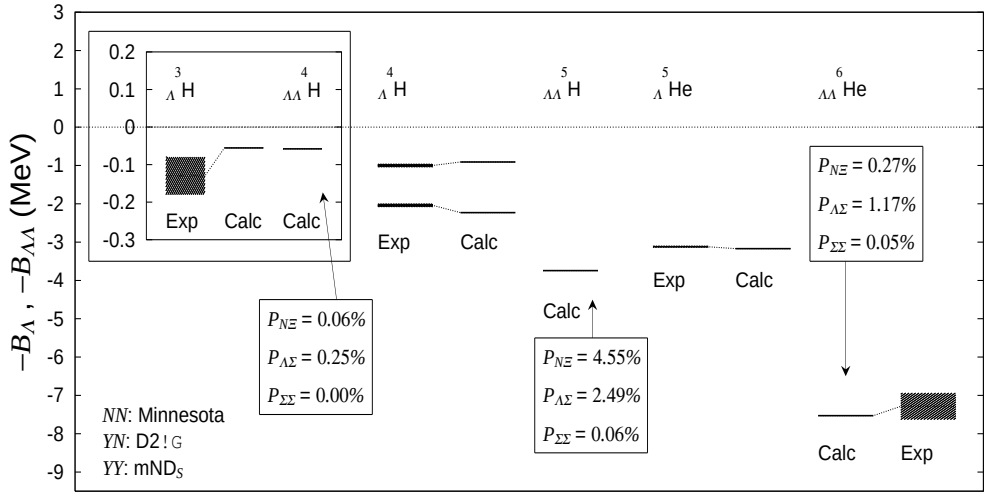

Figure 1. Λ and $\Lambda\Lambda$ separation energies in s-shell hypernuclei, calculated by Nemura et al. [4] using stochastic variational methods.

2.2 $\Lambda\Lambda$ hypernuclei

Several few-body cluster calculations of $\Lambda\Lambda$ hypernuclei in the neighborhood of ${}^{6}_{\Lambda\Lambda}$He have been reported. Two such calculations are depicted in Fig. 2. A nearly linear correlation between $\Delta B_{\Lambda\Lambda}({}^{6}_{\Lambda\Lambda}\mathrm{He})$ and $\Delta B_{\Lambda\Lambda}({}^{5}_{\Lambda\Lambda}\mathrm{H}, {}^{5}_{\Lambda\Lambda}\mathrm{He})$ is shown on the left-hand side, for Faddeev calculations using a variety of $\Lambda\Lambda$ interactions [9]. Here,

$$\Delta B_{\Lambda\Lambda}({}^{A}_{\Lambda\Lambda}Z) = B_{\Lambda\Lambda}({}^{A}_{\Lambda\Lambda}Z) - 2\bar{B}_{\Lambda}({}^{(A-1)}_{\Lambda}Z)\ , \qquad (1)$$

where $B_{\Lambda\Lambda}({}^{A}_{\Lambda\Lambda}Z)$ is the $\Lambda\Lambda$ separation energy of the hypernucleus ${}^{A}_{\Lambda\Lambda}Z$ and $\bar{B}_{\Lambda}({}^{(A-1)}_{\Lambda}Z)$ is the $(2J{+}1)$-average of B_{Λ} values for the ${}^{(A-1)}_{\Lambda}Z$ hypernuclear core levels. The roughly linear increase of $B_{\Lambda\Lambda}$ holds generally in three-body $\Lambda\Lambda C$ models (C standing for a cluster) over a wide range of values for the strength parameter $\bar{V}_{\Lambda\Lambda}$ [9]. Given that $\Delta B_{\Lambda\Lambda}({}^{6}_{\Lambda\Lambda}\mathrm{He}) \approx 1$ MeV, the figure demonstrates that the $I = 1/2$ ${}^{5}_{\Lambda\Lambda}$H - ${}^{5}_{\Lambda\Lambda}$He hypernuclei are particle stable. This conclusion is confirmed by the calculation [4] shown in Fig. 1.

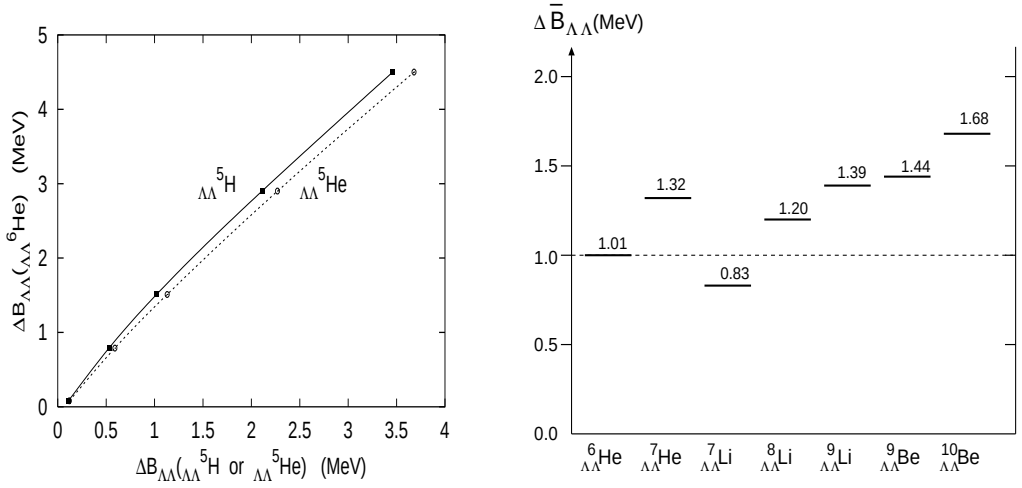

Figure 2. $\Delta B_{\Lambda\Lambda}$ values from Faddeev calculations [9] (left) and from three-body and four-body cluster calculations [10] (right).

The right-hand side of Fig. 2 depicts $\Delta B_{\Lambda\Lambda}$ values for $A = 7{-}10$ in three-body and four-body cluster variational calculations [10], normalizing the $\Lambda\Lambda$ interaction by requiring it to reproduce the well determined $\Delta B_{\Lambda\Lambda}$ value of ${}^{6}_{\Lambda\Lambda}$He within the same calculations. The deviations from the value $\Delta B_{\Lambda\Lambda} \approx 1$ MeV reflect dynamical core polarization effects. Some information is available on ${}^{10}_{\Lambda\Lambda}$Be and few neighboring $\Lambda\Lambda$ hypernuclei. Although the associated $\Delta B_{\Lambda\Lambda}$ values cannot be uniquely assigned to specific $\Lambda\Lambda$ hypernuclear states, acceptable assignments do exist that make these values consistent with the scale of $\Delta B_{\Lambda\Lambda}$ shown here.

3 Σ hyperons

A vast body of reported $(K^-, \pi^\pm)$ and (π^-, K^+) spectra indicate a repulsive Σ nuclear potential, with a substantial isospin dependence which for very light nuclei may conspire in selected configurations to produce Σ hypernuclear quasibound states, as shown on the left-hand side of Fig. 3 for ${}^{4}_{\Sigma}$He.[1] These data suggest that Σ hyperons do not bind in heavier nuclei.

A repulsive component of the Σ nuclear potential is also revealed in Σ^--atom analyses of level shifts and widths, as shown on the right-hand side of Fig. 3. The figure demonstrates that $\mathrm{Re}V_\Sigma$ is attractive at low densities outside the nucleus, changing into repulsion in the nuclear surface region, but well outside of the nuclear radius. Hence this transition is solidly substantiated by fitting to Σ^--atom data. The precise magnitude and shape of the repulsive component within the nucleus is model dependent [13]. The inner repulsion bears interesting consequences for the balance of strangeness in the inner crust of neutron stars [14], primarily by delaying the appearance of Σ^- hyperons to higher densities, as shown on the left-hand side of Fig. 4.

[1] The discovery of ${}^{4}_{\Sigma}$He, in K^- capture at rest, is due to R.S. Hayano et al.: Phys. Lett. **B231**, 355 (1989).

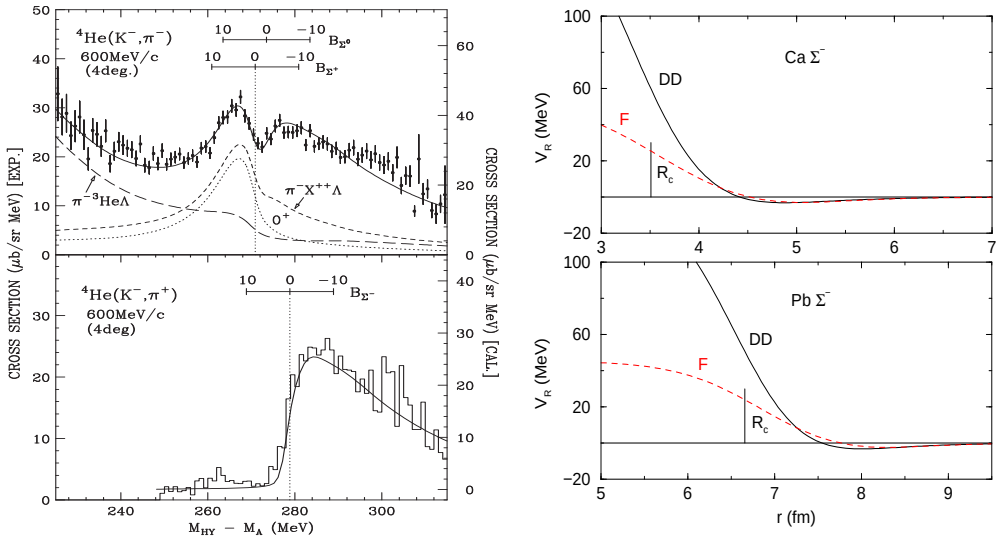

Figure 3. Left: $^4\mathrm{He}(K^-,\pi^\pm)$ spectra, as measured [11] and as calculated by Harada [12], providing evidence for a $^4_\Sigma$He $I=1/2$ quasibound state in the π^- channel, with binding energy $B_{\Sigma^+}=4.4\pm0.3\pm1$ MeV and width $\Gamma=7.0\pm0.7^{+1.2}_{-0.0}$ MeV. Right: ReV_{Σ^-} fitted to Σ^- atomic data, for two potential models [13]. The half-density nuclear charge radius R_c is indicated.

4 Ξ hyperons

Very little is established experimentally on the interaction of Ξ hyperons with nuclei. Inclusive (K^-,K^+) spectra on ^{12}C [15] yield a moderately attractive potential depth $\mathrm{Re}V_\Xi\approx-14$ MeV when fitted near the Ξ^--hypernuclear threshold. The most recent variant ESC04d of the Nijmegen YN potentials, adjusted to this potential depth, gives rise to quasibound states in several light nuclear targets that cope with the strong spin and isospin dependence in ESC04d, beginning with ^{7}Li [16]. For such a shallow potential, Ξ^0 hyperons do not bind to ^{4}He, although Ξ^- hyperons do bind owing to the Coulomb energy.

Ξ hyperons could become stabilized in multi-Λ hypernuclei once the decay $\Xi N\to\Lambda\Lambda$, which releases ≈25 MeV in free space, gets Pauli blocked. The onset of Ξ binding would occur for ${}^{\ }_{\Xi^0\Lambda}{}^{6}$He if $B_{\Xi^0}(^5_{\Xi^0}\mathrm{He})>3$ MeV [17], or for ${}^{\ }_{\Xi^0\Lambda\Lambda}{}^{7}$He if $B_{\Xi^0}(^5_{\Xi^0}\mathrm{He})>1$ MeV [18]. Particle stability for Ξ hyperons becomes robust with few more Λs, even for as shallow Ξ-nucleus potentials as discussed above. Fig. 4, right-hand side, demonstrates that Ξs can be added to a core of ^{56}Ni plus Λs, reaching as high strangeness fraction as $f_S\equiv-S/A\approx0.7$ while retaining particle stability. This leads to the concept of Strange Hadronic Matter (SHM) consisting of equal fractions of protons, neutrons, Λ, Ξ^0 and Ξ^- hyperons, with $f_S=1$, as for Strange Quark Matter (SQM). Both SHM and SQM provide macroscopic realizations of strangeness, but SHM is more plausible phenomenologically.

In a way of interim conclusions, few-body 'strange' systems provide a valuable handle and means of extrapolation into SHM. Several day-1 experiments on Ξ hyperons and $\overline{K}$ mesons in nuclei are scheduled soon, at the high-intensity 50 GeV proton synchrotron in the J-PARC facility in Japan.

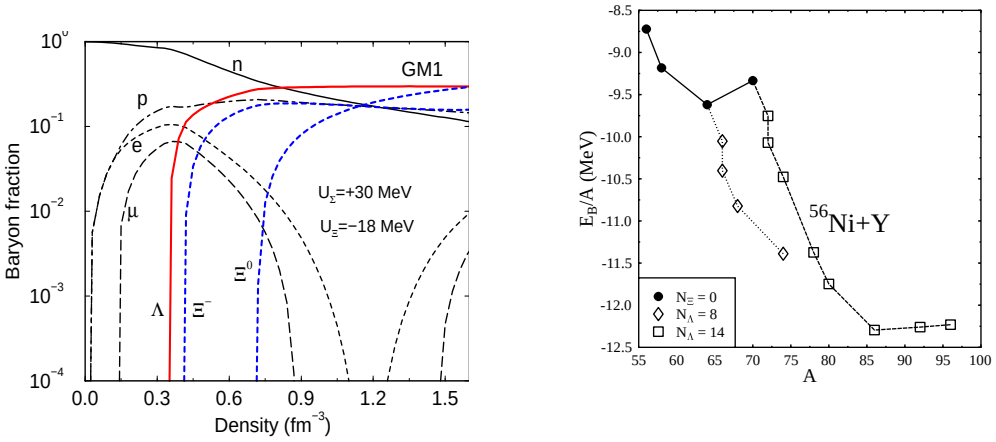

Figure 4. Left: fractions of baryons and leptons in neutron star matter calculated in RMF with weak YY potentials [2]. Right: binding energy of ^{56}Ni with added Λ and Ξ hyperons as a function of baryon number A [18].

5 Addendum: $\overline{K}$ mesons

Table 1. K^-pp binding energies & widths (MeV) calculated without $\bar{K}NN \to YN$

	$\bar{K}NN$ single channel		$\bar{K}NN - \pi\Sigma N$ coupled channels		
	ATMS [20]	AMD [21]	Faddeev [22]	Faddeev [23]	variational [24]
B	48	17–23	50–70	60–95	40–80
Γ	61	40–70	90–110	45–80	40–85

The K^-p interaction near threshold is dominated by the $\Lambda(1405)$, a $\pi\Sigma$ resonance interpreted as a $\bar{K}N$ quasibound state. Some of the topical issues in $\bar{K}$ nuclear physics, as reviewed in Ref. [19], are: (i) would K^- mesons form sufficiently narrow quasibound states in nuclei? and (ii) could strangeness materialize macroscopically in a K^- condensed phase rather than in SHM?

Next to $\Lambda(1405)$, the lightest $\bar{K}$ nuclear state maximizing the strongly attractive $I = 0$ $\bar{K}N$ interaction is $[\bar{K}(NN)_{I=1}]_{I=1/2,J^\pi=0^-}$, loosely denoted K^-pp. Results of few-body calculations for K^-pp are displayed in Table 1. The single-channel calculations are variational, and the difference between the resulting binding energies reflects the difference between the pole positions affecting the $I = 0$ $\bar{K}N$ amplitude, whether at 1405 MeV [20] or at 1420 MeV [21]. In coupled-channel calculations, the explicit use of the $\pi\Sigma N$ channel adds 20 ± 5 MeV with respect to single-channel calculations that use effective $\bar{K}N$ potentials. We note that the K^-pp calculated widths are substantial, before even considering $\bar{K}NN \to YN$ decay widths which become substantial in denser systems [25].

Acknowledgement. I am grateful to the organizers of the Workshop on Critical Stability, October 13-17, 2008, particularly Jean-Marc Richard, for the kind hospitality in Erice and for providing me with the opportunity to visit again this wonderful site after 41 years.

References

1. J. Schaffner-Bielich, A. Gal: Phys. Rev. **C62**, 034311 (2000)
2. J. Schaffner-Bielich: Nucl. Phys. **A804**, 309 (2008)
3. A. Gal: Few-Body Syst. Suppl. **14**, 251 (2003)
4. H. Nemura, S. Shinmura, Y. Akaishi, K.S. Myint: Phys. Rev. Lett. **94**, 202502 (2005)
5. H. Takahashi et al.: Phys. Rev. Lett. **87**, 212502 (2001)
6. I.N. Filikhin, A. Gal: Phys. Rev. Lett. **89**, 172502 (2002)
7. J.K. Ahn et al.: Phys. Rev. Lett. **87**, 132504 (2001)
8. S.D. Randeniya, E.V. Hungerford: Phys. Rev. **C76**, 064308 (2007)
9. I.N. Filikhin, A. Gal: Nucl. Phys. **A707**, 491 (2002)
10. E. Hiyama et al.: Phys. Rev. **C66**, 024007 (2002)
11. T. Nagae et al.: Phys. Rev. Lett. **80**, 1605 (1998)
12. T. Harada: Phys. Rev. Lett. **81**, 5287 (1998)
13. E. Friedman, A. Gal: Physics Reports **452**, 89 (2007)
14. S. Balberg, A. Gal: Nucl. Phys. **A625**, 435 (1997)
15. T. Fukuda et al.: Phys. Rev. **C58**, 1306 (1998);
    P. Khaustov et al.: Phys. Rev. **C61**, 054603 (2000)
16. E. Hiyama et al.: Phys. Rev. **C78**, 054316 (2008)
17. I.N. Filikhin, A. Gal: Phys. Rev. **C65**, 041001(R) (2002)
18. J. Schaffner et al.: Phys. Rev. Lett. **71**, 1328 (2003); Ann. Phys. **235**, 35 (1994)
19. A. Gal: Hyperfine Interactions, in press, arXiv:0812.0144 [nucl-th]
20. T. Yamazaki, Y. Akaishi: Phys. Lett. **B535**, 70 (2002)
21. A. Doté, T. Hyodo, W. Weise: Nucl. Phys. **A804**, 197 (2008)
22. N.V. Shevchenko, A. Gal, J. Mareš: Phys. Rev. Lett. **98**, 082301 (2007)
23. Y. Ikeda, T. Sato: Phys. Rev. **C76**, 035203 (2007)
24. S. Wycech, A.M. Green: Phys. Rev. **C**, submitted, arXiv:0808.3329 [nucl-th]
25. D. Gazda, E. Friedman, A. Gal, J. Mareš: Phys. Rev. **C76**, 055204 (2007)

Few-Body Systems 0, 1–4 (2009)

Few-Body Systems

The *ab initio* no-core shell model*

C. Forssén[1**], J. Christensson[2], P. Navrátil[3], S. Quaglioni[3], S. Reimann[2], J. Vary[4], S. Åberg[2]

[1] Fundamental Physics, Chalmers University of Technology, 412 96 Göteborg, Sweden
[2] Mathematical Physics, LTH, Lund University, Box 118, 22 100 Lund, Sweden
[3] Lawrence Livermore National Laboratory, P.O. Box 808, L-414, Livermore, CA 94551, USA
[4] Department of Physics and Astronomy, Iowa State University, Ames, IA 50011, USA

Abstract. This contribution reviews a number of applications of the *ab initio* no-core shell model (NCSM) within nuclear physics and beyond. We will highlight a nuclear-structure study of the $A = 12$ isobar using a chiral NN+3NF interaction. In the spirit of this workshop we will also mention the new development of the NCSM formalism to describe open channels and to approach the problem of nuclear reactions. Finally, we will illustrate the universality of the many-body problem by presenting the recent adaptation of the NCSM effective-interaction approach to study the many-boson problem in an external trapping potential with short-range interactions.

Introduction. A truly first-principles approach to the nuclear many-body problem requires a nuclear Hamiltonian that is based on the underlying theory of QCD. A candidate for providing the desired connection between QCD and the low-energy nuclear physics sector is chiral perturbation theory (χPT), see, e.g., the review by E. Epelbaum [1] and references therein. A very interesting observation from χPT is that three-nucleon forces (3NF) appear naturally already at the next-to-next-to-leading order of the expansion. This chiral 3NF was recently implemented in nuclear many-body calculations as will be discussed in the next section.

Regardless of its origin, high-precision nuclear Hamiltonians are very difficult to implement when solving the nuclear many-body problem. At this workshop we have heard about a number of methods that are available to solve the few-body problem ($A = 3 - 4$) to basically numerical precision. For more than four particles there are only a handful of methods available when using modern, realistic interactions. Much effort has been spent in studying different unitary transformations of the interaction to make it tractable for actual many-body

*Article based on the presentation by C. Forssén at the Fifth Workshop on Critical Stability, Erice, Sicily, Received December 12, 2008; Accepted December 20, 2008
** *E-mail address:* christian.forssen@chalmers.se

calculations. In particular, the *ab initio* no-core shell model (NCSM) is usually combined with the cluster-approximated, Lee-Suzuki transformation to generate effective interactions, see e.g., Refs. [2]. In short, the NCSM is a general approach for studying strongly interacting, quantum many-body systems. It's a matrix diagonalization technique to solve the translational invariant A-body problem in a finite harmonic oscillator basis. A particularly nice feature of the method is the flexibility of the harmonic-oscillator model space that implies basically no restrictions regarding the choice of Hamiltonian. Specifically, the NCSM method allows to test the modern χPT interactions in many-body calculations.

Recent NCSM Results. The $A = 12$ nuclear systems provide a challenge for modern *ab initio* methods. The systems can potentially act as new benchmarks as relevant observables allow for sensitive tests of the nuclear Hamiltonians and the computed wave functions. The current level of our experimental understanding of ^{12}C includes two bound states and the triple-alpha threshold at 7.3 MeV. Above this the picture becomes very complicated due to overlapping broad resonances. A central question concerns the possible existence of broad 0^+ and 2^+ resonances in this region. An important concept that attracts much theoretical interest is the interplay between triple-alpha and neutron-proton degrees of freedom. Studies of ground- and excited states in $A = 12$ systems are possible within the NCSM. These studies are particularly interesting since the chiral 3NF was recently implemented by P. Navrátil et al. [3]. The inclusion of these terms in the NCSM gives the correct ordering of $T = 1$ states with the isobaric analogue of the ^{12}B and ^{12}N ground states being the lowest. It also provides the correct ordering of the 1^+ and 4^+ states although it over-corrects the spin-orbit strength [3]. Still, regardless of the interaction being used, these results demonstrate a limitation of the NCSM method. Whereas the spectrum and properties of shell-model like states are reproduced very nicely, states that are known to exhibit a high degree of clusterization are missing from the low-energy spectrum. They typically end up at much higher excitation energy and are far from converged.

Open quantum systems. A long-term vision for nuclear theory is to achieve a unified picture of the nuclear many-body system, including both bound and continuum states and the transitions between them. Preferably this picture should be grounded in the fundamental interactions between the constituent nucleons. In addition, the separation of scales known to occur in nuclear systems, should be properly described. This requires the simultaneous modeling of small-scale many-body degrees of freedom and large-scale few-body correlations. A possible route towards achieving such a microscopic picture of open channels and nuclear reactions is explored at Livermore by combining the NCSM formalism with resonating group methods (RGM) [4]. In the RGM approach the many-body wave function is decomposed into contributions from various channels that are distinguished by their different arrangement of the nucleons into clusters. By defining a set of antisymmetrized cluster basis functions, and diagonalizing the Hamiltonian in this space, one obtains a non-local, coupled-channels Schrödinger Equation for the relative motion of the clusters in the different channels. In

Ref. [4] this approach was implemented and tested for certain $A = 4 - 5$ low-energy, single-nucleon scattering problems. In particular, n+^{4}He scattering at low energies represents a convenient training ground for many-body scattering calculations. There is no $A = 5$ bound state, and single-channel scattering is valid up to rather high energies. There is a sharp, low-energy resonance in the $3/2^-$ channel, and a broader, high-energy resonance in the $1/2^-$ channel. Scattering in the s-wave channel is non-resonant but obviously depends critically on proper antisymmetrization. Phase shifts for both n+^{4}He and p+^{4}He scattering, calculated in the NCSM/RGM approach, are presented in Fig. 1. The method

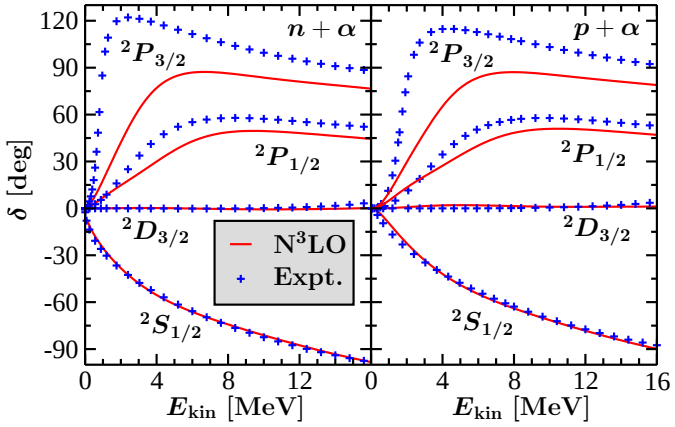

Figure 1. Phase shifts for n-α (left panels) and p-α (right panels) scattering. Recent NCSM/RGM results compared to an R-matrix analysis of experimental data. From Ref. [4].

shows very good convergence behavior, but it's clear that the position and widths of the p-wave resonances depend sensitively on the interaction model.

Effective Interaction Approach to the Many-Boson Problem. The emerging field of cold-atom physics has proven to be a very rich arena of research for few- and many-body physicists. Particle numbers can be varied, the interaction strength can in many cases be tuned through Feshbach resonances, and many different properties can be studied very cleanly in the laboratory. Nuclear physics techniques and tools have proven to be very useful to describe the physics of these systems. With trapping potentials that are very close to harmonic, the NCSM should be a perfect method. We recently adapted the NCSM formalism to describe a two-dimensional system of strongly interacting bosons [5]. A purely repulsive, short-ranged interaction was modeled with a Gaussian potential. Note that the different statistics of the bosonic many-body system required a complete rewrite of the NCSM suite of codes.

The success of the NCSM effective-interaction approach is demonstrated in Fig. 2. Ground- and excited-state energies are presented for a system of nine atoms. The NCSM results are compared to the much slower convergence of the standard configuration interaction (CI) method. The figure illustrates that stronger correlations within the system are obtained when increasing the interaction strength (right panel). In this case, the computed energies still show

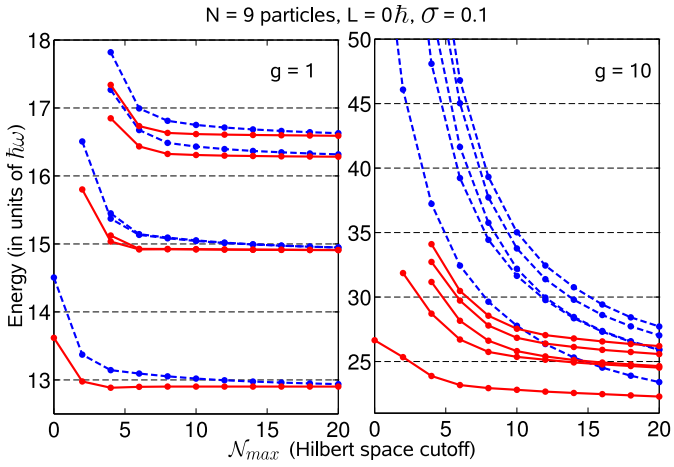

Figure 2. Energies for a system of nine bosons and total angular momentum $L = 0$, for different many-body space cutoffs ($\mathcal{N}_{\max}$). Repulsive Gaussian interactions with range $\sigma = 0.1$ and two different strengths (g) are used (oscillator units). The blue-dashed (red-solid) curves correspond to standard CI (effective interaction approach) calculations. From Ref. [5].

a slow decrease with increasing model space ($\mathcal{N}_{\max}$). Still, in comparison, the energies obtained from the standard CI calculations show a much slower convergence. These results represent an important first step of our new approach. Three-dimensional systems and higher particle numbers should also be within reach for future studies.

Conclusion. Recent applications of the *ab initio* NCSM within nuclear physics and beyond has been reviewed. In particular, we have demonstrated the study of chiral 3NF Hamiltonians in the p-shell, the treatment of open channels using the NCSM/RGM approach, and the effective-interaction approach to the many-boson problem.

Acknowledgement. This research was supported by the Swedish Research Council and the Knut and Alice Wallenberg Foundation. Partly prepared by LLNL under Contract DE-AC52-07NA27344. Support from the U.S. DOE/SC/NP (Work Proposal No. SCW0498), and from the U.S. DOE Grant DE-FC02-07ER41457 is acknowledged. One of us (C.F.) acknowledges financial support from Stiftelsen Lars Hiertas Minne and Längmanska Kulturfonden.

References

1. Epelbaum, E.: Prog. Part. Nucl. Phys. **57**, 654 (2006).
2. Navrátil, P., Vary, J. P., Barrett, B. R.: Phys. Rev. Lett. **84**, 5728 (2000); Navrátil, P., Vary, J. P., Barrett, B. R.: Phys. Rev. C **62**, 054311 (2000.
3. Navrátil, P., et al.: Phys. Rev. Lett. **99**, 042501 (2007).
4. Quaglioni, S., Navrátil, P.: Phys. Rev. Lett. **101**, 092501 (2008).
5. Christensson, J., et al.: arXiv.org:0802.2811 [cond-mat], Phys. Rev. A (in print) (2008).

Few-Body Systems 0, 1–4 (2009)

Few-Body Systems

Analysis of the effects of three-nucleon forces in $A = 3, 4$ systems*

A. Kievsky[1], M. Viviani[1], L. Girlanda[1,2], L.E. Marcucci[1,2], S. Rosati[1,2]

[1] Istituto Nazionale di Fisica Nucleare, Largo Pontecorvo 2, 56127 Pisa, Italy
[2] Dipartimento di Fisica, Università di Pisa, Largo Pontecorvo 2, 56127 Pisa, Italy

Abstract. It is not possible to reproduce both the three- and four-nucleon binding energies using the available two-nucleon potentials. This is one manifestation of the need to include a three-nucleon force in the corresponding Hamiltonian. In this paper we will analyze the capability of a three-nucleon force model to describe not only the aforementioned binding energies but also some $N - d$ low energy scattering observables.

1 Introduction

The realistic presently available NN potentials reproduce the experimental NN scattering data up to energies of 350 MeV with a χ^2 per datum close to 1. However, the use of these potentials for a study of the three- and four-nucleon bound and scattering states gives a χ^2 per datum very much larger than 1 (see for example Ref.[1]). In order to improve that situation, different three-nucleon force (TNF) models have been derived: widely used in the literature are the Tucson-Melbourne (TM) and the Urbana IX (URIX) models [2, 3]. More recently, TNF models have been derived [4] based on chiral effective field theory at next-to-next-to-leading order. The local version of this interaction (hereafter referred as N2LO) can be found in Ref. [5]. All these models contain a certain number of parameters that are fixed to reproduce the three- and four-nucleon binding energies. In this paper we will analyze the quality of this agreement, the prediction for the doublet $n - d$ scattering length ${}^2a_{nd}$ and some polarization observables in $p - d$ scattering. For this purpose we use the hyperspherical harmonic (HH) method (for a recent review see Ref. [6]).

2 Binding energies and scattering lengths for $A = 3, 4$

From the results obtained in Ref. [6], we report in Table 1 the triton and ^{4}He binding energies, and the doublet $n-d$ scattering length ${}^2a_{nd}$. These results were

*Article based on the presentation by A. Kievsky at the Fifth Workshop on Critical Stability, Erice, Sicily, Received January 14, 2009; Accepted January 29, 2009.

obtained using the AV18 or the N3LO-Idaho two-nucleon potentials together with the AV18+URIX and N3LO-Idaho+N2LO TNF models. The results are compared to the experimental values also reported in the table. Worthy of notice is the recent very accurate datum for ${}^2a_{nd}$ [9].

Table 1. The triton and ^{4}He binding energies B (MeV), and doublet scattering length ${}^2a_{nd}$ (fm) calculated using the AV18 and the N3LO-Idaho two-nucleon potentials, and the AV18+URIX and N3LO-Idaho+N2LO two- and three-nucleon interactions.

Potential	$B({}^3\mathrm{H})$	$B({}^4\mathrm{He})$	${}^2a_{nd}$
AV18	7.624	24.22	1.258
N3LO-Idaho	7.854	25.38	1.100
AV18+URIX	8.479	28.48	0.578
N3LO-Idaho+N2LO	8.474	28.37	0.675
Exp.	8.482	28.30	0.645±0.003±0.007

From the table we may observe that only the results obtained using an interaction model that includes a TNF are close to the corresponding experimental values. Moreover, the triton binding energy is well reproduced by choosing an appropriate value for the strength of the TNF. However this is not true for the ^{4}He binding energy and the scattering length ${}^2a_{nd}$, especially in the case of the AV18+URIX model.

The URIX potential has two free parameters which can be conveniently fixed. The first one, called $A_{2\pi}^{PW}$, is related to the strength of the term produced by a 2π-exchange with an intermediate Δ excitation. This term is constructed from the sum of two contributions with a relative strength $D_{2\pi}^{PW}$ of 1/4 and proves to be attractive. The second constant, called A_R, fixes the strength of a purely central repulsive term introduced to compensate the attraction of the previous term, which by itself would produce a large overbinding in infinite nuclear matter. The original values of these parameters, $A_{2\pi}^{PW} = -0.0293$ MeV, $A_R = 0.0048$ MeV and $D_{2\pi}^{PW} = 0.25$, has been fixed using the URIX with the AV18 two-nucleon potential. The corresponding results for the quantities of interest are given in Table 1. In order to improve these results we have varied the constants $A_{2\pi}^{PW}$, A_R and the relative strength $D_{2\pi}^{PW}$. For a given value of $A_{2\pi}^{PW}$, we have varied A_R and $D_{2\pi}^{PW}$ to reproduce $B({}^3\mathrm{H})$ and ${}^2a_{nd}$. Then we have calculated $B({}^4\mathrm{He})$. Surprisingly this last result turned out to be quite close to the experimental value. The results of the analysis are given in Table 2 where five sets of values which reproduce the mentioned quantities are reported.

From the table we observe that the values considered for $D_{2\pi}^{PW}$ and A_R are quite far from the original ones. In particular, the relative strength $D_{2\pi}^{PW}$ differs from the original value of 1/4. To extend the analysis further, the obtained set of values can be used to study $p - d$ scattering at low energy. In Fig 1 the $p - d$ analyzing power A_y at $E_{lab} = 3$ MeV is shown in correspondence to the original AV18+URIX model (solid line) and the first three sets of values given in Table 2 and indicated by (a), (b) and (c). As can be seen, the results for the models (a), (b) and (c) are very close to each other. The same is true for the last two choices of Table 2; however, corresponding results are not shown for

Table 2. Different choices for the parameters of the URIX potential and the corresponding triton and ^{4}He binding energies (in MeV) and scattering length $^2a_{nd}$ (in fm), calculated with the AV18+URIX potential.

$A_{2\pi}^{PW}$(MeV)	$D_{2\pi}^{PW}$	A_R(MeV)	$B(^3\mathrm{H})$	$B(^4\mathrm{He})$	$^2a_{nd}$
-0.0200	1.625	0.0176	8.474	28.33	0.644
-0.0250	1.25	0.0182	8.474	28.34	0.644
-0.0293	1.00	0.0181	8.474	28.33	0.643
-0.0350	0.8125	0.0191	8.474	28.33	0.645
-0.0400	0.6875	0.0198	8.474	28.38	0.645

the sake of clarity. Besides the usual underprediction of the observable given by the AV18+URIX model, we observe a substantially worse description when the new sets of constants are used. In Fig. 2 the tensor analyzing power T_{21} is shown corresponding to the same choice of parameters. The original AV18+URIX model overpredicts the minimum close to 90°. Again the curves listed (a), (b) and (c) nearly overlap and there is a substantially worse description of the observable between 40° and 120°

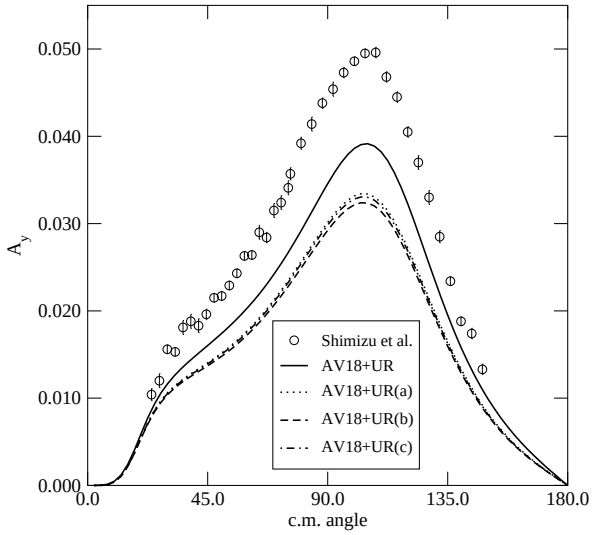

Figure 1. The $p-d$ analyzing power A_y for the models discussed in the text. Experimental data are from Ref. [10].

3 Conclusions

Stimulated by the fact that the commonly used TNF models do not reproduce simultaneously the triton and ^{4}He binding energy and the $n-d$ doublet scattering length, we have analyzed possible modifications of the AV18+URIX potential.

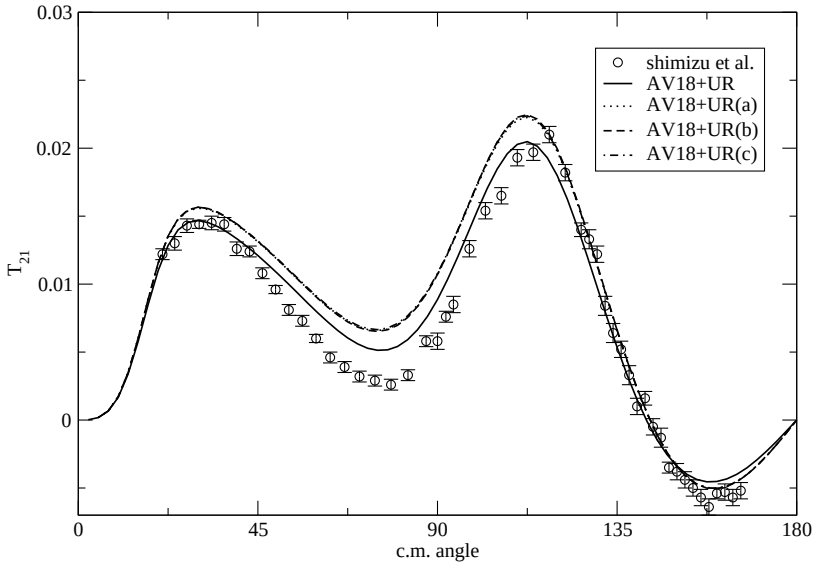

Figure 2. The $d-p$ analyzing power T_{21} for for the models discussed in the text. Experimental data are from Ref. [10].

We have varied the original parameter values of this model so as to improve the description of these quantities. Five choices of the parameters have been considered. However, the new models worsen the description of the shown $p-d$ polarization observables at low energies. Further work on this problem is in progress.

References

1. A. Kievsky, M. Viviani, and S. Rosati, Phys. Rev. C **64**, 024002 (2001)
2. S. Coon and W. Glöckle, Phys. Rev. C **23**, 1790 (1981)
3. B.S. Pudliner *et al.*, Phys. Rev. Lett. **74**, 4396 (1995)
4. E. Epelbaum *et al.*, Phys. Rev. C **66**, 064001 (2002)
5. P. Navratil, Few-Body Syst. **41**, 117 (2007)
6. A. Kievsky, S. Rosati, M. Viviani, L.E. Marcucci, and L. Girlanda, J. Phys. G: Nucl. Part. Phys. **35**, 063101 (2008)
7. A. Kievsky, Nucl. Phys. A **624**, 125 (1997)
8. M. Viviani, A. Kievsky, and S. Rosati, Phys. Rev. C **71**, 024006 (2005)
9. K. Schoen *et al.*, Phys. Rev. C **67**, 044005 (2003)
10. S. Shimizu *et al.*, Phys. Rev. C **52**, 1193 (1995)

Few-Body Systems 0, 1–4 (2009)

Few-Body Systems

Neutron-triton elastic scattering*

M. Viviani[1,**], A. Kievsky[1], L. Girlanda[2,1], L. E. Marcucci[2,1] and S. Rosati[1]

[1] INFN, Sezione di Pisa, Largo Pontecorvo, 3, 56127 Pisa (Italy)
[2] Phys. Dept., University of Pisa, Largo Pontecorvo, 3, 56127 Pisa (Italy)

Abstract. The Kohn variational principle and the hyperspherical harmonics technique are applied to study the $n-{}^3$H elastic scattering at low energies. In this contribution the first results obtained using a non-local realistic interaction derived from the chiral perturbation theory are reported. They are found to be in good agreement with those obtained solving the Faddeev-Yakubovsky equations. The calculated total and differential cross sections are compared with the available experimental data. The effect of including a three-nucleon interaction is also discussed.

1 Introduction

In the last few years the scattering of nucleons by deuterons has been the subject of a large number of investigations. This scattering problem is in fact a very useful tool for testing the accuracy of our present knowledge of the nucleon–nucleon (NN) and three nucleon (3N) interactions. Noticeable progress has been achieved, but a number of relevant disagreements between theoretical predictions and experimental results still remains to be solved [1, 2].

It is therefore of interest to extend the above mentioned analysis to four nucleon scattering processes. In this case, an important goal for both theoretical and experimental analysis is to reach a precision comparable to that achieved in the $N-d$ case. This is particularly challenging from the theoretical point of view, since the study of $A = 4$ systems is noticeably more complicated than the $A = 3$ one. Recently, accurate calculations of four-body scattering observables have been achieved in the framework of the Faddeev-Yakubovsky (FY) equations [3], solved in momentum space, and treating the long-range Coulomb interaction using the screening-renormalization method [4, 5].

In this contribution, the four-body scattering problem is solved using the Kohn variational method and expanding the internal part of the wave function

*Article based on the presentation by M. Viviani at the Fifth Workshop on Critical Stability, Erice, Sicily, Received December 12, 2008; Accepted January 5, 2009.
**E-mail address:* michele.viviani@pi.infn.it

in terms of the hyperspherical harmonic (HH) functions. Previous applications of this method [6, 7, 8] were limited so far to consider only local potentials, as the Argonne V18 [9] NN potential. Recently, for bound-states, the HH method has been extended to treat also non-local potentials, given either in coordinate- or momentum-space [10]. Here, we report the first application of the HH method to the four-body scattering problem with non-local potentials.

The potential used in this paper is the N3LO-Idaho model by Entem & Machleidt [11], with cutoff $\Lambda = 500$ MeV. This potential has been derived using an effective field theory approach and the chiral perturbation theory up to next-to-next-to-next-to-leading order. We have also performed calculations by adding to the N3LO-Idaho potential a 3N interaction, derived at next-to-next-to leading order (N2LO) in Ref. [12] (N3LO-Idaho/N2LO interaction model). The two free parameters in this N2LO 3N potential have been chosen from the combination that reproduces the $A = 3, 4$ binding energies [12]. The development of a 3N interaction including N3LO contribution is still under progress [13].

This paper is organized as follows. In Section 2, a comparison between HH and FY calculations is reported. We have performed this comparison for the N3LO-Idaho potential for incident neutron energy $E_n = 4$ MeV. Finally, in Section 3, the theoretical calculations are compared with the available experimental data.

2 Comparison between HH and FY results

The calculated phase-shift and mixing angle parameters for $n - {}^3\mathrm{H}$ elastic scattering at $E_n = 4$ MeV using the N3LO-Idaho potential are reported in Table 1. The values reported in the columns labeled HH have been obtained using the HH expansion and the Kohn variational principle, whereas those reported in the columns labeled FY by solving the FY equations [4]. As can be seen, there is a good overall agreement between the results of the two calculations.

Table 1. Phase-shift and mixing angle parameters for $n - {}^3\mathrm{H}$ elastic scattering at incident neutron energy $E_n = 4$ MeV calculated using the N3LO-Idaho potential. The values reported in the columns labeled HH have been obtained using the HH expansion and the Kohn variational principle, whereas those reported in the columns labeled FY by solving the FY equations [4].

Phase-shift	HH	FY	Phase-shift	HH	FY
${}^1S_0$	−69.3	−69.1	${}^3P_0$	23.2	23.3
${}^3S_1$	−61.4	−61.2	${}^1P_1$	22.7	22.5
${}^3D_1$	−1.14	−1.10	${}^3P_1$	44.4	44.5
ϵ	0.77	0.80	ϵ	9.80	9.64
${}^1D_2$	−1.72	−1.90	${}^3P_2$	48.4	48.7
${}^3D_2$	−0.94	−1.01	${}^3F_2$	0.07	0.09
ϵ	2.74	2.81	ϵ	1.24	1.26

3 Results

The preliminary results for the $n - {}^3\mathrm{H}$ total cross section calculated with the considered potential models are reported in Figure 1. As already known, the calculated cross section with the AV18 potential overpredicts the experimental data at low energies, and is well under the data in the peak region [8, 4]. The problem at low energies is cured when the Urbana-IX 3N force [14] is considered [8]. In the peak region the inclusion of this 3N force slightly decreases the cross section, increasing the disagreement with the data. On the other hands, using the N3LO-Idaho a better agreement with experimental data is found [4]. Including the N2LO 3N force, there is now a perfect agreement at low energy (in particular, in the minimum around $E_n = 1$ MeV). Also in the peak region a slight better agreement is observed. The origin of the remaining discrepancy is unclear, but it could be related to parts of 3N interaction not yet considered.

The quality of the agreement can be also seen by comparing the theoretical and experimental differential cross sections, avaliable at $E_n = 1$, 2, and 3.5 MeV.

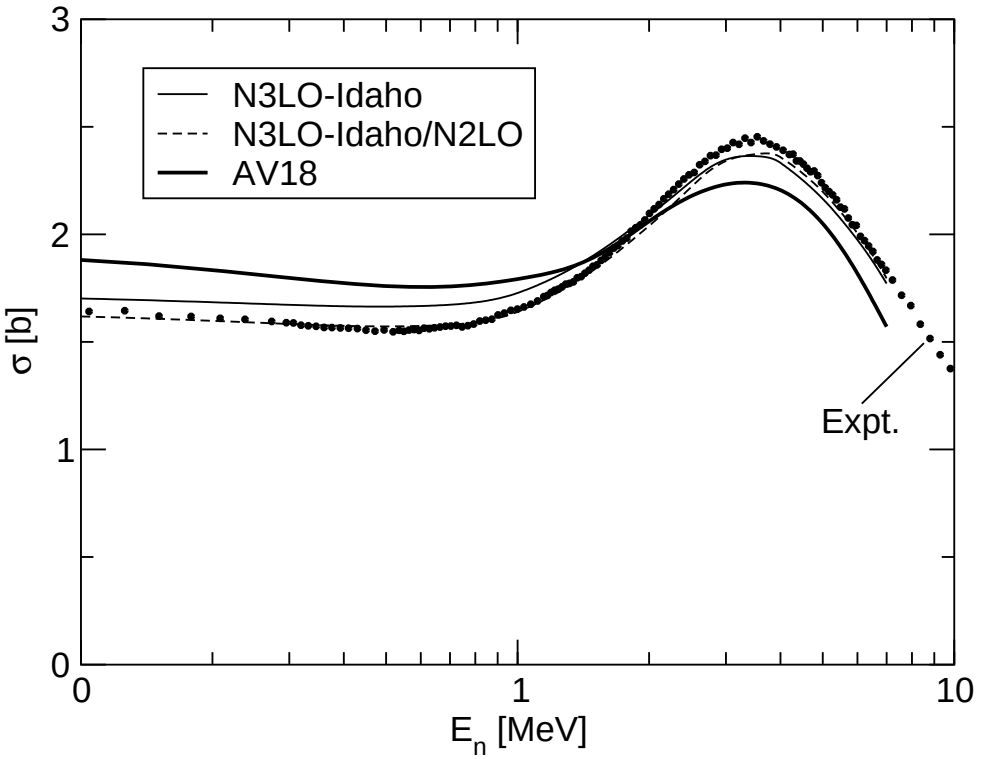

Figure 1. $n - {}^3\mathrm{H}$ total cross sections calculated with the AV18 (thick solid line), N3LO-Idaho (solid line), and the N3LO-Idaho/N2LO (dashed line) as function of the incident neutron energy E_n. The experimental data are form Ref. [15].

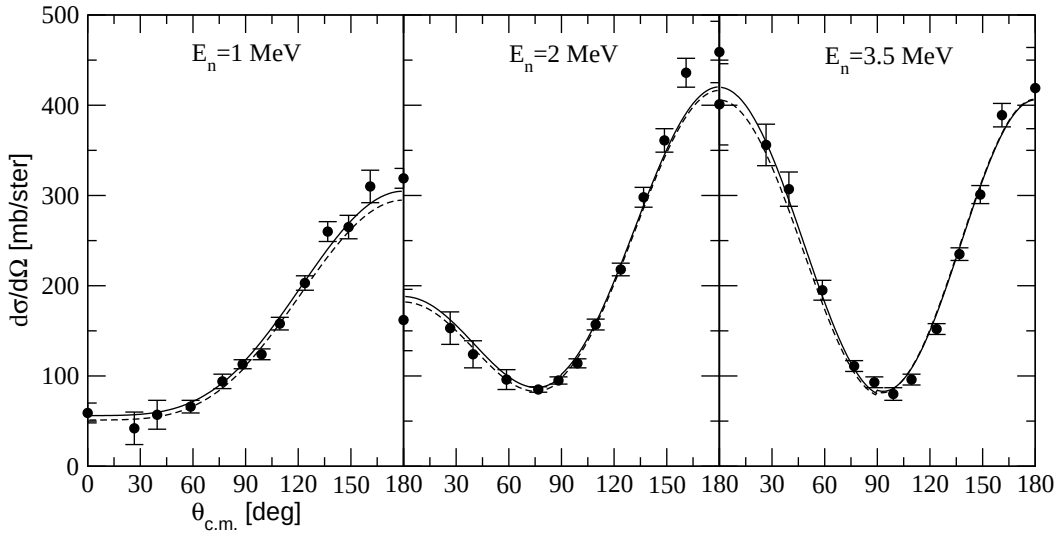

Figure 2. $n - {}^3$H differential cross sections calculated with the N3LO-Idaho (solid line) and the N3LO-Idaho/N2LO (dashed line) interaction models for three different incident neutron energies. The experimental data are from Ref. [16].

References

1. W. Glöckle *et al.*, Phys. Rep. **274**, 107 (1996)
2. A. Kievsky, S. Rosati, W. Tornow and M. Viviani, Nucl. Phys. **A607**, 402 (1996)
3. A. Deltuva and A. C. Fonseca, Phys. Rev. C **75**, 014005 (2007)
4. A. Deltuva and A. C. Fonseca, Phys. Rev. Lett. **98**, 162502 (2007)
5. A. Deltuva and A. C. Fonseca, Phys. Rev. C **76**, 021001 (2007)
6. M. Viviani, S. Rosati, and A. Kievsky, Phys. Rev. Lett. **81**, 1580 (1998)
7. M. Viviani *et al.*, Phys. Rev. Lett. **86**, 3739 (2001)
8. R. Lazauskas *et al.*, Phys. Rev. C **71**, 034004 (2005)
9. R.B. Wiringa, V.G.J. Stoks, and R. Schiavilla, Phys. Rev. C **51**, 38 (1995)
10. M.Viviani *et al.*, Few-Body Syst. **39**, 159 (2006)
11. D.R. Entem and R. Machleidt, Phys. Rev. C **68**, 041001 (2003)
12. P. Navrátil, Few-Body Syst. **41**, 117 (2007)
13. V. Bernard *et al.*, Phys. Rev. C **77**, 064004 (2008)
14. B.S. Pudliner *et al.*, Phys. Rev. C **56**, 1720 (1997)
15. T. W. Phillips, B. L. Berman, and J. D. Seagrave, Phys. Rev. C **22**, 384 (1980)
16. J. D. Seagrave, L. Cranberg, and J. E. Simmons, Phys. Rev. **119**, 1981 (1960)

Few-Body Systems 0, 1–4 (2009)

Few-Body Systems

Scattering states of three-body systems with the Hypersherical Adiabatic method*

P. Barletta[1], A. Kievsky[2]

[1] Department of Physics and Astronomy, University College London, Gower Street, WC1E6BT London, UK
[2] Istituto Nazionale di Fisica Nucleare, Piazza Torricelli 2, 56100 Pisa, Italy

Abstract. In this paper we investigate the feasibility of employing the Hyperspherical Adiabatic (HA) basis set to describe continuum states of the Helium trimer molecule.

1 Introduction

The Helium trimer molecule ($^4He_3$) has recently attracted considerable scientific interest. The peculiar features of the He-He potential, that is, its extremely shallow well associated to a very strong hard core, make the Helium dimer the largest and weakliest bound homonuclear diatomic molecule known in Nature. For the same reasons theoretical investigations of the trimer are computationally challenging, and the Helium trimer has been used in recent years also as a benchmark system for testing different numerical approaches. Most studies addressed the discrete part of the spectrum (see Ref. [1] and references therein), with a particular attention to investigating the Efimov nature of the excited state, but some have also investigated the low-energy part of the continuum [1, 2, 3].

This study represents the continuation of our previous work [4] on the application of the Hyperspherical Adiabatic (HA) method to study the continuum part of the energy spectrum for a three-body system. The HA expansion has found many applications in different fields of few-body physics, from atomic to molecular and nuclear physics. Its main advantage is the possibility to build an optimum basis set by solving a parametric Schrödinger like equation, and allowing for the original Hamiltonian problem to be solved with a two-step procedure. However, most applications were restricted to study bound states, and very few groups have applied to the continuum. Recently, Suno and Esry [1] have investigated the low energy continuum of the Helium trimer using the HA method. The main problem associated with this study is that, contrary to

*Article based on the presentation by P. Barletta at the Fifth Workshop on Critical Stability, Erice, Sicily, Received December 12, 2008; Accepted January 16, 2009.

the bound state case, for the continuum a large number of adiabatic channels is necessary to reach convergence, and the associated system of one-dimensional coupled differential equations becomes numerically more difficult to solve.

2 Method, Results and Conclusions

The set of hyperspherical coordinates $\{\rho, \Omega\}$ is defined in a standard fashion (see for instance Ref. [4] for details) for a system of three identical particles of mass m ($\hbar^2/m = 43.281307$ K a_0^2). The system wavefunction is expanded in terms of the HA basis $\{\Phi_\nu\}$:

$$\Psi = \sum_\nu u_\nu(\rho)\Phi_\nu(\rho, \Omega). \tag{1}$$

The HA basis is constructed by means of an expansion on Hyperspherical Harmonics (HH). The notorious difficulty in obtaining the HA basis at large ρ is overcome by solving numerically the asymptotic equation [5] in the asymptotic region ($\rho > 150$ a_0). The HA basis elements were then represented by using up to 900 HH in the core region and 5000 HH in the asymptotic region, including the symmetrized (over particle permutation) angular channels $(0,0)$, $(2,2)$ and $(4,4)$ (where the pair (l_x, l_y) indicate the partial angular momentum on the x and y Jacobi coordinate, see Ref. [6] for more details). The HA functions and related adiabatic potentials were then calculated on a non-uniform hyperradial grid of 927 points spanning the range $0 - 10000$ a_0.

The He_3 potential energy surface can be effectively modelled as a sum of three pairwise interactions, as three-body effects are minimal. However, due to the weakness of the He-He interaction, the determination of He-He potential has proved challenging to quantum chemists, and there are many different potentials available in the literature. In this work we have used the LM2M2 potential, and the SAPT potential.

The next step is the determination of the set of functions $\{u_\nu(\rho)\}$, and of the scattering observable of interest. As a check of the goodness of HA basis constructed, we have first performed a bound state calculation. The results are presented in Table 1. The pattern of convergence as a function of number of adiabatic channels N_A is relatively slow, possibly due to the very strong repulsive core in the He-He interaction. The results obtained are in general agreement with the literature, as it can be seen from the last rows of the table. For simplicity, not all literature results are cited in the table.

In Ref. [4] two different approaches were investigated to determine the scattering observables. In the first, indicated as "method HA1", the system wavefunction for continuum energy was supplemented by a term containing explicitly the scattering function. The second, "method HA2", is a direct solution of the hyperradial system of equations with the appropriate boundary conditions. Both approaches showed, when tested on the three nucleon system, a poor convergence pattern.Method HA2 was thus preferred in this work, as method HA1 would probably require an intractably large basis, consequence of its unitary correspondence to a HH expansion. Furthermore, we have restricted the wave-

function's expansion to the lowest adiabatic channels. The boundary conditions to be imposed to the hyperradial functions $u_\nu(\rho)$ are the following. As $\rho \to \infty$ the lowest adiabatic function $\Phi_1(\rho, \Omega) \to \rho^{3/2}\phi_d(r)$, with ϕ_d the dimer wave function [4]. Therefore, in a zero energy process, the wave function $\Psi \to \phi_d(1 - a_{1+2}/y)$, and, accordingly, the function u_1 at large ρ is

$$\rho^{5/2}u_1(\rho) \sim \rho - a_s \tag{2}$$

and all the other hyperradial functions $u_\nu(\rho) \to 0$, for $\nu > 1$. Due to the finite range of the dimer wave function, at very large values of the hyperradius we have $\rho \to \sqrt{2/3}y$, with y the relative distance between the dimer and the third particle. Therefore, a_s is related to the $1+2$ scattering length as $a_{1+2} = \sqrt{3/2}a_s$. The approximation of retaining the lowest adiabatic curves in the wave function expansion yields results very close to the converged values, as shown in Table 2. For the sake of comparison, in the table the results using different techniques are also reported. However, a full convergence for the scattering length requires a large number of HA channels, and it is difficult to achieve. Also the set of hyperradial equations becomes more difficult to be solved than for the bound state case [4]. How to obtain a satisfactory and converged solution to the set of hyperradial differential equation is still an open problem .

Table 1. Convergence of the energies of the two $^4He_3$ bound states, in mK, in terms of N_A, for two different He-He potentials. The results of the CHH method of Ref. [6] and the HA expansion of Refs. [7, 8], are reported

	LM2M2		SAPT2	
N_A	E_0	E_1	E_0	E_1
1	-112.45	-2.114	-112.45	-2.663
4	-131.37	-2.258	-131.37	-2.825
8	-125.35	-2.269	-132.77	-2.837
12	-125.83	-2.272	-133.27	-2.841
16	-126.04	-2.274	-133.49	-2.842
20	-126.15	-2.274	-133.61	-2.843
Ref. [6]	-126.4	-2.265	-135.1	-2.885
Ref. [7]	-125.2	-2.269		
Ref. [8]	-125.2	-2.26		

Table 2. Convergence of the atom-diatom scattering length, in Å, in terms of N_A for two different He-He potentials. The results of Refs. [2, 3], using the Faddeev method, are reported.

N_A	1	4	5	20	Ref. [3]	Ref. [2]
LM2M2	149.22	122.10	121.39	120.91	118.7	115.4
SAPT2	140.18	115.54	114.88	113.07	-	123.1

For example, one possibility is to employ a DVR representation for the wave-function [9]. In Fig. 1 the lowest hyperradial functions $u_1(\rho)$ are given for the excited trimer state and for the zero energy state, showing strong similarities between the two states.

In conclusion, the feasibility of the HA approach to calculate low-energy scattering observables was tested on the $^4He_3$ system, which is challenging due to the large basis set required. We have not achieved a full convergence for the He+He_2 scattering length, and further work is required in order to find a satisfactory way of solving the large system of coupled hyperradial equations, in the continuum, derived from the implementation of the HA approach.

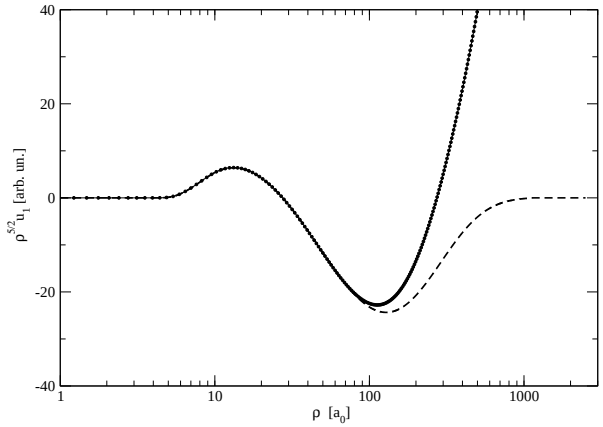

Figure 1. Hyperradial function u_1 for the excited trimer state (dashed line) and zero energy state (dots and continuum line). The excited state function has been rescaled to coincide with the the zero energy function at $\rho = 23$ a_0. The dots represent the DVR amplitudes, whereas the continuum line is the back-transformed function (see Ref. [9]).

References

1. Suno, H., Esry, B.D. : Phys. Rev. A **78** 06271 (2008).
2. Roudnev, V. :Chem. Phys. Lett. **367**, 95 (2003).
3. Kolganova, E.A., Motovilov, A.K., Sandhas, W. : Few-Body Syst. **38**, 205 (2006) .
4. Barletta, P., Kievsky, A. :Few-Body Syst., *in press* (2008).
5. Nielsen, E., et al. : Phys. Rep. **347**, 373 (2001).
6. Barletta, P., Kievsky, A. : Phys. Rev. A, **64**, 042514 (2001).
7. Nielsen, E., Fedorov D.V., Jensen, A.S. : J. Phys. B **31**, 4085 (1998).
8. Blume, D., Greene, C.H., Esry, B.D. : J. Chem. Phys., **113**, 2145 (2000).
9. Lombardi, M., Barletta, P., Kievsky, A. : Phys. Rev. A, **70**, 032503 (2004).

Few-Body Systems 0, 1–?? (2009)

Few-Body Systems

Non symmetrized basis function for identical particles*

M. Gattobigio**[1], A. Kievsky[2], M. Viviani[2], P. Barletta[3]

[1] INLN, Université de Nice-Sophia Antipolis, CNRS, 1361 route des Lucioles, 06560 Valbonne, France
[2] Istituto Nazionale di Fisica Nucleare, Largo Pontecorvo 2, 56127 Pisa, Italy
[3] Department of Physics and Astronomy, University College London, Gower Street, WC1E6BT London, UK

Abstract. We propose to use the hyperspherical harmonics (HH) basis to solve the A-body system problem without explicit symmetrization or anti-symmetrization of the basis functions as required by the statistic of the system. Therefore, the HH basis set is expressed with respect to a given ordering of the A particles. However, after diagonalization, the eigenvectors reflect the symmetries of the Hamiltonian, and it is possible to identify the physical states having the expected symmetry under particle permutation. As an example we study the case of four particles interacting through a short-range spin-dependent interaction and the Coulomb potential.

1 Introduction

A common method for solving the Schrödinger equation for few interacting particles is the variational method, and a widespread choice of basis set is represented by the HH basis. This basis allows for a simple treatment of the kinetic energy, and provides a systematic way of constructing the basis for a general number of particles (see Ref. [**?**] and references therein). The major problem, when using the HH basis, is the rapidly growing dimension of the basis as the number of particles is increased. In the case of a system formed by identical particles, it is common to use combinations of HH functions having the corresponding permutational symmetry. They represent a subset of the basis which in general has a much lower dimension than the complete basis [**?**, **?**]. The problem, however, is the increasing difficulty to carry out the symmetrization procedure as the number of particle increases [**?**].

*Article based on the presentation by M. Gattobigio at the Fifth Workshop on Critical Stability, Erice, Sicily, Received January 15, 2009; Accepted January 31, 2009.
** *E-mail address:* mario.gattobigio@inln.cnrs.fr

The HH functions do not have well defined properties under particle permutation. They depend of the particular choice of Jacobi coordinates and of the hyperangular coordinates used to define the HH functions. Changing the ordering of the particles also defines a new set of Jacobi coordinates and, thus, new HH functions.

In the present paper, we propose to use the HH basis without prior symmetrization procedure. We loose the advantage of a reduced Hilbert space; however, we gain in simplicity in the calculation of the matrix elements. By including all HH basis elements up to a certain grand angular momentum K, the diagonalization of the Hamiltonian matrix will produce eigenvectors reflecting its symmetries. Therefore, it is possible to identify the eigenvectors with the desired symmetry, and the corresponding eigenvalues are variational estimates of the energies of the physical states. The disadvantage of this method lies in the large dimension of the matrices to be diagonalized. However, different techniques are available to treat (at least partially) this problem.

Following a previous study of the $A = 3, 4$ systems interacting through a short-range potential supplemented by the Coulomb interaction [**?**], we analyze the case of a spin-dependent potential. Note that the method allows for a simple treatment of symmetry-breaking terms, such as different particle masses, or the Coulomb interaction between a particle pair.

The paper is organized as follows: in Section **??** we fix the notation introducing the Jacobi coordinates, the HH basis set, and the potential basis (PB). In Section **??** we show how to use the PB to calculate the potential energy. In Section **??** we apply our method to Volkov potential, for $A = 4$ particles, with and without the Coulomb interaction, and to a spin-dependent Volkov-like potential. In Section **??** we draw some conclusions.

2 The HH functions and the potential basis

We briefly review the main properties of the HH functions and we refer to Refs. [**?**, **?**] for the full details. From a particular ordering of the particles, we can define a set of Jacobi coordinates $\boldsymbol{x}_1, \ldots, \boldsymbol{x}_N$, and the corresponding hyperspherical coordinates, $\rho, \Omega_N = (\hat{x}_1, \ldots, \hat{x}_N, \phi_2, \ldots, \phi_N)$. The HH functions, coupled to a given angular momentum LM, are defined as

$$\mathcal{Y}^{LM}_{[K]}(\Omega_N) = \left[Y_{l_1}(\hat{x}_1) \otimes \ldots \otimes Y_{l_N}(\hat{x}_N) \right]_{LM} \left[\prod_{j=2}^{N} {}^{(j)}\mathcal{P}^{l_j, K_{j-1}}_{K_j}(\phi_j) \right] , \qquad (1)$$

with $[K]$ the set of quantum numbers $L, M, l_1, \ldots, l_{N-1}, n_2, \ldots, n_N$ plus $N-2$ intermediate l-values, and the K_j defined as $K_j = \sum_{i=1}^{j} (l_i + 2n_i)\,, l_N = L\,, n_1 = 0\,, K \equiv K_N$. ${}^{(j)}\mathcal{P}^{l_j, K_{j-1}}_{K_j}(\phi_j)$ is an hyperspherical polynomial. With the above definition, the HH functions are eigenvectors of the grand angular operator $\Lambda^2_N(\Omega_N)$, $[\Lambda^2_N(\Omega_N) + K(K+3N-2)]\mathcal{Y}_{[K]}(\Omega_N) = 0$, with K the grand angular momentum quantum number.

The PB elements $\mathcal{P}^{l,m}_{2n+l}(\Omega_{12})$ form a subset of the HH basis, namely the one which satisfies $\Lambda^2_{N-1}(\Omega_{N-1})\mathcal{P}^{l,m}_{2n+l}(\Omega_{12}) = 0$, where the Jacobi variables are

$\boldsymbol{x}_1, \ldots, \boldsymbol{x}_N = \boldsymbol{r}_2 - \boldsymbol{r}_1$, and the hyperspherical variables are split into $\Omega_N = (\Omega_{N-1}, \hat{x}_N, \phi_N)$, with $\Omega_{12} \equiv (\hat{x}_N, \phi_N)$, and $(n, l, m) \equiv (n_N, L, M)$. One can similarly define the PB depending on a generic pair (i, j) as $\mathcal{P}^{l,m}_{2n+l}(\Omega_{ij})$, and a very useful property is that we can express it as a combination of HH functions defined in the reference set with the same grand angular momentum

$$\mathcal{P}^{l,m}_{2n+l}(\Omega_{ij}) = \sum_{[K'=2n+l]} {}^{(N)}C^{n,l}_{[K']}(\varphi^{ij})\, \mathcal{Y}^{lm}_{[K']}(\Omega_N)\,, \tag{2}$$

where the coefficients ${}^{(N)}C^{n,l}_{[K']}(\varphi^{ij})$ are known for each value of K and A. The PB can be used to expand a generic function depending on the pair (i, j). In particular the two-particle potential, can be expanded in the PB as

$$V(\mathbf{r}_i - \mathbf{r}_j) = \sum_{nlm} V_{nlm}(\rho) \mathcal{P}^{l,m}_{2n+l}(\Omega_{ij})\,, \tag{3}$$

where the $V_{nlm}(\rho)$ are the hyperradial multipoles.

3 The potential energy in term of HH functions

Once we have introduced the PB and its properties, we can use it to express the full potential on HH functions. Let us consider, for concreteness, a spin-dependent potential of the form

$$V(i, j) = V^W(r_{ij}) + V^\sigma(r_{ij})\, \boldsymbol{\sigma}_i \cdot \boldsymbol{\sigma}_j\,. \tag{4}$$

Using Eq. (**??**) to expand the central parts of the potential on PB basis, and Eq. (**??**) to rotate the PB on the reference permutation, we obtain ($n = K/2$)

$$V(i, j) = \sum_{[K]} \left(V^W_n(\rho) + V^\sigma_n(\rho)\, \boldsymbol{\sigma}_i \cdot \boldsymbol{\sigma}_j \right) {}^{(N)}C^{n}_{[K]}(\varphi^{ij}) \left[\mathcal{Y}_{[K]}(\Omega_N) \right]_{L=0}\,, \tag{5}$$

where, due to the central nature of the potential, $l = 0$, $m = 0$, and they have been omitted in the notation. The spherical harmonics of the HH's have been coupled to give total zero angular momentum. The total potential is the sum over the pairs, and we obtain

$$V = \sum_{i<j} V(i, j) = \sum_n \left(V^W_n(\rho) \otimes \mathcal{G}_n(\Omega) \otimes \mathbb{I}_\sigma + V^\sigma_n(\rho) \otimes \sum_{i<j} \mathcal{G}^{ij}_n(\Omega) \otimes (\boldsymbol{\sigma}_i \cdot \boldsymbol{\sigma}_j) \right), \tag{6}$$

where we have defined the matrices

$$\mathcal{G}_n(\Omega) = \sum_{[K=2n]} \sum_{i<j} {}^{(N)}C^{n}_{[K]}(\varphi^{ij}) \left[\mathcal{Y}_{[K]}(\Omega_N) \right]_{L=0}\,, \tag{7}$$

and

$$\mathcal{G}^{ij}_n(\Omega) = \sum_{[K=2n]} {}^{(N)}C^{n}_{[K]}(\varphi^{ij}) \left[\mathcal{Y}_{[K]}(\Omega_N) \right]_{L=0}\,. \tag{8}$$

We have written the expressions as an explicit tensor-product form. This simplifies the matrix-vector product used to diagonalize the matrix by iterative methods.

4 Application to $A = 4$

To solve the four-body problem we introduce the following basis set

$$\langle \rho\, \Omega |\, m\, [K]\, \sigma \rangle = \left(\beta^{(\alpha+1)/2} \sqrt{\frac{m!}{(\alpha+m)!}}\, L_m^{(\alpha)}(\beta\rho)\, \mathrm{e}^{-\beta\rho/2} \right) \mathcal{Y}_{[K]}^{LM}(\Omega)\, |\sigma\rangle\,, \qquad (9)$$

where $L_m^{(\alpha)}(\beta\rho)$ is a Laguerre polynomial with $\alpha = 8$ and β a variational non-linear parameter, and $|\sigma\rangle = |s_1 s_2 (s_{12}) s_3 s_4 (s_{34}); s^{\rm tot} s_z^{\rm tot}\rangle$ is the total spin state, obtained by coupling the four spins $s_i = 1/2$. The kinetic-energy matrix is easily calculated within this basis set

$$\langle\, m'\, [K']\, \sigma' | T |\, m\, [K]\, \sigma \rangle = -\frac{\hbar^2\beta^2}{m} (T^{(1)}_{m'm} - K(K+3N-2) T^{(2)}_{m'm}) \delta_{[K'][K]} \delta_{\sigma'\sigma}\,, \quad (10)$$

with

$$T^{(1)}_{m'm} = \frac{1}{4}\delta_{m,m'} + \sqrt{\frac{m'!}{(\alpha+m')!}} \sqrt{\frac{m!}{(\alpha+m)!}} \int_0^\infty x^\alpha\, \mathrm{e}^{-x} dx\, L_{m'}^{(\alpha)}(x) \times \left[\left(-\frac{\alpha+2m}{2x} - \frac{m}{x^2} \right) L_m^{(\alpha)}(x) + \frac{m+\alpha}{x^2} L_{m-1}^{(\alpha)}(x)(1-\delta_{m,0}) \right], \quad (11)$$

and

$$T^{(2)}_{m'm} = \sqrt{\frac{m'!}{(\alpha+m')!}} \sqrt{\frac{m!}{(\alpha+m)!}} \int_0^\infty x^\alpha\, \mathrm{e}^{-x} dx\, L_{m'}^{(\alpha)}(x) \left(\frac{1}{x^2} \right) L_m^{(\alpha)}(x)\,, \qquad (12)$$

and the kinetic energy matrix displays a tensor-product form too.

In the following we fix the value of the nucleon mass such that $\hbar^2/m = 41.47$ Mev fm^{-2} and we introduce two different potentials: (i) the spin-independent Volkov potential ($V^\sigma(r) = 0$); (ii) a modified version of the Volkov potential including a spin-dependent term.

In the first case we have

$$V^W(r) = E_1\, \mathrm{e}^{-r^2/R_1^2} + E_2\, \mathrm{e}^{-r^2/R_2^2}, \qquad (13)$$

with $E_1 = 144.86$ MeV, $R_1 = 0.82$ fm, $E_2 = -83.34$ MeV, and $R_2 = 1.6$ fm. The results are given in Table **??**. The convergence of the ground-state energy E_0 is shown as a function of the grand angular momentum K. The non-linear parameter has been fixed $\beta = 2$, and the quantum number $m = 25$ is such that the convergence has been reached with respect to this quantum number for each value of K. For the sake of comparison, we also report the ground state energy obtained using the stochastic variational method (SVM) [**?**], the shell model with HH basis (SMHH) [**?**], and the symmetrized HH basis [**?**]. On the same table, we calculate the ground state energy E_0^C in presence of a Coulomb potential between two nucleons, with $e^2 = 1.44$ MeV fm. As the basis set is not symmetrized, it can be used when adding a potential term between particles $(1, 2)$

$$V^C(r_{12}) = \frac{e^2}{r_{12}} = \frac{e^2}{\rho \cos\phi_3}\,. \qquad (14)$$

Table 1. The ground-state energy E_0, with Volkov potential, as a function of $K_{\max}$, using 25 Laguerre polynomials, and $\beta = 2\,\mathrm{fm}^{-1}$. We also give the dimension N_H of the HH basis, and the ground-state energy E_0^C in the presence of an additional Coulomb interaction.

$K_{\max}$	N_{HH}	E_0 (MeV)	E_0^C (MeV)
0	1	28.580	27.748
2	6	28.580	27.750
4	21	29.283	28.455
6	56	29.812	28.986
8	126	30.162	29.338
10	252	30.278	29.456
12	462	30.365	29.544
14	792	30.392	29.572
16	1287	30.407	29.587
18	2002	30.413	29.593
20	3003	30.416	29.596
22	4368	30.417	29.597
SVM[**?**]		30.42	
SM[**?**]		29.532	
HH[**?**]		30.406	

Note that, with this kind of potential, a symmetric basis set should involve states with isospin $T = 0, 1, 2$; hence a symmetrized basis would be enlarged by the presence of a symmetry-breaking term.

As a second example, we consider a spin-dependent potential. We use a Volkov-like potential defined for singlet and triplet spin channels, $S = 0, 1$, namely

$$V_{(S)} = E_{(S),1}\,\mathrm{e}^{-r^2/R^2_{(S),1}} + E_{(S),2}\,\mathrm{e}^{-r^2/R^2_{(S),2}}\,, \tag{15}$$

with $E_{(0),1} = 144.86$ MeV, $R_{(0),1} = 0.82$ fm, $E_{(0),2} = -66.7$ MeV, and $R_{(0),2} = 1.6$ fm, and $E_{(1),1} = 144.86$ MeV, $R_{(1),1} = 0.82$ fm, $E_{(1),2} = -97.0$ MeV, and $R_{(1),2} = 1.6$ fm. In terms of the potential defined in Eq. (**??**) we have $V_W = V_{(0)}/4 + 3V_{(1)}/4$, and $V_\sigma = -V_{(0)}/4 + V_{(1)}/4$.

Using this potential, a bound state appears for total spin $s^{\mathrm{tot}} = 0$; in this case the spin-space has dimension two, and the two states $|\sigma\rangle$ are $|0\rangle \equiv |\frac{1}{2}\frac{1}{2}(0)\frac{1}{2}\frac{1}{2}(0); 00\rangle$ and $|1\rangle \equiv |\frac{1}{2}\frac{1}{2}(1)\frac{1}{2}\frac{1}{2}(1); 00\rangle$. The values of the Pauli matrix-scalar product are the following

$$\begin{aligned}
\langle\sigma'|\boldsymbol{\sigma}_1\cdot\boldsymbol{\sigma}_2|\sigma\rangle &= \langle\sigma'|\boldsymbol{\sigma}_3\cdot\boldsymbol{\sigma}_4|\sigma\rangle = \begin{pmatrix} -3 & 0 \\ 0 & 1 \end{pmatrix} \\
\langle\sigma'|\boldsymbol{\sigma}_1\cdot\boldsymbol{\sigma}_3|\sigma\rangle &= \langle\sigma'|\boldsymbol{\sigma}_2\cdot\boldsymbol{\sigma}_4|\sigma\rangle = \begin{pmatrix} 0 & -\sqrt{3} \\ -\sqrt{3} & -2 \end{pmatrix} \\
\langle\sigma'|\boldsymbol{\sigma}_1\cdot\boldsymbol{\sigma}_4|\sigma\rangle &= \langle\sigma'|\boldsymbol{\sigma}_2\cdot\boldsymbol{\sigma}_3|\sigma\rangle = \begin{pmatrix} 0 & \sqrt{3} \\ \sqrt{3} & -2 \end{pmatrix}.
\end{aligned} \tag{16}$$

In Table **??** we showt the results obtained with this potential for the ground-state energy, E_0, and for the first excition, E_1.

Table 2. The ground-state energy E_0, with spin-dependent Volkov potential, as a function of $K_{\max}$, using 25 Laguerre polynomials, and $\beta = 2\,\mathrm{fm}^{-1}$. We also give the energy of the first excited state E_1.

$K_{\max}$	E_0 (MeV)	E_1 (MeV)
0	26.319	2.566
2	26.964	2.881
4	27.793	5.115
6	28.302	6.330
8	28.650	6.982
10	28.768	7.363
12	28.858	7.617
14	28.888	7.782
16	28.904	7.910
18	28.911	8.008
20	28.915	8.088

5 Conclusions

In this paper we propose to solve the A-body system using the hyperspherical harmonics functions without a preliminary symmetry-adaptation of the basis set. We have shown the feasibility of this procedure in the case of four particle interacting through a spin dependent short-range potential. We have also considered a purely central interaction including the Coulomb potential between a pair. Skiping the explicit symmetrization of the basis, we have gained in simplicity when the matrix elements of the potential are to be calculated, and without increasing the dimension of the basis, we have considered potential terms which break the permutational symmetry. This is of fundamental importance if we want to consider a system of protons and neutrons in which the Coulomb interaction between protons has to be included as well as their mass difference. The main difficulty in the present method is the treatment of very large matrices. We have shown that the Hamiltonian matrix can be written as a tensor product and this particular form can be diagonalized very efficiently [**?**].

References

1. Fabre de la Ripelle M (1983) Ann. Phys.(NY) 147:281
2. Novoselsky A, and Katriel J (1994) Phys. Rev A 49:833
3. Barnea N (1999) Phys. Rev. A 59:1135
4. Viviani M, Kievsky A, Rosati S (2005) Phys. Rev. C 71:024006
5. Gattobigio M, Kievsky A, Viviani M, Barletta P (2008) [arXiv:0811.4259 physics]
6. Varga K, Suzuki Y (1995) Phys. Rev. C 52:2885
7. Timofeyuk N K (2002) Phys. Rev. C 65:064306

Few-Body Systems 0, 1–4 (2009)

Few-Body Systems

Few-Body Reactions in Nuclear Astrophysics*

E. Garrido[1]**, R. de Diego[1], C. Romero-Redondo[1], D.V. Fedorov[2], A.S. Jensen[2]

[1] Instituto de Estructura de la Materia, CSIC, Serrano 123, E-28006 Madrid, Spain
[2] Department of Physics and Astronomy, University of Aarhus, DK-8000 Aarhus C, Denmark

Abstract. Nuclear reactions involving light nuclei require few-body models to describe the nuclear structure and the reaction mechanism. The production rates for the $\alpha + n + n \to {}^6\mathrm{He} + \gamma$ and $\alpha + n + n + n \to {}^6\mathrm{He} + n$ processes are discussed. Typically only very low relative energies are relevant. For environments with a high density, processes involving more particles could dominate. The use of the adiabatic approach as a method to compute cross sections at very low energies is proposed.

1 Introduction

When talking about reactions of astrophysical interest we refer to all those nuclear processes playing a role in the nucleosynthesis of the elements in the stars. In particular, in this work we shall concentrate on those reactions involving light nuclei, for which few-body models are needed at two different levels, to describe the structure of the nuclei and also to describe the reaction mechanism.

The basic goal when investigating these reactions is to estimate their production rate, which gives the velocity (number of reactions per unit time and unit volume) at which the products of the reaction are created.

2 Production Rates

The production rate for a reaction involving N particles in the initial state is obtained as $P^T = \int dE B(E,T) P(E)$, where $P(E)$ is the production rate at a given kinetic energy E in the N-body center of mass, and $B(E,T)$ is the Maxwell-Boltzmann distribution giving the probability for finding the N particles with

*Article based on the presentation by I. Mazumdar at the Fifth Workshop on Critical Stability, Erice, Sicily, Received November 17, 2009; Accepted January 19, 2009.
** *E-mail address:* e.garrido@iem.cfmac.csic.es

that precise relative kinetic energy [1]. This distribution takes the form:

$$B(E,T) = \frac{1}{\Gamma(\frac{3N-3}{2})} \frac{1}{K_B T} \left(\frac{E}{K_B T}\right)^{\frac{3N-5}{2}} e^{-\frac{E}{K_B T}}, \tag{1}$$

where K_B is the Boltzmann constant and T is the temperature of the star.

The exponential in the previous expression implies that for a given temperature T, the only relevant energies correspond to $E \lesssim K_B T$. Typical temperatures in the stars (i.e., in the core of the sun) are of the order of 10^7 K, which leads to $K_B T \approx 0.001$ MeV. Therefore, in the stellar medium only very low relative kinetic energies are relevant.

The total production rate at a given energy ($P(E)$) is the product of the so called *reaction rate* and the densities n_i of the N nuclei ($i = 1, \cdots, N$) involved in the initial state. These densities are usually written as $n_i = \rho N_A \frac{X_i}{A_i}$, where N_A is the Avogrado number, A_i and X_i are the mass number and mass abundance of the nucleus i, and ρ is the density of the star [1]. The density is, together with the temperature, the crucial property of the star determining the production rate. In fact, $P(E)$ is proportional to ρ^N, meaning that, for a sufficiently large ρ, processes involving more particles could play a role.

Finally, the reaction rate ($R(E)$) is given by the Fermi's golden rule integrated over all the possible momenta for the final products of the reaction. Assuming M particles in the final state, $R(E)$ is written as:

$$R(E) = \int \frac{2\pi}{\hbar} \left|\langle \Psi_i(E)|W|\Psi_f(E_f)\rangle\right|^2 \delta(E - E_f) \frac{d^3 p_1}{(2\pi)^3} \cdots \frac{d^3 p_M}{(2\pi)^3}, \tag{2}$$

where Ψ_i and Ψ_f are the initial and final wave functions, $\boldsymbol{p}_1, \cdots, \boldsymbol{p}_M$ are the momenta of the final nuclei, and W represents the interaction. When only two particles are involved in the initial state, the reaction rate is the cross section of the process times the relative velocity between the two particles.

Obviously, the matrix element contained in the integrand of Eq. (2) is the same for a given reaction and for the inverse process. It is then possible to relate the reaction rates (and therefore the production rates) corresponding to both processes. This means that the production rate for a reaction leading to two particles in the final state can be written in terms of the cross section of the inverse process. This is what happens in the two reactions briefly discussed in the following subsections.

2.1 Two-Neutron Radiative Capture: The $\alpha + n + n \rightarrow {}^6He + \gamma$ Process

This a pure electromagnetic process where only the bound ^{6}He nucleus and a photon are found in the final state. Following the discussion above, the corresponding production rate can be written in terms of the photo-dissociation cross section (σ_γ) of ^{6}He. To be precise, this production rate takes the form:

$$P_{\alpha,2n}(\rho,T) = n_\alpha n_n^2 \frac{\hbar^3}{c^2} \left(\frac{m_\alpha + 2m_n}{m_\alpha m_n^2}\right)^{\frac{3}{2}} \frac{2\pi}{(K_B T)^3} e^{-\frac{Q}{K_B T}} \int_{|Q|}^{\infty} E^2 \sigma_\gamma(E) e^{-\frac{E}{K_B T}} dE \tag{3}$$

where $Q = m_{^6\mathrm{He}} - m_\alpha - 2m_n$, and $m_{^6\mathrm{He}}$, m_α, and m_n are the masses of ^{6}He, the α particle, and the neutron, respectively.

The cross section $\sigma_\gamma(E)$ is usually expanded in terms of electric and magnetic multipoles, each of them given by a well known expression in terms of the strength function of the reaction [2].

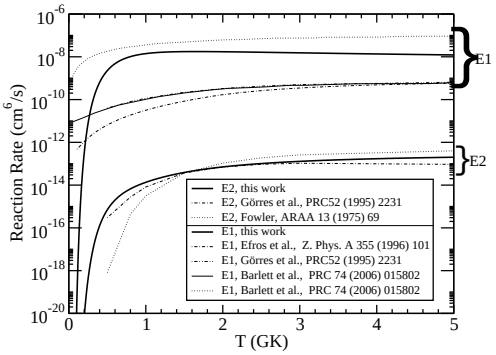

Figure 1. Dipole and quadrupole reaction rates for the $\alpha + n + n \rightarrow^6$ He $+ \gamma$ process. (*ARAA: Ann. Rev. Astron. Astrophys.*)

In the figure, the thick solid lines are the computed electric dipole and quadrupole reaction rates when the corresponding strength functions are obtained as described in [3]. This procedure includes all the possible capture mechanisms: Resonant, sequential, and direct. As seen in the figure, the quadrupole result agrees with previous estimates by Görres (dot-dashed) and Fowler (dotted). For the dipole contribution our reaction rate is about one order of magnitude higher than Görres, Efros and Barlett. The reason is that in these calculations a fully sequential capture process is assumed. In fact, in the work by Barlett et al. they also estimated the dipole reaction rate including the contribution from dineutron capture. This estimate (dotted line) is above our calculation.

2.2 Four-Body Recombination: The $\alpha + n + n + n \rightarrow {}^6He + n$ Process

In this process one neutron takes the excess of energy released when the remaining particles combine into a bound state. Again, only two particles are found in the final state, and the production rate takes the following form in terms of the cross section $\sigma_n(E)$ for the inverse process (neutron breakup of ^{6}He):

$$P_{\alpha,3n}(\rho,T) = n_\alpha n_n^3 \mu_{n^6\mathrm{He}} \left(\frac{m_\alpha + 3m_n}{m_\alpha m_n^3}\right)^{\frac{3}{2}} \frac{\hbar^6 (2\pi)^{\frac{5}{2}}}{(K_B T)^{\frac{9}{2}}} e^{-\frac{Q}{K_B T}} \int_{|Q|}^{\infty} E\sigma_n(E) e^{-\frac{E}{K_B T}} dE. \quad (4)$$

Calculation of $\sigma_n(E)$ requires the proper description of the four-body inital and final states. The initial state is described as a bound three-body system (^{6}He) plus a free neutron, and $\sigma_n(E)$ is estimated assuming that the transition amplitude can be written as the sum of the three amplitudes corresponding to the interaction between the incident neutron and each of the three constituents in ^{6}He. Each of them factorizes into a term depending on the initial (bound) and final (continuum) three-body structure of ^{6}He, and a second term giving the two-body transition amplitude for the scattering of the incident neutron and the corresponding constituent [4].

For a mass density of ρ =150 g/cm^3 (like in the core of the sun) and a temperature of 15 GK the four-body recombination production rate is about four orders of magnitude smaller than for the electromagnetic two-neutron capture. However, since this production rate goes like ρ^4, while for the electromagnetic

capture it goes like ρ^3, the four-body recombination mechanism could dominate in an environment with a sufficiently large density ($\rho > 1.5 \cdot 10^6$ g/cm^3).

However, for very low temperatures the approximation described above is very likely failing, and a proper calculation of $\sigma_n(E)$ is required.

3 The Adiabatic Approach and Nuclear Reactions at Low Energies

Given a particle hitting an N-body system, the adiabatic approach appears as an efficient method to compute the corresponding cross section at very low energies. The adiabatic expansion of the $(N+1)$-body wave function permits to solve the angular part of the equations for individual (frozen) values of the radial coordinate. As a second step, one has to deal with a coupled set of radial equations where a series of effective adiabatic potentials enters [5].

It can be proved that at large distances the eigenfunctions associated to each of the adiabatic potentials correspond to very specific structures. A reduced number of potentials are associated to the different possible asymptotics corresponding to one (or more) bound subsystems and the remaining particle(s) in the continuum. They are all the possible outgoing channels corresponding to elastic, inelastic or rearrangement scattering. The incoming channel (N-body bound target plus one particle in the continuum) is typically described by a single adiabatic potential. Therefore, in this approximation a limited and small number of S-matrix elements are enough to describe the scattering process.

However, for a breakup process leading to $N+1$ particles in the continuum, the asymptotics is described by infinitely many adiabatic potentials. One of the open questions is to establish how many of these potentials are needed to obtain a converged breakup cross section.

4 Summary and Conclusions

Temperature and density are two crucial star properties which determine the production rate of a given reaction. Typical temperatures are such that only very low relative energies are relevant. A proper description of the radiative capture processes requires inclusion of all the possible capture mechanisms. Usually those processes involving less particles dominate over the competing reactions with more particles involved. However, if the star density is large enough the latter could be relevant. Finally, we propose the adiabatic approximation as a very useful method in order to compute cross sections at very low energies.

References

1. Fowler, W. A., et al.: Annu. Rev. Astron. Astrophys. **5**, 525 (1967)
2. Forssén C., Shul'gina, N. B., Zhukov, M.V.: Phys. Rev. **C67**, 045801 (2003)
3. de Diego, R., et al.: Phys. Rev. **C77**, 024001 (2008)
4. Garrido, E., Fedorov D. V., Jensen, A. S.: Nucl. Phys. **A695**, 109 (2001)
5. Nielsen, E., et al.: Phys. Rep. **347**, 373 (2001)

Few-Body Systems 0, 1–4 (2009)

Few-Body Systems

Light nuclei in the continuum*

F.M. Marqués**

Laboratoire de Physique Corpusculaire,
IN2P3-CNRS, ENSICAEN et Université de Caen, F-14050 Caen cedex, France

Abstract. The development of light, neutron-rich beams has opened in the last decade new perspectives for the study of many-neutron systems. Breakup experiments at GANIL are described, using beams of ^{6,8}He, ^{11}Li, ^{14}Be and ^{15}B at several tens of MeV/N. Our approach is based on the detection in coincidence of the breakup fragment and the neutrons in order to investigate the different correlations in the final state of these very neutron-rich systems. Several particular cases are discussed: fragment-n correlations in unbound ^{7}He, ^{10}Li and ^{9}He; 2n correlations in ^{6}He, ^{11}Li and ^{14}Be; and three-body and 4n correlations in ^{8}He and ^{14}Be.

1 Introduction

The very neutron-rich, light nuclei provide a fertile testing ground for our understanding of nuclear structure. From an experimental point of view this region is the only one for which nuclei lying at and beyond the neutron dripline may be accessed. Theoretically a wide range of models, including various shell model approaches (e.g., the shell model in the continuum, the no-core shell model) and more *ab initio* type models are capable of providing predictions. In addition, the structure of some unbound systems, such as ^{10}Li, is key to constructing three-body descriptions of two-neutron halo nuclei, such as ^{11}Li.

One of the best adapted tools to the study of nuclei far from stability is that of "knockout" or breakup of a high-energy radioactive beam. The high cross-section of these reactions make up for the low intensity of these very exotic beams. Our group has been studying these systems at GANIL for the last decade, with very neutron-rich beams accelerated at several tens of MeV/N. The fragments following breakup are detected in coincidence with the multidetector arrays CHARISSA (charged fragments) and DEMON (neutrons). Some examples are described in the following.

*Article based on the presentation by F.M. Marqués at the Fifth Workshop on Critical Stability, Erice, Sicily, Received December 30, 2008; Accepted January 8, 2009.

** *E-mail address:* marques@lpccaen.in2p3.fr

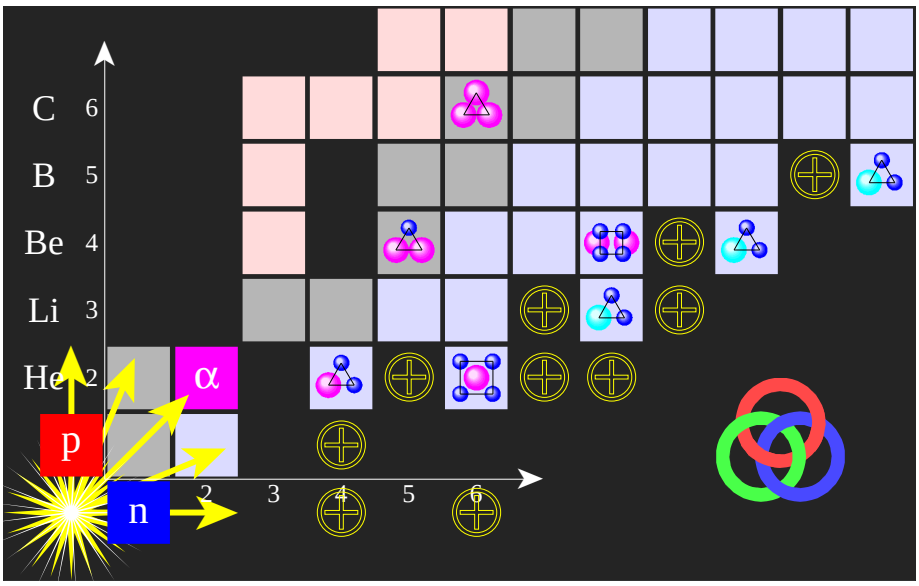

Figure 1. Zoom on the lighter part of the nuclear chart. The crosses correspond to unbound nuclei studied at GANIL by our group.

2 Two-body, unbound systems

The unbound nuclei ^{7,9}He and ^{10}Li have been investigated via the high-energy breakup of ^{8}He, ^{11}Be and ^{14}B. The decay-energy spectra were reconstructed from coincident measurements of the charged fragments (^{6,8}He and ^{9}Li) with Si-CsI telescopes from CHARISSA and the neutrons with the DEMON array. A theoretical approach based on the sudden approximation was used to model the reactions populating the unbound final states. The calculated decay-energy spectra were convoluted with the response function of the experimental setup using a simulation developed specifically for the present study and compared with the experimental results [1].

The ^{7}He system was investigated with the three different beams. No evidence for the existence of the proposed low-lying ($E_r > 1$ MeV) spin-orbit partner ($1/2^-$) of the ground state ($3/2^-$) could be found.

The ^{10}Li system was produced using an ^{11}Be beam and the results confirm the continuation of the inversion of the $1/2^+$ and $1/2^-$ levels in the $N = 7$ isotopic chain (Fig. 2). The virtual s state is found to be the ground state with a scattering length of $a_s = -14 \pm 2$ fm. The production of ^{10}Li using the ^{14}B beam exhibits, in addition, a low-lying p excited state at about 500 keV.

The ^{9}He system was similarly produced using both ^{11}Be and ^{14}B beams, and was the most exotic system studied. A structure was observed at very low decay energy which very probably corresponds to a virtual s state ($a_s > -3$ fm). This result suggests that the level inversion also occurs in ^{9}He, but with a much weaker core-neutron interaction than for ^{10}Li. For the data acquired from the breakup of the ^{14}B beam, the decay energy spectrum exhibits a resonance

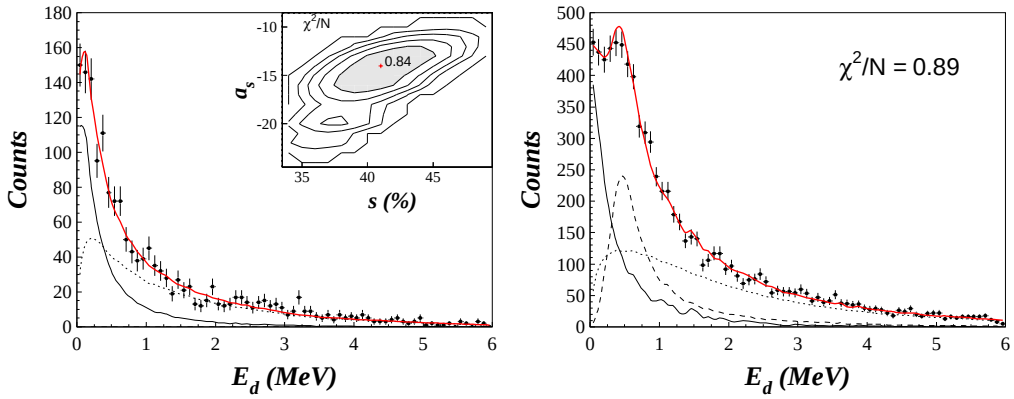

Figure 2. Decay energy of the ^{10}Li system from the breakup of ^{11}Be (left) and ^{14}B (right) [1]. The red line is the non-resonant background obtained by event mixing (dotted line) plus a virtual s state at an energy corresponding to a scattering length of -14 fm (solid line) plus, on the right, a p wave at 500 keV (dashed line).

around $E_r = 1.2$ MeV, which most probably corresponds to an excited $1/2^-$ state in ^{9}He.

3 Three- and Four-body systems

The unbound systems described above were formed by knocking out some nucleons from a heavier, exotic beam. More complex systems, like the two-neutron haloes ^{6}He, ^{11}Li and ^{14}Be (core+2n), or the four valence neutrons inside ^{8}He and ^{14}Be (α+4n and ^{10}Be+4n), can be studied with the same techniques through the excitation of these systems leading to breakup.

Concerning the former, the breakup of ^{6}He, ^{11}Li and ^{14}Be into their core plus the two valence neutrons was studied using the technique of intensity interferometry, and the rms distances between the two neutrons at breakup were measured [2]. These distances were about 5-7 fm, relatively large. A more sophisticated analysis on the breakup of ^{8}He into ^{6}He+2n [3] lead to the measurement of both the relative distance and the relative time between the neutrons in the sequential channel (formation of an unbound ^{7}He resonance). The delay was found to be consistent with the lifetime of ^{7}He.

The 4n system was studied in the breakup of ^{14}Be [4] and ^{8}He [5]. Few events were found to be consistent with the correlated decay of the four neutrons, either as a bound or a low-lying resonant state [6]. The breakup of a higher intensity beam of ^{15}B was studied in 2006 at GANIL using the same techniques. The idea is to knock out one proton from the beam and form an excited ^{14}Be that will decay in flight, either to ^{12}Be+2n or ^{10}Be+4n. Many events with a ^{10}Be in coincidence with the neutron detectors were recorded, and the analysis is in progress [7].

4 Conclusion and perspectives

The recent study of very exotic unbound systems has lead to new results: absence of low-lying excited state in ^{7}He independently of the entrance channel, precission measurement of the ^{9}Li+n scattering length, and s/p level inversion in the $N = 7$ isotopic chain up to ^{9}He. The breakup of two-neutron halo systems has been "mapped" in both space and time using the technique of intensity interferometry. And the most neutron rich isotopes of He and Be have been excited in order to liberate their four valence neutrons, leading to events consistent with the formation of a correlated tetraneutron. All these axes are being studied in depth following the breakup of a high intensity ^{15}B beam, which lead to many fragment+n, core+2n and core+4n exit channels [7].

References

1. H. Al Falou, PhD Thesis, Université de Caen (2007).

2. F.M. Marqués *et al.*, Phys. Rev. C **64**, 061301 (2001).

3. B. Laurent, PhD Thesis, Université de Caen (2007).

4. F.M. Marqués *et al.*, Phys. Rev. C **65**, 044006 (2002).

5. V. Bouchat, PhD Thesis, Université Libre de Bruxelles (2005).

6. F.M. Marqués *et al.*, arXiv:nucl-ex/0504009v1.

7. A. Leprince, PhD Thesis, Université de Caen, in preparation.

Few-Body Systems 0, 1–4 (2009)

Few-Body Systems

Efimov Effect in 2-Neutron Halo Nuclei*

Indranil Mazumdar

Department of Nuclear & Atomic Physics, Tata Institute of Fundamental Research, Mumbai 400 005, India

Abstract. We provide a brief overview of our theoretical investigations, carried out in recent years, to study Efimov effect in 2-n halo nuclei. The calculations provide the evidence for the occurrence of at least two Efimov states in ^{20}C. These states disappear one by one as the two-body binding energy is increased and show up as asymmetric resonances in the elastic scattering cross section of n-^{19}C system. The asymmetric nature of the resonances is explained by invoking the mechanism of Fano resonance.

1 Introduction

The remarkable advancements in the production of Radioactive Ion Beams and detection facilities have opened up new vistas in contemporary nuclear physics. It is now possible to produce exotic light nuclei close to the neutron drip line and study their structural properties. The discovery of the halo structure formed by the valence one or two neutrons outside a compact core has been one of the most important findings of these studies. The very small one or two-neutron separation energy and abnormally large root mean square radius, as confirmed by measurements of interaction cross section and by momentum distribution studies are some of the novel structural features of the halo nuclei. Some of the 2-neutron halo nuclei are also characterized by what is now known as the Borromean property, which implies that while the binary subsystems, such as n-core and n-n are unbound the three-body system comprising the n-n core gives rise to a bound state. A typical example is that of ^{11}Li, the most studied 2-n halo nucleus. In addition to the studies of the structural properties of the halo nuclei from a purely nuclear physics standpoint, the three-body structure of the 2-n halo nuclei comprising a compact core and two neutrons with very low separation energy makes them ideally suited for studying the Efimov effect. Efimov showed, over three decades ago, that a three-body quantum mechanical system with resonating binary interactions gives rise to an effective attractive inverse

*Article based on the presentation by I. Mazumdar at the Fifth Workshop on Critical Stability, Erice, Sicily, Received January 1st, 2009, Accepted January 8, 2009.

quadratic potential as function of the three-body radial variable supporting an infinite number of weakly bound states [1]. There have been extensive searches for Efimov states in many areas of physics by both experimentalists and theorists. Indeed, the Efimov effect is now being recognised to play a central role in Bose-Einstein condensation in dilute atomic gases. Very recently, the first experimental observation of Efimov states has been reported in ultracold cesium trimers [2]. The material that follows will present our attempts to search for Efimov states in 2-n halo nuclei.

2 Efimov Effect in ^{14}Be, ^{19}B, and ^{20}C

Our formalism is based upon a three-body model of the 2-n halo nucleus comprising a compact core and two valence neutrons. We assume s-wave separable potentials for the binary sub-systems [3]. Solving the three-body Schrodinger equation in momentum space we obtain two coupled integral equations for the spectator functions F(p) and G(p). These equations are recast involving only dimensionless quantities for studying the sensitive computational details of the Efimov effect. In this process the two-body strength and range parameters for the n-n and n-core systems are made dimensionless. The details are provided in [4] and will not be presented here. The first 2-n halo nucleus studied using this formalism was ^{14}Be considered to be a three-body system of a ^{12}Be core and two loosely bound valence neutrons [4]. Keeping the n-core range parameter fixed the strength parameter was varied corresponding to n-^{12}Be virtual states from 50 keV to 0.01 keV. At 50 keV virtual state, the three-body system is found to have binding energy close to the experimental value, but no excited state is predicted. As the virtual state energy of n-^{12}Be is decreased, we not only get the ground state energy, but also the excited state energy for the ^{14}Be system. In fact the first excited state appears for n-^{12}Be virtual state of about 4 keV followed by the emergence of the second excited state at n-core virtual state of 2 keV. This methodology was followed to search for Efimov states in ^{19}B, ^{22}C and ^{20}C [5]. It was shown by numerical analysis and also from analytical considerations that Borromean-type halo nuclei like ^{19}B and ^{22}C, where n-n and n-core are both unbound, are much less vulnerable to respond to the existence of the Efimov effect. On the contrary, those nuclei, like ^{20}C in which the halo neutron is supposed to be in the intruder low lying bound state with the core, appear to be promising candidates to search for the occurrence of Efimov states at energies below the n-(n-core) breakup threshold.

3 Movement of Efimov states in ^{20}C to resonances in n-^{19}C Scattering

In light of the uncertainties in the experimental data we have studied the effect on the behaviour of Efimov states in ^{20}C by scanning a wide region of the n-core binding energy from 60 to 500 keV. It has been noticed that as the two-body binding energy reaches around 140 keV, the second Efimov state has its energy less than that of the two-body leading to an unstable state. Similarly, the first Efimov state also becomes unstable for the two-body binding energy

around 240 keV. This is in conformity with what was originally predicted by Amado and Noble about the movement of Efimov states into the unphysical sheet associated with the two-body unitarity cut on increasing the strength of the binary interaction [6]. This particular behaviour was investigated by extending the study in the scattering sector. We studied the elastic scattering amplitude for n-^{19}C system as a function of incident neutron energy by computing the integral equations for the amplitude at energies below the three-body break up threshold [7]. It was found that for binding energies greater than or equal to 250 keV for the n-^{18}C system the disappearance of the first Efimov state gives rise to a resonance at the neutron energy of 1.6 keV with a full width of around 0.25 keV. The same trend was also observed for binding energies of 200 and 350 keV with the resonances appearing at the same position with similar widths of around 0.25 keV. The second excited state was also found to disappear above the n+^{18}C threshold of about 140 keV with the appearance of a resonance showing the generality of this behaviour.

4 Fano Resonances of Efimov States in ^{20}C

A very intriguing feature of the resonances described in the previous section are their asymmetric profiles. This is unlike the symmetric Breit-Wigner or Lorentzian shapes encountered more often in nuclear physics. We have interpreted the asymmetric shapes of the resonances as Fano resonances widely observed and studied in atomic and molecular systems. The Fano resonances originate from the presence of two alternative pathways to the final state. One directly into the continuum and the other through the embedded discrete state, interfere both constructively and destructively to give the asymmetric resonance. In ^{20}C, the very weak binding and large spatial spread of the Efimov states lead to a strong overlap with the continuum states leading to comparable amplitudes of the two pathways and the very asymmetric profile. We have fitted the resonances by Fano profiles and have extracted the best fit Fano indices for the resonances [8]. The fits to the resonances at 250 and 150 keV n-^{18}C binding energies yield the same fano index (q), displaying their origin as members of the same family of Efimov states. In very recent calculations we have revisited the problem of the movement of Efimov states into resonances with increasing strength of the n-core binary system. For a system of very heavy core ($\sim$100) with two valence neutrons we reproduce the same behaviour as seen in ^{20}C. The results further establish the finding of the movement of Efimov states into resonances beyond a certain strength of the n-core bound system. The right panel of the Fig. 1. shows the asymmetric resonance structures in the elastic scattering cross sections (for a very heavy core) for three different n-core binding energies. We have also checked the scattering length of the n-(n+core) system for the incident energy tending to zero to be positive and large, thereby, supporting a bound state. This result for a hypothetical nucleus with a very heavy core (mass $\sim$ 100) with two valence halo neutrons show the same behaviour as that of a realistic 2-n halo nuclei, the ^{20}C. This helps establishing the results obtained on a firmer foundation and over a large mass range. The left panel shows the peak position of the elastic cross

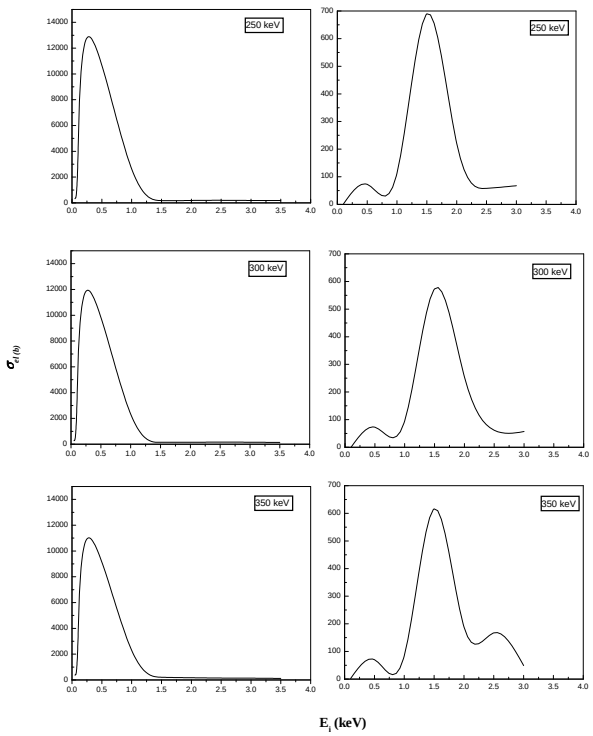

Figure 1. The peak structures in the scattering cross sections for 1) one very heavy core and two valence neutrons and 2) three equal masses.

sections for a system of three equal masses for three different n-core binding energies. In this case the peak position has shifted towards the origin with very large cross sections hinting at virtual states. The case for equal masses are being studied and will be reported elsewhere. It would be really interesting to search for the same effect of movement of Efimov states to resonances in lighter 2-n halo nuclei with the halo neutron and the core forming a bound system. While ^{20}C is by far the most promising case for an experimental campaign we may suggest a few more nuclei, like, ^{38}Mg and ^{32}Ne. For both these nuclei the 2-n separation energies are comparable to that of ^{20}C (2570 and 1970 keV respectively) with the n-core systems of ^{37}Mg and ^{31}Ne are nominally bound by 250 and 330 kev.

Acknowledgement. The results presented above have been arrived at in collaboration with V. Arora, V.S. Bhasin and A.R.P. Rau. The author thanks them all.

References

1. V.N. Efimov, Phys.Rev.**C47**,1876 (1993) and references therein to earlier papers.
2. T. Kraemer *et al*, Nature **440**, 315 (2006)
3. S. Dasgupta, I. Mazumdar and V.S. Bhasin, Phys.Rev.**C50**,R5510 (1994)
4. I. Mazumdar and V.S. Bhasin, Phys.Rev.**C56**,R5 (1997)
5. I. Mazumdar, V. Arora and V.S. Bhasin, Phys.Rev.**C61**, 051303(R) (2000)
6. R. D. Amado and J. V. Noble, Phys. Lett. **35B**, 25 (1971)
7. V. Arora, I. Mazumdar, and V. S. Bhasin, Phys. Rev. C **69**, 061301 (R) (2004)
8. I. Mazumdar, A.R.P. Rau and V.S. Bhasin, Phys. Rev. Lett. **97**,062503 (2006)

Few-Body Systems 0, 1–4 (2009)

Few-Body Systems

Microscopic Description of Few-Body Systems in the Fermionic Molecular Dynamics Approach*

T. Neff**, H. Feldmeier

GSI Helmholtzzentrum für Schwerionenforschung GmbH, Planckstraße 1, 64291 Darmstadt, Germany

Abstract. Fermionic Molecular Dynamics (FMD) is a microscopic approach for the description of light nuclei in the *p*- and *sd*-shell. Many-body basis states are Slater determinants of Gaussian wave-packets localized in phase space. Brink-type cluster states and harmonic oscillator shell model states are contained as special limiting cases in FMD. The FMD approach is used to study the spectrum of ^{12}C with special emphasis on states with pronounced α-clustering including the Hoyle state. The FMD approach is also used to study ^{17}Ne which is a candidate for a two-proton halo nucleus.

1 Introduction

The nuclear-many problem is notoriously difficult to solve. Few-body approaches provide exact solutions for the three- and four-body problem. For heavier nuclei we can try to solve the many-body problem for example with the no-core shell model. But there are problems for loosely bound systems with halo or cluster structures. Cluster models – microscopic or non-microscopic – are often used to study such systems. With the Fermionic Molecular Dynamics model we have a microscopic approach that allows to treat well bound states with shell model structure and loosely bound states with clustering or halos on the same footing.

2 Fermionic Molecular Dynamics

In the Fermionic Molecular Dynamics model [1, 2] Slater determinants are used as many-body basis states

$$\big|Q\big\rangle = \mathcal{A}\left\{\big|q_1\big\rangle \otimes \cdots \otimes \big|q_A\big\rangle\right\} \tag{1}$$

*Article based on the presentation by T. Neff at the Fifth Workshop on Critical Stability, Erice, Sicily, Received December 1st, 2009; Accepted December 12, 2009.

** *E-mail address:* t.neff@gsi.de

where the single-particle states $\big|q\big\rangle$ are given by a single or a superposition of two Gaussian wave packets localized in phase space

$$\big\langle \boldsymbol{x}\big|q\big\rangle = \sum_i c_i \exp\left\{-\frac{(\boldsymbol{x}-\boldsymbol{b}_i)^2}{2a_i}\right\}\big|\chi_i^{\uparrow},\chi_i^{\downarrow}\big\rangle \otimes \big|\xi\big\rangle\,. \tag{2}$$

The complex parameter $\boldsymbol{b}$ encodes mean position and mean momentum of the wave packet. The width a can be different for each wave packet. The spin can assume any orientation, whereas the isospin is $\pm\frac{1}{2}$ describing either protons or neutrons. The wave packet basis is very flexible. Harmonic oscillator single-particle states are obtained as linear combinations of slightly shifted Gaussians. Bloch-Brink type cluster states can be obtained by localizing groups of wave packets.

The FMD solution on the Hartree-Fock level is obtained by minimizing the intrinsic Hamiltonian with respect to all the parameters of the single-particle states.

$$\min_{\{q_i\}} \frac{\big\langle Q\big|H-T_{\rm cm}\big|Q\big\rangle}{\big\langle Q\big|Q\big\rangle} \tag{3}$$

To restore the symmetries of the Hamiltonian the intrinsic state $\big|Q\big\rangle$ is projected on parity, angular momentum and total linear momentum

$$\big|Q;J^\pi MK,\boldsymbol{P}=0\big\rangle = P^\pi P^J_{MK} P^{\boldsymbol{P}=\boldsymbol{0}}\big|Q\big\rangle \tag{4}$$

As the correlation energies can be very large a variation after projection (VAP) should be performed. This is numerically very expensive and only done for light nuclei. For heavier nuclei we perform a variation after projection in a generator-coordinate sense. The intrinsic state $\big|Q\big\rangle$ is minimized under certain constraints like radius, quadrupole or octupole deformation and we search for the minimum in the projected energy surface as a function of the generator coordinates. With either approach we generate a set of intrinsic states $\big|Q^{(a)}\big\rangle$. In the end we solve the generalized eigenvalue problem

$$\sum_{K'b}\big\langle Q^{(a)}\big|(H-T_{cm})P^\pi P^J_{KK'}P^{\boldsymbol{P}=0}\big|Q^{(b)}\big\rangle\, c^{J^\pi\alpha}_{K'b} = E^{J^\pi\alpha}\sum_{K'b}\big\langle Q^{(a)}\big|P^\pi P^J_{KK'}P^{\boldsymbol{P}=0}\big|Q^{(b)}\big\rangle\, c^{J^\pi\alpha}_{K'b} \tag{5}$$

to obtain the multi-configuration mixing result.

We use an effective interaction that is based on the $V_{\rm UCOM}$ interaction. In the Unitary Correlation Operator Method [3, 4] short-range central and tensor correlations are included explicitly by means of a unitary correlation operator. To account for missing three-body correlations and three-body interactions a momentum-dependent two-body term is added to the interaction and fitted to binding energies and radii of closed-shell nuclei [1].

3 Hoyle State in ^{12}C

The second 0^+ state in ^{12}C, the famous Hoyle state, has been studied intensively for many years. It is located slightly above the three-α threshold and is supposed

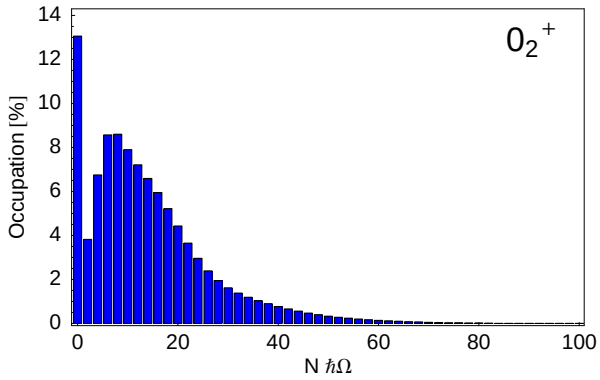

Figure 1. Decomposition of the ^{12}C FMD Hoyle state wave function into N-$\hbar\Omega$ shell model components.

to feature a pronounced α-cluster nature. Microscopic cluster model calculations within the RGM approach [5] were quite successful in describing its properties but use simple effective interactions. Based on the cluster model wave function an interpretation of this state as a Bose condensate of α-particles was proposed recently [6].

In the FMD approach [7] α-cluster configurations are a subset of the Hilbert space. Further configurations are obtained by VAP calculations with constraints on radius and quadrupole deformation. These additional configurations are necessary to describe properties of the ground state band where α-clusters are broken due to the spin-orbit force. In a Hilbert space that consists only of α-cluster configurations the FMD ground state is underbound by more than 10 MeV. Including all configurations we can reproduce the properties of the ground state band as well as that of the Hoyle state. The Hoyle state has an overlap of 85% with three-α configurations and has a very large radius of 3.38 fm. The spatially extended nature of the Hoyle state is also tested by electron scattering data, measuring the transition from the ground state to the Hoyle state. In Fig. 1 the FMD Hoyle state is decomposed into $N\hbar\Omega$ shell model configurations. The admixture of shell model components manifests itself in the $0\hbar\Omega$ contribution. The three-α configurations appear as coherent state extending beyond $50\hbar\Omega$ excitations.

4 Two-proton Halo in ^{17}Ne

^{17}Ne is considered as two-proton halo candidate because of its small two-proton separation energy of 930 keV. Large interaction radii and narrow momentum distributions support the idea of a halo. Theoretical attempts to describe ^{17}Ne in the shell model and in cluster models came to different conclusions regarding the valence protons. Shell model calculations [8] focused on the Coulomb displacement energies between ^{17}Ne and ^{17}N and predicted an s^2-component of only 20%, while cluster model calculations [9, 10] found rather large s^2-components of about 45%.

Recent measurements of the charge radii by the COLLAPS group at ISOLDE

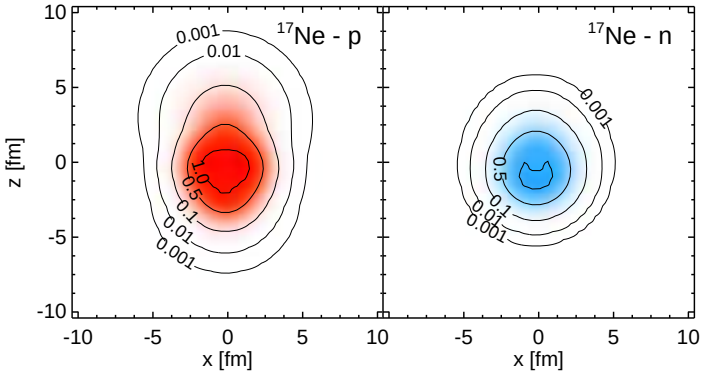

Figure 2. Proton and neutron density distribution for dominant intrinsic configuration of ^{17}Ne. Contours are in units of half nuclear matter density.

now allow for a direct test of the wave function. In a joint paper the experimental results for the charge radii of $^{17-22}$Ne are compared with FMD calculations [11]. Minimizing the energy of the parity projected Slater determinant we find for ^{17}Ne two minima which correspond to s^2- and d^2-dominated configurations for the valence protons around an ^{15}O core. Additional configurations are created by cranking the strength of the spin-orbit force. The intrinsic state with the greatest weight in the multiconfiguration mixing calculation is shown in Fig. 2. The FMD calculations reproduce the large experimental charge radius of 3.042(21) fm with an s^2-contribution of about 42%. A further test for the wave function is provided by the $B(E2)$ values [12] that are reproduced within the experimental error bars.

References

1. Roth, R., Neff, T., Hergert, H., Feldmeier, H.: Nucl. Phys. **A745**, 3 (2004)
2. Neff, T., Feldmeier, H.: Eur. Phys. J Special Topics **156**, 69 (2008)
3. Neff, T., Feldmeier, H.: Nucl. Phys. **A713**, 311 (2003)
4. Roth, R., et al.: Phys. Rev. C **72**, 034002 (2005)
5. Kamimura, M.: Nucl. Phys. **A351**, 456 (1981)
6. Funaki, Y., et al.: Phys. Rev. C **67**, 051306(R) (2003)
7. Chernykh, M., et al.: Phys. Rev. Lett. **98**, 032501 (2007)
8. Fortune, H. T., Sherr, R.: Phys. Lett. **B503**, 70 (2001)
9. Grigorenko, L. V., et al.: Nucl. Phys. **A713**, 372 (2003)
10. Garrido, E., Fedorov, D. V., Jensen, A. S.: Phys. Rev. C **69**, 024002 (2004)
11. Geithner, W., Neff, T., et al.: accepted for publication in Phys. Rev. Lett.
12. Chromik, M. J., et al.: Phys. Rev. C **66**, 024313 (2002)

Few-Body Systems 0, 1–5 (2009)

Few-Body Systems

Three-body decays: structure, decay mechanism and fragment properties*

R. Álvarez-Rodríguez [1**], A.S. Jensen [1], E. Garrido [2], D.V. Fedorov [1], H.O.U. Fynbo [1], O.S. Kirsebom [1]

[1] Department of Physics and Astronomy, University of Aarhus, DK-8000 Aarhus C, Denmark
[2] Instituto de Estructura de la Materia, CSIC, Serrano 123 E-28006 Madrid, Spain

Abstract. We discuss the three-body decay mechanisms of many-body resonances. R-matrix sequential description is compared with full Faddeev computation. The role of the angular momentum and boson symmetries is also studied. As an illustration we show the computed α-particle energy distribution after the decay of ^{12}C(1^+) resonance at 12.7 MeV.

1 Introduction

The three-body decay of many-body resonances can be accurately measured in complete kinematics. Information about the decaying state and the decay mechanism is usually extracted from the measurement of the three fragments after the decay. Although this is a common practice, the situation is ambiguous. The experimental analyses of these processes are based on the R-matrix formalism which inherently assumes two successive two-body decays. The input are the properties of the intermediate two-body states and the population of the nuclear many-body initial state approximated as a three-body system.

Occasionally, in principle contrary descriptions are able to explain the observed distributions making the understanding of the underlying physics difficult. An example demonstrating the difficulties is the 3α decay of 1^+ state in ^{12}C which was successfully described by two opposite mechanisms: a sequential decay via the 2^+ state in ^{8}Be [1], and a direct decay into the three-body continuum [2]. This requires an explanation. What information is contained in a full-kinematics measurement of three-body decay? Apparently unique information can only be extracted under favorable conditions. The crux of the matter is that the decay mechanism is related to a "decay path", an intermediate structure,

*Article based on the presentation by R. Álvarez-Rodíguez at the Fifth Workshop on Critical Stability, Erice, Sicily, Received November 28, 2008; Accepted January 19, 2009.

**Present address:* INFN Sezione di Pisa, Largo B. Pontecorvo 3, I-56127 Pisa, Italy. Electronic address: raquel.alvarez@pi.infn.it.

which in contrast to the final state signal in the detector is not an observable. We shall in this contribution compare the results from three-body calculations and experimental R-matrix analyses.

2 Energy distributions

The large-distance observable structure of the many-body initial state is a three-body continuum state, therefore we compute the resonance structure in a three-body cluster model [3]. We use the complex scaled hyperspherical adiabatic expansion method to solve the Faddeev equations which describe the 3-body system. The appropriate coordinates are the so-called hyperspherical coordinates and consist of the hyperradius $\rho^2 = 4\sum_{i=1}^{3}(\boldsymbol{r}_i - \boldsymbol{R})^2$, and five hyperangles. In the adiabatic hyperspherical expansion method the angular part of the Faddeev equations is solved first and the angular eigenfunctions Φ_{nJM} are then used as a basis to expand the total wave function Ψ^{JM}.

We include short-range [4] and Coulomb potentials. The many-body effects that are present at short distances are assumed to be unimportant except for the resonance energy. This is taken into account by using a structureless 3-body interaction that fits the position of the resonance.

The resonance wave-function contains information about the decay mechanism, and the large-distance properties reflect directly the measurable fragment momentum distributions. The single particle probability distributions are obtained after integration of the absolute square of the wave function over the four hyperangles describing the directions of the momenta.

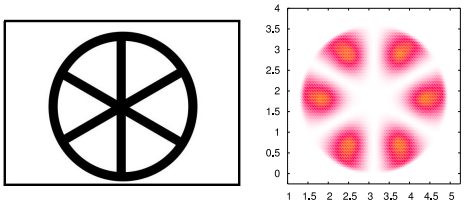

Figure 1. (Color online) Regions of the 3α Dalitz plot where the density must vanish (in black) for a 1^+ state (left). Dalitz plot for the 1^+ state of ^{12}C. x-axis corresponds to $(E_{\alpha 1}/2E_{\alpha 2})/\sqrt{(3)}$ and y-axis to $E_{\alpha 1}$ in MeV.

The many-body initial state resonance evolves into three clusters at large distances. The total angular momentum and parity J^π is conserved in the process. This symmetry combined with Bose-statistics imposes constraints on the resulting momentum distributions. An early example of these effects applied to three pion decays can be found in ref. [5]. Fig. 1 shows the regions of the Dalitz plot where the density must vanish for the decay of a 1^+ state into three α-particles. This gives rise to the minima in the single α-particle energy distribution. The Dalitz plot computed within the Faddeev framework is also shown and is in agreement with these symmetry constraints.

Fig. 2 shows the single-α energy distributions, i.e. the probability for emergence of one α particle with a given energy divided by its maximum allowed, for the 1^+ state of ^{12}C computed with R-matrix analysis [1,6]. This corresponds to the projection of the Dalitz plot in fig. 1 on the y-axis. The decay is assumed to be sequential via ^{8}Be(2^+) since angular momentum forbids the decay via ^{8}Be(0^+). We have varied the two-body energy and width. When both the two-body energy

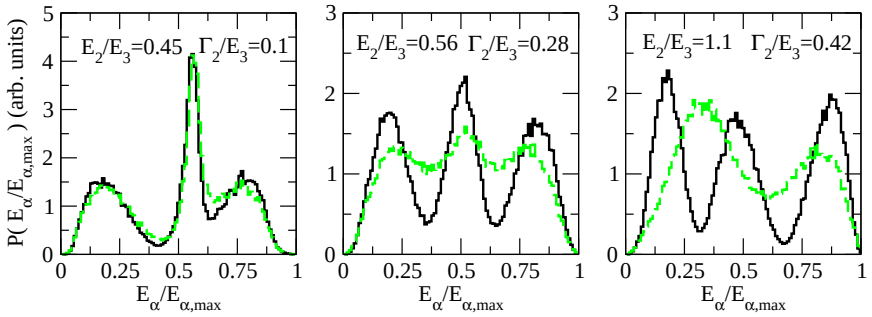

Figure 2. (Color online) Single α energy distributions from R-matrix analysis for the decay into three α-particles of the $^{12}C(1^+)$ resonance at 12.7 MeV of excitation energy. The energies and widths of the intermediate $^8Be(2^+)$ state are varied as specified in the panels. The green dashed curve corresponds to the case where the symmetrization of the wave function is omitted. The middle panel corresponds to the measured resonance energy.

and width are small (left) a narrow peak corresponding to the emission of the first α arises. The other two α's are related to the broad peaks. By increasing the two-body energy and width the three-peak distribution becomes rather pronounced and insensitive to the two-body parameters when either E_{2r}/E_{3r} is larger than about 0.5 or the two-body width is large. The same figure contains the curves corresponding to the case where the boson symmetry is omitted. For a low and narrow two-body state the effect of this symmetry seems to be unimportant, but an increase on the width leads to a two-peak (not three-peak) distribution.

Fig. 3 shows the results from the full three-body computation and the computation from the lowest continuum three-body wave function (K=8) from ref. [7] (democratic decay). This is the simplest assumption with the correct symmetries. We have varied the three-body energy and consequently the three-body width. Two rotation angles have been considered: one of them is large enough to accumulate the contribution of sequential decay through the ^{8}Be resonance in a single adiabatic potential, while the other is not. The calculations include the boson symmetry of the α-particles. The results from the large rotation angle do not include the contribution from the decay via $^8Be(2^+)$ and are very close to the democratic decay. In the result from the full Faddeev computation the three peaks are closer to each other and this approaches better the experiment. The fractions of population at large distance are given in table 2 for the different values of E_{3r} shown in fig. 3. We can observe that the sequential decay probability increases as we increase the three-body energy.

3 Conclusions

We have computed the observable momentum distributions from decay of three-body resonances by use of R-matrix simulations and from full Faddeev calculations. We have considered the example of the 1^+ resonance of ^{12}C. The angular momentum and boson symmetries constrain the resulting momentum distributions. The same measured momentum distributions can be described in differ-

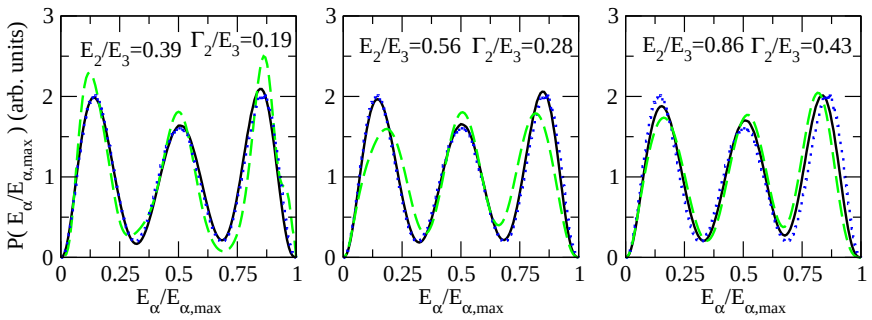

Figure 3. (Color online) Single α energy distributions from Faddeev computation for direct decay of the ^{12}C(1^+) resonance. The three-body energy is varied by changing the strength of the three-body potential. The relative energies and widths of the intermediate ^{8}Be(2^+) resonance are specified in the panels. The solid (black) and dashed (green) curves correspond to complex rotation angles of $\theta = 0.25$ and 0.1 respectively. The dotted (blue) curve corresponds to democratic decay [7]. For $\theta = 0.25$ only direct decay is shown.

Table 1. The probability P_{seq} for populating the component related to the decay via ^{8}Be(2^+) at large distances in the computation of the 1^+ resonance of ^{12}C for a complex rotation angle $\theta = 0.25$. The three-body energy (E_{3r}) is varied by adjusting the strength of the three-body potential. The ^{8}Be(2^+) two-body energy is maintained $E_{2r} = 2.7$ MeV. The energies are referred to the 3α or 2α separation threshold.

^{12}C(J^π)	E_{2r}/E_{3r}	Γ_{2r}/E_{3r}	E_{3r} (MeV)	Γ_{3r} (MeV)	l_y	P_{seq}
	0.86	0.43	3.5	0.005	2	0.001
1^+	0.56	0.28	5.4	0.09	2	0.12
	0.39	0.19	7.8	1.15	2	0.89

ent complete basis sets, e.g. either direct products of two-body states and their center-of-mass motion relative to the third particle (R-matrix) or three-body continuum wave functions (Faddeev). The fact that different descriptions seem to work indicates that the same wave function could be described in different ways. Extracting information of both structure and decay mechanism can then be misleading and requires model interpretations. Full Faddeev computations successfully reproduce the measured distributions.

References

1. Fynbo, H.O.U., et al.: Phys. Rev. Lett. **91**, 082502 (2003).
2. Álvarez-Rodríguez, R., et al.: Phys. Rev. Lett. **99**, 072503 (2007).
3. Nielsen, E., Fedorov, D.V., Jensen, A.S., Garrido, E.: Phys. Rep. **347**, 373 (2001).
4. Ali, S., Bodmer, A.R.: Nucl. Phys. **80**, 99 (1966).
5. Zemach, Z.: Phys. Rev. **133**, B1201 (1964).
6. Fynbo, H.O.U., et al.: in preparation.
7. Korsheninnikov, A.A.: Yad. Fiz. **52**, 1034 (1990) [Sov. J. Nucl. Phys. **52**, 827 (1990)].

Few-Body Systems 0, 1–4 (2009)

Few-Body Systems

Consistent description of the $^{12}C(0_2^+)$ state*

S. I. Fedotov, O. I. Kartavtsev** and A. V. Malykh

Joint Institute for Nuclear Research, Dubna, 141980, Russia

Abstract.

The excited 0_2^+ state of ^{12}C is of key importance for description of the triple-α reaction, which is the only way for helium burning in stars. Authors' efforts to calculate the lowest 0^+ states within the framework of the α-cluster model are summarized and discussed. In particular, the recently calculated 0_2^+ state's width and $0_2^+ \to 0_1^+$ transition density are in good agreement with the experimental data.

The $^{12}C(0_2^+)$ state was predicted by Hoyle [1] and experimentally observed [2, 3] more than 50 years ago. This amazing prediction is based merely on observable abundance of elements in the universe by assuming that sufficiently fast helium burning in stars proceed via the resonance reaction $3\alpha \to {}^8\mathrm{Be} + \alpha \to {}^{12}C(0_2^+) \to {}^{12}C+\gamma$. During the recent years, there is a continuous interest to the experimental and theoretical study of the ^{12}C nucleus [5, 6, 7, 8]. While the Hoyle state is fairly well studied experimentally, e.g., its extremely small width Γ and $0_2^+ \to 0_1^+$ transition density (in particular, the monopole transition matrix element M_{12} and the transition radius R_{tr}) have been accurately measured, the theoretical description of a comparable accuracy is still lacking. One of the tough problems in the theory is connected with the necessity to describe the continuum wave function of few charged particles.

In a set of calculations [9, 10, 11, 12] the α-cluster model is used to obtain the lowest $^{12}C(0^+)$-states properties with particular attention to reliable description of the 0_2^+ state. These results are summarized and discussed in order to determine the ability of the α-cluster model to describe the experimentally observed 0_2^+ state's width Γ, $0_2^+ \to 0_1^+$ monopole transition matrix element M_{12}, and $0_2^+ \to 0_1^+$ transition radius R_{tr}.

The effective two-body potential of the α-cluster model is taken in the Ali-Bodmer form [13] as a sum of two Gaussians, which parameters in the s-wave channel are chosen to fix the ^{8}Be energy $E_{2\alpha}$ and its width γ at the experimental values 92.04 ± 0.05 keV and 5.57 ± 0.25 eV [14]. Generally, the parameters of the

*Article based on the presentation by O. I. Kartavtsev at the Fifth Workshop on Critical Stability, Erice, Sicily, Received December 4, 2008; Accepted January 30, 2009.

** *E-mail address:* oik@nusun.jinr.ru

two-body potential in s-, d-, g-channels are determined to adjust the experimental α-α elastic-scattering phase shifts.

The effective three-body potential V_3 is introduced to take into account those effects, which are not described by a sum of the effective two-body potentials. A simple dependence of V_3 on the hyperradius ρ is assumed [6, 9, 10, 11, 12]; the parameters of V_3 are chosen to fix the ground-state E_{gs} and excited-state E_r energies of ^{12}C, as well as the ground-state root-mean-square (rms) radius $R^{(1)}$ at their experimental values $E_{gs} = -7.2747$ MeV, $E_r = 0.3795$ MeV [15], $R^{(1)} = 2.48 \pm 0.022$ fm [16, 17]. Although the ground state is not of the α-cluster structure, the calculation of the ground state within the α-cluster model is necessary to provide the overall description of the non-α-cluster component, which contribute substantially also in the excited state. Furthermore, both the excited and ground state wave functions have to be calculated within the framework of the same approach to obtain the experimentally available M_{12} and R_{tr}.

The method of calculation is based on the expansion of the total wave function in a set of eigenfunctions on a hypersphere (at the fixed ρ); the detailed description is given in [9, 10]. It is of most importance that the properties of the 0_2^+ state are obtained by solving the scattering problem of two clusters (α and ^{8}Be), which greatly simplifies the calculations by avoiding a tremendous problem of determination of the wave function of three outgoing charged particles. The reliability of this approximation is closely related to the sequential decay mechanism via intermediate emission of ^{8}Be ($^{12}\mathrm{C}(0_2^+) \to \alpha + {}^8\mathrm{Be} \to 3\alpha$). The sequential mechanism was approved in the experiment [4] where the branching ratio for the non-sequential decay $^{12}\mathrm{C} \to 3\alpha$ is estimated to be less than 1%.

In calculations [9, 10, 11], the local two-body potential was used to understand how sensitive are the characteristics of the 0_2^+ state to variations of the potential parameters. In addition, dependences of M_{12}, Γ, and the excited-state rms radius $R^{(2)}$ on one of the parameters of V_3 are studied provided other parameters of V_3 (taken as a sum of two Gaussians) are chosen to fix E_{gs}, E_r, and $R^{(1)}$. It is found that for any reliable three-body potential the values of Γ, M_{12}, and $R^{(2)}$ are located within the narrow intervals, which are marked by triangles in Fig. 1. The calculations performed for two families of the two-body potentials show that Γ, M_{12}, and $R^{(2)}$ are comparatively stable under variations of the two-body potential (Fig. 1). Thus, the results are robust to the variations of the effective potentials and the calculated Γ and M_{12} overestimate the experimental values by a factor 2. This surprising agreement gives a clear evidence that the dominant contribution to the final result comes from the s-wave part of the interaction.

To provide better agreement of the calculated and experimental values, the recent caculations have been performed by using the effective two-body potential properly describing the $\alpha - \alpha$ interaction also in higher partial waves. The preliminary results will be presented below while the details of calculations will be published elsewhere [12]. The three-parameter's Woods-Saxon form is found to be suitable for the three-body potential V_3, which turns out to be flexible enough to fix at the experimental values E_{gs}, E_r, and mostly $R^{(1)}$. As a result, a set of two-body potentials and corresponding V_3 is found, for which both Γ and M_{12}

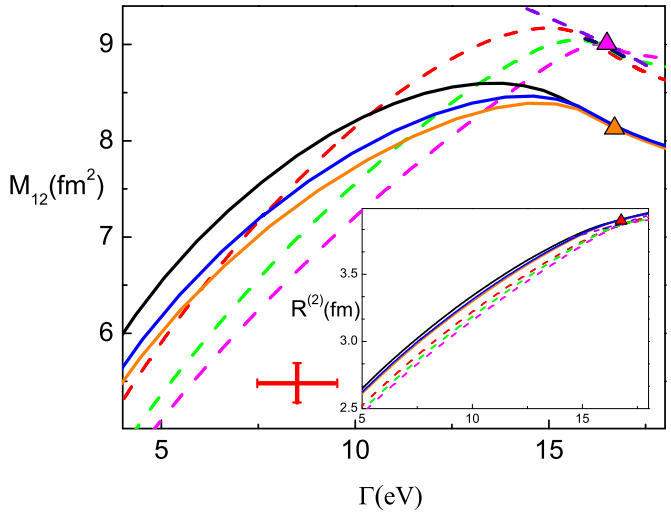

Figure 1. Dependences of the monopole $0_2^+ \to 0_1^+$ transition matrix element M_{12} vs the width Γ of the 0_2^+ state for two families of local two-body potentials (shown by solid and dashed lines). The point with errorbars shows the experimental data $\Gamma = 8.5 \pm 1.0$ eV [19] and $M_{12} = 5.48 \pm 0.22$ fm^2 [19]. The corresponding dependences $R^{(2)}$ vs Γ are shown in the inset.

are in excellent agreement with the experimental data (Fig. 2). Correspondingly, the transition radius R_{tr} varies within the interval 4.84 fm $< R_{tr} <$ 4.90 fm being slightly above the experimental value 4.396 ± 0.27 fm [19]. The R_{tr} is defined as in [19] by $R_{tr}^2 = \sum_k \langle \Psi^{(1)} | \mathbf{r}_k^4 | \Psi^{(2)} \rangle / M_{12}$, where $\mathbf{r}_k$ is a center-of-mass position vector of the k-th proton and a sum is taken over all protons.

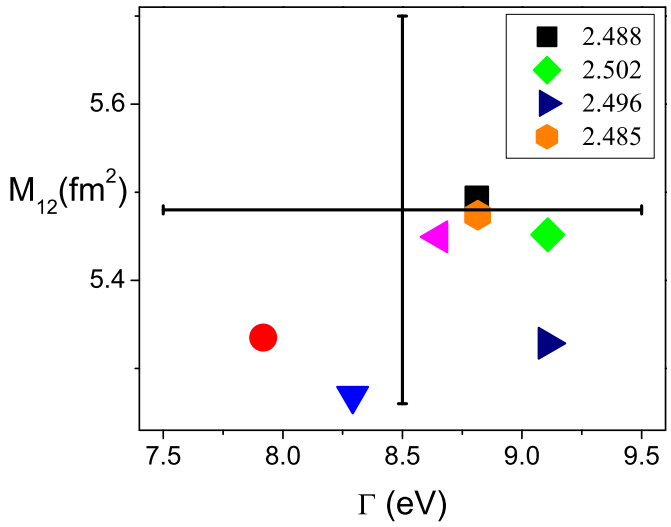

Figure 2. Monopole $0_2^+ \to 0_1^+$ transition matrix element M_{12} and width Γ of the 0_2^+ state for a set of seven two-body potentials. The point with errorbars shows the experimental data. The ground-state rms radius $R^{(1)}$ is fixed either at the experimental value 2.48 fm or at slightly different values specified in the inset.

In conclusion, it is found that the α-cluster model, in spite of its simplicity, is amazingly effective in description of ^{12}C (0^+) states. One should note that the three-body calculations leave enough room for further improvement of the model. In particular, the investigation of the electromagnetic (α-α bremsstrahlung) and (α, α) reactions could be used for construction of the exact effective potentials. Furthermore, the calculation of the ^{12}C (0_2^+) state is a necessary step towards study of helium burning at ultra-low temperatures and high densities, which takes place, e.g., in accretion on white dwarfs and neutron stars [20]. The present approach is promising for calculation of the triple-α reaction below the three-body resonance thus providing the unified treatment of the crossover from the resonant to the non-resonant mechanism of the reaction.

References

1. F. Hoyle, Astrophys. J. Suppl. **1**, 121 (1954).
2. D. N. F. Dunbar, R. E. Pixley, W. A. Wenzel, and W. Whaling, Phys. Rev. **92**, 649 (1953).
3. C. W. Cook, W. A. Fowler, C. C. Lauritsen, and T. Lauritsen, Phys. Rev. **107**, 508 (1957).
4. M. Freer, A. H. Wuosmaa, R. R. Betts et al., Phys. Rev. C **49**, R1751 (1994).
5. H. O. U. Fynbo, C. A. Diget, U. C. Bergmann et al., Nature **433**, 136 (2005).
6. I. Filikhin, V. M. Suslov, and B. Vlahovic, J. Phys. G **31**, 1207 (2005).
7. R. Álvarez-Rodríguez, E. Garrido, A. S. Jensen et al., Eur. Phys. J. A **31**, 303 (2007).
8. M. Chernykh, H. Feldmeier, T. Neff et al., Phys. Rev. Lett. **98**, 032501 (2007).
9. S. I. Fedotov, O. I. Kartavtsev, V. I. Kochkin, and A. V. Malykh, Phys. Rev. C **70**, 014006 (2004).
10. S. I. Fedotov, O. I. Kartavtsev, and A. V. Malykh, Eur. Phys. J. A **26**, 201 (2005).
11. S. I. Fedotov, O. I. Kartavtsev, and A. V. Malykh, In: Models and Methods in Few- and Many-Body Systems. Proc. of the DST-UNISA-JINR Symposium /Ed.: S. A. Sofianos (Pretoria, UNISA Press, 2007), pp. 64-73.
12. S. I. Fedotov, O. I. Kartavtsev, and A. V. Malykh, to be published.
13. S. Ali and A. R. Bodmer, Nucl. Phys. **80**, 99 (1966).
14. S. Wüstenbecker, H. W. Becker, H. Ebbing et al., Z. Phys. A **344**, 205 (1992).
15. F. Ajzenberg-Selove, Nucl. Phys. A **506**, 1 (1990).
16. W. Ruckstuhl, B. Aas, W. Beer, I. Beltrami et al., Nucl. Phys. A **430**, 685 (1984).
17. E. A. J. M. Offermann, L. S. Cardman, C. W. de Jager et al., Phys. Rev. C **44**, 1096 (1991).
18. F. Ajzenberg-Selove, Nucl. Phys. A **490**, 1 (1988).
19. P. Strehl and Th. H. Schucan, Phys. Lett. B **27**, 641 (1968).
20. A. G. W. Cameron, Astrophys. J. **130**, 916 (1959).

Few-Body Systems 0, 1–4 (2009)

Few-Body Systems

Poincaré Invariant Three-Body Scattering*

Ch. Elster**[1], T. Lin[1], W.N. Polyzou[2], W. Glöckle[3],

[1] Institute of Nuclear and Particle Physics, and Department of Physics and Astronomy, Ohio University, Athens, OH 45701, USA
[2] Department of Physics and Astronomy, The University of Iowa, Iowa City, IA 52242, USA
[3] Institute for Theoretical Physics II, Ruhr-University Bochum, D-44780 Bochum, Germany

Abstract. Relativistic Faddeev equations for three-body scattering are solved at arbitrary energies in terms of momentum vectors without employing a partial wave decomposition. Relativistic invariance is incorporated withing the framework of Poincaré invariant quantum mechanics. Based on a Malfliet-Tjon interaction, observables for elastic and breakup scattering are calculated and compared to non-relativistic ones.

A consistent treatment of intermediate energy reactions requires a Poincaré symmetric quantum theory [1]. In addition, the standard partial wave decomposition, successfully applied below the pion-production threshold [2], is no longer an adequate numerical scheme due to the proliferation of the number of partial waves. Thus, the intermediate energy regime is a new territory for few-body calculations, which waits to be explored.

This work addresses two aspects in this list of challenges: exact Poincaré invariance and calculations using vector variables instead of partial waves. In Ref. [3] the non-relativistic Faddeev equations were solved directly as function of vector variables for scattering at intermediate energies. A key advantage of this formulation lies in its applicability at higher energies, where the number of partial waves proliferates. The Faddeev equation, based on a Poincaré invariant mass operator, has been formulated in detail in [4] and has both kinematical and dynamical differences with respect to the corresponding non-relativistic equation.

The formulation of the theory is given in a representation of Poincaré invariant quantum mechanics where the interactions are invariant with respect to kinematic translations and rotations [5]. The model Hilbert space is a three-nucleon Hilbert space (thus not allowing for absorptive processes). The method introduces the NN interactions in the unitary representation of the Poincaré group and allows to input e.g. high-precision NN interactions in a way that reproduces the measured two-body observables. However in this study we use a

*Article based on the presentation by Charlotte Elster at the Fifth Workshop on Critical Stability, Erice, Sicily, Received November 29, 2008; Accepted January 8, 2009.
** *E-mail address: charlotte.elster@gmail.com*

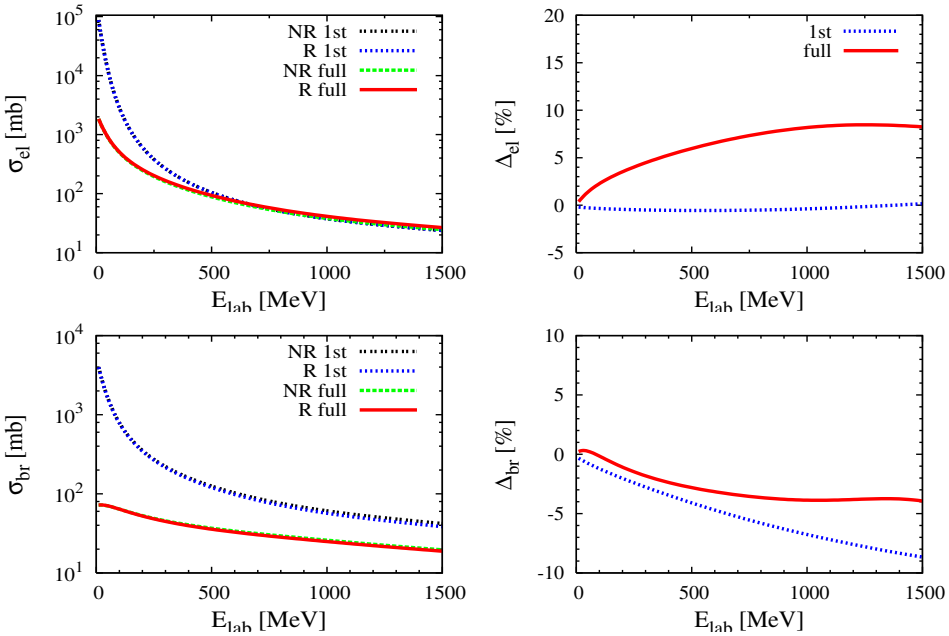

Figure 1. The total elastic c.m. cross section for elastic (top left) and for breakup scattering (bottom left) calculated from a Malfliet-Tjon type potential as function of the projectile kinetic laboratory energy. The labels 'R' ('NR') stand for relativistic (non-relativistic) calculations. The Faddeev calculations in the first order in t are marked with '1st', the converged full Faddeev calculations with 'full'. To show the difference, the percentage difference between the relativistic and corresponding non-relativistic calculations are displayed on the right.

simpler interaction consisting of a superposition of an attractive and a repulsive Yukawa interaction with parameters chosen such that a bound state at E_d = -2.23 MeV is supported [4]. Poincaré invariance and S-matrix cluster properties dictate how the two-body interactions must be embedded in the three-body dynamical generators. Scattering observables are calculated using Faddeev equations formulated with the mass Casimir operator (rest Hamiltonian) constructed from these generators.

To obtain a valid estimate of the size of relativistic effects, it is important that the interactions employed in the relativistic and non-relativistic calculations are phase-shift equivalent. We follow the suggestion by Coester, Piper, and Serduke (CPS) and construct a phase equivalent interaction from a non-relativistic 2N interaction [6] by adding the interaction to the square of the mass operator. In this CPS method the relativistic interaction can not be analytically calculated from the non-relativistic one. However, there is a simple analytic connection between the relativistic and non-relativistic two-body t-matrices

$$t_{re}(\mathbf{p},\mathbf{p}';2E_p^{rel}) = \frac{2m}{\sqrt{m^2+p^2}+\sqrt{m^2+p'^2}}\, t_{nr}(\mathbf{p},\mathbf{p}';2E_p^{nr}),$$

where $2E_p^{rel} = 2\sqrt{m^2+p^2}$ and $2E_p^{nr} = \frac{p^2}{m} + 2m$. This relativistic two-body t-

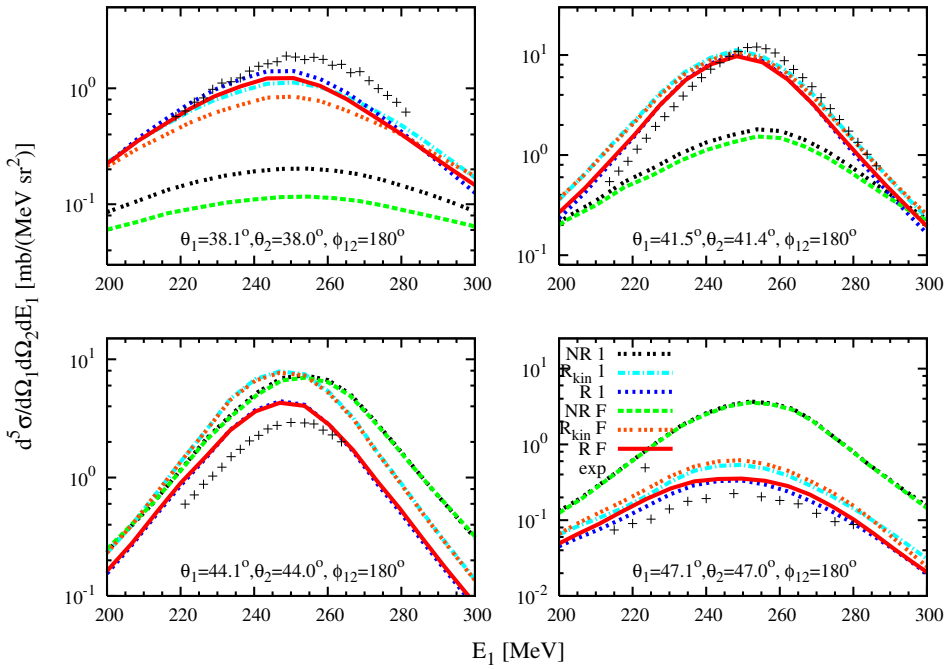

Figure 2. The exclusive differential cross section for the reaction ^{2}H(p,2p)n at 508 MeV laboratory projectile energy for different proton angle pairs $\theta_1 - \theta_2$ symmetric around the beam axis as function of the laboratory kinetic energy of one of the outgoing protons. The meaning of the curves are the same as in Fig. 1, except that here '1' denotes the 1st order Faddeev calculation, 'F' the fully converged one. In the curves labeled $R_{\rm kin}$ only relativistic kinematics is taken into account. The data are taken from Ref. [10].

matrix $t_{re}(\mathbf{p}, \mathbf{p}'; 2E_p^{rel})$ is scattering equivalent to the non-relativistic one at the same relative momentum $\mathbf{p}$ [7]. This t-matrix is the input for the Poincaré invariant transition amplitude of the 2N subsystem embedded in the three-particle Hilbert space obtained via a first resolvent method as layed out in Ref. [4].

By construction, differences in the relativistic and non-relativistic calculations first appear in the three-body calculations. Those differences are in the choice of kinematic variables (Jacobi momenta are constructed using Lorentz boosts rather then Galilean boosts) and in the embedding of the two-body interactions in the three-body problem, which is a consequence of the non-linear relation between the two and three-body mass operators. These differences modify the permutation operators and the off-shell properties of the kernel of the Faddeev equations [9].

In Fig. 1 the total cross sections for elastic and breakup cross sections are displayed as function of the projectile kinetic energy up to 1.5 GeV obtained from our fully converged relativistic Faddeev calculation as well as the one obtained from the first-order term, $T^{1st} = tP$, with P being the permutation operator for three identical particles. It is obvious that, especially for energies below 300 MeV, the contribution of rescattering terms is huge. However, for extracting the size of

relativistic effect, it is more useful to consider the relative difference between the relativistic and non-relativistic calculations. In first order, there is essentially no effect in the total elastic cross section, which is consistent with the observation that the relativistic two-body t-matrix is constructed to be phase-shift equivalent to the non-relativistic one. The same comparison with fully converged Faddeev calculations indicates that relativistic effects in the three-body problem increase the total cross section for elastic scattering with increasing energy, whereas it is slightly reduced in the total breakup cross section.

Considering exclusive breakup reactions, differences between a relativistic and non-relativistic calculation are more pronounced and strongly depend on the configuration. Though our two-body force is simple, we compare to a ^{2}H(p,2p)n experiment at 508 MeV [10] to see if our calculation captures essential features of the measurement. Differences in the predictions of our relativistic and non-relativistic calculations are very pronounced at this energy as can be seen in Fig. 2, which shows selected angle pairs $\theta_1 - \theta_2$ from Ref. [10], which are symmetric around the beam axis. The cross section is plotted against the laboratory kinetic energy of one of the outgoing protons. It is interesting to observe that for smaller angle pairs the relativistic cross sections (RF) are considerably larger than the non-relativistic ones (NRF). For larger angle pairs the situation reverses. It is further noteworthy, that in the configurations of Fig. 2, which are close to quasi-free, rescattering effects (or equivalently higher order contributions of the Faddeev multiple scattering series) are very small (curves '1' and 'F' are almost identical). To show that peak-positions are given by kinematics, we added curves labeled 'R_{kin}', which stands for a non-relativistic calculation in which only kinematics and phase space factors are replaced by the relativistic ones. We want to note that the above comparisons do not involve a non-relativistic limit, instead relativistic and non-relativistic three-body calculations with interactions that are fit to the same two-body data are compared. All of the differences are due to the different ways two-body dynamics is incorporated in the three-body problem.

References

1. E.P. Wigner, Ann. Math. C **40**, 149 (1939).
2. W. Glöckle, H. Witała, D. Hüber, H. Kamada, J. Golak, Phys. Rep. **274**, 107 (1996).
3. H. Liu, Ch. Elster, W. Glöckle, Phys. Rev. C**72**, 054003 (2005).
4. T. Lin, Ch. Elster, W. N. Polyzou, W. Glöckle, Phys. Rev. C**76**, 014010 (2007).
5. F. Coester, Helv. Phys. Acta. **38**, 7 (1965).
6. F. Coester, S.C. Piper, and F.J.D. Serduke, Phys. Rev. C**11**, 1 (1975).
7. B. D. Keister and W. N. Polyzou, Phys. Rev. C**73**, 014005 (2006).
8. T. Lin, Ch. Elster, W. N. Polyzou, W. Glöckle, Phys. Lett. **B 660**, 345 (2008).
9. T. Lin, Ch. Elster, W. N. Polyzou, H. Witała, W. Glöckle, Phys. Rev. C**78**, 024002 (2008).
10. V. Punjabi *et al.*, Phys. Rev. C**38**, 2728 (1988).

Few-Body Systems 0, 1–4 (2009)

Few-Body Systems

Three- and Four-Body Scattering Calculations including the Coulomb Force*

A. Deltuva

Centro de Física Nuclear da Universidade de Lisboa, P-1649-003 Lisboa, Portugal

Abstract. The method of screening and renormalization for including the Coulomb interaction in the framework of momentum-space integral equations is applied to the three- and four-body nuclear reactions. The Coulomb effect on the observables and the ability of the present nuclear potential models to describe the experimental data is discussed.

The Coulomb interaction, due to its long range, does not satisfy the mathematical properties required for the formulation of the standard scattering theory. However, since in nature the Coulomb potential is always screened, one could expect that the physical observables become insensitive to the screening provided it takes place at sufficiently large distances R and, therefore, the $R \to \infty$ limit should correspond to the proper Coulomb. This was proved by Taylor [1] in the context of the two-particle system: though the on-shell screened Coulomb transition matrix diverges in the $R \to \infty$ limit, after renormalization by (an equally) diverging phase factor it converges as a distribution to the well known proper Coulomb amplitude and therefore yields identical results for the physical observables. A similar renormalization relates screened and proper Coulomb wave functions [2].

The method of screening and renormalization can be used for the systems with more particles [3], albeit with some limitations. Here we briefly recall the procedure which is described in detail in ref. [4]. In the transition operators derived from nuclear plus screened Coulomb potentials one has to isolate the diverging screened Coulomb contributions in the form of a two-body on-shell transition matrix and two-body wave function with known renormalization properties. This can be achieved using the two-potential formalism as long as in the initial/final states there are no more than two charged bodies (clusters). At the same time this procedure separates long-range and Coulomb-distorted short-range parts of the transition amplitude, the former being the two-body on-shell transition matrix derived from the screened Coulomb potential between the centers of mass

*Article based on the presentation by A. Deltuva at the Fifth Workshop on Critical Stability, Erice, Sicily, Received November 7, 2008; Accepted January 16, 2009.

(c.m.) of the two charged bodies that is present in the elastic scattering only. After renormalization this contribution converges towards its $R \to \infty$ limit very slowly but the result, the pure Coulomb amplitude of two-body nature, is known analytically. The remaining part of the elastic scattering amplitude as well as the amplitudes for transfer and breakup are complicated short-range operators that are externally distorted by Coulomb. However, due to their short-range nature, convergence with R after the renormalization by the corresponding phase factors is fast and, therefore, they are calculated numerically at finite R using the standard scattering theory and making sure that R is large enough for the convergence of the results. We solve Faddeev-like Alt, Grassberger, and Sandhas (AGS) equations for three- and four-particle scattering [5, 6] using the momentum-space partial-wave basis as described in detail in refs. [7, 8, 9] for three- and four-nucleon scattering without the Coulomb force. However, the screened Coulomb interaction, due to its longer range, compared to the nuclear interaction, brings additional difficulties: quasisingular nature of the potential and slow convergence of the partial-wave expansion. The right choice of the screening is essential in resolving those difficulties. The convergence of the partial-wave expansion with our new screening function [4] is fast enough and thereby allows us to avoid the approximations used in the previous implementations [10, 11] of the screening and renormalization approach and obtain reliable results.

The most important criterion for the reliability of the screening and renormalization method is the convergence of the observables with the screening radius R used to calculate the Coulomb-distorted short-range part of the amplitudes. Numerous examples can be found in refs. [4, 12, 13]. In most cases the convergence is impressively fast and only becomes slower for the observables at very low energies. Furthermore, as demonstrated in ref. [14], our results for p-d elastic scattering agree well over a wide energy range with those of ref. [15] obtained from the variational solution of the three-nucleon Schrödinger equation in configuration space with the inclusion of an *unscreened* Coulomb potential and imposing the proper Coulomb boundary conditions explicitly.

The present method was used to study three-nucleon hadronic and electromagnetic (e.m.) reactions in refs. [4, 16, 17, 18]. Furthermore, it was applied to the nuclear reactions dominated by three-body degrees of freedom like $\alpha + d$ [12], $d + {}^{12}\mathrm{C}$, and $p + {}^{11}\mathrm{Be}$ [19, 20]. Finally, in refs. [9, 13, 21] all elastic and transfer four-nucleon reactions below three-body breakup threshold have been studied. The importance of the Coulomb at low energies is demonstrated in Fig. 1 for elastic d-α scattering. It may be very strong at all energies in p-d breakup and three-body e.m. disintegration of ^{3}He in kinematical regimes with low relative pp energy where the Coulomb repulsion converts the cross section peak obtained in the absence of Coulomb into a minimum as can be seen in the the experimental data as well [16, 18]. However, even after the inclusion of the Coulomb interaction and the three-nucleon force some discrepancies between experiment and theory like the space star anomaly in p-d breakup [4, 18] and the A_y-puzzle in p-d [4, 15] and p-^{3}He [13, 24] elastic scattering still persist. Furthermore, A_y is described quite well in the n-^{3}He and p-^{3}H elastic scattering but not in the $p + {}^3\mathrm{H} \to n + {}^3\mathrm{He}$ transfer reaction. A very strong Coulomb effect manifests itself

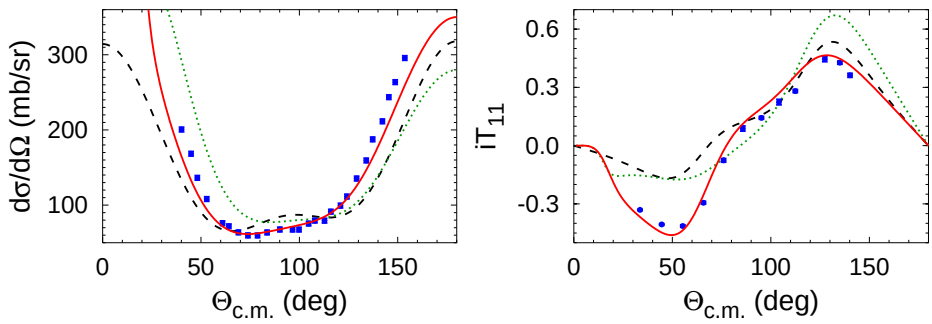

Figure 1. Differential cross section and deuteron vector analyzing power iT_{11} of d-α elastic scattering at $E_d = 4.81$ MeV. Results derived from the N-α potential that is attractive in S-wave and supports Pauli-forbidden bound state which is projected out are shown as solid (dashed) curves with (without) Coulomb. The results including Coulomb but with local repulsive N-α S-wave potential are given by dotted curves. The experimental data are from refs. [22, 23]

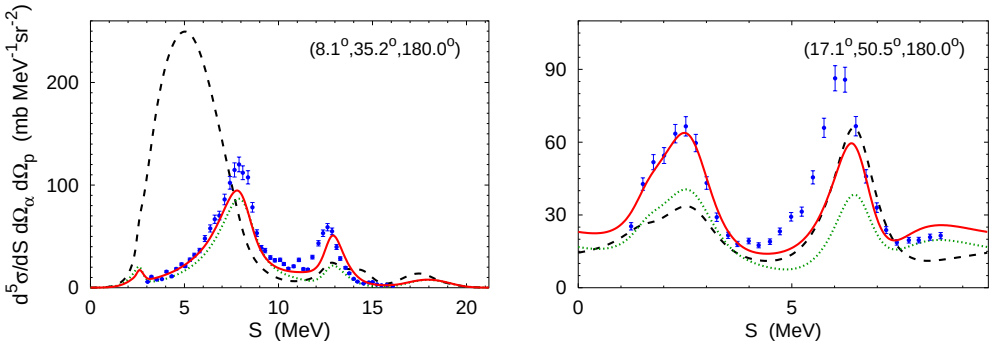

Figure 2. Differential cross section of α-d breakup at $E_\alpha = 15$ MeV in selected kinematical configurations. Curves as in Fig. 1. The experimental data are from ref. [22, 23]

in the α-d breakup where the shift of αp P-wave resonance position leads to the corresponding shifts of the differential cross section peaks as shown in Fig. 2. In addition, Figs. 1 and 2 as well as the results of ref. [12] demonstrate the superiority of the attractive N-α S-wave potentials supporting a Pauli-forbidden bound state that is projected out over the local repulsive S-wave potentials which, because of their simplicity, are very often used in the configuration space calculations of resonances and e.m. reactions.

In conclusion, the Coulomb interaction between the charged particles was included in few-body scattering calculations using the old idea of screening and renormalization [1] but with novel practical realization that avoids all the approximations of the previous works [10, 11] and yields fully converged results.

Acknowledgement. This work has been performed in collaboration with A. C. Fonseca and P. U. Sauer. The author is supported by the Fundação para a Ciência e a Tecnologia (FCT) grant SFRH/BPD/34628/2007.

References

1. Taylor, J. R.: Nuovo Cim. **B23**, 313 (1974)
2. Gorshkov, V. G.: Sov. Phys.-JETP **13**, 1037 (1961)
3. Alt, E. O., Sandhas, W.: Phys. Rev. **C21**, 1733 (1980)
4. Deltuva, A., Fonseca, A. C., Sauer, P. U.: Phys. Rev. **C71**, 054005 (2005); Phys. Rev. Lett. **95**, 092301; Phys. Rev. **C72**, 054004 (2005); Phys. Rev. **C73**, 057001 (2006); Annu. Rev. Nucl. Sci. **58**, 27 (2008)
5. Alt, E. O., Grassberger, P., Sandhas, W.: Nucl. Phys. **B2**, 167 (1967)
6. Grassberger, P., Sandhas, W.: Nucl. Phys. **B2**, 181 (1967); Alt, E. O., Grassberger, P., Sandhas, W.: JINR report No. E4-6688 (1972)
7. Chmielewski, K., et al.: Phys. Rev. **C67**, 014002 (2003)
8. Deltuva, A., Chmielewski, K., Sauer, P. U.: Phys. Rev. **C67**, 034001 (2003)
9. Deltuva, A., Fonseca, A. C.: Phys. Rev. **C75**, 014005 (2007)
10. Alt, E. O., Rauh, M.: Few-Body Systems **17**, 121 (1994)
11. Alt, E. O., et al.: Phys. Rev. **C65**, 064613 (2002)
12. Deltuva, A.: Phys. Rev. **C74**, 064001 (2006)
13. Deltuva, A., Fonseca, A. C.: Phys. Rev. Lett. **98**, 162502 (2007); Phys. Rev. **C76**, 021001 (2007)
14. Deltuva, A., et al.: Phys. Rev. **C71**, 064003 (2005)
15. Kievsky, A., Viviani, M., Rosati, S.: Phys. Rev. **C64**, 024002 (2001)
16. Kistryn, S., et al.: Phys. Lett. **B641**, 23 (2006)
17. Deltuva, A., Fonseca, A. C., Sauer, P. U.: Nucl. Phys. **A790**, 344c (2007)
18. Sagara, K., et al.: Nucl. Phys. **A790**, 348c (2007)
19. Deltuva, A., et al.: Phys. Rev. **C76**, 064602 (2007)
20. Crespo, R., et al.: Phys. Rev. **C76**, 014620 (2007)
21. Deltuva, A., Fonseca, A. C., Sauer, P. U.: Phys. Lett. **B660**, 471 (2008)
22. Bruno, M., et al.: Lett. Nuovo Cim. **27**, 265 (1980)
23. Grüebler, W., et al.: Nucl. Phys.**A134**, 686 (1969)
24. Viviani, M., et al.: Phys. Rev. Lett. **86**, 3739 (2001)
25. Koersner, I., et al.: Nucl. Phys. **A286**, 431 (1977)

Few-Body Systems 0, 1–4 (2009)

Few-Body Systems

Experimental Low-Energy Antiproton Physics*

Eberhard Widmann**

Stefan Meyer Institute for Subatomic Physics, Austrian Academy of Sciences, Boltzmanngasse 3, 1090 Vienna, Austria

Abstract. An overview is given on experiments under progress at the Antiproton Decelerator of CERN which aim at precision spectroscopy of antiprotonic helium, an exotic three-body system containing an antiproton, a helium nucleus, and an electron. An outlook towards the next generation Facility for Low-energy Antiproton and Ion Research (FLAIR) at Darmstadt is presented.

1 Introduction

The only currently available source of low-energy antiprotons is the Antiproton Decelerator (AD) which is in operation at CERN since 2000. Two collaborations, ATRAP and ALPHA, are devoted to the formation of cold antihydrogen ($\overline{\mathrm{p}}\mathrm{e}^+$) with the goal of measuring the 1s-2s two-photon transition for a comparison to hydrogen as a test of CPT symmetry. The ASACUSA collaboration, of which the author is a member, studies exotic atomic systems containing an antiproton as well as collision processes with low-energy antiprotons. Most relevant for this conference is the precision spectroscopy of antiprotonic helium ($\overline{\mathrm{p}}\mathrm{He}^+$) as well as the plan to measure the ground-state hyperfine structure of antihydrogen as a complementary measurement to the 1s-2s spectroscopy pursued by the other two collaborations. Just recently a fourth collaboration AEGIS has been approved which aims at a study of the gravitation of antimatter using ultra-cold antihydrogen.

A broader physics program will be available at the FLAIR facility (Facility for Low-energy Antiproton and Ion Research) planned at the FAIR facility in Darmstadt. The availability of cooled antiprotons in pulsed and continuous extraction at a factor 100 lower energy than at the AD will greatly improve the progress of current experiments and make many new experiments in nuclear and particle physics possible as described in [1].

*Article based on the presentation by E. Widmann at the Fifth Workshop on Critical Stability, Erice, Sicily, Received December 22, 2008; Accepted January 9, 2009.

** *E-mail address:* eberhard.widmann@oeaw.ac.at

2 Antiprotonic helium: a unique three-body system

Antiprotonic helium is an exotic three-body system consisting of a helium nucleus, an antiproton and an electron (He^{2+}–$\overline{p}$–e^- = $\overline{p}He^+$) which has a series of long-lived metastable states with principal and angular quantum numbers of the antiproton of $(n, l) = 31 \ldots 39$ (cf. Fig. 1). It has been studied in great detail by the PS205 collaboration at LEAR [2] and by ASACUSA at the AD [3].

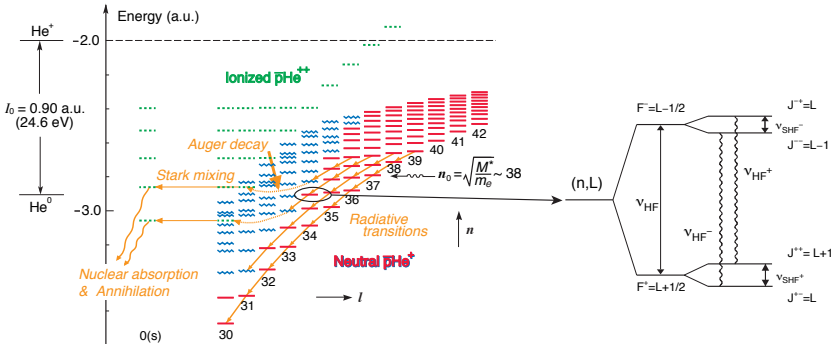

Figure 1. Level diagram of antiprotonic helium. Straight lines correspond to metastable states (life time $\sim \mu$s), wavy lines denote Auger-dominated short-lived states (life time < 10 ns). The lines shown in the left-side diagram actually consist of quadruplets due to the magnetic interaction of its constituents, leading to the hyperfine structure shown at the right-hand side.

In a series of laser spectroscopy experiments, the energy levels of the antiproton have been measured with increasing precision, while the theoretical description has similarily improved. Fig. 2 left shows a comparison of the most recent laser spectroscopy results with two calculations by Korobov and Kino. The agreement of our experimental values to the caclulations of Korobov is in general within the experimental error bars which are of the order of 20 ppb. Since theory uses the numerical value of the proton mass for thr antiproton, a comparison of theory and experiment can be used to extract a CPT test of the proton and antiproton mass. Averaging over all transitions measured in $\overline{p}^4He^+$and $\overline{p}^3He^+$, a precision of 2 ppb was reached for the relative difference of $\overline{p}$ mass and charge.

A second quantity of interest for testing CTP with $\overline{p}He^+$is the magnetic moment $\boldsymbol{\mu}_{\overline{p}}$ of the antiproton, which is known experimentally only to 0.3 % [7]. It manifests itself in a unique hyperfine splitting (cf. Fig. 1) where the dominant splitting arises from the interaction of the antiproton magnetic moment and the electron spin magnetic moment (hyperfine HF structure), while $\boldsymbol{\mu}_{\overline{p}}$ leads to a finer splitting (super hyperfine SHF structure). Using a laser-microwave-laser method, the two M1 transitions labelled $\nu^+_{\rm HF}$ and $\nu^-_{\rm HF}$ in Fig. 1 were measured first in 2001 to a precision of 30 ppm [8], slightly better than the estimated error of theory of $\sim 10^{-4}$ [9]. Since the M1 transitions are dominated by a spin flip of the electron, they are only indirectly sensitive to $\boldsymbol{\mu}_{\overline{p}}$. The combination $\Delta\nu_{\rm HF} = \nu^-_{\rm HF} - \nu^+_{\rm HF} = \nu^+_{\rm SHF} - \nu^-_{\rm SHF}$ on the other hand is directly proportional to $\boldsymbol{\mu}_{\overline{p}}$, but since it is determined by subtracting two large frequencies, its accuracy is much

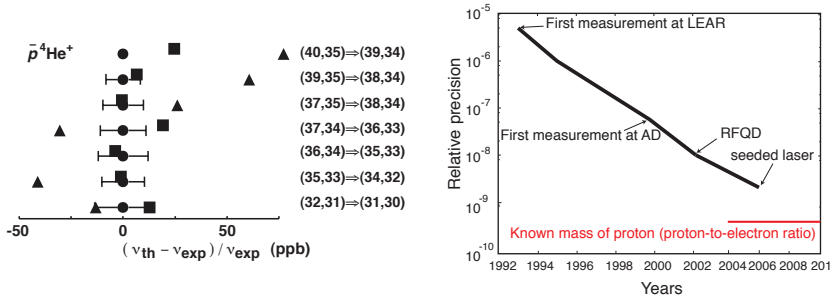

Figure 2. Left: comparison of the most recent laser spectroscopy results (filled circles with error bars [4]) with two calculations by Korobov (squares [5]) and Kino (triangles [6]). Plotted is the relative deviation of theory and experiment in ppb (10^{-9}). Right: Achieved precision of the laser spectroscopy of antiprotonic helium as a function of time.

smaller. The 2001 result corresponds to an error of 1.6 % .

With the aim of improving the experimental accuracy by a factor of 10, a new experiment was performed using a newly developed seeded pulsed laser system similar to the one employed for the precision laser spectroscopy experiments [4]. In a first step, an statistical uncertainty for $\nu_{\mathrm{HF}}^{\pm}$ of 2.3 ppm was already achieved [13] (cf. Fig. 3 left). Likewise, the statistical error on $\Delta\nu_{\mathrm{HF}}$ was reduced to 0.2 %. Fig. 3 (right) shows a comparison of our experimental results for $\Delta\nu_{\mathrm{HF}}$ compared to several theoretical calculations. As can be seen, the experimental value moved closer to theory, although there is still a difference of $\sim 2\sigma$ to the most precise calculation BK [9]. This might be explained by a density shift of the resonance lines as predicted by Korenman [14], so further measurements at different densities as well as checks of other possible systematic errors are needed before a final comparison to theory to extract a value of the antiproton spin magnetic moment can be made.

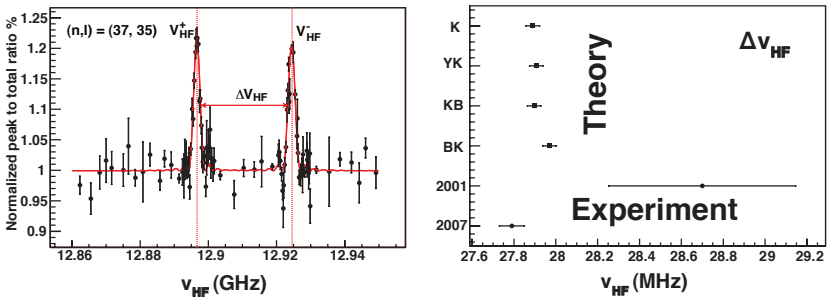

Figure 3. Left: Recent results of the microwave spectroscopy of antiprotonic helium. Right: Comparison of two experimental results with theoretical calculations (K [10] YK [11] KB [9] BK [12]) for $\Delta\nu_{\mathrm{HF}}$.

3 Outlook

Antiprotonic helium is a unique example of how the common efforts by theory and experiment can advance the understanding of the structure of a three-body system, which can generate a means to make precision comparison of the properties of its constituents. The laser spectroscopy measurements have lead to one of the most sensitive tests of CPT in the baryon sector, and the microwave spectroscopy will provide a value of the spin magnetic moment of the antiproton with higher precision than currently known.

Acknowledgement. The author wants to thank all members of the ASACUSA spectroscopy group for their long-lasting collaboration and the AD staff for providing the antiproton beam. This work was supported by Monbukagakusho (Grant No. 15002005), by the Hungarian National Research Foundation (OTKA T046095), by the FP6 project MKTD-CT-2004-509252, and by the Austrian Ministry for Science and Education.

References

1. Widmann, E.: Physica Scripta **72** C51 (2005).
2. Yamazaki, T. et al.: Phys. Rep. **366** 183 (2002).
3. Hayano, R. et al.: Rep. Prog. Phys. **70** 1995 (2007).
4. Hori, M. et al.: Physical Review Letters **96** 243401 (2006).
5. Korobov, V. I.: in: A. Hirtl, J. Marton, E. Widmann and J. Zmeskal (Eds.), Proceedings of the International Conference on Exotic Atoms and Related Topics (EXA'05), Vienna, 2005, Austrian Academy of Sciences Press, Vienna, 2005, pp. 391–400.
6. Kino, Y., Kamimura, M. and Kudo, H.: Nucl. Instrum. Methods Phys. Res. B **412** 84 (2004).
7. Kreissl, A. et al.: Z. Phys. C **37** 557 (1988).
8. Widmann, E. et al.: Phys. Rev. Lett. **89** 243402 (2002).
9. Korobov, V. I. and Bakalov, D.: J. Phys. B: At. Mol. Opt. Phys **34** L519 (2001).
10. Kino, Y. et al.: Hyperfine Interactions **146-147** 331 (2003).
11. Yamanaka, N. et al.: Phys. Rev. A **63** 012518 (2000).
12. Bakalov, D. and Korobov, V. I.: Phys. Rev. A **57** 1662 (1998).
13. Pask, T. et al.: J. Phys. B: At. Mol. Opt. Phys **41** 081008 (2008).
14. Korenman, G. and Yudin, S.: J. Phys. B: At. Mol. Opt. Phys **39** 1473 (2006).

Few-Body Systems 0, 1–4 (2009)

Few-Body Systems

Binding in some few-body systems containing antimatter*

E. A. G. Armour**

School of Mathematical Sciences, University of Nottingham, University Park, Nottingham NG7 2RD, UK

Abstract. It is well known that the system made up of a fixed proton and antiproton and an electron (or a positron) has no bound states if the internuclear distance $R < 0.639a_0$. In this paper, I consider the more complicated system in which the electron and the positron are both present and investigate the possibility of obtaining a lower bound on the value of R for which the system has no bound states. I also investigate the implications of the existence of bound states of the simpler, one light particle system regarding bound states of the more complicated system.

1 Introduction

The system made up of a fixed proton and antiproton and an electron or a positron is a particular case of a charged particle in a dipole field. Many calculations have been carried out on this system.

The first determination of the critical internuclear distance, R_c, below which the dipole cannot bind an electron (or a positron) was carried out by Fermi and Teller. They stated that $R_c = 0.639a_0$. No details were given of the calculation.

Turner [1] gives a good overall review of the calculations on this system, starting with Fermi and Teller. Crawford [2] was able to show that if the internuclear distance $R > R_c$, a *countable infinity* of bound states exists.

It is of interest to consider the more complicated system in which both the electron and the positron are present. In this case the threshold for binding moves down from zero to $-\frac{1}{4}$ a.u., the ground state energy of positronium (Ps). Clearly, there is no binding if $R = 0$. It is reasonable to assume that there exists a critical value of R, R_{cp}, below which the nuclei are unable to bind the electron and the positron.

*Article based on the presentation by E. A. G. Armour at the Fifth Workshop on Critical Stability, Erice, Sicily, Received November 28, 2008; Accepted January 9, 2009.

** *E-mail address:* edward.armour@nottingham.ac.uk

Armour et al. [3] showed using a variational calculation with trial function with 32 basis functions in terms of prolate spheroidal coordinates, some of them Hylleraas-type functions and one basis function representing very weakly bound positronium, that $R_{cp} \leq 0.8a_0$. More recently, Strasburger [4] showed using a variational calculation with a trial function containing 64 to 256 explicitly correlated Gaussian functions that $R_{cp} \leq 0.744a_0$.

In this paper, I will investigate the possibility of obtaining a lower bound on R_{cp} and other conditions on the existence of bound states.

2 Towards a lower bound on R_{cp}

One way to obtain a lower bound on R_{cp} would be to show that $R_{cp} \geq R_c = 0.639a_0$, the critical value for $p\bar{p}e^-$ and $p\bar{p}e^+$, when only the electron or the positron is present. This could be proved if it were possible to show that:

A bound state of $\mathrm{H\overline{H}}$ at $R < R_c \Longrightarrow$ A bound state of

$$p\bar{p}e^- \text{ and } p\bar{p}e^+ \text{ at } R < R_c. \tag{1}$$

For we know that no such bound state of $p\bar{p}e^-$ and $p\bar{p}e^+$ exists. Thus taking the *contrapositive* of (1) $\Rightarrow$ no bound state of $\mathrm{H\overline{H}}$ at $R < R_c$.

Can we prove proposition (1)?

The Hamiltonian, $\hat{H}_f$, for the system is of the form

$$\hat{H}_f = -\tfrac{1}{2}\nabla_1^2 - \tfrac{1}{2}\nabla_2^2 + V - \frac{1}{r_{12}} = \hat{H}_{\text{dip}} - \frac{1}{r_{12}}, \tag{2}$$

where V is the dipole potential. $\hat{H}_f$ can also be expressed in the form

$$\hat{H}_f = -\tfrac{1}{4}\nabla_{\boldsymbol{\rho}}^2 - \nabla_{\boldsymbol{r}_{12}}^2 + V - \frac{1}{r_{12}}, \tag{3}$$

where $\boldsymbol{\rho}$ is the position vector of the centre of mass of the positronium w.r.t. the centre of mass of the nuclei. $\boldsymbol{r}_{12}$ is the position vector of the positron (particle 2) w.r.t. the electron (particle 1).

Suppose that a bound state of the full system does exist for some value of R, i.e., there exists some square-integrable function $\phi(\boldsymbol{r}_1, \boldsymbol{r}_2)$, within the domain of $\hat{H}_f$, for which

$$\hat{H}_f\phi = E\phi \tag{4}$$

where

$$E = -\tfrac{1}{4} - \epsilon \quad (\epsilon > 0). \tag{5}$$

If more than one exists, we shall assume that ϕ is the lowest in energy.

It follows from (4) that

$$\hat{H}_{fc}\phi_c = E\phi_c, \tag{6}$$

where

$$\hat{H}_{fc} = C\hat{H}_f C^{-1}\ , \qquad \phi_c = C\phi. \tag{7}$$

Take

$$C = \exp\left[\frac{ar_{12}}{1+\delta r_{12}}\right], \tag{8}$$

where a and δ are positive constants. Note that C is non-singular as $r_{12} \geq 0$ and $\delta > 0$. Since

$$\lim_{r_{12}\to\infty} C = \exp\left[\frac{a}{\delta}\right], \tag{9}$$

as ϕ is square-integrable, so is ϕ_c.

As $\delta \to 0+$, ϕ_c becomes more and more diffuse, and the effect of the Coulombic interaction becomes less and less. The aim is to use this to uncover the role in binding of the dipole potential V in $\hat{H}_f$.

It follows from equation (5) and (6) that

$$\frac{\langle \phi_c \mid \hat{H}_{fc} \mid \phi_c \rangle}{\langle \phi_c \mid \phi_c \rangle} = E = -\tfrac{1}{4} - \epsilon \quad (\epsilon > 0). \tag{10}$$

It is shown in ref. [5] that it follows from this that

$$\frac{\langle \phi_c \mid \hat{H}_{\rm dip} \mid \phi_c \rangle}{\langle \phi_c \mid \phi_c \rangle} \leq \frac{\langle \phi_c \mid \frac{1}{r_{12}} \mid \phi_c \rangle}{\langle \phi_c \mid \phi_c \rangle} - \epsilon \quad (\epsilon > 0). \tag{11}$$

A tentative proof is given in ref. [5] that it follows from (11) that

$$\frac{\langle \phi_c \mid \hat{H}_{\rm dip} \mid \phi_c \rangle}{\langle \phi_c \mid \phi_c \rangle} \leq \omega\delta^{\frac{1}{2}} + O(\delta) - \epsilon \quad (\epsilon > 0;\ 0 < \omega < \tfrac{3}{2}). \tag{12}$$

This result would imply that, for sufficiently small δ, there exists a square-integrable function, ϕ_c, such that

$$\frac{\langle \phi_c \mid \hat{H}_{\rm dip} \mid \phi_c \rangle}{\langle \phi_c \mid \phi_c \rangle} < 0. \tag{13}$$

It follows from the variational theorem that a bound state of the system exists when the interaction between the electron and the positron is set to zero. This would imply that a bound state of the dipole system made up of the proton and the antiproton and the electron or the positron exists.

3 Qualification

We know from Strasburger's variational calculation [4] that for $R = 0.8a_0$,

$$\epsilon \geq 0.0013148\ a.u. \tag{14}$$

Also we know from Wallis et al.'s exact solution [6] for the system made up of a proton, an antiproton and an electron or a positron, that in the case of the binding energy, ϵ_{ni}, for the two non-interacting particles, if $R = 0.8a_0$,

$$\epsilon_{ni} < 0.0000464\ a.u. \tag{15}$$

Take

$$\epsilon \geq 0.0013148.$$

The inequality (13) implies that it should be possible to find a δ such that

$$\frac{\langle \phi_c \mid \hat{H}_{\rm dip} \mid \phi_c \rangle}{\langle \phi_c \mid \phi_c \rangle} < -\epsilon_{ni} = -0.0000464.$$

This is a contradiction. Further investigation is necessary to determine its cause.

4 Implications from the existence of a bound state of the non-interacting system regarding the existence of bound states of the interacting system

Suppose that the electron and the positron interact through a potential, $-\gamma/r_{12}$, where $\gamma > 0$. Suppose $\hat{H}_{\text{dip}}$ has a bound state, ϕ_d, of energy $-\eta$, where $\eta > 0$.

Recall that there are a countable infinity of bound states of the non-interacting system if $R > R_c$. Thus, for sufficiently small γ, it can be shown that

$$\frac{\langle \phi_d \mid \hat{H}_f(\gamma) \mid \phi_d \rangle}{\langle \phi_d \mid \phi_d \rangle} < -\tfrac{1}{4}\gamma^2 \tag{16}$$

for as many of these states as we please [5]. It is straightforward to show using the Hylleraas–Undheim theorem that it follows from (17) that if γ is such that N such states exist, there must exist M bound states where $1 \leq M \leq N$. M can be expected to increase as N increases.

Strasburger [4] has shown that a bound state of $\hat{H}_f(\gamma)$ exists for $\gamma = 1$ if $R \geq 0.744a_0$. It would thus seem likely that $\gamma_c > 1$ if $R \geq 0.744a_0$.

5 Conclusion

I have set out a tentative proof that $R_{cp} \geq R_c$, where $R_c = 0.639a_0$ is the critical value below which the proton and the antiproton cannot bind an electron (or a positron), on its own. The proof is not satisfactory at present as it gives rise to a contradiction. I hope to be able to resolve this problem.

I have shown that it is comparatively straightforward to make predictions about the existence of bound states of the system containing both light particles from known results for the one particle system, provided the interaction between them is of the form $-\gamma/r_{12}$, where γ is a sufficiently small, positive number.

References

1. Turner, J. E.: *Am. J. Phys.* **45**, 758 (1977).
2. Crawford, O. H.: *Proc. Phys. Soc. (London)* **91**, 279 (1967).
3. Armour, E. A. G., Zeman, V. and Carr, J. M.: *J. Phys. B* **31**, L679 (1998).
4. Strasburger, K.: *J. Phys. B* **35**, L435 (2002).
5. Website, Conference on 'Critical Stability', Ettore Magorana Centre for Scientific Culture, Erice, Sicily, October 2008.
6. Wallis, R. F., Herman, R. and Milnes, H. W.: *J. Molec. Spectroscopy* **4**, 51 (1960).

Few-Body Systems 0, 1–6 (2009)

Few-Body Systems

Can one bind three electrons with a single proton?*

D. Bressanini[1]**, R. Brummelhuis[2] ***,†, P. Duclos[3] ††, R. Ruamps[4] †††

[1] Dipartimento di Scienze Chimiche, Fisiche e Matematiche - Universita'dell'Insubria, Italy
[2] Université de Reims, FRE 3111, Département de mathématique et informatique, Moulin de la Housse, BP 1039 51687 Reims cedex 2, France
[3] Centre de Physique Théorique de Marseille UMR 6207 - Unité Mixte de Recherche du CNRS et des Universités Aix-Marseille I, Aix-Marseille II et de l' Université du Sud Toulon-Var - Laboratoire affilié à la FRUMAM, Luminy Case 907, 13288 Marseille cedex 9, France
[4] 7 place des Pradettes 31100 Toulouse

Abstract. Of course not for an ideal H^{--} atom. But with the help of an intense homogeneous magnetic field B, the question deserves to be reconsidered. It is known (see e.g. [BSY, BD]) that as $B \to \infty$ and in the clamped nucleus approximation, this ion is described by a one dimensional Hamiltonian

$$\sum_{i=1}^{N} -\frac{\Delta_i}{2} - Z\delta(x_i) + \sum_{1\le i<j\le N} \delta(x_i - x_j) \quad \text{acting in} \quad L^2(\mathbb{R}^3) \tag{1}$$

where $N = 3$, $Z = 1$ is the charge of the nucleus, and δ stands for the well known "delta" point interaction. We present an extension of the "skeleton method", see [CDR1, CDR2], to the case of three degree of freedom . This is a tool, that we learn from [R] for the case $N = 2$, which reduces the spectral analysis of (1) to determining the kernel a system of linear integral operators acting on the supports of the delta interactions. As an application of this method we present numerical results which indicates that (1) has a bound state for $Z = 1$ and $N = 3$.

*Article based on the presentation by P. Duclos at the Fifth Workshop on Critical Stability, Erice, Sicily, Received December 16, 2008; Accepted January 27, 2009.
** *E-mail address:* dario.bressanini@uninsubria.it
*** *Alternative address:* Birkbeck, University of London, School of Economics, Mathematics and Statistics, Malet Street, WC1E 7HX, London, UK
† *E-mail address:* raymond.brummelhuis@univ-reims.fr
†† *E-mail address:* duclos@univ-tln.fr
††† *E-mail address:* renaudruamps@free.fr

1 Introduction

It is known by Lieb's inequality [L] that an atom with a nucleus charge Z and an infinite nuclear mass can bind at most N electrons with $N < 2Z + 1$, so that the answer to the question posed in the title is no for such an atom. Even it is strongly believed and numerically and experimentally verified that the bound should be $N \leq Z + 1$. However if one puts the atom in an intense homogeneous magnetic field the number of electrons that can be bound by a nuclear charge Z may increase drastically. The Hamiltonian in such conditions reads

$$H^B(N,Z) := \sum_{j=1}^{N} \frac{(-i\nabla_j - \frac{1}{2}\mathbb{B} \wedge r_j)^2}{2m} - \frac{Z}{|r_j|} + \sum_{1\leq j<k\leq N} \frac{1}{|r_j - r_k|}, \qquad (2)$$

where r_j is the position of the j^{th} electron with respect to the fixed nucleus and $\mathbb{B}$ is a constant magnetic field of strength B. If one introduces the critical number of electrons as (spect $_d X$ stands for discrete spectrum of X)

$$N_c(B,Z) := \max\{N, \text{spect}\,_d H^B(N,Z) \neq \emptyset\}$$

it was shown in [LSY, Th. 1.5] that

$$\liminf_{Z\&\frac{B}{Z^3}\to\infty} \frac{N_c(B,Z)}{Z} \geq 2$$

and they conjectured that the above limit should be indeed 2. The main motivation of the present work is to start the study of the ratio $N/Z_c(B,N)$ with

$$Z_c(B,N) := \inf\{Z, \text{spect}\,_d H^B(N,Z) \neq \emptyset\}$$

for finite Z and N and large B in order to explore how many electrons a charge Z can bind thanks to this strong magnetic field.

The mechanism by which this binding enhancement occurs is well understood: high intensity magnetic fields make the atom one dimensional. It has even been shown, see [BD, Th.1.5], that $H^B(N,Z)$, restricted to any fixed total angular momentum along the magnetic field axis, is asymptotic in the norm resolvent sense to a rescaled version of (1) as $B \to \infty$, at least for spectral parameters in a suitable neighbourhood of the bottom of the spectrum of $H^B(N,Z)$. Thus if we prove that (1) has a discrete eigenvalue for a given charge Z, we can guarantee that this remains true for $H^B(N,Z)$, for a large enough intensity of the magnetic field $\mathbb{B}$. To appreciate the importance of this binding enhancement we shall compare the ratio $N/Z_c(B=\infty,N)$ with the same ones for zero magnetic field with bosonic statistics, see Table 1.

As often in these atomic problems it is convenient to work with the following rescaled version of (1)

$$h(N,\lambda) := \sum_{i=1}^{N} -\frac{\Delta_i}{2} - \delta(x_i) + \lambda \sum_{1\leq i<j\leq N} \delta(x_i - x_j), \quad \lambda := \frac{1}{Z}. \qquad (3)$$

We also remark that to prove the existence of a bound state for $N = 3$ we need only consider $h := h(3, Z)$ in the bosonic sector, see [BD, Th. 1.8 and the discussion in §IX], providing we take the part of $H^B(N, Z)$ with total angular momentum with respect to the magnetic field axis $\mathbb{M} \geq \frac{1}{2}N(N-1)$ with $N = 3$, i.e. $\mathbb{M} \geq 3$.

2 Simple variational approaches

We define a critical value of Z attached to (1) as follows

$$\hat{Z}(N) \quad := \quad \inf\{Z, \text{spect}_{\,\mathrm{d}} h(N, \lambda = \frac{1}{Z}) \neq \emptyset\}$$

which may be considered according to the discussion in §1 as $Z_c(B = \infty, N)$. It is natural to try to find a wave function Ψ so that $(h\Psi, \Psi)$ is below $\Sigma(Z = 1/\lambda)$, the infimum of the essential spectrum of h; $\Sigma(Z)$, which, by the HVZ theorem, is equal to $\inf h(2, \lambda)$, is known only numerically but thanks to the skeleton methods of Rosenthal, [R, Table I], the curve $Z \to \Sigma(Z)$ is known with a fairly good accuracy, sufficient for our purposes, see the solid curve in Figure 1 below. The trial function we take is $\Psi(x) := P_{\text{bose}} \prod_{i=1}^{3} a_i e^{-|a_i|x_i}$, $a_i > 0$ where P_{bose} denotes the projector on the functions which are invariant under the exchange of particles. With $a_1 = a_2 = a_3 = a$ one gets: $(h\Psi, \Psi) = \frac{3}{2}a^2 - 3a + \frac{3\lambda}{2}a$ and optimizing over a leads to $(h\Psi, \Psi) = -\frac{3}{8}(\lambda - 2)^2$. Requiring that this value is below Σ gives $\hat{Z}_c(3) \leq 1.75$. Then with a two parameter function with $a_1 = a_2 = a$ and $a_3 = b$ we get

$$(h\Psi, \Psi) = \frac{2a^3b + 4a^2b^2}{(a+b)^2} - \frac{4a^2b}{(a+b)^2} - \frac{4ab}{a+b} + \lambda\left(\frac{8a^2b}{(3a+b)(a+b)} + \frac{ab}{a+b}\right).$$

Looking for the highest possible value of λ so that $(h\Psi, \Psi)$ is below Σ by a "contour plot", gives $\hat{Z}_c(3) \leq 1.45$. We have also done the computation with three parameters and obtained $\hat{Z}_c(3) \leq 1.32$. One could of course try more elaborate trial functions; we prefer instead to switch to:

3 The skeleton method

Let τ_i, resp. $\tau_{i,j}$ denote the trace (restriction) operators to the plane $x_i = 0$, resp. $x_i = x_j$. To identify these planes with $\mathbb{R}^2$, we choose an oriented basis in each of them as follows: let $\{A_1, A_2, A_3\}$ denote the canonical basis of $\mathbb{R}^3$

equ.	basis	normal	trace op.
$x_1 = 0$	$b^{(1)} := \{A_2, A_3\}$	A_1	τ_1
$x_2 = 0$	$b^{(2)} := \{A_3, A_1\}$	A_2	τ_2
$x_3 = 0$	$b^{(3)} := \{A_1, A_2\}$	A_3	τ_3
$x_1 = x_2$	$b^{(4)} := \{\frac{A_1+A_2}{\sqrt{2}}, A_3\}$	$\frac{-A_2+A_1}{\sqrt{2}} =: A_4$	$\tau_4 := \tau_{1,2}$
$x_2 = x_3$	$b^{(5)} := \{\frac{A_2+A_3}{\sqrt{2}}, A_1\}$	$\frac{-A_3+A_2}{\sqrt{2}} =: A_5$	$\tau_5 := \tau_{2,3}$
$x_3 = x_1$	$b^{(6)} := \{\frac{A_3+A_1}{\sqrt{2}}, A_2\}$	$\frac{-A_1+A_3}{\sqrt{2}} =: A_6$	$\tau_6 := \tau_{3,1}$

.

and define: $(\tau_i\Psi)(s) = \psi(s_1 b_1^{(i)} + s_2 b_2^{(i)})$. Let $\mathcal{H}^1(\mathbb{R}^3)$ denote the usual Sobolev space and $\tau : \mathcal{H}^1(\mathbb{R}^3) \to \oplus_{i=1}^6 L^2(\mathbb{R}^2)$ be defined by $\tau\Psi := (\tau_1\Psi, \tau_2\Psi, \tau_3\Psi, \tau_{1,2}\Psi, \tau_{2,3}\Psi, \tau_{3,1}\Psi)$. Let $h_0 := -\Delta/2$ acting on $L^2(\mathbb{R}^3)$ and $r_0(E) := (h_0 - E)^{-1}$ its resolvent. One can rewrite $h := h(3,\lambda)$ in the sense of quadratic forms as $h = h_0 + \tau^\star g \tau$ where g stands for the 6×6 diagonal matrix with diagonal $(-1,-1,-1,\lambda/\sqrt{2},\lambda/\sqrt{2},\lambda/\sqrt{2})$. If we let $r(E) := (h-E)^{-1}$ then one has using the second resolvent equation that $r(E) = r_0(E) - r_0(E)\tau^\star S(E)^{-1}\tau r_0(E)$ with $S(E) := g^{-1} + K(E)$ and $K(E) := \tau r_0(E)\tau^\star$. We shall use a theorem (see e.g. [CDR2, Th. 2.3] for a proof) which asserts that

$$\Sigma(Z) > -k^2 \in \operatorname{spect}_{\mathrm{d}} h \iff \ker S(-k^2) \neq \{0\}. \tag{4}$$

It will be easier to work in the Fourier image and to perform a scaling so that $S(-k^2)$ appears to be unitarily equivalent to $k(g^{-1}k + \widehat{K(-1)})$. In view of (4) we have to find $k > \sqrt{-\Sigma}$ so that $\ker g^{-1}k + \widehat{K(-1)} \neq \{0\}$ where the hat stands for the Fourier transform. Such a spectral problem in k is sometimes call an operator pencil. We shall call $g^{-1}k + \widehat{K(-1)}$ the *skeleton* of h. $\widehat{K(-1)}$ is a 6×6 matrix of integral operators on $L^2(\mathbb{R}^2)$. To give a flavour we explicitly write down two of them; with the notations: $T_0 := \widehat{K_{i,i}(-1)}$, $T_{i,j} := \tau_i \widehat{r_0(-1)} \tau_j^\star$

$$T_0(p,q) = \tau_i \widehat{r_0(-1)} \tau_i^\star = \frac{\delta(p-q)}{\sqrt{p^2+2}}, \quad T_{1,2}(p,q) = \frac{\delta(q_1 - p_2)}{\pi\left((p_1^2 + p_2^2 + q_2^2) + 2\right)}.$$

It turns out that these integral operators $T_{i,j}$ depend mostly on the angle between the planes on which τ_i and τ_j operate their restriction. That is why we adopt the following notations: $T_{\frac{\pi}{2}} = T_{1,2}$, $T_{\frac{\pi}{4}} = T_{1,4}$, $\tilde{T}_{\frac{\pi}{2}} := T_{1,5}$, $T_{\frac{\pi}{3}} = T_{4,5}$. Thanks to the fact that we are working in the bosonic sector, the skeleton reduces by symmetry to

$$\begin{pmatrix} -k + T_0 + 2T^\sharp_{\frac{\pi}{2}} & 3T^\sharp_{\frac{\pi}{4}} \\ 3(T^\sharp_{\frac{\pi}{4}})^\star & \frac{\sqrt{2}}{\lambda}k + T_0 + 2T_{\frac{\pi}{3}} \end{pmatrix} \tag{5}$$

with $(\varepsilon\psi(p,q) := \psi(q,p))$ $T^\sharp_{\frac{\pi}{2}} := \frac{1}{2}\left(T_{\frac{\pi}{2}} + T^\star_{\frac{\pi}{2}}\right)$, $T^\sharp_{\frac{\pi}{4}} := \frac{1}{3}\left((1+\varepsilon)T_{\frac{\pi}{4}} + \widetilde{T}_{\frac{\pi}{2}}\right)$. Multiplying (5) on the left by the diagonal matrix with diagonal $(1, \lambda/\sqrt{2})$ we arrive at a classical but non selfadjoint eigenvalue problem. We analyse its spectrum numerically using the set of 9 trial functions $\Phi_\beta(p) := \varphi_{\beta_1}(p_1)\varphi_{\beta_2}(p_2)$, with $\beta \in \{0.27, 1.7, 6\}^2$ and $\varphi_{\beta_i}(u) := \exp(-\beta_i u^2), \quad u \in \mathbb{R}$. We get the highest (generalized) eigenvalue k of (5) as a function of λ see Figure 1. This shows that

$$\hat{Z}_c(3) \leq 0.86.$$

Although we do believe that this value 0.86 is very likely to be an upper bound on $\hat{Z}_c(3)$ we warn the reader that beside the uncertainty due to numerics there is also a gap in our reasoning since we are not yet able to justify our use of variational technics for a non selfadjoint operator.

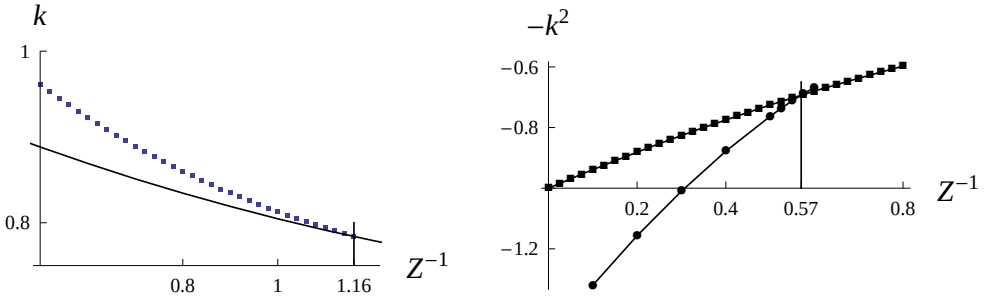

Figure 1. On the letf: the dotted line gives the highest eigenvalue of (5) and the solid line the essential spectrum of (3). On the right: the square dots stand for the energy of the three electrons atoms in $\mathbb{R}^3$ with bosonic statistics obtained by the Diffusion Monte Carlo method [BMBM] and the circle dots for the corresponding two electrons system.

Table 1. Critical ratio

N	2	3
$N/Z_c(0,N)$	2.19	1.71
$N/\hat{Z}_c(N)$	5.31	≥ 3.48

4 Conclusions

As announced in the introduction, we display in Table 1 the numbers of electron per unit of nucleus charge at the critical values of these charges. We have used $Z_c(0,2) \simeq 0.9112$ from [StSt, (2.12) and references therein] and $\hat{Z}_c(2) \simeq 0.377$ from [R]. $\hat{Z}_c(3)$ has been studied in §3. In order to estimate the critical charge $Z_c(0,3)$ for binding three bosonic electrons we used the Diffusion Monte Carlo method [BMBM], which is known to give exact results, within the statistical uncertainty of the method, for bosonic systems. This method employs a guided random walk that sample the exact, unknown ground state function. To guide the random walk and reduce the statistical uncertainty of the results we used a properly symmetrized guiding function of the kind

$$\Psi = P_{\text{bose}} \prod_{i=1}^{3} \exp(-|a_i| r_i) \prod_{i<j} \exp(b_{i,j} r_{i,j}/(1 + c_{i,j} r_{i,j})).$$

The parameters have been optimized for each value of $\lambda = 1/Z$. We performed simulations for $\lambda = 0.1, 0.2, 0.3, 0.4, 0.5, 0.6$. Comparing the energies with the corresponding ones of the 2-body system we located the critical λ between 0.5 and 0.6. In order to locate it more precisely we performed additional simulations in that interval, at steps of 0.025, fitted the results, for both two and three body systems, with quartic polynomials and computed the intersection. We estimate $\lambda_c = 0.570$, see Figure 1 on the right.

References

BMBM. D. Bressanini, G. Morosi, L. Bertini, M. Mella Few Body Systems **31**, 199 (2002)

BSY. B. Baumgartner, J.-Ph. Solovej, J. Yngvason: *Atoms in strong magnetic fields: The high field limit at fixed nuclear charge*, Commun. Math. Physics **212** (3), 703 - 724 (2000)

BD. R. Brummelhuis, P. Duclos: *Effective Hamiltonians for atoms in very strong magnetic fields*. J. Math. Phys. **47**, 032103 (2006)

CDR1. H. Cornean, P. Duclos, B. Ricaud: *Three quantum charged particles interacting through delta potentials*, Few-Body Systems **38**(2-4), 125-131

CDR2. H. Cornean, P. Duclos, B. Ricaud: *On the skeleton method and an application to a quantum scissor* Proceedings and Symposia in Pure Mathematics of the AMS **77** (2008) 657-672,

L. Lieb E.H. : *Bound on the maximum negative ionization of atoms and molecules*. Phys. Rev. A 29, 3018-3028 (1984)

LSY. Lieb H.L., Solovej J. Ph., Yngvason J.: *Asymptotics of Heavy Atoms in High Magnetic Fields: I. Lowest landau band Regions*. Commun. Pure Appl. Math. **47**(4), 513591 (1994)

R. C.M. Rosenthal: *Solution of Delta Function Model for Heliumlike Ions* Journ. Chem. Phys. **35**(5) 2474-2483 (1971)

StSt. F. H. Stillinger and D. K. Stillinger, *Nonlinear variational study of perturbation theory for atoms and ions*, Phys. Rev. A **10** (1974), 1109-1122

Few-Body Systems 0, 1–5 (2009)

Few-Body Systems

Adiabatic spectrum for relativistic hydrogen in a strong homogeneous magnetic field*

R. Brummelhuis[1,2**], Ph. Briet[3***], P. Duclos[3†]

[1] Université de Reims, FR 3111, Département de Mathématique et Informatique, BP 1039, 51687 Reims Cedex 2, France

[2] Birkbeck, University of London, School of Economics, Mathematics and Statistics, Malet Street, N1PB, London, UK

[3] Centre de Physique Théorique de Marseille UMR 6207, Unité Mixte de Recherche du CNRS et des Universités Aix-Marseille I, Aix-Marseille II et de l'Université du Sud Toulon-Var, Laboratoire affilié á la FRUMAM, Luminy Case 907, 13288 Marseille Cedex 9, France

Abstract. We study the bound states of relativistic hydrogen-like atoms coupled to strong homogeneous magnetic fields, assuming a fixed, infinitely heavy nucleus. Working in the adiabatic approximation in which the electron is confined to the lowest Landau level, we show that the corresponding Dirac Hamiltonian always has an infinite discrete spectrum accumulating at mc^2, m being the electron mass, and that, as the field strength increases, its eigenvalues successively descend into the lower part of the continuous spectrum, $(-\infty, -mc^2]$. This phenomenon is for large B roughly periodical in log B.

1 Introduction

The Dirac Hamiltonian for a hydrogen-like atom with nuclear charge Z in a constant magnetic field $\mathbb{B}$ of size B in the z-direction is given by

$$D^B = D_0^B - \frac{\gamma}{|r|}, \quad D_0^B = \overrightarrow{\alpha} \cdot (p + \mathbb{A}) + \beta, \tag{1.1}$$

where we use coordinates $r = (x, y, z) \in \mathbb{R}^3$ and where $p = i^{-1}\nabla_r$. Furthermore, $\gamma := \alpha Z$ with α the fine structure constant, β and $\overrightarrow{\alpha} = (\alpha_x, \alpha_y, \alpha_z)$ are the Dirac matrices:

$$\alpha_j = \begin{pmatrix} 0 & \sigma_j \\ \sigma_j & 0 \end{pmatrix} \ (j = x, y, z), \quad \beta = \begin{pmatrix} 0 & I \\ I & 0 \end{pmatrix},$$

*Article based on the presentation by R. Brummelhuis at the Fifth Workshop on Critical Stability, Erice, Sicily, Received December 16, 2008; Accepted January 27, 2009.

**E-mail address:* raymond.brummelhuis@univ-reims.fr

***E-mail address:* briet@univ-tln.fr

†*E-mail address:* duclos@univ-tln.fr

with σ_j the well-known Pauli matrices, I is the 2×2-identity matrix, and $\mathbb{A}$ is the vector potential, which we choose as $\mathbb{A} := \frac{1}{2}\mathbb{B} \wedge r = \frac{1}{2}B\,(-y, x, 0)$.

1.1 Spectral decomposition of D_0^B

Since $\mathbb{A}$ has a component 0 in the z-direction, we can decompose D_0^B into a transversal and a parallel operator with respect to the magnetic field: $D_0^B = D_{0,\mathrm{tr}}^B + D_{0,//}$, where $D_{0,//} := \alpha_z p_z + \beta m$ is independent of B, and where $D_{0,\mathrm{tr}}^B := \alpha_x(p_x - \frac{1}{2}By) + \alpha_y(p_y + \frac{1}{2}Bx)$. One has $(D_{0,\mathrm{tr}}^B)^2 = H^B \otimes I$, where $H^B = (p_x - \mathbb{A}_x)^2 + (p_y - \mathbb{A}_y^2 + B\sigma_z = -\Delta_{x,y} + \frac{1}{4}B(x^2+y^2) + BL_z + B\sigma_z$ is the Pauli-Hamiltonian in a constant magnetic field, which has an explicitly known pure point-spectrum, consisting of non-negative integer multiples of $2B$, each of which is has infinite multiplicity (cf. e.g. [2]). Let $\Pi_{\mathcal{L}}^B$ be the orthogonal projection onto the (infinite dimensional) kernel of $(D_{0,\mathrm{tr}}^B)^2$. Since for a self-adjoint operator A, $\mathrm{Ker}(A^2) = \mathrm{Ker}(A)$, this is also the orthogonal projection onto the kernel of $D_{0,\mathrm{tr}}^B$, which we will call the *relativistic lowest Landau-level*, $\mathcal{L}^B$, of $D_{0,\mathrm{tr}}^B$; here "lowest" has to be interpreted in the sense of absolute value: the spectrum of $D_{0,\mathrm{tr}}^B$ can be shown to be $\sqrt{2B}\mathbb{Z}$, and consequently $|D_{0,\mathrm{tr}}^B| \geq \sqrt{2B}$ on the orthogonal complement of $\mathcal{L}^B$.

To remove the infinite degeneracy, we take advantage of the fact that D^B, D_0^B and $D_{0,\mathrm{tr}}^B$ all commute with $J_z = L_z + S_z$, the total angular momentum in the z-direction, and that we can therefore fix an angular momentum channel $J_z = j$, $j \in \frac{1}{2} + \mathbb{Z}$. If we indicate restrictions to this angular momentum channel by the superscript "$J_z = j$", then we have that the image of $\Pi_{\mathcal{L}}^{B,J_z=j}$ is non-zero iff $j = \ell - 1/2$ with $\ell \leq 0$. Moreover, for such j, $\mathrm{Im}\,\Pi_{\mathcal{L}}^{B,J_z=j}$ is one-dimensional and spanned by the spinor

$$\chi_\ell(x+iy)\begin{pmatrix} 0 \\ 1 \\ 0 \\ 1 \end{pmatrix}, \quad \chi_\ell\left(\rho e^{i\varphi}\right) := (2\pi 2^\ell \ell!)^{-1/2} B^{1/2}\, \rho^\ell e^{-i\ell\varphi} e^{-B\rho^2/4}.$$

We still have that $|D_0^{B,J_z=j}| \geq \sqrt{2B}$ on the orthogonal complement of $\mathrm{Im}\,\Pi_{\mathcal{L}}^{B,J_z=\ell}$. For simplicity we will limit ourselves to the case of $j = -1/2$. This is not an essential restriction, though, and our calculations will carry through, with modifications, for general $j \in -\frac{1}{2} - \mathbb{N}$.

2 Adiabatic approximation

We will work in the adiabatic approximation, in which, for large B, the electron is assumed to be "frozen" in its lowest Landau orbits in directions perpendicular to the field $\mathbb{B}$. This means replacing the exact Hamiltonian D^B by the "lowest Landau" Hamiltonian $d_{\mathcal{L}}^B := \Pi_{\mathcal{L}}^{B,J_z=-1/2} D^B \Pi_{\mathcal{L}}^{B,J_z=-1/2}$ (where we henceforth leave off the superscript indicating the angular momentum channel). The Hamiltonian $d_{\mathcal{L}}^B$ is one-dimensional, and effectively acts on two-component wave-functions as

$$d_{\mathcal{L}}^B \;=\; d_{0,z} + V_{\mathcal{L}}^B(z),\; d_{0,z} = \begin{pmatrix} m & p_z \\ p_z & -m \end{pmatrix}; \tag{2.1}$$

with $V_{\mathcal{L}}^B(z) := -\gamma\langle\chi_0^B||r|^{-1}|\chi_0^B\rangle = \sqrt{B}V_{\mathcal{L}}^1(\sqrt{B}z)$; explicitly,

$$V_{\mathcal{L}}^1(z) = -\gamma\int_0^\infty \frac{e^{-u}}{\sqrt{2u+z^2}}\,du. \tag{2.2}$$

Note that d_0^B is the free Dirac operator in dimension 1.

This of course begs the question of whether we can relate the spectra of D^B and $d_{\mathcal{L}}^B$. For large B, a large amount of (positive or negative) energy is needed to go from the lowest Landau level into one of the others, and the question is whether the attractive Coulomb potential can provide that energy. In the non-relativistic case the answer was "no", at least asymptotically for very large B; mathematically, this translated into the norm-resolvent convergence of the full Hamiltonian to its projection onto the lowest Landau level in [2]. In the relativistic case, the situation is not that clear, basically because both Coulomb potential and the Dirac operator have the same order of homogeneity -1, a well-known problem in rigorous relativistic quantum mechanics. A further analysis, using the techniques of [2], shows that one can prove norm-resolvent convergence of D^B to $d_{\mathcal{L}}^B$ if we allow γ to be B-dependent and require that $\gamma\sqrt{B}\to 0$, cf. [1]. More generally, we can do perturbation theory around $d_{\mathcal{L}}^B$ of $\gamma\sqrt{B}\ll 1$, that is $B\ll\alpha^2\simeq 18769$ for hydrogen. Since in our units $B=1$ already corresponds to $4.4\,10^9$ Tesla, this may not be an unreasonable assumption for the lighter atoms.

3 Large-B approximation of $d_{\mathcal{L}}^B$

The eigenvalue-problem for $d_{\mathcal{L}}^B$ does not seem to be directly solvable in closed form, but we can further simplify the operator for large values of B. If $U_{\pi/2}$ denotes the rotation of $\mathbb{C}^2$ by $\pi/4$, it is convenient to introduce

$$\widetilde{d}_{\mathcal{L}}^B := U_{\pi/4}^{-1}\,d_{\mathcal{L}}^B\,U_{\pi/4} = \begin{pmatrix} p_z+V_{\mathcal{L}}^B & -m \\ -m & -p_z+V_{\mathcal{L}}^B \end{pmatrix}.$$

We note that for $z\neq 0$, $V_{\mathcal{L}}^B(z)\to -\gamma|z|^{-1}$. One can now show that as $B\to\infty$, $\widetilde{d}_{\mathcal{L}}^{\infty,B}$ is asymptotic, in norm-resolvent sense, to a suitably defined regularization of the one-dimensional Dirac + Coulomb Hamiltonian (rotated by $\pi/4$):

Proposition 3.1 *Define the operator $d_{\mathcal{L}}^{\infty,B}$ on $L^2(\mathbb{R},\mathbb{C}^2)$ by*

$$\widetilde{d}_{\mathcal{L}}^{\infty,B} := \begin{pmatrix} p_z-\gamma/|z| & m \\ m & -p_z-\gamma/|z| \end{pmatrix},$$

with domain those $u=(u_1,u_2)\in L^2(\mathbb{R},\mathbb{C}^2)$ such that $u_j\in H^1(|z|\geq\varepsilon)$ for all $\varepsilon>0$ ($j=1,2$) and satisfying the following boundary condition in 0:

$$e^{i(-1)^j\gamma(\log B+c)}\varepsilon^{i(-1)^j\gamma}u_j(\varepsilon)\simeq\varepsilon^{-i(-1)^j\gamma}u_j(-\varepsilon),\quad \varepsilon\downarrow 0,\quad j=1,2,$$

where $c=\log 2-\Gamma'(1)$, and $\simeq$ means that the difference tends to 0 with ε. Then $d_{\mathcal{L}}^{\infty,B}$ is self-adjoint and we have that for all complex $\xi\notin\mathbb{R}$,

$$\lim_{B\to\infty}||\,(\widetilde{d}_{\mathcal{L}}^B-\xi)^{-1}-(\widetilde{d}_{\mathcal{L}}^{\infty,B}-\xi)^{-1}\,||=0.$$

Observe that $\widetilde{d}_{\mathcal{L}}^{\infty,B}$ still depends on B, through the boundary conditions, which in fact are periodic in $\log B$. The eigenvalue problem for $\widetilde{d}_{\mathcal{L}}^{\infty,B}$ can be explicitly solved with the help of Whittaker functions. Before stating the result, we note the following symmetry of the operator: let $P : u(z) \to u(-z)$ be the parity operator, and let $\mathcal{E} : (u_1, u_2) \to (u_2, u_1)$ exchange the components of the spinor u. Then $\widetilde{d}_{\mathcal{L}}^{\infty,B}$ commutes with $P\mathcal{E}$, which has eigenvalues ± 1, and we can reduce the operator accordingly.

Theorem 3.2 *Let $F_\pm : (-m, m) \to \{\zeta \in \mathbb{C} : |\zeta| = 1\}$ be given by*

$$F_\pm(E) := (\mp)\,\frac{E + i\tau/2}{|E + i\tau/2|} \cdot \frac{\Gamma(1 - 2i\gamma)}{\Gamma(1 + 2i\gamma)} \cdot \frac{\Gamma(1 + i\gamma - \kappa)}{\Gamma(1 - i\gamma - \kappa)} \cdot \tau^{2i\gamma} e^{-ic\gamma} \tag{3.1}$$

where $\tau = \tau(E) := 2\sqrt{m^2 - E^2}$ and $\kappa := \kappa(E) := \gamma E/\sqrt{m^2 - E^2}$. Then $E \in (-m, m)$ is an eigenvalue of $\widetilde{d}_{\mathcal{L}}^{\infty,B}$ in the $\pm$-sector of the Parity & Exchange operator $P\mathcal{E}$ iff $F_\pm(E) = e^{i\gamma \log B} = B^{i\gamma}$.

An equivalent way of stating the eigenvalue condition is that $A_\pm(E) := \mathrm{Arg}\,(F_\pm(E)) = i\gamma \log B \bmod 2\pi$, where $\mathrm{Arg}(\zeta) \in (-\pi, \pi]$ denotes the principal value of the argument of $\zeta \in \mathbb{C} \setminus 0$. Graphical analysis shows that for small γ and given $B > 0$, $\widetilde{d}_{\mathcal{L}}^{\infty,B}$ will have infinitely many eigenvalues $E_0^\pm(B) < E_1^\pm(B) < \cdots$ in $(-m, m)$ accumulating at m, see figure 1 below, for an illustration for $\gamma = 0.5$. The eigenvalues in either sector are monotonically decreasing in B, and the lowest eigenvalue $E_0^+(B)$ will, for a certain critical value B_c of the field, be absorbed into lower continuous spectrum $(-\infty, -m]$, at which point $E_0^-(B)$ will become the new lowest eigenvalue, and the whole process will repeat itself, periodically in $\log B$ with period $2\pi/\gamma$. As a consequence of norm-resolvent convergence, the same phenomenon will occur for $d_{\mathcal{L}}^B$ if B is sufficiently large, the periodicity becoming approximate. We note that in reference [3] it was recently shown, by a variational argument involving a min-max characterisation of the ground state of Dirac operators in the spectral gap $(-m, m)$ and comparison with $d_{\mathcal{L}}^B$, that the ground state of D^B enters the negative continuous spectrum for a certain $B_c = B_c(\gamma)$. This left open the question of whether there remained other eigenvalues. Our result answers this for $d_{\mathcal{L}}^B$ when B is sufficiently large, and also for D^B in the limit of $\gamma\sqrt{B} \to 0$.

Concerning the critical values of B, one can use Stirling's formula to show that

$$\lim_{E \to -m} F_\pm(E) = \mp \frac{\Gamma(1 - 2i\gamma)}{\Gamma(1 + 2i\gamma)} \left(\frac{2\gamma m}{e^{c/2}}\right)^{2i\gamma}, \tag{3.2}$$

The critical values B_c of the magnetic field for which $E_0^\pm(B_c) = -m$ will have to satisfy $B_c^{i\gamma} =$ Right Hand Side of (3.2). We note that if $B_c(\gamma)$ is the first critical $B > 1$, then $\lim_{\gamma \to 0} \gamma \log B_c = \pi$, confirming a result of [3]; (3.2) allows us to derive an asymptotic expansion of $\gamma B_c(\gamma)$ for small γ.

*Acknowledgement.*This research was supported by a grant from *Alliance: Franco-British Partnership Programme 2006 and 2007*, project Number PN 06.015.

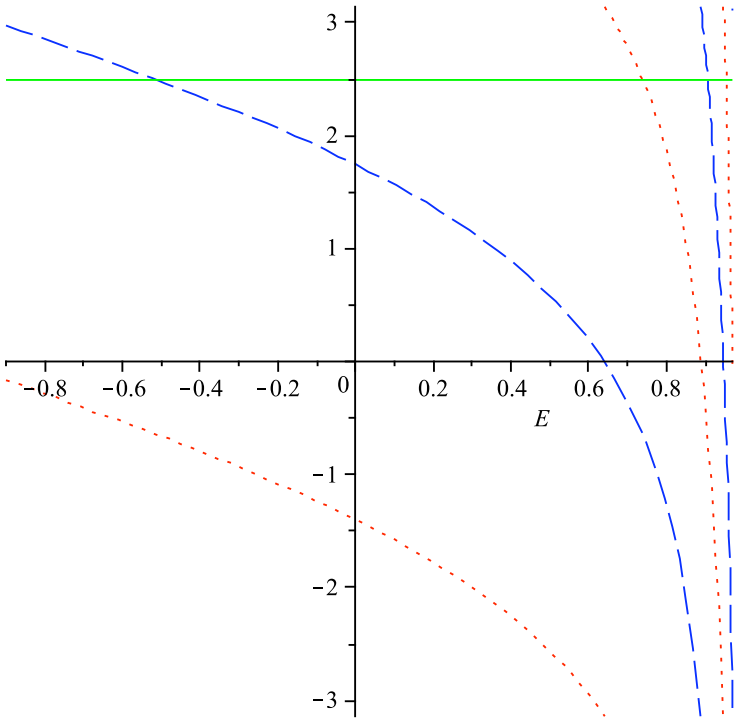

Figure 1. Graphs of $A_+(E)$ (dots), $A_-(E)$ (dashes) and $\gamma \log B = 2.5 \bmod 2\pi$ (solid), $\gamma = 0.5$

References

1. Briet, Ph., Brummelhuis, R., and Duclos, P.: in preparation.
2. Brummelhuis, R. , Duclos, P.: J. Math. Phys. **47**, 032103 (2006).
3. Dolbeault, J., Esteban, M., Loss, M.: Ann. H. Poincare **8**, 749 (2007).

Few-Body Systems 0, 1–4 (2009)

Few-Body Systems

A Mathematical Theory for Vibrational Levels Associated with Hydrogen Bonds*

George A. Hagedorn[1] , Alain Joye[2]

[1] Department of Mathematics and Center for Statistical Mechanics, Mathematical Physics, and Theoretical Chemistry, Virginia Polytechnic Institute and State University, Blacksburg, Virginia 24061–0123, U.S.A.

[2] Université de Grenoble, Institut Fourier, Unité Mixte de Recherche CNRS-UJF 5582, BP 74, F–38402 Saint Martin d'Hères Cedex, France,

Abstract. We describe recent work in which we propose an alternative to the usual time independent Born-Oppenheimer approximation that is specifically designed to describe molecules with Hydrogen bonds. In our approach, the masses of the Hydrogen nuclei are scaled differently from those of the heavier nuclei, and we employ a specialized form for the electron energy level surface. Consequently, anharmonic effects play a role in the leading order calculations of vibrational levels for symmetric molecules. For non-symmetrical molecules, the different vibrational modes appear at different orders of approximation.

1 Introduction

The standard time-independent Born-Oppenheimer (BO for short) approximation [1] takes advantage of the large masses of the nuclei relative to the mass of the electrons. With mass unit given by the mass of the electrons, the masses of the nuclei are of order ϵ^{-4}, with ϵ small. It allows one to compute the low-lying vibrational states of the nuclear motion from knowledge of the ground state electron energy surface near its minimum, under the following two assumptions: the ground state is isolated from the other energy surfaces near its minimum and the minimum is non-degenerate. To leading order, as is well known, the vibrational energy levels are those of a harmonic oscillator (HO for short) associated with the non-degenerate minimum, see [3] for a recent review and references.

Despite its many successes, this approximation may fail to give accurate results when applied to molecules that contain hydrogen bonds. The binding energy of such bonds is typically very small, and the mass of the Hydrogen nucleus is an order of magnitude smaller than that of other nuclei such as Carbon.

*Article based on the presentation by A. Joye at the Fifth Workshop on Critical Stability, Erice, Sicily, Received December 22, 2008; Accepted January 25, 2009.

Moreover, the experimental vibrational spectra of some tri-atomic molecules with hydrogen bonds, such as F-H-F^- and F-H-Cl^-, display significant deviations from the approximate harmonic spectrum, see [2].

In [4, 6], we revisit the BO approximation in order to propose an alternative taking into account the specificities of simple molecules that contain hydrogen bonds. Our approach differs from the standard BO approximation in the following way. First, we scale the masses of the Hydrogen nuclei as ϵ^{-3} while keeping the heavier nuclei scale as ϵ^{-4}. Note that for $\epsilon \simeq 0.082$ corresponding to the mass of the Carbon nucleus, the mass of the Hydrogen nucleus is approximately equal to $1.015\epsilon^{-3}$ times that of the electrons. Second, we model the electron energy surface in a special way that depends on ϵ. This takes into account the smallness of some coefficients of the harmonic potential associated with the hydrogen bond. The case of symmetric linear tri-atomic molecules in which bending is ignored is dealt with in [4], whereas [6] is devoted to asymmetric tri-atomic molecules in which rotations are included. Note that the local behaviour of the ground state energy surface around a minimum is enough to describe the low energy vibrational levels because the corresponding wave packets are strongly localized close to this minimum, as $\epsilon \to 0$. We describe these two model cases in an informal way below.

In order to keep things simple, we only discuss here the scalar Hamiltonians obtained by reducing the molecular Hamiltonian to kinetic energy plus smooth potential given by the ground state energy surface, E_{GS}. Extensions of these results to the full molecular Hamiltonians are provided in [4, 6].

2 The symmetric case

We consider here a tri-atomic molecule of the form A-H-A, where the A's are nuclei of masses ϵ^{-4} and H is a Hydrogen nucleus of mass ϵ^{-3}. The nuclei are constrained to move on a fixed axis. The reduced scalar Hamiltonian reads

$$H_S(\epsilon) = -\frac{\epsilon^4}{2}\Delta_W - \frac{\epsilon^3}{2}\Delta_Z + E_{GS}(\epsilon, W, Z) \tag{1}$$

where the Jacobi coordinates $(W, Z) \in \mathbb{R}^2$ give the distance between the two nuclei A and the location of the H nucleus w.r.t. the center of mass of the two A's, see Fig. 1. Some inessential factors coming from reduced masses are

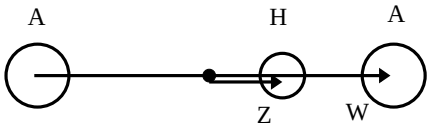

Figure 1. Coordinate system for A-H-A

simplified by a trivial rescaling of the variable Z. At equilibrium, we assume the molecule is symmetrical so that the minimum of the ground state energy surface lies at $(W_0, 0)$, with $W_0 > 0$. Numerics on the ion F-H-F^- suggest the expansion

$$\begin{aligned} E_{GS}(\epsilon, W, Z) &= E_0 + a_1(W - W_0)^2 + (a_2\epsilon - a_3(W - W_0))Z^2 + a_4 Z^4 + \cdots \\ &\equiv E_1(\epsilon,\, W,\, Z) + O((W - W_0)^\alpha Z^{2\beta}), \quad \alpha, \beta \in \mathbb{N},\ \alpha + \beta \geq 3, \end{aligned} \tag{2}$$

where the ϵ dependence only enters in the coefficient of Z^2, which is much smaller than the other coefficients. Note that symmetry implies an expansion in Z^2 and $E_1(\epsilon, W, Z)$ is bounded below in case the following condition holds:

$$a_1, a_3, a_4 > 0, \quad \text{and either} \quad a_3^2 < 4a_1a_4, \quad \text{or} \quad a_3^2 = 4a_1a_4 \quad \text{and} \quad a_2 \geq 0. \tag{3}$$

Keeping only the leading term E_1 in the expansion defines the approximation $H_1(\epsilon) = -\frac{\epsilon^4}{2}\Delta_W - \frac{\epsilon^3}{2}\Delta_Z + E_1(\epsilon, W, Z)$. By rescaling the variables according to $w = (W - W_0)/\epsilon$, $z = Z/\epsilon^{1/2}$, $H_1(\epsilon)$ is equivalent to $E_0 + \epsilon^2 H_{NF}$, where the ϵ-independent, anharmonic, normal form Hamiltonian reads

$$H_{NF} = -\frac{1}{2}\Delta_w - \frac{1}{2}\Delta_z + a_1w^2 + (a_2 - a_3w)z^2 + a_4z^4. \tag{4}$$

It is proven in [4] that under condition (3) the spectrum of H_{NF} is discrete and that it is related to the spectrum of $H_S(\epsilon)$, $\sigma(H_S(\epsilon))$, in the following sense: *For any eigenvalue $\mathcal{E}_{NF}^{(j)}$ of H_{NF}, there exists $\mathcal{E}_S(\epsilon)$ in $\sigma(H_S(\epsilon))$ such that*

$$\mathcal{E}_S(\epsilon) = E_0 + \epsilon^2\mathcal{E}_{NF}^{(j)} + O(\epsilon^3), \quad as \quad \epsilon \to 0. \tag{5}$$

Such results hold for more mass scales and other ϵ-dependent potentials, see [5].

3 The non-symmetric case

Here a tri-atomic molecule of the form *A-H-B* is considered, in a full three dimensional setting. Again, we start from the reduced scalar Hamiltonian in Jacobi coordinates. They are defined as in Fig. 2: $\boldsymbol{X}$ is the vector from the heavy nucleus A to the Hydrogen nucleus H whereas $\boldsymbol{Y}$ links the center of mass of AH to the other heavy nucleus B. We express $\boldsymbol{Y}$ by means of spherical coordinates with respect to the center of mass frame of reference as $\boldsymbol{Y} = (Y, \theta, \phi)$. For $\boldsymbol{X}$, we use a moving frame with third axis z' parallel to $\boldsymbol{Y}$ and first axis parallel to $\boldsymbol{Y} \wedge z$, z being the third axis of the fixed frame. Using cylindical coordinates in the moving frame, we get $\boldsymbol{X} = (R, \gamma, X)$. In these variables, the ground state

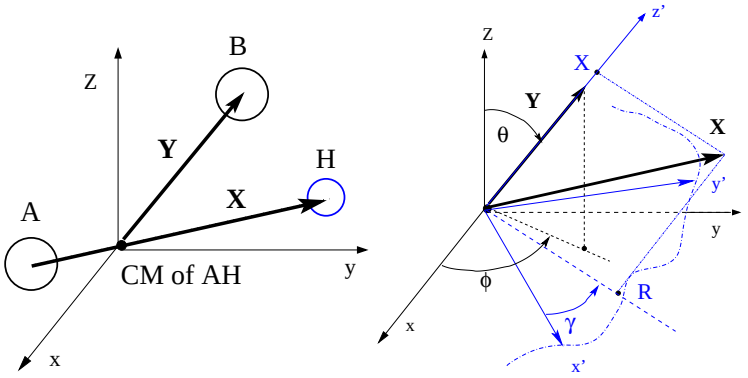

Figure 2. Coordinate system for *A-H-B*

energy surface does not depend on the angles, but the kinetic energy becomes messy. Taking mass scales as above, the scalar Hamiltonian reads

$$H_S(\epsilon) = -\frac{\epsilon^3}{2\mu_1(\epsilon)}\Delta_{\boldsymbol{X}} - \frac{\epsilon^4}{2\mu_2(\epsilon)}\Delta_{\boldsymbol{Y}} + E_{GS}(\epsilon, X, R, Y), \tag{6}$$

where $\mu_j(\epsilon)$ are reduced masses that are regular in ϵ. The molecule is assumed to be linear, *i.e.* at equilibrium, $\boldsymbol{X}$ and $\boldsymbol{Y}$ are colinear, so that $R_{\rm eq} = 0$.

The behaviour of the ground state close to the equilibrium point $(X_0, 0, Y_0)$ is modelled after comparisons with numerics on a typical case, here F-H-Cl^-, and taking into account the symmetries. We consider

$$\begin{aligned} E_{GS}(\epsilon, X, R, Y) &= V_1(X) + \epsilon V_2(X, R, Y), \qquad (7)\\ \text{with} \qquad V_1(X) &= a_0 + a_2(X - X_0)^2 + \cdots \\ V_2(X, R, Y) &= b_{0,2,0}R^2 + b_{1,0,1}(X - X_0)(Y - Y_0) + b_{0,0,2}(Y - Y_0)^2 + \cdots \end{aligned}$$

The decomposition (7) reflects the fact that the molecule behaves like a compound AH interacting weakly with B, depending on the "proton affinities" of A and B. Also, the quadratic term in $(X - X_0)$ in V_2 is incorporated in V_1.

Making explicit the kinetic energy, expanding $H_S(\epsilon)$ in powers of $\epsilon^{1/4}$ and taking into account the scales of the quantum fluctuations leads to

$$\begin{aligned} H_S(\epsilon) = a_0 &- \frac{\epsilon^3}{2\mu_1}\left(\frac{\partial^2}{\partial R^2} + \frac{1}{R}\frac{\partial}{\partial R} + \frac{1}{R^2}\,\frac{\partial^2}{\partial \gamma^2}\right) + \epsilon\, b_{0,2,0}R^2 \\ &- \frac{\epsilon^3}{2\mu_1}\frac{\partial^2}{\partial X^2} + a_2(X - X_0)^2 - \frac{\epsilon^4}{2\,\mu_2}\frac{\partial^2}{\partial Y^2} + \epsilon\, b_{0,0,2}(Y - Y_0)^2 + \cdots \qquad (8) \end{aligned}$$

where the remaining terms can be safely neglected. This leading term is the sum of a one dimension HO describing the A-H streching modes, a two dimensional HO corresponding to degenerate bending modes and a one dimensional HO associated with the AH-B streching modes. The corresponding eigenvalues appear at different orders in ϵ and are given by

$$\begin{aligned} \mathcal{E}_X^{(n_1)}(\epsilon) &= \epsilon^{3/2}\sqrt{2a_2/\mu_1}(n_1 + 1/2), \qquad \mathcal{E}_{R,\gamma}^{(n_2)}(\epsilon) = \epsilon^{4/2}\sqrt{2b_{0,2,0}/\mu_1}(n_2 + 1), \\ \mathcal{E}_Y^{(n_3)}(\epsilon) &= \epsilon^{5/2}\sqrt{2b_{0,0,2}/\mu_2}(n_3 + 1/2). \qquad (9) \end{aligned}$$

It is shown in [6] that these HO approximate $H_S(\epsilon)$ in the sense that:
For any choice of eigenvalue (9), there exists $\mathcal{E}_S(\epsilon)$ in $\sigma(H_S(\epsilon))$ such that

$$\mathcal{E}_S(\epsilon) = a_0 + \mathcal{E}_X^{(n_1)}(\epsilon) + \mathcal{E}_{R,\gamma}^{(n_2)}(\epsilon) + \mathcal{E}_Y^{(n_3)}(\epsilon) + O(\epsilon^3), \quad \textit{as} \quad \epsilon \to 0. \qquad (10)$$

Acknowledgement. A.J. wishes to thank the organizers of "Critical Stability V" for a very interesting and enjoyable meeting.

References

1. Born, M., Oppenheimer, J.R. , *Ann. Phys.* (Leipzig) **84**, 457, (1927)
2. Elghobashi, N. and González, L. , *J. Chem. Phys.* **124**, article 174308 (2006).
3. Hagedorn, G.A., Joye, A., *AMS Proc. of Symp. in Pure Math.* **76** , 203, (2007)
4. Hagedorn, G.A., Joye, A. , *Commun. Math. Phys.* **274**, 691, (2007)
5. Hagedorn, G.A., Joye, A., *AMS Contemp. Math. Series*, **447**, 139, (2007)
6. Hagedorn, G.A., Joye, A., *Rev. Math. Phys.*, to appear.

Few-Body Systems 0, 1–4 (2009)

Few-Body Systems

How to model p-scattering using point interactions and related problems*

P. Kurasov**,***

Department of Mathematics, LTH, Box 118, Lund University, 221 00 Lund, Sweden,
Department of Mathematics, Stockholm University, 106 91 Stockholm, Sweden,
Department of Physics, S:t Petersburg University, 198904 St. Peterhof, Russia

Abstract. A new type of point interactions for the Laplacian in $\mathbb{R}^3$ is constructed generalizing classical Fermi pseudopotential. This model leads to a new resolvent formula and a non-trivial scattering matrix in p-channel.

1 Introduction

It is well-known that the celebrated Fermi delta potential [2, 3] leads to non-trivial scattering in the s-channel only. We propose a new family of point interaction models which may be used to describe particles with non-trivial interaction also in the p-channel while preserving exact solvability and point character of the interaction [4]. These models are given by self-adjoint operators and their spectral and scattering properties are discussed. Similar physical models have been discussed during the conference (see contributions by J. Macek, S. Wycech and others). The developed method can be also applied to model the system of three quantum particles. One may expect that the corresponding operator is semibounded (in contrast to the Landau Hamiltonian studied by Skorniakov-Ter-Martirosyan and Minlos-Faddeev in the sixties [5]).

2 Fermi-Berezin-Faddeev point interaction

The stationary Schrödinger operator with delta potential is formally defined by

$$-\Delta + \alpha\delta \equiv -\Delta + \alpha\delta\langle\delta, \cdot\rangle. \tag{1}$$

F.A. Berezin and L.D. Faddeev [2] interpreted this operator as the Laplace operator L_θ defined on the domain of functions from the Sobolev space $W_2^2(\mathbb{R}^3 \setminus \{0\})$[1]

*Article based on the presentation by P. Kurasov at the Fifth Workshop on Critical Stability, Erice, Sicily, Received November 27, 2008; Accepted January 27, 2009.
**Supported in part by Swedish Research Council Grant number 500092501
***E-mail address:* pak@math.su.se
[1]The Sobolev space W_2^s is best characterized using Fourier transform as $(1 + |\mathbf{p}|)^s \hat{f}(\mathbf{p}) \in L_2(\mathbb{R}^3)$.

possessing the asymptotic representation $U(x) = \frac{u_-}{4\pi|\mathbf{x}|} + u_0 + o(1)$, as $\mathbb{R}^3 \ni \mathbf{x} \to 0$ and the boundary conditions $u_0 = \cot\theta\ u_-,\ \ \theta \in [0, \pi)$. In general there is no relation between the parameters α and θ, but it may be established using homogeneity requirements [1].

The operator L_θ can also be seen as the differential Laplace operator defined on the set of functions satisfying the representation $U = U_r + u_1 \frac{e^{-\beta|x|}}{4\pi|x|}$, where $U_r \in W_2^2(\mathbb{R}^3), u_1 \in \mathbb{C}$, $\beta > 0$, and the boundary condition $U_r(0) = (\cot\theta + \frac{\beta}{4\pi})u_1$. The parameters β and θ determining L_θ in this representation are not independent.

The operator L_θ is self-adjoint in $L^2(\mathbb{R}^3)$, its absolutely continuous spectrum is $[0, \infty)$ and it has a unique eigenvalue $E_0 = -(4\pi\cot\theta)^2$, provided $\cot\theta < 0$. The corresponding bound state eigenfunction is spherically symmetric and the scattering amplitude does not depend on the angle between the incoming and outgoing waves.

3 Why p-type point interactions are impossible in $L_2(\mathbb{R}^3)$?

Several attempts to define higher order point interactions lead to operators in Pontryagin spaces (with indefinite metrics), making these models not very attractive for physical applications.[2] The impossibility to define such interactions in the original Hilbert space follows from the fact that all self-adjoint extensions of the operator $-\Delta|_{C_0^\infty(\mathbb{R}^3\setminus\{0\})}$ coincide with the family L_θ. It is expected that the operator with a high order interaction at the origin is defined on the functions possessing the representation $U_r(x) + u_1 g_1$, where g_1 is a certain solution of the Helmholtz equation having singularity at the origin. Every such solution different from $e^{-\beta|\mathbf{x}|}/4\pi|\mathbf{x}|$ has a non square integrable singularity. The corresponding boundary condition should contain derivatives of U_r at the origin, which are properly defined only if U_r belongs to the Sobolev space W_2^s with $s > 2$. For example the first derivatives are defined if U_r belongs to W_2^3, which is precisely the domain of the Laplacian considered as an operator in W_2^1 instead of L_2.[3]

4 Cascade model for p-scattering

A mathematically rigorous interpretation for the formal operator

$$-\Delta + \sum_{i=1}^{3} \alpha \partial_{x_i} \delta \langle \partial_{x_i} \delta, \cdot \rangle, \qquad \alpha \in \mathbb{R} \tag{2}$$

can be given in the following way.[4] Consider the following three singular solutions

[2] See in particular papers by Yu. Shondin, A. Tip, J.F. van Diejen, A. Dijksma, H. Langer and C.G. Zeinstra.

[3] This fact is usually known as *Sobolev embedding theorem*.

[4] The first model of this type was developed using abstract mathematical language by K. Watanabe and the author when they tried to analyse an article by I. Andronov. It was realized later that this model leads to a natural generalization of von Neumann extension theory [4].

to the Helmholtz equation $(-\Delta+\beta_1^2)g_j=0,\ \mathbf{x}\neq 0$, where $\beta_1>0$

$$g_j=\frac{\partial}{\partial x_j}\frac{e^{-\beta_1|\mathbf{x}|}}{4\pi|\mathbf{x}|}=-\frac{\beta_1|\mathbf{x}|+1}{4\pi|\mathbf{x}|^3}e^{-\beta_1|\mathbf{x}|}x_j\notin L_2(\mathbb{R}^3),\quad g_j=(-\Delta+\beta_1^2)^{-1}\partial_{x_j}\delta$$

and the Hilbert space

$$\mathbb{H}=W_2^1(\mathbb{R}^3)\dot{+}\mathcal{L}\{g_1,g_2,g_3\}\ni\mathbb{U}=U+\sum_{i=1}^3u_1^ig_i=U-\frac{\beta_1|\mathbf{x}|+1}{4\pi|\mathbf{x}|^3}e^{-\beta_1|\mathbf{x}|}\mathbf{x}^t\cdot\mathbf{u}_1,$$

with the norm $||\mathbb{U}||^2_{\mathbb{H}}=||\sqrt{-\Delta+\beta_1^2}U||^2_{L_2}+\gamma||\mathbf{u}_1||^2$, where $\gamma>0$. The operator associated with (2) in $\mathbb{H}$ is defined as a restriction of the operator $\mathbb{A}$ acting as the differential Laplace operator outside the origin $\mathbb{A}\mathbb{U}=-(\mathbb{U}_{x_1x_1}+\mathbb{U}_{x_2x_2}+\mathbb{U}_{x_3x_3}),\ \mathbf{x}\neq 0$. Consider another positive parameter $\beta\neq\beta_1$ and introduce

$$G_i=\frac{1}{\beta_1^2-\beta^2}(g_i(-\beta^2)-g_i(-\beta_1^2)),\quad G_i=(-\Delta+\beta^2)^{-1}g_i.$$

Then the family of self-adjoint in $\mathbb{H}$ operator $\mathbb{A}_\theta$, $\theta\in[0,\pi)$ is defined on the functions possessing the representation

$$\mathbb{U}=U_r+\sum_{i=1}^3u^iG_i+\sum_{i=1}^3u_1^ig_i,\quad U_r\in W_2^3(\mathbb{R}^3),\mathbf{u},\mathbf{u}_1\in\mathbb{C}^3,$$

and the boundary conditions $\sin\theta\,(\nabla U_r(0)+\gamma\mathbf{u}_1)=\cos\theta\,\mathbf{u}$, by the formula

$$\mathbb{A}_\theta\left(U_r+\sum_{i=1}^3u^iG_i+\sum_{i=1}^3u_1^ig_i\right)=-\Delta U_r-\beta^2\sum_{i=1}^3u^iG_i+\sum_{i=1}^3(u^i-\beta_1^2u_1^i)g_i.$$

The self-adjoint operator $\mathbb{A}_\theta$ - rigorous interpretation for the formal operator (2), - is defined on the functions forming cascade of less and less singular elements. It is described by four real parameters $\beta,\beta_1,\gamma,\theta$ (not all independent).

5 Properties of the cascade model

The operator $\mathbb{A}_\theta$ is self-adjoint in the Hilbert space $\mathbb{H}$, and describes a certain point interaction, which is not of s-type as Berezin-Faddeev one. The operator commutes with the rotations around the origin and reflections in planes passing through the origin, *i.e.* this constructed point interaction is spherically symmetric. The spectrum has an absolutely continuous branch $[0,\infty)$ and negative eigenvalues having multiplicity three. The spectral properties of the operator are encoded in the following rational Nevanlinna function

$$Q(\lambda)=\frac{1}{12\pi}\left\{ik+\frac{\beta_1^2}{ik-\beta_1}+\beta+\frac{\beta_1^2}{\beta+\beta_1}\right\}+\frac{\gamma}{-\beta_1^2-k^2},\quad k\sqrt{\lambda}.$$

Continuous spectrum (generalized) eigenfunctions are

$$\mathbb{V}(\lambda,\mathbf{k}/k,\mathbf{x})=e^{i\mathbf{k}\cdot\mathbf{x}}+\frac{i}{(k^2+\beta_1^2)(Q(k^2)+\cot\theta)}\frac{ik|\mathbf{x}|-1}{4\pi|\mathbf{x}|^3}e^{ik|\mathbf{x}|}\mathbf{x}^t\cdot\mathbf{k},$$

and we see that the scattering amplitude $\frac{-\lambda\cos(\widehat{\mathbf{x},\mathbf{k}})}{4\pi(\lambda+\beta_1^2)(Q(\lambda)+\cot\theta)}$ depends on the angle between the incoming and outgoing waves. Hence the scattering matrix is non-trivial in the p-channel.

The bound state eigenfunctions are

$$\mathbb{V}_{\lambda_0} = -\frac{\chi|\mathbf{x}|+1}{4\pi|\mathbf{x}|^3}e^{-\chi|\mathbf{x}|}\mathbf{x}\cdot\mathbf{a}, \quad \lambda_0 = -\chi^2,$$

where $\chi > 0$ is a solution to the equation $Q(-\chi^2) + \cot\theta = 0$.

The function Q appears also in the denominator of the resolvent $(\mathbb{A}-\lambda)^{-1}$ in $\mathbb{H}$. The restriction of the resolvent to the infinite dimensional subspace $W_2^1(\mathbb{R}^3) \subset \mathbb{H}$ has the form which reminds of classical Krein's resolvent formula[5]

$$(\mathbb{A}_\theta - \lambda)^{-1}U = \frac{1}{-\Delta-\lambda}U - \frac{1}{(\lambda+\beta_1^2)(Q(\lambda)+\cot\theta)}\times \left(\int_{\mathbb{R}^3}\frac{(ik|\mathbf{y}|-1)e^{ik|\mathbf{y}|}}{4\pi|\mathbf{y}|^3}\mathbf{y}^t U(\mathbf{y})d^3\mathbf{y}\right)\frac{(ik|\mathbf{x}|-1)e^{ik|\mathbf{x}|}}{4\pi|\mathbf{x}|^3}\mathbf{x}. \quad (3)$$

Note that the function appearing in the denominator is not any longer a Nevanlinna function as it is growing like $\lambda^{3/2}$, $\lambda\to\infty$.

6 Perspectives

The suggested model can be generalized to include even higher order point interactions. Analytic properties of these operators and new families of eigenfunction expansions based on the resolvent formula (3) were discussed by A. Luger and the author.

Acknowledgement. The author would like to thank the organizers for putting together an extremely stimulating conference, which allowed to develop new ideas and find listeners to the old ones.

References

1. S. Albeverio and P. Kurasov, Singular Perturbations of Differentail Operators, Cambridge Univ. Press, 2001.
2. F.A.Berezin, L.D.Faddeev, Remark on the Schrödinger equation with singular potential. (Russian) *Dokl. Akad. Nauk SSSR*, **137** (1961), 1011–1014.
3. E. Fermi, Sul moto dei neutroni nelle sostanze idrogenate, *Ricerca Scientifica*, **7** (1936), 13–52 (In Italian.), English translation in E.Fermi, Collected papers, vol. I, Italy 1921–1938, Univ. of Chicago Press, Chicago, 1962, pp. 980–1016.
4. P. Kurasov, Triplet extensions I: semibounded operators in the scale of Hilbert spaces, accepted for publication in *J. d'Analyse Mathématique*.
5. R.A. Minlos and L.D. Faddeev, Comment on the problem of three particles with point interactions, *Soviet Physics JETP*, **14** (1962), 1315–1316.

[5]Note that we consider here not the bordered resolvent, but just the restriction of $(\mathbb{A}-\lambda)^{-1}$ to the subspace $W_2^1 \subset \mathbb{H}$.

Few-Body Systems 0, 1–6 (2009)

Few-Body Systems

Calculating few-body resonances using an oscillator trap*

D.V. Fedorov[1]**, A.S. Jensen[1], M. Thøgersen[1], E. Garrido[2], R. de Diego[2]

[1] Aarhus University, 8000 Aarhus C, Denmark
[2] Instituto de Estructura de la Materia, CSIC, Serrano 123 E-28006 Madrid, Spain

Abstract. We investigate the possibility of calculating the parameters of few-body resonances using the oscillator trap boundary conditions. We place the few-body system in an oscillator trap and calculate the energy spectrum and the strength function of a suitably chosen transition. Broader resonances are identified as Lorentzian peaks in the strength function. Narrower resonances are identified through the pattern of avoided crossings in the spectrum of the system as function of the trap size. As an example we calculate 0_2^+ and 0_3^+ resonances in ^{12}C within the 3α model.

1 Introduction

Few-body resonances are often calculated using the complex scaling method where the resonances are identified as generalized complex eigenvalues of the Hamiltonian with the corresponding generalized eigenfunctions (see e.g. [1, 2] and references therein). The method has the advantage of having a simple boundary condition: the few-body wave-function vanishes at large distances. However, it also has certain disadvantages. Complex arithmetics and algorithms are generally slower and complex matrices need more computer memory. Calculating extremely narrow resonances is difficult as it demands calculations of the eigenvalues with exceedingly high accuracy. Interpretation of the generalized eigenfunctions is also not trivial [1], especially for heavy complex scaling needed for broader resonances.

In this contribution we investigate the possibility of calculating the parameters of few-body resonances using the same simple boundary condition as in complex scaling method but working with real energies and real wave-functions.

We place the few-body system in an artificial oscillator trap of length b which is significantly larger than the characteristic length of the few-body system. We

*Article based on the presentation by D. Fedorov at the Fifth Workshop on Critical Stability, Erice, Sicily, Received December 10, 2008; Accepted January 23, 2009
** *E-mail address:*fedorov@phys.au.dk

then calculate the (discrete) spectrum of the system in the trap and estimate the strength function of a certain transition from a suitable chosen initial state to the positive-energy states of the system in the trap.

The broader resonances with width $\Gamma \gtrsim \hbar^2/(2mb^2)$, where m is the characteristic mass of the few-body system, can be identified as Lorentzian peaks in the strength function. A similar idea of identifying resonances through a strength function has been suggested in [3] in connection with the Lorentz-integral-transform method.

The narrow resonances with $\Gamma < \hbar^2/(2mb^2)$ need an investigation of the spectrum of the system in the trap as function of the trap length. When an energy level in the trap, following its general behavior as b^{-2}, approaches the system's resonance level to within its width, the two levels interfere and avoid crossing. The pattern of avoided crossings in the spectrum of the system in the trap reveals the position of the narrow resonance. The width of the resonance can be estimated from the size of the region of avoided crossing, or, more precisely, from the variation of the energy levels with respect to the trap length.

The approach is similar to the box method (also called the stabilization method) [4, 5]. However, the difference is that we use an oscillator trap instead of a box and that we resort to strength function method for broader resonances where the avoided crossings method is less reliable. The box boundary condition is more complicated as the wave-function has to vanish identically at the box boundary which for few-body systems is a multi-dimensional surface. The oscillator trap can be potentially used in stochastic variational calculations with correlated Gaussians [6].

As an example we apply the approach to the 3α system in the $J^\pi{=}0^+$ channel where there exist a narrow, 0^+_2, and a broader, 0^+_3, resonance. We show that the approach allows to reliably calculate the two resonances in this system.

2 The few-body system and the trap

We consider the 3α system with the total angular momentum and parity $J^\pi{=}0^+$. The Ali-Bodmer type α-α potential is taken from [7],

$$\begin{aligned} V_{\alpha\alpha}(r) &= \left(125\hat{P}_{l=0} + 20\hat{P}_{l=2}\right) e^{-\left(\frac{r}{1.53}\right)^2} - 30.18\, e^{-\left(\frac{r}{2.85}\right)^2} \\ &+ \frac{4\cdot 1.44}{r}\,\mathrm{erf}\left(\frac{r}{2.32}\right), \end{aligned} \tag{1}$$

where all energies are in MeV, all lengths in fm, $\hat{P}_l$ is the projection operator onto a state with relative orbital momentum l, and r is the distance between α-particles. In addition a three-body force

$$V_3(\rho) = -76\,\mathrm{MeV}\,\exp(-\rho^2/(4\mathrm{fm})^2)\,, \tag{2}$$

is employed to simulate the contribution of "compound nucleus" degrees of freedom at shorter distances where all three α-particles overlap. The three-body force is defined in terms of the hyper-radius

$$\rho^2 = \frac{m_\alpha}{m}\sum_{i=1}^{3} r_i^2\,, \tag{3}$$

where r_i are the c.m. coordinates of the α-particles, m=939 MeV is the chosen mass scale and m_α=3.97m.

The system is placed in an oscillator trap

$$V_{\rm trap} = \frac{\hbar^2}{2m}\frac{\rho^2}{b^4} \ , \tag{4}$$

where the trap length b is varied around 30-40 fm.

The three-body problem in the trap is solved using the adiabatic hyperspherical method (see e.g. [2] and references therein). First for every fixed hyperradius ρ the eigenvalue problem for all remaining variables (denoted collectively as hyper-angles Ω) is solved and the spectrum of hyper-angular eigenvalues $\epsilon_i(\rho)$ together with the angular eigenfunctions $\Phi_i(\rho,\Omega)$ are obtained. The functions $\Phi_i(\rho,\Omega)$ are then used as a full basis in the Ω space and the total wave-function ψ is represented as a series

$$\psi(\rho,\Omega) = \sum_{i=1}^{\infty} f_i(\rho)\Phi_i(\rho,\Omega) \ , \tag{5}$$

where the expansion coefficients $f_i(\rho)$ are obtained by solving the hyper-radial equations where the eigenvalues $\epsilon_i(\rho)$ serve as effective potentials.

3 Strength function

A resonance can be identified as a peak in a reaction cross-section with approximately Lorentzian shape. The amplitude of a quantum transition, caused by an operator F, from some initial state ψ_a into one of the discrete state ψ_n (with the energy E_n) of the system in the trap, is given in the Born approximation as

$$M_{n\leftarrow a} = \langle\psi_n|F|\psi_a\rangle \ . \tag{6}$$

Since a resonance per definition must be seen in any reaction channel, the particular choice of the excitation operator F and the initial state ψ_a should be irrelevant as soon as the matrix element does not vanish identically. We thus choose the initial state in the form of the large ρ asymptotics of a bound three-body state [8, 9],

$$f_i(\rho) = \rho^{-5/2}\exp(-\rho/b_3), \tag{7}$$

in every hyper-radial channel i. The constant b_3=4 fm is chosen close to the size of the bound state of 3α system. The excitation operator is taken as

$$F = \rho^2 \ . \tag{8}$$

The cross-section of a reaction into the final states with energies $E \pm \frac{\Delta E}{2}$ is determined by the strength function, defined as

$$S(E) = \frac{1}{\Delta E}\sum_{E_n\in E\pm\frac{\Delta E}{2}} |M_{n\leftarrow a}|^2 \ . \tag{9}$$

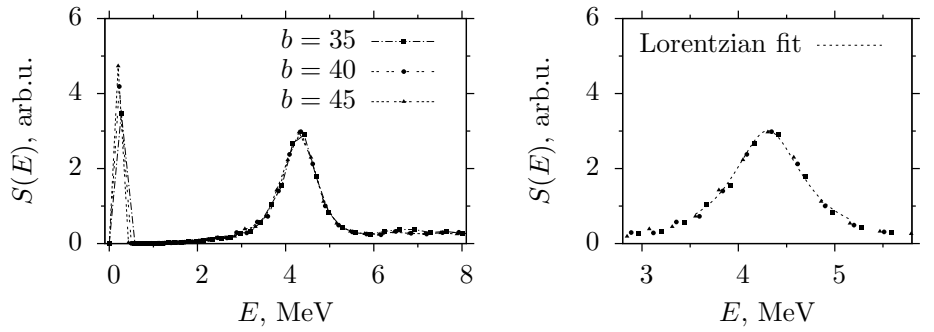

Figure 1. Left: the strength function $S(E)$ as function of the 3α energy E for different oscillator lengths b. Right: the peak at 4.3 MeV is fitted with a Lorentzian, Const/$[(E - E_r)^2 + \Gamma^2/4]$, where E_r=4.3 MeV and Γ=0.9 MeV.

The energy bin size ΔE has to be chosen on the one hand small enough as not to smear out the essential features of the cross-section, and on the other hand large enough to include many states. In our calculations the energy bins include four states each.

The calculated strength function is shown on Figure 1. It reveals a broader peak at 4.3 MeV and a narrow unresolved peak at ∼0.4 MeV. In the region of the broader peak the strength function is well converged with respect to the trap length, and the bin size is quite appropriate for the description of the width of the peak as there are many points within the peak region.

The shape of the peak is well described by a Lorentzian

$$S(E) \overset{E\approx E_r}{\propto} \frac{1}{(E - E_r)^2 + \frac{\Gamma^2}{4}} \tag{10}$$

with E_r=4.3 MeV and Γ=0.9 MeV. These numbers are consistent with [2].

The narrow peak at in the strength function ∼0.4MeV is represented by only one point. The position of the point reveals the resonance energy but not the width. To resolve the width at least several points are needed within the peak region. For resonances width exceedingly narrow width Γ this would demand unreasonably large trap lengths of the order $b \sim \sqrt{\hbar^2/(2m\Gamma)}$.

However instead of the strength function the avoided crossings method can be used to calculate narrow resonances using reasonably sized traps.

4 Avoided crossings

For large trap lengths the energy levels in the trap, E_n, scale with the trap size as $\hbar\omega \propto b^{-2}$. By varying the trap size a level in the trap can be moved close to the resonance level of the system. If the resonance were behind a completely impenetrable barrier (thus having a vanishing width) there would be no interference through the barrier between the resonance and the state in the external trap. The resonance would then be insensitive to the trap size. The spectrum of the system in the trap, as function of the trap size, would thus show the trap levels scaling as b^{-2} and crossing the resonance energy represented by a horizontal line.

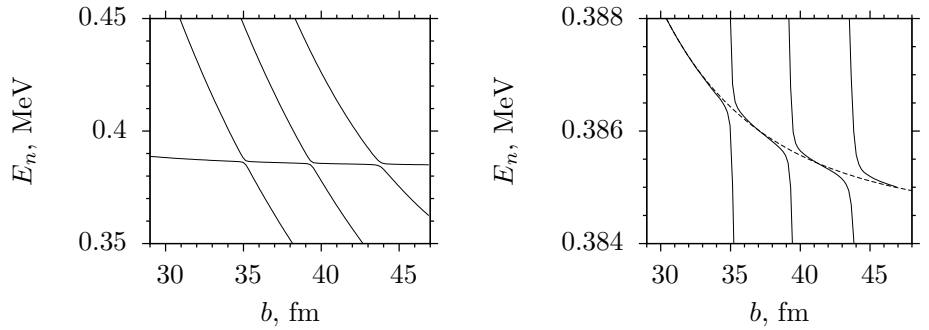

Figure 2. Left: the spectrum of the 3α system in an oscillator trap as function of the trap size b in the region of the narrow peak on Figure 1: the sequence of avoided crossings indicates a resonance at ~ 0.38 MeV; Right: zoom-in into the region of avoided crossings: the resonance energy is fitted with $E(b) = E_r + Kb^{-4}$ with $E_r = 0.38435$ MeV and K=7.471^4 MeV fm^4.

If the barrier has small but finite penetrability the trap level approaching the resonance to within its width becomes perturbed by the resonance resulting in the "repulsion" of the two interfering levels. This shows up as a sequence of avoided crossings in the spectrum of the system in the trap as function of the trap size in the vicinity of the narrow resonance, see Figure 2 (left).

The resonance state gets a contribution from the oscillator potential (4) which at large b is proportional to b^{-4}. This contribution can be determined by a fit $E_r + Kb^{-4}$ through the resonance energies as shown on Figure 2 (right). The fit also provides the asymptotic estimate of the resonance energy $E_r = 0.38435\,\mathrm{MeV}$.

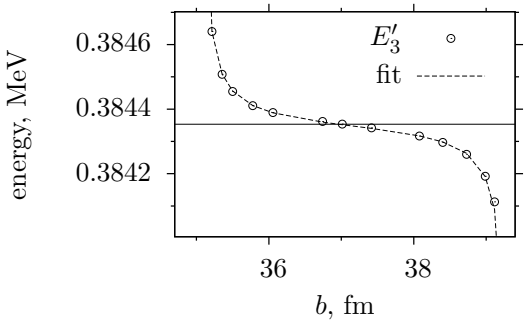

Figure 3. The reduced energy $E_3' \equiv E_3 - Kb^{-4}$ of the third level of the 3α system in an oscillator trap as function of the trap length b in the region of the resonance $E_r = 0.38435\,\mathrm{MeV}$ (indicated as a horizontal line) where the parameters K and E_r are from the fit of the resonance energy on Figure 2. The energy E_3' is fitted with the curve $\frac{b-b_3}{\Delta b_3} = \arctan\frac{\Gamma/2}{E-E_r}$ where b_3, Δb_3, and Γ are fitting parameters. The fit gives $\Gamma = 77\,\mathrm{eV}$.

Figure 3 shows the reduced energy of the third level, $E_3' \equiv E_3 - Kb^{-4}$, where the oscillator contribution is subtracted. It is possible to estimate the width Γ of the resonance from the plot assuming that the energy region where the avoided

crossing takes place is determined by the width of the resonance,

$$\frac{\Gamma}{2} = \Delta b \left. \frac{\partial E'_n}{\partial b} \right|_{E_n = E_r} , \tag{11}$$

where Δb is the distance between the neighboring avoided crossings.

However, instead of numerical differentiation it is better to estimate the width by fitting the calculated energies with the curve

$$\frac{b - b_n}{\Delta b_n} = \arctan \frac{\Gamma/2}{E'_n - E_r} , \tag{12}$$

where b_n, Δb_n, and Γ are fitting parameters. Figure 3 (right) shows such a fit for E_3 which gives $\Gamma = 77\,\mathrm{eV}$. This value is consistent with the estimates of 10-30 eV in [7, 10] taking into account that our three-body potential provides a slightly higher E_r.

5 Conclusion

Using the two lowest $J^\pi{=}0^+$ resonances in the 3α system as an example, we have investigated the possibility of calculating the energies and widths of few-body resonances by placing the few-body system in an artificial oscillator trap. The oscillator trap has particularly simple boundary condition and can be potentially used in stochastic variational calculations with correlated Gaussians.

We have shown that broader resonances with the width $\Gamma \gtrsim \hbar^2/(2mb^2)$, where b is the trap size, can be identified as Lorentzian peaks in the strength function of a suitably chosen "gedanken" transition. Narrower resonances can be identified through the pattern of avoided crossings in the spectrum of the system in the trap as function of the trap size.

References

1. Elander N, et. al.: AIP Conf. Proc. 998, 43 (2008)
2. Fedorov DV, Garrido E, Jensen AS: Few Body Systems 33, 153 (2003)
3. Leidemann W, Few-Body Systems 42, 139 (2008)
4. Maier CH, Cederbaum LS, Domcke W: J. Phys. B 13, L119 (1980)
5. Zhang L, et. al.: Phys. Rev. C 77, 014312 (2008)
6. Thøgersen M, Fedorov DV, Jensen AS: EPL 83, 30012 (2008)
7. Fedorov DV, Jensen AS: Phys. Lett. B 389, 631 (1996)
8. Nielsen E, et. al.: Physics Reports, 347, 373 (2001)
9. Pushkin A, Jonson B, Zhukov MV: J. Phys. G 22, L95 (1996)
10. Fedotov SI, et. al.: Phys. Rev. C 70, 014006 (2004)

Few-Body Systems 0, 1–6 (2009)

Few-Body Systems

Quantum scattering with the driven Schrödinger approach and complex scaling *

Nils Elander**, Mikhail Volkov***, Åsa Larson†, Michael Stenrup††, J. Zsolt Mezei†††, Evgeny Yarevsky‡ and Sergey Yakovlev‡‡

Molecular Physics Division, AlbaNova University Center, Stockholm University, SE 106 91 Stockholm, Sweden

Abstract. Quantum scattering calculations of two and three-body systems with Coulomb interaction using the driven Schrödinger equation combined with exterior complex scaling are discussed. A rigorous formulation for two-body scattering is reported, and its generalization to three-body scattering is considered.

1 Introduction.

The understanding of the dynamics of small molecular systems have made a considerable progress during the past ten years. The identification of the measured peak in the cross section of the reaction $F + HD(v', j') \rightarrow FHD \rightarrow FH(v'', j'') + D$ as an isolated resonance would not have been possible if not for the simultaneous theoretical and computational developments described in [1]. A number of other experimental and theoretical studies demonstrate the existence of resonances in several primary chemical reactions [2, 3]. Theoretical methods to describe these reactions were created by Manolopoulos, Schatz, Clary, Launay, Alexander and others and are reviewed in Refs. [2, 3]. Most of these methods are based on the hyperspherical approach and are limited to at most a few potential energy surfaces and neutral reactants and products.

*Article based on the presentations by M. Volkov and N. Elander at the Fifth Workshop on the Dynamics and Structure of Critically Stable Quantum Few-Body Systems, Erice, Italy, 2008. December 4, 2008; Accepted January 13, 2009

** *E-mail address:* elander@physto.se
*** *E-mail address:* miha@physto.se
† *E-mail address:* aasal @physto.se
†† *E-mail address:* stenrup@physto.se
††† *E-mail address:* mezeijzs@physto.se
‡ *E-mail address:* yarevsky@gmail.com, *Permanent address: Chair of Computational Physics, Department of Physics, St. Petersburg State University, St. Petersburg, Russia*
‡‡ *E-mail address:* sl-yakovlev@yandex.ru *Permanent address: Chair of Computational Physics, Department of Physics, St. Petersburg State University, St. Petersburg, Russia*

Naturally abundant reactions may also include charged reactants or products. Some such processes may be studied in the double electrostatic storage ring DESIREE [4], which is currently being built at Stockholm university. The mutual neutralization reaction $H^+ + H^- \to H_2^* \to H(1) + H(n)$ [5], where n is a principal quantum number, will be one of the first experiments in this ring. The charge transfer reaction $N^{3+} + H \to NH^{3+} \to N^{2+} + H^+$ [6] is another candidate for early experiments. Another interesting experiment is the similar three-body reaction $H_2^+ + H^- \to H_3^* \to H_2 + H$. A theoretical-computational study of this reaction can be performed using a method that can describe many-channel, three-body scattering of charged particles in a full angular momentum framework (MCTSCPFAM) which includes the features of Refs. [5, 6].

In a well quoted short paper Nuttal and Cohen [7] propose the use of the driven Schrödinger equation combined with complex scaling [8] to compute quantum cross sections for short range potentials. McCurdy, Rescigno and coworkers [9] have recently explored this method [7] combined with exterior complex scaling [8] (ECS) in several electron-atom (molecule) scattering studies.

The present study is focused on developing theoretical and computational methods for MCTSCPFAM. The driven Schrödinger approach is discussed in section 2. In the following section 3 we give an outline of a new proof showing that the method of ref. [9], in the two-body case, can be rigorously generalized to include a potential composed of a short range potential and a long range Coulomb contribution. For a more complete discussion of this work we refer to recent work of Volkov *et al.* [10]. We then outline how to generalize the method [10] to a many channel, three-body problem in section 4.

2 The driven Schrödinger equation - an introduction

The idea in Ref. [7] was to consider the Schrödinger equation and split the wave function into an incoming Ψ_{in} and a scattered Ψ_{scat} part, $\Psi = \Psi_{in} + \Psi_{scat}$. As the incoming wave satisfies the free Schrödinger equation, we find

$$(H - E)\Psi = 0 \quad \Rightarrow \quad (H - E)\Psi_{scat} = -(H - E)\Psi_{in} = -V\Psi_{in}, \qquad (1)$$

where V is the potential energy. With given boundary conditions, including ECS we can compute the scattered wave for an arbitrary energy E. Following Ref. [7] one can use complex scaling to obtain zero boundary condition at infinity if the potential there decreases exponentially or faster. McCurdy, Rescigno and coworkers [9] realized, without presenting rigorous arguments, that this method could be extended to long-range potentials. Scattering quantities like the amplitude and the S-matrix can then be computed. Below we use atomic unit.

3 The two-body problem for Coulomb plus short-range potentials.

Let the reduced mass be one. The partial wave $\Psi_\ell(k, r)$ with angular momentum ℓ satisfies the radial Schrödinger equation $(H_\ell + V - k^2)\Psi_\ell = 0$. Here, the "free" Hamiltonian is $H_\ell = -\partial_r^2 + \ell(\ell + 1)/r^2$ and the interaction potential $V(r) = 2q/r + V_s(r)$, where q is a charge. The short-range potential V_s is assumed to vanish faster than $1/r^2$ at large r.

The asymptotic form of the scattering solution is defined in terms of the Coulomb wave functions [11]. Let $\eta = q/k$. The scattering amplitude $\mathcal{A} = e^{2\mathrm{i}\sigma_\ell}(e^{2\mathrm{i}\delta_\ell} - 1)/(2\mathrm{i})$, where $\sigma_\ell = \arg\Gamma(1 + \ell + \mathrm{i}\eta)$, is determined by the phase shift δ_ℓ, which is due to the presence of the potential V_s.

In order to reformulate the problem in terms of a driven Schrödinger equation, the potential V is split into a sum of an interior part, V_R, and an exterior part, V^R, such that $V = V_R + V^R$. Here R is a parametrical radius chosen such that $V(r) \ll E$ for $r \geq R$. The finite-range interior potential V_R is introduced in such a way that $V_R = V$, if $r \leq R$, and $V_R = 0$ otherwise. The splitting of the wave function $\Psi_\ell = \Psi_R + \Psi^R$ leads to the inhomogeneous equation

$$(H_\ell + V - k^2)\Psi_R = -V_R\Psi^R \tag{2}$$

provided that Ψ^R obeys the Schrödinger scattering problem for the exterior potential

$$(H_\ell + V^R - k^2)\Psi^R = 0, \tag{3}$$

with the corresponding amplitude $\mathcal{A}^R$. Eq. (3) defines Ψ^R. For $r \leq R$ the potential V^R vanishes ($V^R(r) = 0$). Therefore, the function $\Psi^R(k, r)$ must be proportional to the Riccati-Bessel function $\hat{j}_\ell$:

$$\Psi^R(k, r) = a^R \hat{j}_\ell(kr). \tag{4}$$

The function $\Psi^R(k, r)$ for $r > R$ can be expressed in terms of Jost solutions [11]. The requirement for the wave function and its derivative to obey the continuity conditions at the point $r = R$ completes the construction of Ψ^R. This construction provides a way to calculate a^R and the amplitude $\mathcal{A}^R$, defined through the relation $\mathcal{A}^R = e^{2\mathrm{i}\sigma_\ell}(e^{2\mathrm{i}\delta^R} - 1)/(2\mathrm{i})$.

Once the wave function Ψ^R has been constructed, Eq. (2) is well defined. By imposing the boundary conditions

$$\Psi_R(k, 0) = 0, \qquad \Psi_R(k, r) \sim \mathcal{A}_R\, u_\ell^+(\eta, kr), \quad r \to \infty, \tag{5}$$

where $u_\ell^+ = e^{-\mathrm{i}\sigma_\ell}(G_\ell + \mathrm{i}F_\ell)$ is the sum of the regular and irregular Coulomb wave functions, this equation determines the remainder of the scattering wave function $\Psi_R = \Psi_\ell - \Psi^R$. As we solve the boundary value problem (2,5) for Ψ_R on the interval $[0, R]$ only, the function Ψ^R is well-defined through (4). The amplitude $\mathcal{A}_R$ is given by $\mathcal{A}_R = \mathcal{A} - \mathcal{A}^R$. The representation of the amplitude $\mathcal{A}_R$ in terms of the residual phase shift $\delta_R = \delta_\ell - \delta^R$ has the standard form

$$\mathcal{A}_R = e^{2\mathrm{i}(\sigma_\ell + \delta^R)}(e^{2\mathrm{i}\delta_R} - 1)/(2\mathrm{i}). \tag{6}$$

The boundary problem (5) becomes simpler when the radius R is chosen large enough. If $kR \gg \ell(\ell + 1) + \eta^2$, then the asymptotic form of $\Psi_R(k, r)$ reduces to

$$\Psi_R(k, r) \sim \mathcal{A}_R\ e^{\mathrm{i}(kr - \ell\pi/2 - \eta\log 2kr)}. \tag{7}$$

For the phase shift δ^R, we find the asymptotic behavior $\delta^R \sim \eta\log 2kR - \sigma_\ell$. The asymptotic form (7) can be used in order to calculate the amplitude $\mathcal{A}_R$ in its

local representation. Using the Green's function formalism, we can also find its integral representation

$$\mathcal{A}_R = -k^{-1} \int_0^R dr' \;\; \Psi^R(k,r') V(r') \left[\Psi^R(k,r') + \Psi_R(k,r') \right]. \tag{8}$$

The success in solving the driven Schrödinger equation by ECS depends on whether the driving term vanishes for complex values of the radial coordinates. The driven Schrödinger equation formulation (2,5) perfectly meets this requirement since the potential on the right hand side is of finite range. Another useful observation made from the representation (8) is that the scattering amplitude $\mathcal{A}_R$ is completely determined by that part of the solution Ψ_R, which is restricted on the finite domain $0 \le r \le R$. After the ECS transformation of the coordinate, the boundary condition (5) becomes the zero boundary condition, and the Schrödinger equation (2) can be easily solved.

Summarizing the description of our approach, we can say that the only parameter affecting the results is the radius R. It is important that the scattering problem (1) is exactly reduced to the boundary value problem on the interval $[0, R]$ for an arbitrary finite value R [10]. For the numerical calculations, however, we need to use the asymptotics of the wave function at the right boundary R. This gives an error, those magnitude is defined by the accuracy of the asymptotics.

In order to find the solution, we first ECS-transform and solve Eq. (2) with the zero boundary conditions and compute the function $\Psi_R(k,r)$. Then we find the amplitude $\mathcal{A}_R$ using the local representation (7) or with the integral representation (8). Using Eq. (6) with $\delta^R = \eta \log 2kR - \sigma_\ell$, we calculate the phase shift δ_R and finally reconstruct δ_ℓ with the relation $\delta_\ell = \delta^R + \delta_R$. The numerical implementation of this approach has recently been shown to have both good accuracy and high efficiency [10].

4 The driven Schrödinger approach to the three-body problem

Three possible arrangements for an atom-diatom can be distinguished and denoted $\alpha = a, b, c$. Let the mass-scaled Jacobi coordinates $\mathbf{R}_\alpha$ and $\mathbf{r}_\alpha$ be the dissociative and diatomic coordinates respectively. The total wave function $\Psi(\mathbf{R}_\alpha, \mathbf{r}_\alpha)$ of the system is given as the solution to the Schrödinger equation in one of the three Jacobi coordinate systems

$$\Big[-\Delta_{\mathbf{R}_\alpha} - \Delta_{\mathbf{r}_\alpha} + \sum_\beta V_\beta(\mathbf{r}_\beta) - E \Big] \Psi(\mathbf{R}_\alpha, \mathbf{r}_\alpha) = 0, \quad \alpha = a, b, c. \tag{9}$$

Here, $V_\beta(\mathbf{r}_\beta)$ is the atom-atom interaction. The total wave function can be represented as the sum of the incoming wave and an unknown function $\Phi(\mathbf{R}_\alpha, \mathbf{r}_\alpha)$. The incoming wave describes the initial state of the system when the third particle is far away from the diatom in the rovibrational state j

$$\Psi(\mathbf{R}_\alpha, \mathbf{r}_\alpha) = \Phi(\mathbf{R}_\alpha, \mathbf{r}_\alpha) + \varphi_\alpha^j(\mathbf{r}_\alpha) e^{\mathrm{i}(\mathbf{q}_\alpha^j, \mathbf{R}_\alpha)}. \tag{10}$$

Here, the third particle momentum q_α^j is defined according to $E = (q_\alpha^j)^2 - \epsilon_\alpha^j$, where $\varphi_\alpha^j(\mathbf{r}_\alpha)$ and ϵ_α^j are the wave function and the energy of the diatom rovibrational state, respectively. Substituting representation (10) into Schrödinger equation (9), we get its inhomogeneous (driven) form

$$\Big[-\Delta_{\mathbf{R}_\alpha} - \Delta_{\mathbf{r}_\alpha} + \sum_\beta V_\beta(\mathbf{r}_\beta) - E\Big]\Phi(\mathbf{R}_\alpha, \mathbf{r}_\alpha) = -\varphi_\alpha^j(\mathbf{r}_\alpha) e^{\mathrm{i}(\mathbf{q}_\alpha^j, \mathbf{R}_\alpha)} \sum_{\beta\neq\alpha} V_\beta(\mathbf{r}_\beta). \quad (11)$$

In order to find the solution to Eq. (11) the asymptotic boundary condition should be taken into account. This condition for large hyperradius $\rho = \sqrt{R_\alpha^2 + r_\alpha^2}$ reads [12]

$$\Phi(\mathbf{R}_\alpha, \mathbf{r}_\alpha) \sim \sum_{\alpha=a,b,c} \sum_j \left[A_\alpha^j(\hat{\mathbf{R}}_\alpha)\varphi_\alpha^j(\mathbf{r}_\alpha)\frac{e^{\mathrm{i}q_\alpha^j R_\alpha}}{R_\alpha}\right] + A_\alpha^0(\hat{\mathbf{r}}_\alpha, \hat{\mathbf{R}}_\alpha, \phi_\alpha)\frac{e^{\mathrm{i}\sqrt{E}\rho}}{\rho^{5/2}}. \quad (12)$$

The amplitudes A_α^j, $j > 0$ describe the elastic and rearrangement processes while A_α^0 is the breakup amplitude.

The asymptotic form (12) has different forms in different arrangements. Therefore, its implementation into a practical numerical method for the solution of the three-body Schrödinger Eq. (11) is problematic. Hence, the use of the idea of the previous section leads in the three body case to drastic simplifications. If we apply ECS to the coordinates r_α, R_α with some exterior radius, the scattered wave $\Phi(\mathbf{R}_\alpha, \mathbf{r}_\alpha)$ (12) vanishes exponentially. For exponentially decreasing potentials, the r.h.s. of Eq. (11) also vanishes, while for long-range potentials we need to use a technique similar to that outlined in the previous section. We then arrive at the equation (11) with zero boundary conditions at infinity, which can be solved with already developed methods.

Finally, we should extract the scattering amplitudes from the wave function $\Phi(\mathbf{R}_\alpha, \mathbf{r}_\alpha)$. The simplest way is to define the elastic and rearrangement amplitudes from the asymptotic boundary conditions. To do so, we choose the exterior radius large enough so that asymptotics (12) is already satisfied with sufficient accuracy. For smaller distances R_α, the first terms in (12) dominate over the breakup term. For a chosen Jacobi coordinate frame (i.e. rearrangement channel α), we project the wave function Φ onto $\varphi_\alpha^j(\mathbf{r}_\alpha)$. As the overlap integral of $\varphi_\alpha^k(\mathbf{r}_\alpha)$ with $\varphi_\beta^k(\mathbf{r}_\beta)$ for $\alpha \neq \beta$ is zero, other arrangement channels do not contribute. In the same channel, the vibrational eigenfunctions are orthogonal implying

$$\int d\mathbf{r}_\alpha \varphi_\alpha^k(\mathbf{r}_\alpha)\Phi(\mathbf{R}_\alpha, \mathbf{r}_\alpha) \sim A_\alpha^k(\hat{\mathbf{R}}_\alpha)\frac{e^{\mathrm{i}q_\alpha^k R_\alpha}}{R_\alpha}. \quad (13)$$

This equation gives both the elastic and rearrangement amplitudes.

A numerical generalization of the present MCTSCPFAM theory could be accomplished with the framework of our three-body finite element method [13] (ECSFEMFAM).The three-body eigenvalue problem for the bound state wave function $\Phi(\mathbf{R}_\alpha, \mathbf{r}_\alpha)$ is there formulated in terms of Eq. (11) with r.h.s. put to zero. The coordinate space is described by a set of rectangular finite elements. The solution wave function to the eigenvalue is described as the expansion over

the FEM basis function f_i, $\Phi = \sum_i c_i f_i$, i.e. as an eigenvector $\mathbf{c}$. In this code the Hamiltonian $\mathbf{H}$ is expressed as finite element matrix elements H_{ij}, and the finite element overlap matrix is expressed as S_{ij}. If the inhomogeneous term in the r.h.s. of Schrödinger equation (11) is represented as a vector $\mathbf{b}$, we can formulate the eigenvalue problem, `EP` , and the driven Schrödinger equation scattering problem, `DP` , as

$$\texttt{EP}: \quad \mathbf{Hc} = E\mathbf{Sc} \qquad \texttt{DP}: \quad (\mathbf{H} - E\mathbf{S})\mathbf{c} = \mathbf{b} \tag{14}$$

Starting with the ECSFEMFAM code we need to add the $\mathbf{b}$ term to compute the scattering wave function in terms of $\mathbf{c}$. The amplitudes are then obtained from a numerical realization of Eq. (13).

5 Summary

We have here outlined the use of the driven Schrödinger equation combined with exterior complex scaling in order to treat quantum scattering of few particles. A rigorous formulation for two-body scattering is reported, and its generalization to three-body scattering is considered. Finally, we indicate how the theory may be realized numerically based on an existing finite element parallel coded which is suitable for several potential energy surfaces.

Acknowledgement. This work is supported by Swedish Research Council. EY and MV acknowledges support from the Swedish Institute, ZM acknowledges support from Wenner Gren Foundation and MS, EY and SY acknowledge support from Stockholm University.

References

1. Liu K., Skodje R. T., Manolopoulos D. E., Phys. Chem. Comm. **5** (2002) 27.
2. *Theory of Chemical Reaction Dynamics*, Ed. A. Lagana and G. Lendvay, NATO Science Series **145**, Kluwer Acad. Publ., Dordrecht, (2004).
3. *Non-adiabatic Effects in Chemical Dynamics*, Faraday Discussions, **127** (2004).
4. Schmidt, H.T. *et al.*, Internat. J. Astrobiology **7** (2008) 205.
5. Stenrup M., Larson Å. and Elander N., Phys. Rev A. **79** (2009) 012713.
6. Shilyaeva K., Yarevsky E. and Elander N., J. Phys. B: At. Mol. Opt. Phys. 42, (2009) 044011.
7. Nuttal J. and Cohen H. L., Phys. Rev. **188** (1969) 1542.
8. Hislop P.D. and Sigal I.M., *Introd. Spectral Theory*, Springer, New York, (1996).
9. Rescigno T. N., Baertschy M., Byrum D. and McCurdy C. W., Phys. Rev. **A 55** (1997) 4253 .
10. Volkov M. V., Elander N., Yarevsky E. and Yakovlev S. L., EPL 85, (2009) 30001.
11. Newton R.G. *Scattering Theory of Waves and Particles*, Springer-Verlag, New-York, 1982.
12. Faddeev L.D. and Merkuriev S.P. *Quantum Scattering Theory of Several Particle Systems*, Kluwer Acad Publ., Dordrect, 1993.
13. Alferova T., Andersson S., Elander N., Levin S. and Yarevsky E., Few Body Systems **31**(2002) 177 .

Few-Body Systems 0, 1–5 (2009)

Few-Body Systems

A Quantum Version of Wigner's Transition State Theory*

R. Schubert[1**], H. Waalkens[1,2***], S. Wiggins[1†],

[1] School of Mathematics, University Walk, University of Bristol, Bristol BS8 1TW, United Kingdom
[2] Department of Mathematics, University of Groningen, Nijenborgh 9, 9747 AG Groningen, The Netherlands

Abstract. A quantum version of a recent realization of Wigner's transition state theory in *phase space* is presented. The theory developed builds on a quantum normal form which locally decouples the quantum dynamics near the transition state to any desired order in $\hbar$. This leads to an explicit algorithm to compute cumulative quantum reaction rates and the associated Gamov-Siegert resonances with high accuracy. This algorithm is very efficient since, as opposed to other approaches, it requires no quantum time propagation.

1 Introduction

High resolution spectroscopic techniques allow one to study chemical reaction processes in unprecedented detail (see, e.g., the review paper [1]). A reaction can often be viewed as a transition across a saddle point of the potential energy surface which describes the interaction between the constituent atoms. In the 30's Eyring, Polanyi and Wigner developed transition state theory (TST) which is a computationally efficient way to compute *classical* reaction rates without integrating trajectories. The main idea is to define a dividing surface that partitions the energy surface into a reactant and a product component and compute the rate from the directional phase space flux through this surface. In order not to overestimate the rate the dividing surface must not be recrossed by reactive trajectories. For two degrees of freedom such a dividing surface was constructed from a periodic orbit in the 70's by Pechukas, Pollak and others [2, 3]. In higher dimensions it has recently been shown that a dividing surface free of local recrossings is spanned by a *normally hyperbolic invariant manifold* (NHIM) [4].

*Article based on the presentation by H. Waalkens at the Fifth Workshop on Critical Stability, Erice, Sicily, Received December 1st, 2008; Accepted January 8, 2009.
** *E-mail address:* r.schubert@bris.ac.uk
*** *E-mail address:* h.waalkens@rug.nl
† *E-mail address:* s.wiggins@bris.ac.uk

The NHIM and the dividing surface can be explicitly constructed from an algorithm which computes the (classical) *normal form* of the system near the saddle and leads to a local nonlinear decoupling of the classical dynamics [5].

Much effort has been devoted to developing a quantum TST which inherits the computational benefits of classical TST. The mere existence of such a theory is discussed controversially in the literature. For example, in [6] Miller states that "... there is no uniquely well defined quantum version of TST in the sense that there is in classical mechanics. This is because tunneling along the reaction coordinate necessarily requires one to solve the (quantum) dynamics for some finite region about the TS dividing surface, and if one does this quantum mechanically there is no theory' left, *i.e.*, one has a full dimensional quantum dynamics treatment that is *ipso facto* exact, a quantum simulation." In this short note we present a quantum TST based on a quantum version of the normal form procedure which, classically, yields the realization of TST. Similar to the classical case this quantum normal form (QNF) leads to a local decoupling of the quantum dynamics to any desired order in $\hbar$ in terms of elementary operators with well known spectral properties. This supersedes a full quantum simulation. In this approach the cumulative reaction probability can be viewed as the quantum mechanical flux through a (classically recrossing free) dividing surface which inherently includes tunneling. In this sense, our approach completely sidesteps the issues and concerns expressed by Miller. The QNF computation can be implemented as an explicit algorithm which leads to an efficient procedure to compute cumulative reaction rates and the corresponding Gamov-Siegert resonances [7]. For the technical details of this note we refer to [8, 9], which also includes the historical background for the development of the QNF theory.

2 The Quantum Normal Form

The key idea of our approach is to find a unitary transformation which simplifies the Hamilton operator near the saddle point of the corresponding classical dynamics (for the precise meaning of 'near' and the classical-quantum correspondence see [8, 9]). More precisely, suppose that the classical system has an equilibrium point of saddle-center-$\cdots$-center stability type ('saddle' for short), i.e. the matrix in the associated linearized classical Hamilton equations of motion has one pair of real eigenvalues $\pm\lambda$ associated with the saddle or 'reaction coordinate' and $f-1$ pairs of imaginary eigenvalues $\pm\mathrm{i}\omega_k$, $k=2,\ldots,f$, associated with the center or 'bath' degrees of freedom. Suppose furthermore that the ω_k are rationally independent. Then for each $N\geq 2$, there is a unitary transformation U_N such that

$$U_N^\star \widehat{H} U_N = H_{\mathrm{QNF}}^{(N)}(\widehat{I},\widehat{J}_2,\ldots,\widehat{J}_f) + \widehat{R}^{(N+1)}\ , \tag{1}$$

where $H_{\mathrm{QNF}}^{(N)}$ is a polynomial of order $[N/2]$ in the elementary operators

$$\widehat{I} = \frac{\hbar}{\mathrm{i}}\left(q_1\frac{\mathrm{d}}{\mathrm{d}q_1}+\frac{1}{2}\right),\quad \widehat{J}_k = -\frac{\hbar^2}{2}\frac{\mathrm{d}^2}{\mathrm{d}q_k^2}+\frac{1}{2}q_k^2\quad (k=2,\ldots,f)\,. \tag{2}$$

We call $H^{(N)}_{\rm QNF}(\widehat{I},\widehat{J}_2,\ldots,\widehat{J}_f)$ the QNF of order N. The properties of the reaction operator $\widehat{I}$ (which is unitarily equivalent to the inverted harmonic oscillator, see [9]) and the harmonic bath operators $\widehat{J}_k$ are explicitly known. Since they also commute we can solve the quantum problem described by $H^{(N)}_{\rm QNF}(\widehat{I},\widehat{J}_2,\ldots,\widehat{J}_f)$ analytically. The remainder $\widehat{R}^{(N+1)}$ is an operator which is small near the saddle in a semiclassical sense, see [9]. Similar to the classical normal form the QNF and U_N can be computed order by order using the explicit algorithm developed in [8, 9]. We note that if we give up the rational independence of the ω_k, $k=2,\ldots,f$, one can find a unitary transformation which brings the original Hamiltonian into a quantum version of the classical normal form reported in [10]. However, similar to the classical case, the quantum problem can in general not be solved explicitly if the ω_k are rationally dependent.

3 Cumulative Reaction Probabilities and Quantum Resonances

The eigenfunctions of $H^{(N)}_{\rm QNF}(\widehat{I},\widehat{J}_2,\ldots,\widehat{J}_f)$ are products the harmonic oscillator wave functions for the operators $\widehat{J}_k$, $k=2,\ldots,f$, and eigenstates of the operator $\widehat{I}$ which can be chosen to be pairs of incoming or outgoing scattering wavefunctions associated with reactants and products [9]. Relating the pairs of incoming and outgoing states leads to a 'local' S-matrix which has a simple block structure with the 2×2 matrices

$$S_n(E)=\frac{\mathrm{e}^{\mathrm{i}(\frac{\pi}{4}-\frac{I}{\hbar}\ln\hbar)}}{\sqrt{2\pi}}\Gamma\left(\frac{1}{2}-\mathrm{i}\frac{I}{\hbar}\right)\begin{pmatrix}-\mathrm{i}\mathrm{e}^{-\frac{\pi}{2}\frac{I}{\hbar}} & \mathrm{e}^{\frac{\pi}{2}\frac{I}{\hbar}}\\ \mathrm{e}^{\frac{\pi}{2}\frac{I}{\hbar}} & -\mathrm{i}\mathrm{e}^{-\frac{\pi}{2}\frac{I}{\hbar}}\end{pmatrix} \tag{3}$$

along the diagonal. Here n denotes the vector $(n_2,\ldots,n_f)$ of quantum numbers of the modes in the center directions, and $I(E)$ is implicitly defined by

$$H^{(N)}_{\rm QNF}\big(I,\hbar(n_2+1/2),\ldots,\hbar(n_f+1/2)\big)=E\,. \tag{4}$$

This matrix incorporates the effects of tunneling for energies close to the saddle-energy.

Interestingly, the local S-matrix contains the full information required to compute the cumulative reaction probability $N(E)$ and Gamov-Siegert resonances. In fact, $N(E)$ is given as the sum over the individual transmission probabilities of all modes n, i.e.

$$N(E)=\sum_n T_n(E)\,,\quad \text{where}\quad T_n(E)=|S_{n\,12}(E)|^2=(1+\mathrm{e}^{-2\pi\frac{I}{\hbar}})^{-1}\,. \tag{5}$$

Moreover, the poles of $S_n(E)$ at $I=-\mathrm{i}\hbar(n_1+1/2)$, $n_1\in\mathbb{N}_0$, give the complex energies of the resonances via (4).

4 Examples

In Fig. 1 we compare the cumulative reaction probability and Gamov Siegert resonances computed from the QNF to the corresponding exact results for

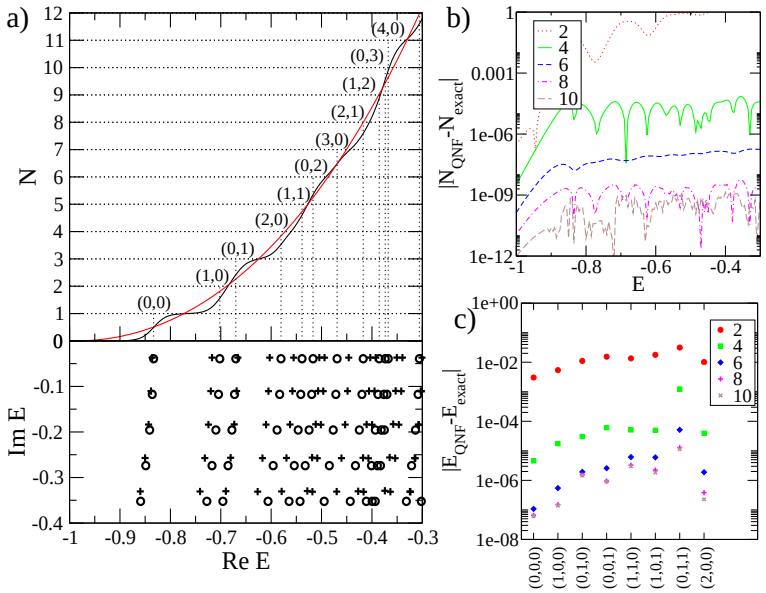

Figure 1. (a) The top panel shows $N(E)$ (oscillatory curve) and the classical flux [11] divided by $(2\pi\hbar)^2$ (smooth curve) for the Eckart-Morse-Morse potential defined in the text with $\epsilon = 0$. The integers (n_2, n_3) mark the energies at which the corresponding Morse oscillator modes contribute a quantization step to $N(E)$. The bottom panel shows the resonances in the complex energy plane marked by circles for the uncoupled case $\epsilon = 0$ and by crosses for the strongly coupled case $\epsilon = 0.3$. (b) Errors for the cumulative reaction probability in (a) for different orders of the QNF. (c) Errors for a selection of resonances (n_1, n_2, n_3) computed from the QNF for $\epsilon = 0.3$. (The parameters are $A = B/10 = 0.5$, $D_{e;1} = 1$, $D_{e;2} = 1.5$, $m = 1$, and $\hbar = 0.1$.)

a 3-degree-of-freedom system consisting of an Eckart potential $V_{\text{Eckart}}(x) = A\exp(x + x_0)/\big(1 + \exp(x + x_0)\big) + B\exp(x + x_0)/\big(1 + \exp(x + x_0)\big)^2$ with $x_0 = \ln(B + A)/(B - A)$ $(B > A \geq 0)$ in one degree of freedom, and two Morse oscillators $V_{\text{Morse};k}(x_k) = D_{e;k}\big(\exp(-2x_k) - 2\exp(-x_k)\big)$, $k = 2, 3$, in the other degrees of freedom, plus the kinetic coupling $\epsilon(p_1p_2 + p_1p_3 + p_2p_3)$.

In the uncoupled case, $\epsilon = 0$, $N(E)$ increases as a function of E at integer steps each time a new transition channel opens, i.e., when the transmission probability $T_{(n_2,n_3)}(E)$ of a mode (n_2, n_3) of the two Morse oscillators switches from 0 to 1. For both the uncoupled and strongly coupled case the resonances form a distorted lattice parametrized by the mode quantum numbers (n_2, n_3) in horizontal direction and the quantum number n_1 in vertical direction. Each string of constant (n_2, n_3) is related to one step of $N(E)$. The agreement of the QNF results with the exact results is excellent and this remains the case even for the strongly coupled system.

5 Conclusions

We presented a quantum version of TST which is fully in the spirit of classical TST in the sense that it requires no quantum simulation although it gives a

full account of the tunneling near the transition state. Our approach is based on a quantum normal form which leads to a local decoupling of the quantum dynamics. The quantum normal form can be cast into an explicit algorithm which leads an efficient way to compute cumulative reaction probabilities and Gamov Siegert resonances for multi-degree-of-freedom systems, for which other methods are no longer feasible.

Acknowledgement. H.W. acknowledges support by EPSRC under grant number EP/E024629/1.

References

1. Skodje, R. T., Yang, X.: Int. Rev. Phys. Chem. **23**, 253 (2004)
2. Pechukas, P., McLafferty F. J.: J. Chem. Phys. **58** 1622 (1973)
3. Pechukas, P., Pollak, E.: J. Chem. Phys. **69** 1218 (1978)
4. Wiggins S.: Normally Hyperbolic Invariant Manifolds in Dynamical Systems. Springer: Berlin 1994
5. Uzer, T., Jaffé, C., Palacián, J., Yanguas, P., Wiggins, S.: Nonlinearity **15** 957 (2001)
6. Miller, W. H.: *Spiers Memorial Lecture*, Farad. Discuss. **110** 1 (1998)
7. Friedman, R. S., Truhlar, D. G.: Chem. Phys. Lett. **183** 539 (1991)
8. Schubert, R., Waalkens, H., Wiggins, S.: Phys. Rev. Lett. **96** 218302 (2006)
9. Waalkens, H., Schubert, R., Wiggins, S.: Nonlinearity **21** R1 (2008)
10. Wiggins, S., Wiesenfeld, L., Jaffé, C., Uzer, T.: Phys. Rev. Lett. **86** 5478 (2001)
11. Waalkens, H., Wiggins, S.: J. Phys. A **37** L435 (2004).

Few-Body Systems 0, 1–4 (2009)

Few-
Body
Systems

Multiparticle interactions of zero-range potentials*

J. H. Macek[1,2]

[1] Department of Physics and Astronomy, University of Tennessee, Knoxville TN 37996-1501,
[2] Oak Ridge National Laboratory, Oak Ridge, TN (USA)

Abstract. For two particles it is often convenient to replace local or non-local potentials by zero-range interactions. Since they are zero-range, these interactions can often be replaced by boundary conditions at a point where the separation between two particles vanishes. In either case, zero-range potentials are useful when the details of the interaction at small distances are not critical for the dynamics. The description of Bose condensates is an example where zero-range interactions are basic to theories of the condensed aggregates. These theories employ the model interactions to obtain a mean field description of large numbers of particles. On a more fundamental level, zero-range interactions are employed to model the interactions of three particles, where they have been used to study the properties of loosely-bound Efimov states. Owning to their success in these areas they have been generalized to allow for multichannel interactions, interactions for states with non-zero angular momentum and energy dependent zero-range potentials. Properties of these generalized potentials and their applications will be illustrated for the interaction of three particles at vanishingly small kinetic energy.

The interactions of many particles near the threshold where all particles are free is a topical subject owing to the ongoing investigations of dilute cold gasses of Bosons and Fermions. In the theory of such systems, a single, low energy, two-body parameter, namely the s-wave scattering length a, plays a central role. This role is incorporated into many-body theories by defining pseudo-potentials [1], here called zero-range potentials, according to

$$V(r)\psi = 2\pi \frac{(\ell+1)[(2\ell-1)!!]}{[(2\ell)!!]} a_\ell^{2\ell+1} \frac{\delta^3(\boldsymbol{r})}{r^\ell} \frac{\partial^{2\ell+1}}{\partial r^{2\ell+1}} r^{\ell+1} \tag{1}$$

where the potential has been written for arbitrary ℓ. The potential is strictly zero-range only for $\ell = 0$ since then quantities such as overlap integrals are defined.

*Article based on the presentation by J.H. Macek at the Fifth Workshop on Critical Stability, Erice, Sicily, Received December 5, 2008; Accepted December 20, 2008

For $\ell > 0$ one must introduce additional conditions since, *e.g.* the matrix elements $\langle\psi_i|\psi_j\rangle$ where i and j refer to different energy eigenstates, are not defined. Such potentials are still useful [6], but one must take the zero-range limit explicitly. For that reason, and because it is the most import case, only $\ell = 0$ is considered here.

The zero-range potentials have been generalized in two other ways, namely, energy dependent scattering lengths have been considered [1–4] and multichannel versions have been employed [5]. The multichannel potentials are used to incorporate the effect of Feshbach resonances, *i.e.* quasi-bound states in closed channels. The multichannel generalization is well-founded for this purpose. Its main drawback is the multiplicity of channels that are needed. Even for one of the simplest non-trivial problems of three boson there are 2 states per boson thus possible $2^3 = 8$ channels for three particles. Symmetry considerations can often reduce this number but the large number of channels is a distinct disadvantage relative to a simple one-channel model.

To avoid the multiplicity of channels, but still incorporate some of the physics of closed channels, one can introduce energy-dependent scattering lengths [2–4]. For example, by setting

$$k \cot \delta = 2(E_r - E)/\gamma \tag{2}$$

where E_r is a resonance energy and $k\gamma = \Gamma$ is the Wigner form for the resonance width, one obtains an energy dependent scattering length $a(E) = \gamma/(2(E - E_r))$. There is, however, a fundamental difficultly with energy-dependent potentials, namely, two-body energy eigenstates including continuum eigenstates are not orthogonal. If the pseudo-potential varies linearly with E so that $V(r) = V_0(r) + V_1(r)E$ then one can redefine the inner product so that in coordinate space the states are orthogonal relative to the weight function $w(r) = 1 - V_1(r)$ and the othogonality relation becomes

$$\langle i|j\rangle = \int \psi_1(\boldsymbol{r})\psi_j(\boldsymbol{r})w(r)d^3r \tag{3}$$

With this definition one can employ standard techniques to use the energy-dependent pseudo-potentials for many-body interactions. In particular, scattering matrix elements S_{ij} are well-defined since the two-body channel eigenstates i and j are well defined.

Unfortunately, the linear dependence on E is too restrictive for many applications of physical interest. For example, the resonance expression of Eq. (2) has a pseudo-potential with a pole at $E = E_r$ so that two-body eigenstates are not orthogonal. This complicates the use of these potentials to model physical problems, however, one can still use them as approximations to more firmly based interactions. One can hope to get some qualitative insights even though the underlying theory is not well-founded. In this brief report I will compare results for three-body interactions obtained using energy-dependent models with those obtained using multichannel, but energy-independent, pseudo-potentials.

The many-body theory used here is the hyperspherical close-coupling representation which is based upon what are now called adiabatic hyperspherical

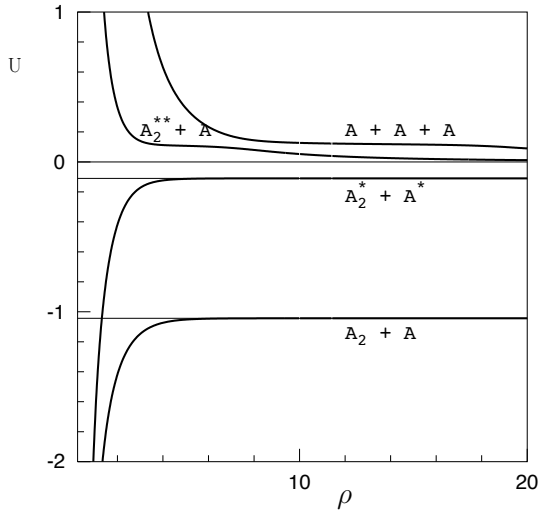

Figure 1. Plot of adiabatic energy curves $U(\rho)$ *vs.* the hyper-radius ρ for the multichannel ZRP model. Data taken from Ref. [5]

.

basis functions [7]. This theory is well adapted to the computation of threshold phenomena, such as three-body recombination, weakly bound states and other processes near thresholds. For example, the effect of Feshbach resonances on three-body processes is a topic of current interest since the constant term on the right hand side of Eq. (2), namely, $E_r/2\gamma$ is just $-1/a$. Because E_r in atom-atom scattering can be varied by applying external fields, the scattering length can be adjusted across a range of values near the threshold for three-body recombination while with the multichannel ZRP this is done by adjusting energy-independent two-body interactions. With the energy-dependent potentials this is done by adjusting constants in the two-body energy dependent scattering length. The multichannel ZRP approach with hyperspherical coordinates was pioneered by Oleg Kartestev [5] who computed the hyperspherical potential energy curves for three bosons using a model interaction which employed a pseudospin formalism to enumerate the two-body channels. Each atom A had two states A and A^* and the Feshbach resonance correlates with the A_2^{**} dimer. The adiabatic energy curves $U(\rho)$, where ρ is the hyper-radius, are shown in Fig. (1). In these graphs, the label U refers to ν^2/ρ^2, whereas the adiabatic potentials are actually $V_{\rm eff}(\rho) = (n^2 - 1/4)/(2\rho^2)$. The curves that correlate to negative values of U for large ρ are channels with bound dimers, either A_2 or A_2^*, while channels that correlate to positive U for large ρ are channels corresponding to three particle breakup $A + A + A$. The section labeled $A_2^{**} + A$ corresponds to a section of the energy curves corresponding to the Feshbach resonance at $U = 2E_r$.

To compare this multichannel curves with similar curves computed using the energy-dependent two-channel model with Eq. (2) for the energy-dependent effective range, first plot the generalized angular momentum term n^2/ρ^2 for $n = 2, 6, 8 \ldots$ as in Fig. 2. They correspond to the pure hyperspherical free-particle channels $A + A + A$. The dotted curve corresponding to the constant Feshbach energy $2E_r$ is shown as a dashed line which crosses all of the free-particle energy curves. When Eq. (2) is used for the energy-dependent scattering length with the two-body energy $k^2/2$ replaced by the "local" two-body energy $\nu^2/(2\rho^2)$ one gets nearly identical potential curves except that the real crossings between the $A_2^{**} + A$ curve and the $A + A + A$ curves become avoided crossings and the

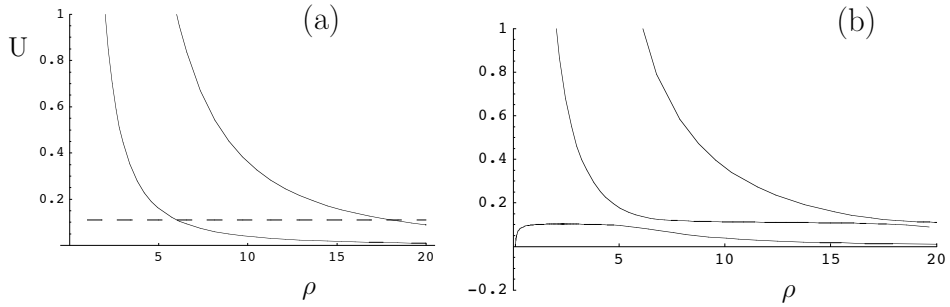

Figure 2. (a) Solid lines- generalized angular momentum barrier in hyper-radial coordinates, dashed line-Constant value of the parameter $2E_r$. (b) Adiabatic potential curves using the energy dependent effective range of Eq. (1) with a Feshbach resonance at E_r.

resonance curve turns down near $\rho = 0$ and goes to $\approx -1/\rho^2$ near $\rho = 0$.

Comparison of Fig. 1 and Fig. 2 shows qualitative agreement between approximate results and exact results for the energy curves of the breakup channels. The dimer channels are missing in the approximate calculation, as expected. It is non-the-less apparent that much of the dynamics in the $A + A + A$ three-body channels are well-represented in Fig. 2b over most of the range of ρ.

There is, however, one important discrepancy with the multichannel ZRP curves, namely, the behavior of the resonance curve near $\rho = 0$ is significantly different. All multichannel curves becomes positively infinite, while the lowest approximate curve becomes negatively infinite. This means that the approximate result could have positive energy resonances while the full multichannel results do not. This could mean that spurious structure may appear in the recombination cross section near threshold.

In addition to spurious or incorrectly located resonances, the non-orthogonality of the two-body channels implies that their non-adiabatic coupling does not vanish for large values of ρ, although the effect of this, possibly spurious, coupling remains to be investigated.

In summary, qualitative understanding of many body dynamics can be obtained using energy-dependent pseudo-potentials, however, they can also give spurious effects owing to non-orthogonality and incorrect behavior for small ρ.

References

1. R. Stock, *et al.*, *Phys. Rev. Lett.*, **94**, 023202 (2005)
2. J. H. Macek and James Sternberg, *NIM B*, **241**, 1 (2005).
3. D. V. Fedorov and A. S. Jensen, *Nuc. Phys. A*, **697**, 783 (2002).
4. M. Massingnan and H. T. C. Stoof, *Phys. Rev. A*, **78**, 030701(R) (2008).
5. O. I. Kartavtsev and J. H. Macek, *Few-Body Systems*, **31**, 249 (2002).
6. M. V. Frolov *et al.*, *J. Phys. B* **39**, S283 (2006).
7. J. H. Macek, *Few-Body Systems*, **31**, 241 (2002).

Few-Body Systems 0, 1–4 (2009)

Few-
Body
Systems

Universality and Leading Corrections in Few-Body Systems*

L. Platter

Department of Physics, Ohio State University, Columbus, OH 43120, USA

Abstract. A large two-body scattering length leads to universal behavior in few-body systems. In particular, the three-body system displays interesting features such as exact discrete scale invariance in the bound state spectrum in the limit of infinite scattering length. Here, I will discuss how an effective field theory (EFT) can be used to study these features and how the finite range of the underlying interaction impacts the bound state spectrum at first order in the EFT expansion.

1 Introduction

Few-body systems with a large two-body scattering length a display interesting universal features. In the two-body system a large positive two-body scattering length will lead to a bound state with binding energy proportional to $1/(Ma^2)$ (where M denotes the mass). Vitaly Efimov showed that the situation in the three-body system is more complicated. For example, for infinite scattering length the binding energies of different states labeled with n and n_* are related by

$$B_3^{(n)} = (e^{-2\pi/s_0})^{n-n_*} B_3^{(n_*)} \ , \tag{1}$$

where $s_0 \approx 1.00624$. The geometric spectrum is a signature of discrete scaling symmetry with scaling factor $e^{-2\pi/s_0}$. Efimov pointed out furthermore that these results are also relevant for finite scattering length a as long as $a \gg l$, where l denotes the range of the underlying interaction [1, 2].

Over the last years an effective field theory (EFT) has been developed which is tailored to calculate the low-energy properties of few-body systems with a large two-body scattering length [3]. This short-range EFT is the appropriate description of ultracold atoms close to a Feshbach resonance and nucleons at very low energies. At leading order, the short-range EFT provides a powerful

*Article based on the presentation by L. Platter at the Fifth Workshop on Critical Stability, Erice, Sicily, Received December 30, 2008; Accepted January 8, 2009.

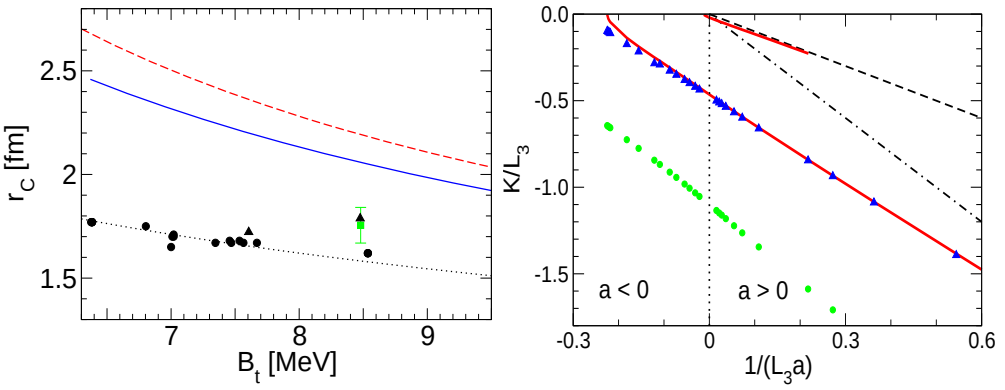

Figure 1. Left panel: The correlation between the triton charge radius and binding energy. The solid and dashed lines denote the leading-order result using different two-body input parameters The circles and triangles indicate Faddeev calculations using different internucleon potentials. The square indicates the experimental values. Right panel: The $a^{-1} - K$ plane for the four-body and three-body problems. The circles and triangles indicate the four-body ground and excited state energies, respectively , while the lower (upper) solid lines give the thresholds for decay into a ground state (excited state) trimer and a particle. The dash-dotted (dashed) lines give the thresholds for decay into two dimers (a dimer and two particles). The vertical dotted line indicates infinite scattering length. All quantities are given in units of a three-body parameter L3

framework to calculate observables in the zero-range limit and reproduces therefore the results derived by Efimov for the three-body sector exactly. It allows furthermore to calculate the effects of the finite range of the underlying interaction systematically and to compute electroweak reactions relevant to nuclear astrophysics.

2 One-Parameter Correlations and Universality

A particular feature of the short-range EFT is the appearance of a three-body force at leading order. Once this three-body counterterm is adjusted such that a known three-body datum is reproduced all remaining observables can be predicted. Three-body observables will therefore depend not only on the scattering length a but also on one additional three-body parameter.

The necessity of this counterterm is more than just an artefact of the field-theoretic formulation of the problem but is instead strongly tied to the aforementioned discrete scale invariance in the three-body system. Its appearance at leading order implies furthermore that two types of one-parameter correlations can be generated within this framework. Either the three-body counterterm is kept constant while the two-body scattering length is varied or a is kept constant while the three-body counterterm is varied.

One example for each of these types of one-parameter correlations is shown in Fig. 1. The correlation between the charge radius of the triton and its binding energy is shown in the left panel of Fig. 1. The two different solid lines correspond

to two different choices of fixing the two-body counterterms, the circles and triangles denote Faddeev calculations with different potentials, the square denotes the experimental value. The difference between the experimental result and the short-range EFT result is due to the importance of finite range corrections.

The right panel shows an Efimov plot which includes results for the four-body system obtained with the short-range EFT. The circles and triangles denote the binding momentum of two different four-body bound states which lie between two successive three-body states. The lower solid line denotes the shallower of these two three-bound states. The upper solid line denotes the next three-body state in the Efimov spectrum. The dashed and dot-dashed lines denote the thresholds for decay into atom plus dimer and two dimers, respectively.

3 Finite Range Corrections

A systematic calculation of higher order corrections is required for an appropriate description of observables if the range of the underlying interaction leads to a sizeable expansion parameter. This is the case in nuclear physics where the ratio of effective range over scattering length is roughly $\sim 1/3$.

Higher order corrections in the EFT expansion have been studied extensively over the last years [6, 7, 8], however, analytical information on the form of these range corrections is very limited. In [9] we used the fact that the wave functions of the Efimov trimers are known in the unitary limit. This allowed us to calculate the shift in the binding energies linear in the effective range in perturbation theory. It is therefore necessary to calculate first the perturbing hyperspherical potential [10, 11, 9]

$$V_{\rm NLO} = -\frac{s_0^2 \xi_0 r_s}{R^3} \ , \tag{2}$$

which is done by implementing a next-to-leading order Bethe-Peierls condition into the hyperangular equation. The shift in the binding energy of the nth bound state can then be found by calculating the integral

$$\frac{2M}{\hbar^2}\Delta B_n^{(1)} = s_0^2 r_s \xi_0 \left[\int_{\frac{1}{\Lambda}}^{\infty} dR {f_n}^2(R) \frac{1}{R^3} - \frac{2H_1 M}{\hbar^2 s_0^2\, r_s\, \xi_0} \Lambda^2 {f_n}^2 \left(\frac{1}{\Lambda}\right) \right] \ , \tag{3}$$

where $f_n(R)$ is the leading-order wave function of the nth three-body bound state. The second term on the right hand side arises from a three-body force

$$V_{SR}^{(1)}(R) = H_1(\Lambda)\Lambda^2 \delta\left(R - \frac{1}{\Lambda}\right) \tag{4}$$

which has been included to regularize the divergent first term. The expression is renormalized by demanding that the shift in the binding energy of the state with index n_* is 0. It turns out that this condition leads to the surprising result that the complete three-body spectrum remains unperturbed, i.e.

$$\Delta B_n^{(1)} = 0 \ , \tag{5}$$

for all n. This result which was also found numerically by Thøgersen *et al.* [12] shows that the discrete scaling symmetry in the three-body system constrains the form of higher order corrections strongly.

4 Summary

Effective field theories can be applied to any system in which a separation of scales is present. They are not only perfectly suited to calculate observables in a systematic low-energy expansion, but also provide a reliable error estimate and a well-defined domain of applicability. An EFT appropriate for short-range interactions has been applied to a large variety of physical systems. I discussed how this short-range EFT can be used to study universal relations in the three-body sector and how range corrections affect the three-body bound state spectrum.

It is a surprising result that the Efimov spectrum in the unitary limit remains unchanged at next-to-leading order. It will be interesting to see how a finite range effects the universal relations between different three-body observables such as the relation between the minima in the three-body recombination rate and the binding energy of Efimov trimers in the unitary limit. It might furthermore be possible to obtain analytic results at next-to-next-to-leading order in the unitary limit.

The consistent inclusion of finite range corrections is required for future calculations of electroweak reactions in few-body systems relevant to nuclear astrophysics and will also be useful in applications of the short-range EFT to Halo-nuclei [13] or α-clusters [14].

Acknowledgement. This work was supported in part by the National Science Foundation under Grant No. PHY–0653312, and the UNEDF SciDAC Collaboration under DOE Grant DE-FC02-07ER41457.

References

1. V. Efimov, Sov. J. Nucl. Phys. **12**, 589 (1971).
2. V. Efimov, Sov. J. Nucl. Phys. **29**, 546 (1979).
3. E. Braaten and H.-W. Hammer, Phys. Rept. **428**, 259 (2006) and references therein.
4. L. Platter and H.-W. Hammer, Nucl. Phys. A **766**, 132 (2006).
5. H.-W. Hammer and L. Platter, Eur. Phys. J. A **32**, 113 (2007).
6. H.-W. Hammer and T. Mehen, Phys. Lett. B **516**, 353 (2001).
7. P. F. Bedaque, G. Rupak, H. W. Grießhammer and H.-W. Hammer, Nucl. Phys. A **714**, 589 (2003).
8. L. Platter and D. R. Phillips, Few Body Syst. **40**, 35 (2006).
9. L. Platter, C. Ji and D. R. Phillips, arXiv:0808.1230 [cond-mat.other].
10. V. Efimov, Phys. Rev. C **44**, 2303 (1991).
11. V. Efimov, Phys. Rev. C **47**, 1876 (1993).
12. M. Thøgersen, D. V. Fedorov and A. S. Jensen, Phys. Rev. A **78**, 020501 (2008).
13. D. L. Canham and H.-W. Hammer, Eur. Phys. J. A **37**, 367 (2008).
14. R. Higa, H.-W. Hammer and U. van Kolck, Nucl. Phys. A **809**, 171 (2008).

Few-Body Systems 0, 1–4 (2009)

Few-Body Systems

Virtual states, halos and resonances in three-body atomic and nuclear systems*

T. Frederico(1) **, M. T. Yamashita(2) and Lauro Tomio(2)

(1) Instituto Tecnológico de Aeronáutica, 12.228-900, São José dos Campos, Brazil
(2) Instituto de Física Teórica, UNESP, 01405-900, São Paulo, Brazil.

Abstract. By considering nuclear and ultracold trapped atomic systems, we review the trajectory of Efimov excited states in the complex plane by changing the two-body scattering lengths and one three-body scale.

Large three-body systems in the maximally symmetric state with the interaction range much smaller than the two-body subsystem scattering lengths have their low-energy observables depending on few physical scales. These scales are the subsystem scattering lengths (or the corresponding two-body energies) and one three-body scale that can be identified with the three-body bound state energy (see ref. [1]). In particular, the ratio between the energy of two consecutive Efimov bound states, N and $N+1$, for the $\alpha\alpha\beta$ three-body system, for a zero-range potential, can be written as a scaling function:

$$\frac{E_3^{(N+1)}}{E_3^{(N)}} = \mathcal{F}\left(\frac{\kappa_{\alpha\alpha}}{\sqrt{|E_3^{(N)}|}}, \frac{\kappa_{\alpha\beta}}{\sqrt{|E_3^{(N)}|)}}\right) \equiv \mathcal{F}_N, \tag{1}$$

where $\kappa_{\alpha\alpha}$ and $\kappa_{\alpha\beta}$ are, respectively, the inverse of the subsystems scattering lengths $a_{\alpha\alpha}$ and $a_{\alpha\beta}$. If α is a fermion, its momentum space wave function should have a symmetric component, otherwise the Efimov phenomena with $s-$wave potentials is absent. As $N \to \infty$, a limit cycle (see ref. [1]) is reached for the scaling function (1). However, in practice, the scaling function is already close to its limiting value even for a small N.

The $\mathcal{F}_N$, given by Eq. (1), can also be identified with the threshold condition, $\xi_{thresh} \equiv \mathcal{F}_N$, for the existence of a bound Efimov state $(N+1)$. For a Borromean system, i.e., $a_{\alpha\beta} < 0$ and $a_{\alpha\alpha} < 0$, $\xi_{thresh} = 0$, while for the other three possibilities given by at least one scattering length larger than zero, the threshold is set by the smallest two-body binding energy. The solutions of $\xi_{thresh} \equiv \mathcal{F}_N$

*Article based on the presentation by T. Frederico at the Fifth Workshop on Critical Stability, Erice, Sicily, Received December 2, 2008; Accepted December 12, 2008

** *E-mail address: tobias@ita.br*

define the border of a bi-dimensional map, with axis given by $\kappa_{\alpha\alpha}/\sqrt{|E_3^{(N)}|}$ and $\kappa_{\alpha\beta}/\sqrt{|E_3^{(N)}|}$. A system lying inside such boundary presents at least one excited state $(N+1)$ (see ref. [1]) as shown in Fig. 1 for $\alpha = n$ and $\beta = c$. The exact Efimov limit is given by the point $(0,0)$. In this parametric space, crossing the critical curve, two possibilities occur for the trajectory of an Efimov excited state in the complex energy plane: *i)* For the Borromean case the excited state turns into a continuum resonance (see ref. [1]); and, *ii)* in the case that at least one subsystem is bound the excited state becomes a virtual one. In the nuclear context, the two-neutron halo nucleus system $n-n-^{18}$C, with a $s-$wave short-range interaction between the pairs, has an Efimov excited state that moves when the ^{19}C binding is changed [2]. Indeed, this system presents a virtual state that turns into an excited state when the ^{19}C binding is decreased [4]. Close to this condition, the $s-$wave $n-^{19}$C effective range expansion has a pole, which is sensitive to the position of the excited bound or virtual state. In the Borromean case, only the three-body cut is present in the T-matrix in the complex energy plane (upper right panel of Fig. 1). In the case of a $\alpha\alpha\alpha$ system, by decreasing the dimensionless quantity $|\kappa_{\alpha\alpha}|/\sqrt{|E_3^{(N)}|}$, one continuum three-body resonance hits the critical border and turns into a $(N+1)$ bound Efimov state. In the case when at least one subsystem is bound there are two branch points (lower right panel). Again, by decreasing the dimensionless quantities $|\kappa_{\alpha\alpha}|/\sqrt{|E_3^{(N)}|}$ one virtual state cross the boundary and turns into a $(N+1)$ bound Efimov

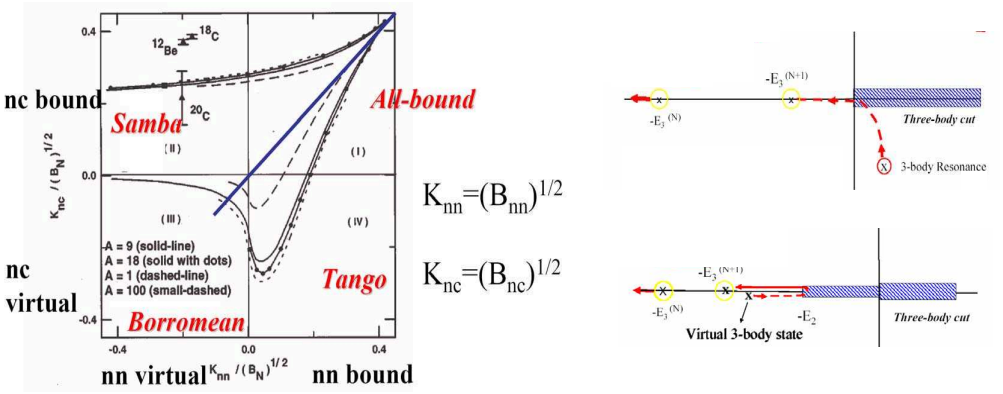

Figure 1. Critical boundary for a neutron-neutron-core $(n-n-c)$ system (left frame), where K_{nn} and K_{nc} correspond, respectively, to two-body bound (virtual) state energies for positive (negative) values. In the right frame, we have the analytic cut structures of the scattering amplitude in the complex energy plane. The Efimov-state trajectories are shown, for a Borromean system, in the upper-right frame, with the state moving from a continuum resonance to a bound system; and, when at least one subsystem is bound, moving from a virtual to a bound system.

The effect of a finite range force changes the boundary according to the expansion parameter r_0/a (r_0 effective range parameter). For a three-boson system, it was found that the critical boundary enlarges for $a > 0$, while it shrinks for

$a < 0$ [5]. The qualitative understanding of that can be seen by approximating the two-body scattering amplitude near the two-body pole as:

$$f(k) = (-a^{-1} + \frac{1}{2} r_0 k^2 - ik)^{-1} \approx \left(1 \pm \frac{r_0}{2}|E_2|^{\frac{1}{2}}\right)\left(\mp|E_2|^{\frac{1}{2}} - ik\right)^{-1} \ , \quad (2)$$

where in the numerator + and − refers to $a > 0$ and $a < 0$, respectively. Therefore, for $a > 0$ the scattering amplitude increases providing more attraction implying in smaller values of a that still can hold an excited Efimov state, while for $a < 0$ the effect is opposite, qualitatively consistent with [5]. One expects that the region delimited by the critical boundary of Fig. 1, with all bound subsystems is somewhat enlarged, while for the Borromean case it shrinks. In the two other quadrants, i.e., for tango and samba configurations there will be a competition between the two effects, that may enlarge or shrink the region for an excited Efimov state.

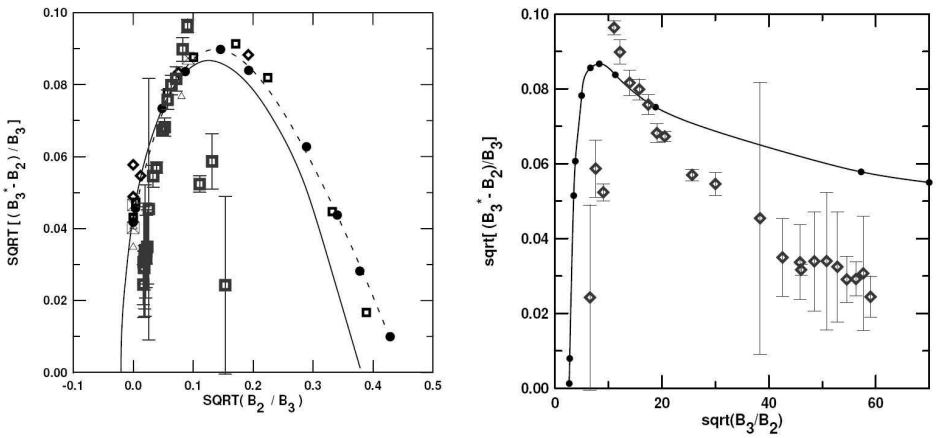

Figure 2. Scaling plots relating the three-boson excited-state energy B_3^* with $\sqrt{B_2/B_3}$ (left frame); and with $\sqrt{B_3/B_2}$ (right frame), where B_2 is the dimer binding energy and B_3 is the ground-state energy. The solid lines represent the zero range model. In the left frame, the symbols correspond to results from realistic models for $^4He_3$ (see details in ref.[3]). The data with bars were extracted from the three-body recombination values for trapped ultracold caesium atoms [6].

Experimental evidence of the trajectory in the complex energy plane of an Efimov state in the Borromean case was recently obtained with trapped ultracold caesium gas near a Feshbach resonance [7] from the measured three-body recombination rate. The excited Efimov state moves to a three-boson continuum resonance when the value of $|a|$ decreases [8], and near the crossing point decreasing further $|a|$ the energy and width of the resonance increases. Such behavior was also indirectly observed. The existence of a three-boson continuum resonance was evidenced by a peak in the recombination rate, that moves toward smaller values of $|a|$ with the increase of temperature. That effect is understood

as an increase of the average kinetic energy that puts the resonance effect at larger values of the energy with a corresponding decrease in the value of $|a|$ [9].

For $a > 0$, an Efimov state moves by changing a according to the universal scaling plot [3], as shown in Fig. 2. The support of that curve delimits the region where one Efimov state above another exists. Some indirect evidence for the scaling plot can be extracted from the three-body recombination rate measured for caesium atoms [7]. The recombination rate to an atom plus a shallow dimer state is an universal function of the shallowest trimer energy [10]. Therefore, knowing the experimental values of the recombination rate and scattering length, one can obtain from the theoretical curve of the recombination rate the binding energy of the shallowest trimer. The binding energy of the caesium trimer below the shallowest one, needed in the plot of Fig. 2 is $B_3 = 1.31$mK [9]. This value comes from the position of the peak of the recombination rate at negative value of a for the lowest possible temperature. In this way, we extract the data points shown in Fig. 2. Of course, this comparison can only be viewed as indicative. In the right panel of the figure, the Efimov state cross the critical point in a much smaller value than the theoretical one. The discrepancy can be due to several reasons. Let us mention, for example, that we have not considered range effects, absorption to deep dimer channels, and possible changes of in B_3 as one varies the two-body scattering length. A measurement of the atom-dimer relaxation at nanokelvin temperatures also indicates that the value of the scattering length, for which the Efimov state crosses the threshold, differs from the universality prediction [11]. Therefore, experimental verification of the trajectory of an Efimov state is still a challenge to be pursued and understood.

Acknowledgement. We thank the Brazilian Funding agencies FAPESP and CNPq for partial financial support.

References

1. Frederico, T., Yamashita, M. T., Nucl. Phys. **A 790**, 116c (2007); and references therein
2. Mazumdar, I., Rau, A. R. P., Bhasin, V. S., Phys. Rev. Lett. **97**, 062503 (2006); Phys. Rev. Lett. **99**, 269202 (2007)
3. Frederico, T., Tomio, L., Delfino, A., Amorim, A. E. A., Phys. Rev. **A 60**, R9 (1999); Canham, D. L., Hammer, H.-W., Eur. Phys. J. **A 37**, 367 (2008)
4. Yamashita, M. T., Frederico, T., Tomio, L., Phys. Rev. Lett. **99**, 269201 (2007); Phys. Lett. **B 660**, 339 (2008); Phys. Lett. **B 670**, 49 (2008)
5. Thogersen, M., Fedorov, D. V., Jensen, A. S., Phys. Rev. **A 78**, 020501 (2008)
6. Tobias Kraemer, private communication
7. Kraemer, T. et al., Nature **440**, 315 (2006)
8. Bringas, F., Yamashita, M. T., Frederico, T., Phys. Rev. **A 69**, 0410702 (2004)
9. Yamashita, M. T., Frederico, T., Tomio, L., Phys. Lett. **A 363**, 468 (2007)
10. Yamashita, M. T., Frederico, T., Tomio, L., Delfino, A., Phys. Rev. **A 68**, 033406 (2003)
11. Knoop, S. et al., arXiv:0807.3306

Few-Body Systems 0, 1–5 (2009)

Few-Body Systems

Interaction Blockade and Pairing in Two-Dimensional Finite Fermion Systems*

J. R. Armstrong[1], M. Rontani[2], S. Åberg[1], V. G. Zelevinsky[3], and S. M. Reimann[1]

[1] Mathematical Physics, Lund Institute of Technology, Box 118, SE-22100 Lund, Sweden
[2] CNR-INFM National Research Center S3, Via Campi 213/A, I-41100 Modena, Italy
[3] NSCL and Department of Physics and Astronomy, Michigan State University, East Lansing, MI, 48824, USA

Abstract. The properties of two-component fermionic quantum systems in two dimensions, such as they nowadays may be realized with cold atoms in traps, are studied within the pairing model adapted from nuclear physics. We compare the results with those of a full numerical diagonalization of the many-body Hamiltonian. The chemical potential differences, excitation energies and angular momentum spectra show that when the zero-range attractive interaction is varied in strength, strong odd-even effects, gaps and shell structure emerge.

1 Introduction

In optical lattices, atom-trapping potentials may be designed with a high degree of precision (see for example [1, 2] and references therein). This allows one to examine a variety of quantum effects for many physical systems which are often close to the immaculate systems usually assumed by theory. In addition to comparisons with condensed matter systems, trapped atoms in optical lattices have connections in nuclear and high energy physics [3, 4, 5, 6]. If the depth of a sinusoidal lattice is large enough, an individual lattice site resembles an isolated harmonic trap. When loading the lattice with fermionic (or bosonic) atoms, the energy levels at the single sites are filled according to statistics and temperature. The interactions between the cold atoms are tunable in strength, and can even be changed from attractive to repulsive. In the case of attractive fermions, the single trap at a lattice site may share some of its characteristics with nuclei, such as shell structure, and pairing [7, 8, 9]. In two dimensions, for repulsive interactions the occurrence of shell structure is in fact very similar to that of quantum

*Article based on the presentation by S. Reimann at the Fifth Workshop on Critical Stability, Erice, Sicily, Received December 1st, 2008; Accepted January 8, 2009.

dots [10]. The discrete transport of electrons through a quantum dot manifests itself in oscillations of the conductance, the so-called "Coulomb blockade" [11, 12]. For different types of interactions other than the Coulomb repulsion between the electrons in a quantum dot, such as the short-ranged interactions between the fermionic atoms, one may analogously observe an "interaction blockade" when an atom is added or removed from the system [13]. For double wells in optical lattices, this was recently reported by Cheinet *et al.* [14, 15].

In these proceedings, we explore the question how far the pairing model adapted from nuclear physics can describe the ground and excited states of two-dimensional few-fermion systems with attractive short-range interactions.

The Hamiltonian of N fermions confined harmonically in a two-dimensional (2D) trap and interacting through an attractive contact interaction is

$$H = \sum_{i}^{N} \left(-\frac{\hbar^2}{2m}\nabla_i^2 + \frac{1}{2}m\omega_0^2 r_i^2 \right) + \frac{1}{2}g' \sum_{i \neq j} \delta^{(2)}(\mathbf{r}_i - \mathbf{r}_j), \tag{1}$$

where the coupling constant g' has units of energy times area. The dimensionless coupling constant, g, is the ratio of the coupling strength to the characteristic energy and length scale of the system $g = g'/(\hbar\omega_0\ell^2)$, where the trap length is $\ell = (\hbar/m\omega_0)^{1/2}$. We solve equation (1) using the pairing model adapted from nuclear physics [16, 17]. In this model, the sum in the second term in Eq. (1) is restricted to summing over time-reversed orbits (the pairs). We use the seniority scheme, where seniority is the number of unpaired particles. Unpaired particles participate beyond the mean field only by blocking certain final states. The unpaired particles also completely determine the possible angular momenta of a given configuration. Compared to the full diagonalization, this model reduces the numerical effort of the calculations significantly, and thus could be used to reach much higher particle numbers. However, for the sake of comparison, Eq. (1) was solved also by the full configuration interaction method [24]. The contact interaction in Eq. (1) is rather disagreeable when one attempts to diagonalize a Hamiltonian in more than one spatial dimension. An approximation is to impose a cut-off [19, 20, 21, 22, 23] effectively renormalizing the interaction strength [25]. The pairing calculations, as well as the CI results, were performed in a model space of six oscillator shells.

2 Results

Figure 1 *(left)* shows the excitation spectra calculated in the pairing model for $2 \leq N \leq 9$ fermionic particles with a quasi-spin degree of freedom, confined in a 2D circular harmonic trap. One can see quite clearly the transition from an oscillator-like system to a strongly-paired system. When the pairing interaction is weak ($g = -0.3$), for all particle numbers one observes essentially a sequence of equally spaced levels, i.e. the $\hbar\omega$ level spacing of the oscillator. For $g = -1$, the equidistant level spacing begins to break down. For the mid-shell particle numbers 4 and 8, a low-lying first excited state appears. This is the first broken pair state, which otherwise has the same single-particle configuration as the fully paired ground state (in the occupation number representation $|\{n_i\}\rangle =$

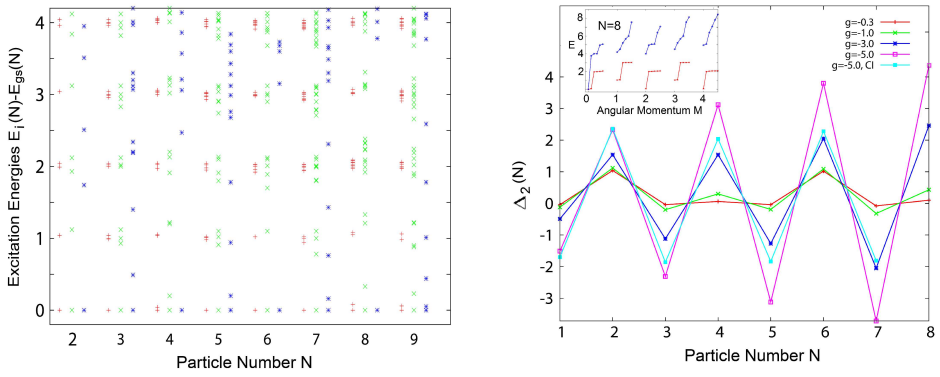

Figure 1. *Left:* Excitation spectra relative to the ground state energy, $E_i(N) - E_{gs}(N)$, calculated for $2 \leq N \leq 9$ harmonically confined contact-interacting fermions in a model space of six oscillator shells, for three values of the coupling constant (from left to right for each particle number), $g = -0.3, -1.0, -5.0$. The excitation energy is capped at 4 $\hbar\omega$ in order to focus on the low energy features of the spectra. *Right:* Differences in chemical potential, $\Delta_2(N)$, for four values of the coupling constant calculated in the pairing model and the $g = -5.0$ result for the CI calculation. The *Inset* shows for $N = 8$ the excitation eneries vs. M, in *red* for $g = -0.3$ and in *blue* for $g = -5.0$, obtained in the pairing model. The first six excited states are shown for each value of M.

$|2, 2, 0, 0, 0, 0\rangle$ for $N = 4$ and $|2, 4, 2, 0, 0, 0\rangle$ for $N = 8$, where $\{n_i\}$ is the sequence of occupancies of the oscillator shells). This state moves steadily higher as the pairing interaction strength is increased. This is seen generally for all considered particle numbers, that for even-N systems, the first excited state moves steadily higher, while in odd-N systems there always remains at least a small number of energetically close, low-lying states.

Figure 1 (*right*) shows the so-called "fundamental energy gap" [13] Δ_2, calculated in the pairing model and with the full Hamiltonian in a CI calculation. $\Delta_2(N)$ is defined as the chemical potential difference for a system with $N + 1$ and N particles,

$$\Delta_2 = E(N + 1) + E(N - 1) - 2E(N) \tag{2}$$

where $E(i)$ is the ground state energy of the i-particle system. In a oure mean field picture, Δ_2 is only non-zero at shell closures, which is seen in the figure. As the attractive interaction is increased, odd-even oscillations appear, as it is now more difficult to remove a particle from an even-numbered system than an odd-numbered one. Except for the case of the largest interaction strength, the pairing model follows the CI data, where the mid-shell peak at $N = 4$ is smaller than the shell closure peaks at $N = 2$ and $N = 6$. For the largest interaction strength, however, in the pairing model the peaks increase with each pair added to the system.

The Inset to the right panel of Figure 1 shows the progression of excited states of a certain angular momentum projection, M, for the eight-particle system. From the weak interaction data, one recognizes the degenerate spectra of the

oscillator, where the excitation spectra of zero, two, and four angular momenta are degenerate, as are both odd-M spectra, and the odd-even yrast line is offset by one $\hbar\omega$. When the interaction strength is increased, degeneracies are broken, as seen from the splitting of the lowest-lying even- and odd-M states. The fully paired ground state is pulled down in energy and the pair vibrations (excited states with seniority zero) also come down, as breaking a pair becomes more costly in energy than moving a pair to a higher mean-field energy level. The $g = -5$ calculation shows a smoothing out of the $\hbar\omega$ staggering and the yrast line now slowly increases with angular momentum.

When comparing with the CI results [25], the mean field-dominated results are similar, but the CI results show reduced degeneracies (since all particles participate in the two-body interaction). Thus, the large-g spectra show a more narrow spread in excitation, and only the $M = 0$ spectrum has a similar band widths in the excitation energies.

In the literature [7, 8, 9] for 3D systems three types of pairing are identified: single-level pairing (in the same ℓ-multiplet), single-shell pairing (within the same oscillator shell), and multi-shell pairing (across oscillator shells). Which type of pairing is prevalent depends on the particle number and pairing strength relative to the oscillator strength [7]. In 2D, there is no distinction between single-level pairing and single-shell pairing. We can, however, distinguish between intra- and inter-shell pairing [7], which comes from the off-diagonal terms in the Hamiltonian (1). For $g = -0.3$, the contribution of the off-diagonal terms to the ground state energy is only a hundredth of a percent, but when $g = -5$, the off-diagonal contribution is 25%. Further analysis should be done to examine the collectivity of the states as the pairing strength is increased.

3 Conclusions

Cold fermions trapped in a 2D harmonic well were examined with a pairing model Hamiltonian. The results of these calculations were compared with results from CI calculations with the same attractive zero-range interaction. For excited states and for strong interactions the terms neglected by the pairing Hamiltonian may cause some difference. However, it was found that ground state properties agree fairly well. When the zero-range attractive interaction is varied in strength, strong odd-even effects, gaps and shell structure emerge in the chemical potential differences, as well as in the angular momentum spectra.

Further studies could be done on how the wave functions evolve with the strength of the pairing interaction and examine collective behavior and perhaps look for evidence of chaos in the spectra. It would also be interesting to perform density calculations and compare them with the CI results. Also, the small size of the pairing calculations should be exploited and calculations should be done for much larger systems.

Acknowledgement. This work was supported by FIRB No. RBIN04EY74 and No. RBIN06JB4C, PRIN No. 2006022932, and INFM-CINECA Supercomputing Project 2007 and 2008, MAE Italy-Japan 2008, the Swedish Research Council, the Swedish Foundation for Strategic Research and NordForsk.

References

1. I. Bloch, *Nature Phys.***1**, 23(2005).
2. I. Bloch, *Nature* **453**, 1016 (2008).
3. A. Gezerlis and J. Carlson, *Phys. Rev. C*, **77**, 032801(R), (2008).
4. T. Schafer, *Prog. Theo. Phys. Suppl.*, **168**, 303, (2007).
5. T. Schafer, *Int. J. Mod. Phys. E*, **16**, 853, (2007).
6. H. Abuki and T. Brauner, *Phys. Rev. D*, **78**, 125010, (2008).
7. H. Heiselberg and B. Mottelson, *Phys. Rev. Lett* **88**, 190401 (2002).
8. H. Heiselberg, *Phys. Rev. A* **68**, 053616 (2003).
9. G. Bruun and H. Heiselberg, *Phys. Rev. A* **65**, 053407 (2002).
10. S. M. Reimann and M. Manninen, *Rev. Mod. Phys.*, **74**, 1283 (2002).
11. D. V. Averin and K. K. Likharev, *J. Low Temp. Phys.* **62**, 345 (1986).
12. H. Grabert and M. H. Devoret, Eds. *Single Charge Tunneling.* New York, NY: Plenum 1991.
13. K. Capelle, M. Borgh, K. Kärkkäinen, and S. M. Reimann, *Phys. Rev. Lett.* **99**, 010402 (2007).
14. P. Cheinet *et al.*, *Phys. Rev. Lett.* **101**, 090404 (2008).
15. S. Fölling *et al.*, *Nature*, **448**, 1029,(2007).
16. A. Volya, B. A. Brown, and V. Zelevinsky, *Phys. Lett. B*, **509**, 37, (2001).
17. V. Zelevinsky and A. Volya, *Phys. At. Nucl.*, **66**, 1829 (2003).
18. M. Rontani, C. Cavazzoni, D. Bellucci, and G. Goldoni, *J. Chem. Phys.* **124**, 124102 (2006).
19. B. D. Esry and C. H. Greene, *Phys. Rev. A* **60**, 1451 (1999).
20. A. Bulgac, J. E. Drut, and P. Magierski, *Phys. Rev. Lett.* **96**, 090404 (2006).
21. I. Stetcu, B. R. Barrett, and U. Van Kolck, *Phys. Lett. B* **653**, 358 (2007).
22. I. Stetcu, B. R. Barrett, U. Van Kolck, and J. P. Vary, *Phys. Rev. A* **76**, 063613 (2007).
23. Y. Alhassid, G. F. Bertsch, and L. Fang, *Phys. Rev. Lett.* **100**, 230401 (2008).
24. M. Rontani, S. Åberg, and S. M. Reimann, arXiv: 0810.4305 (2008).
25. M. Rontani, *et al.*, arXiv:0806.3780 (2008)

Few-Body Systems 0, 1–5 (2009)

Few-Body Systems

Two-boson Correlations in Various One-dimensional Traps*

A. Okopińska **, P. Kościk ***

Institute of Physics, University of Humanities and Sciences, Świętokrzyska 15, 25-406 Kielce, Poland

Abstract. A one-dimensional system of two trapped bosons which interact through a contact potential is studied using the optimized configuration interaction method. The rapid convergence of the method is demonstrated for trapping potentials of convex and non-convex shapes. The energy spectra, as well as natural orbitals and their occupation numbers are determined in function of the inter-boson interaction strength. Entanglement characteristics are discussed in dependence on the shape of the confining potential.

1 Introduction

Entanglement as a measure of quantum correlations is investigated in the hope of better understanding the structure of strongly-coupled many-body systems. Recently there is a growing interest in studying few-particle trapped systems, since they became accessible in experiments with ultracold gases in optical lattices and microtraps. The interatomic interaction can be there considered as a contact one. By choosing the transverse confinement much stronger than the longitudinal one, the quasi-one-dimensional systems with an effective interaction $g_{1D}\delta(x_2 - x_1)$ of an adjustable strength g_{1D} may be experimentally realized [1]. In the Tonks–Girardeau (TG) limit of $g_{1D} \to \infty$ the system is solvable for arbitrary trapping potential [2]. Theoretical consideration of such a system evolution from weak to strong interactions is thus of interest.

We discuss entanglement properties for a system of two bosons interacting through a contact potential and subject to a confining potential $V(x)$. The dimensionless Schrödinger equation takes a form

$$H\phi(x_1, x_2) = E\phi(x_1, x_2), \tag{1}$$

*Article based on the presentation by A. Okopińska at the Fifth Workshop on Critical Stability, Erice, Sicily, Received November 30, 2008; Accepted January 8, 2009

** *E-mail address:* okopin@fuw.edu.pl
*** *E-mail address:* koscik@pu.kielce.pl

where the Hamiltonian reads

$$H = -\frac{1}{2}\frac{\partial^2}{\partial x_1^2} - \frac{1}{2}\frac{\partial^2}{\partial x_2^2} + V(x_1) + V(x_2) + g_{1D}\delta(x_2 - x_1). \tag{2}$$

Since the two-boson function is symmetric and may be chosen real, there exists an orthonormal real basis $\{v_l\}$ such that

$$\phi(x_1, x_2) = \sum_l k_l v_l(x_1) v_l(x_2), \tag{3}$$

where the coefficients k_l are real and $\sum_l k_l^2 = 1$. Therefore

$$\int_{-\infty}^{\infty} \phi(x, x') v_l(x') dx' = k_l v_l(x), \tag{4}$$

which means that v_l are eigenvectors of the two-particle function. It may be shown that v_l are also eigenvectors of the density matrix, known as natural orbitals. Density matrix decomposition is given by $\rho(x, x^{'}) = \sum \lambda_l v_l(x) v_l(x^{'})$, where the occupancies $\lambda_l = k_l^2$. The number of nonzero coefficients k_l and the distribution of their values characterize the degree of entanglement.

2 Optimized Configuration Interaction Method

The configuration interaction method (CI) consists in choosing the orthogonal basis set in the Rayleigh-Ritz (RR) procedure so as to ensure proper symmetry under exchange of particles [3]. For the two-boson system, the CI expansion reads

$$\phi(x_1, x_2) = \sum a_{ij} \psi_{ij}(x_1, x_2), \tag{5}$$

where $\langle x_1, x_2 | ij \rangle = \psi_{ij}(x_1, x_2) = b_{ij}[\varphi_i(x_1)\varphi_j(x_2) + \varphi_j(x_1)\varphi_i(x_2)]$ with $b_{ij} = 1/2$ for $i = j$ and $b_{ij} = 1/\sqrt{2}$ for $i \neq j$. Exact diagonalization of the infinite Hamiltonian matrix $H_{nmij} = \langle nm | H | ij \rangle$ determines the whole spectrum of the system. Truncated matrices $[H]_{N \times N}$ allow determination of successive approximations to the larger and larger number of states by increasing the order N. We use the one-particle basis of the harmonic oscillator eigenfunctions

$$\varphi_i^{\Omega}(x) = \left(\frac{\sqrt{\Omega}}{\sqrt{\pi} 2^i i!} \right)^{\frac{1}{2}} H_i(\sqrt{\Omega} x) \exp\left[-\Omega x^2 / 2 \right]. \tag{6}$$

Following the optimized RR scheme [4], we adjust the value of the frequency Ω so as to make stationary the approximate sum of N bound-state energies, by requiring

$$\frac{\delta Tr[H]_{N \times N}}{\delta \Omega} = 0. \tag{7}$$

Such a way of proceeding has been shown to improve strongly the convergence of the RR method [4, 5]. The Nth order calculation provides approximations to many eigenstates, which enables a direct determination of natural orbitals by

representing them in the same basis (6) as $v(x) = \sum p_n \varphi_n^{\Omega}(x)$. This turns the eigenequation (4) into an algebraic problem

$$\sum (A_{mn} - k_n \delta_{mn}) p_n = 0,$$
$$A_{mn} = \int \psi_m^{\Omega}(x_1)\phi(x_1, x_2)\psi_n^{\Omega}(x_1)dx_1 dx_2 = \begin{cases} a_{nn} & \text{for} \quad m = n \\ 2^{-1/2} a_{mn} & \text{for} \quad m \neq n \end{cases} \tag{8}$$

and a_{nm} are determined from diagonalization of $[H]_{N\times N}$. By diagonalization of the matrix $[A]_{N\times N}$, the approximate coefficients k_n may be determined. Due to the fact that $\sum A_{nm}^2 = 1$, their numerical values satisfy $\sum k_n^2 = 1$.

3 Results

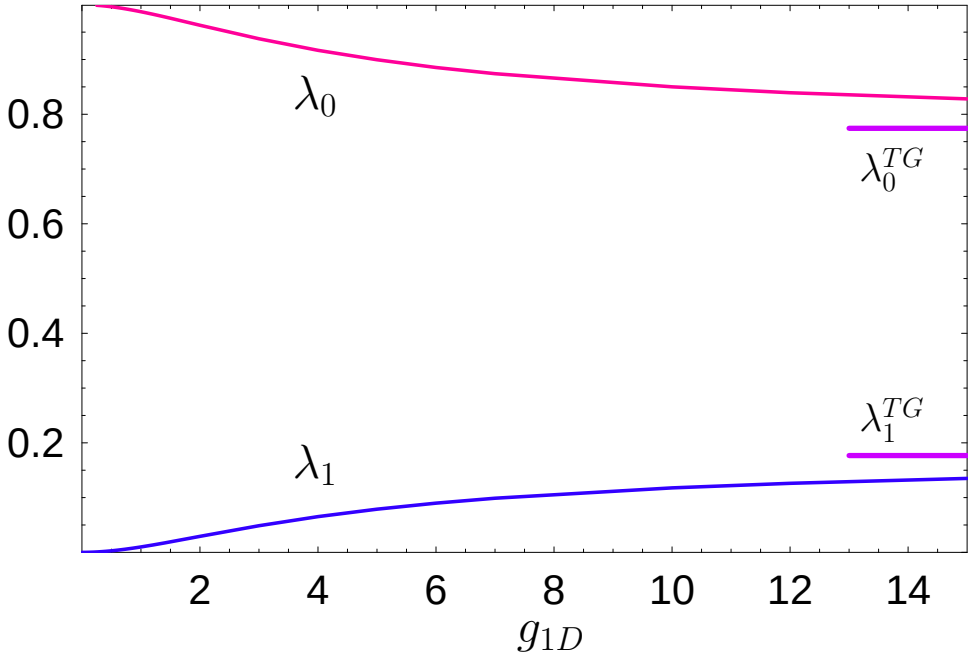

Figure 1. The occupancies λ_0 and λ_1 for a harmonically confined two-boson system in function of g_{1D}, their TG limits are marked by horizontal lines.

In the case of harmonic confinement $V(x) = mx^2/2$ and the contact interaction, the two-particle wave function may be analytically expressed [6]. This allows determination of the occupancies $\lambda_i = k_i^2$ by discretizing (4). The two largest occupancies for the ground state are shown in Fig. 1 in function of g_{1D}. The state is non-entangled ($\lambda_0 = 1$) only if the bosons do not interact. The weakly entangled "condensed" state with only one orbital significantly occupied is realized at very weak interactions, $g_{1D} \lesssim 0.1$. With increasing g_{1D}, the entanglement grows, which shows up in the increase of λ_1 at the cost of λ_0. The occupancies monotonically approach their TG limits $\lambda_0^{TG} \approx 0.7745$ and $\lambda_1^{TG} \approx 0.1765$.

Entanglement properties in the case of multi-well potentials are markedly different. Using the optimized RR method, we calculated the natural orbital oc-

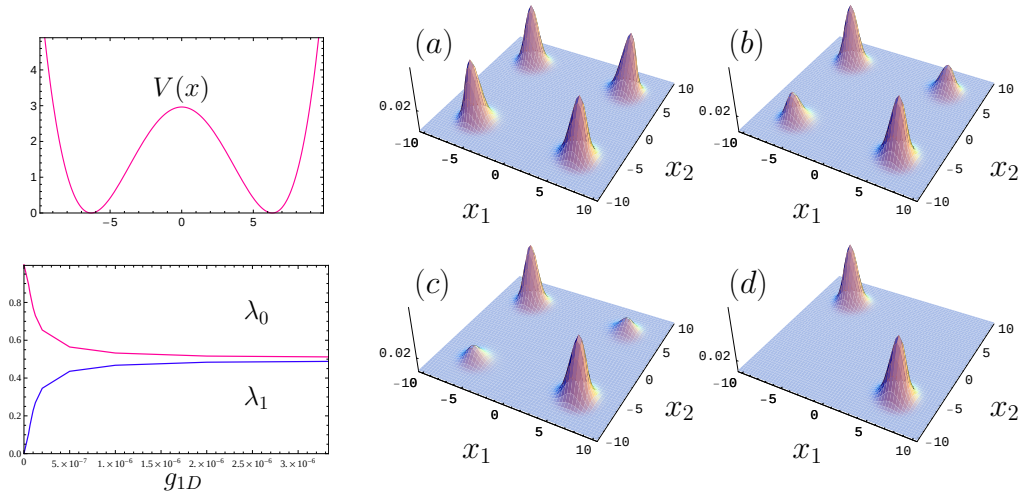

Figure 2. Double-well potential (upper left), the occupancies λ_0 and λ_1 in function of g_{1D} (lower left) and two-boson densities (right) for (a) $g_{1D} = 0$, (b) $g_{1D} = 2.5 \cdot 10^{-8}$, (c) $g_{1D} = 5 \cdot 10^{-8}$, (d) $g_{1D} = 10^{-6}$

cupancies of ground states in double-well potential $V_{2\text{well}}(x) = \frac{2}{27a}(1-ax^2)^2$ and triple-well potential $V_{3\text{well}}(x) = \frac{1}{2}x^2 - ax^4 + \frac{a^2}{2}x^6$. The potentials have minima of the same depth and the maxima of the same height, controlled by the parameter a. The results for $a = 0.025$ are plotted in Figs. 2 and 3, where the upper left presents the shapes of the potentials, and the lower left, the two largest occupancies λ_0 and λ_1 in function of g_{1D}. For $g_{1D} = 0$, the ground state is non-entangled, as $\lambda_0 = 1$. With increasing interactions, λ_0 decreases and λ_1 grows, monotonically approaching the TG limit of non-entangled "fragmented" state, $\lambda_0^{TG} = \lambda_1^{TG} = 0.5$. The critical value g_{1D}^{cr}, above which $\lambda_0 \approx \lambda_1$, is much larger for the triple-well potential than for the double-well one. The dependence of the two-boson density on g_{1D} for the double-well potential is shown on the right of Fig. 2. For noninteracting bosons, the probability of both being in different wells is the same as being in the same well. With increasing g_{1D}, the probability of finding the bosons in the same well quickly decreases and above g_{1D}^{cr} the state is almost fragmented. In the triple-well case (right of Fig. 3) the particles live in the middle well, only above g_{1D}^{cr} the probability of finding a particle in an external well becomes considerable. In the TG limit of non-entangled "fragmented" state, one particle is localized in the middle and the other in one of external wells.

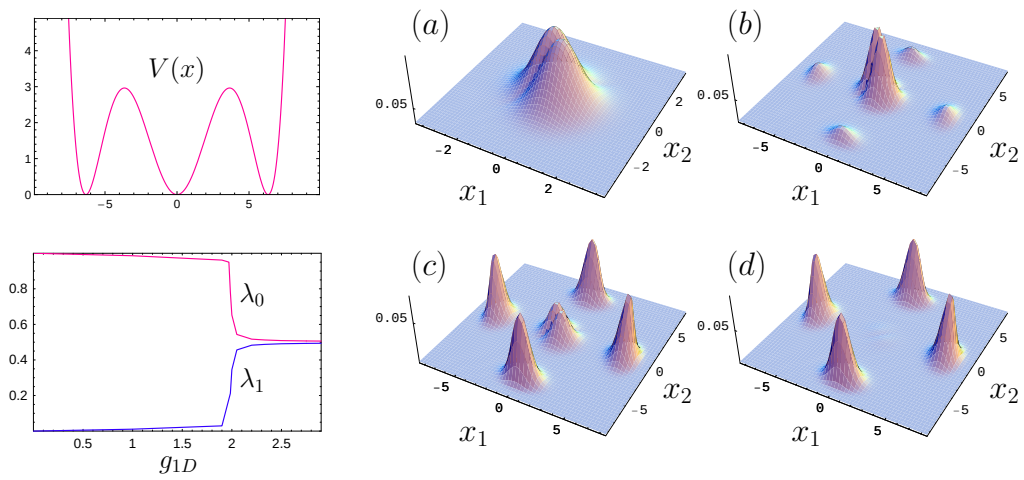

Figure 3. Same as Fig.2 but for the triple-well potential. The two-boson densities (right) for (a) $g_{1D} = 1$, (b) $g_{1D} = 1.97$, (c) $g_{1D} = 1.985$, (d) $g_{1D} = 2.05$

4 Conclusion

The optimized CI method proves very effective in determining the spectrum and the natural orbitals of the two-particle confined systems.

References

1. Kinoshita, T., Wenger, T., Weiss, D. S.: Science **305**, 1125 (2004).
2. Girardeau, M.: J.Math.Phys. **1**, 516 (1960)
3. Helgaker, T., Jørgensen P., Olsen J.: Molecular Electronic- Structure Theory (Wiley, Chichester, 2000).
4. Okopińska, A.: Phys.Rev. **D36**, 1273 (1987)
5. Kościk, P., Okopińska, A.: J. Phys. A: Math. Theor. **40**, 10851 (2007)
6. Busch, T., et al.: Found. Phys. **28**, 549 (1998)

Few-Body Systems 0, 1–8 (2009)

Few-Body Systems

Feshbach Resonances and Medium Effects in ultracold atomic Gases*

G. M. Bruun

The Niels Bohr Institute, University of Copenhagen, DK-2100 Copenhagen Ø, Denmark

Abstract. We develop an effective low energy theory for multi-channel scattering of cold atomic alkali atoms with particular focus on Feshbach resonances. The scattering matrix is expressed in terms of observables only and the theory allows for the inclusion of many-body effects both in the open and in the closed channels. We then consider the frequency and damping of collective modes for Fermi gases and demonstrate how medium effects significantly increase the scattering rate determining the nature of the modes. Our results obtained with no fitting parameters are shown to compare well with experimental data.

1 Introduction

The study of cold atomic gases has now been at the forefront of low temperature physics for more than a decade. One can manipulate these gases with impressive experimental flexibility using the powerful tools of quantum optics. This has produced a string of ground breaking results relevant across many fields of physics including quantum optics, AMO and condensed matter physics [1, 2]. A particularly attractive feature of cold atomic gases is the ability to manipulate the atom-atom interaction with the use of Feshbach resonances. The interaction can be made strong/weak and attractive/repulsive simply by tuning an external magnetic field. This has resulted in many important discoveries concerning strongly interacting many-body systems and the pace at which new results are being reported shows no sign of slowing down.

Sophisticated and very precise coupled channels calculations have been developed to describe atomic Feshbach resonances at the two-body level [3]. Such coupled channels approaches are in general not easily generalized to study the intriguing many-body effects observed in the atomic gases. Several effective theories have therefore been developed which include a simplified version of the two-body Feshbach physics such that many-body calculations are tractable [2].

*Article based on the presentation by G. Bruun at the Fifth Workshop on Critical Stability, Erice, Sicily, Received January 9, 2009; Accepted January 30, 2009

Most of these theories either neglect the Feshbach molecule entirely using so-called single channel models [4] or put it in by hand as a point boson [5]. Such approaches have been very successful in calculating various many-body properties of the atomic gases for wide resonances where the multi-channel nature of the scattering is less important. For narrow resonances however, single channel approximations cannot be expected to be accurate, and even for wide resonances there are observables which depend specifically on the multi-channel nature of the scattering.

To address this, we describe in this paper an effective theory for the Feschbach scattering which in the spirit of Landau expresses the multi-channel scattering matrix in terms of observables only. The Feshbach molecule emerges dynamically as a proper two-body state, yet the theory is still simple enough to be easily generalized to treat many-body effects. As an application of this theory, we consider the collective modes of trapped atomic Fermi gases. The study of collective modes is a powerful probe into the properties of interacting quantum liquids. In cold atomic Fermi gases, collective mode spectroscopy has revealed a wealth of information about zero temperature $T = 0$ [2] as well as $T > 0$ properties [6, 7, 8]. We outline how one can calculate the frequency and damping of the collective modes in the normal phase above the critical temperature T_c for superfluidity. Focus is on how the modes reveal information about the collisional properties and many-body effects.

2 Landau Theory for in-medium Scattering

First we develop an effective low energy theory for fermionic alkali atom-atom scattering in a medium. Consider alkali atoms in a magnetic field B oriented along the z-direction. The strongest part of the atom-atom interaction is the electrostatic central potential given by

$$V(r) = \frac{V_s(r) + 3\,V_t(r)}{4} + [V_t(r) - V_s(r)]\,\boldsymbol{S}_1 \cdot \boldsymbol{S}_2 \tag{1}$$

where $V_s(r)$ and $V_t(r)$ are the singlet and triplet potentials and $\mathbf{S}_1$ and $\mathbf{S}_2$ are the spins of the valence electrons of the two alkali atoms [1]. Scattering via the potential (1) is characterized by channels of anti-symmetrized two-particle states with the same z-projection M_z of the total spin $\boldsymbol{F}$. For a given M_z, the two-particle state with the lowest energy $\epsilon_{\alpha_2} + \epsilon_{\alpha_1}$ constitutes the open channel $|o\rangle = |\alpha_1, \alpha_2\rangle$. Here $\hat{H}_{\rm spin}|\alpha\rangle = \epsilon_\alpha|\alpha\rangle$ are the eigenstates of the single particle hyperfine Hamiltonian [1]. The interaction (1) couples this channel to a number of higher energy states which form a set of closed channels $|c^{(n)}\rangle = |\alpha_3^{(n)}, \alpha_4^{(n)}\rangle$. The threshold energies for the closed channels are then $E_{\rm th}^{(n)}(B) = \epsilon_{\alpha_4^{(n)}} + \epsilon_{\alpha_3^{(n)}} - \epsilon_{\alpha_2} - \epsilon_{\alpha_1}$ and they depend on the magnetic field.

Focus now on the case where there is one open $|o\rangle$ and one closed scattering channel $|c\rangle$. It should be emphasized that our effective theory is readily generalized to more than two channels if appropriate. To arrive at an effective theory for the scattering, we want to eliminate the bare microscopic interaction (1) which has a complicated momentum dependence. The high energy physics is eliminated

by introducing an effective interaction U_{ij} which is a solution to the zero energy Lippmann-Schwinger equation when the hyperfine splitting of the channels is ignored. This results in a momentum independent low energy interaction given by [9]

$$\hat{U}(\mathbf{q}', \mathbf{q}) = \frac{4\pi}{m}\left[\frac{a_s + 3a_t}{4} + (a_t - a_s)\mathbf{S}_1 \cdot \mathbf{S}_2\right] \tag{2}$$

where a_s and a_t are the scattering lengths for the singlet $V_s(r)$ and triplet $V_t(r)$ potentials, respectively. Any finite range effects can be introduced through form factors which we have suppressed here for clarity. Using this low energy interaction, the Lippmann-Schwinger equation reduces to a simple 2×2 matrix equation

$$\begin{bmatrix} T_{cc} & T_{co} \\ T_{oc} & T_{oo} \end{bmatrix}^{-1} = \begin{bmatrix} U_{cc} & U_{co} \\ U_{oc} & U_{oo} \end{bmatrix}^{-1} - \begin{bmatrix} \Pi_c & 0 \\ 0 & \Pi_o \end{bmatrix} \tag{3}$$

where $T_{ij}(\omega, \boldsymbol{K})$ is the scattering matrix between the channels i and j. In addition to the usual dependence on the energy ω, it also depends on the center-of-mass momentum $\boldsymbol{K}$ since Galilean invariance is broken by the presence of the medium. The expressions for the pair propagators in the open and closed channels $\Pi_0(\omega, \boldsymbol{K})$ and $\Pi_c(\omega, \boldsymbol{K}, B)$ with medium effects included through the ladder approximation are given in Ref. [9]. Equation (3) is easily solved and the open channel scattering matrix can be written as

$$T_{oo} = \frac{U_{oo}}{1 - U_{oo}\Pi_o} + \frac{U_{oc}}{1 - U_{oo}\Pi_o} D \frac{U_{co}}{1 - U_{oo}\Pi_o} \tag{4}$$

where

$$D^{-1}(\mathbf{K}, \omega) = {\Pi_c}^{-1} - U_{cc} - {U_{oc}}^2 \frac{\Pi_o}{1 - U_{oo}\Pi_o} \tag{5}$$

is the in-medium pair propagator in the closed channel. Equation (4) provides a transparent physical interpretation of the multi channel scattering: The first term in (4) describes scattering induced by the open channel interaction only and the second term describes the scattering via the closed channel. The diagrammatic structure of (4)-(5) is shown in Fig. 1.

The scattering of alkali atoms depends on the magnetic field B both through the hyperfine states and the matrix elements U_{ij}. Close to a Feshbach resonance located at a given field B_0, the zero energy two-body scattering matrix in the open channel can be parametrized as

$$T_{oo}^{vac} \equiv \frac{4\pi a}{m} = \frac{4\pi a_{\rm bg}}{m}\left(1 - \frac{\Delta B}{B - B_0}\right). \tag{6}$$

Here, $a_{\rm bg}$ is the (non-resonant) background scattering length and ΔB the width of the resonance. The Feshbach resonance comes from the presence of a molecular state in the closed channel. It is thus contained in the second term in (4). The energy $\omega_{\mathbf{K}}$ of a Feshbach molecule (including medium effects) with momentum $\mathbf{K}$ is determined by $D^{-1}(\mathbf{K}, \omega_{\mathbf{K}}) = 0$. By making a pole expansion of (4) around $B = B_0$ and comparing with (6), one can write the scattering matrix in the very

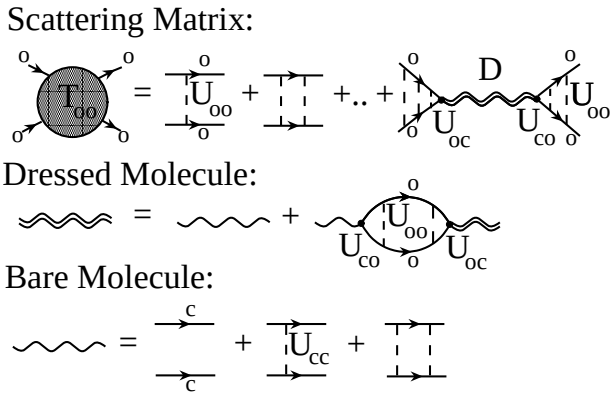

Figure 1. The scattering matrix (4) decomposed into scattering in the open and closed channels. The closed channel molecule is dressed via its coupling to the open channel. Fermions are indicated by straight lines, interaction within a channel is indicated by dashed lines, and coupling between the open and closed channels is indicated by •.

useful form [9]

$$T_{oo} = \frac{T_{\rm bg}}{\left(1 + \frac{\Delta\mu\Delta B}{\tilde{\omega}+h(\omega)-\Delta\mu(B-B_0)}\right)^{-1} - T_{\rm bg}\Pi_o(\omega)}. \tag{7}$$

Here $T_{\rm bg} = 4\pi a_{bg}/m$, $\tilde{\omega} = \omega - K^2/4m$, and $\Delta\mu$ is the magnetic moment of the Feshbach molecule with respect to the open channel. A detailed analysis of the molecular propagator (5) shows that $\Delta\mu$ can be split into a contribution from the magnetic dependence of the bare closed channel state and a contribution from screening due to coupling to high energy states in the open channel. This screening which reduces the magnetic moment from its bare value is often ignored in the literature. It comes from a *linear* frequency dependence of the molecule self energy in addition to the well known $\sqrt{\omega}$ threshold dependence, and it can lead to a significant reduction of the magnetic moment of the molecule [9, 10]. The function $h(\omega)$ is given in Ref. [9]. It describes effects coming from the composite two-fermion nature of the Feshbach molecule, and it is here that many-body effects in the closed channel enter.

With (7), we have arrived at an effective low energy theory for scattering in a medium. The complicated energy and momentum dependent multichannel scattering matrix is expressed in a simple way through the physical observables $a_{\rm bg}$, B_0, ΔB, and $\Delta\mu$. The parameters $a_{\rm bg}$, B_0, ΔB can be measured in scattering experiments whereas the magnetic moment of the Feshbach molecule can be measured in rethermalization experiments [9]. Contrary to many other approaches in the literature, the theory allows one to include non-trivial many-body effects in the closed channel as well as in the open channel. Examples of such closed channel medium effects were considered in Ref. [9].

3 Collective Modes and Viscous Damping

We now consider the collective modes of trapped Fermi gases and examine how they can reveal information about the scattering properties discussed in the previous section. We focus on the normal state for temperatures $T \geq T_c$. The dynamics of the gas is assumed to be described by a semiclassical distribution function $f(\mathbf{r}, \mathbf{p}, t)$ which satisfies the Boltzmann equation. A collective mode corresponds to a deviation $\delta f = f - f^0$ away from the equilibrium distribution $f^0(\mathbf{r}, \mathbf{p})$. By expanding δf in a set of basis states with the symmetry appropriate for the particular mode considered, one can express the Boltzmann equation in matrix form [8, 11]. The corresponding determinants determine the mode frequency ω.

To be specific, we model the collective modes studied experimentally in Ref. [8], where the atoms are trapped in a very elongated harmonic potential of the form $V(\mathbf{r}) = m(\omega_x^2 x^2 + \omega_y^2 y^2 + \omega_z^2 z^2)/2$ with $\omega_z \ll \omega_y \leq \omega_x$. The motion of the collective modes is then mainly in the xy-plane. For the scissors mode, the determinant equation determining the mode frequency becomes [12]

$$\frac{i\omega}{\tau}(\omega^2 - \omega_h^2) + (\omega^2 - \omega_{c1}^2)(\omega^2 - \omega_{c2}^2) = 0. \tag{8}$$

Here $\omega_h = \sqrt{\omega_x^2 + \omega_y^2}$ is the mode frequency in the hydrodynamic limit when $\omega\tau \ll 1$ characteristic of many collisions, and $\omega_{c1} = \omega_x + \omega_y$ and $\omega_{c2} = |\omega_x - \omega_y|$ are the mode frequencies in the collisionless limit $\omega\tau \gg 1$ [13]. The collision rate $1/\tau$ is

$$\frac{1}{\tau} = \frac{\int d^3r d^3p p_x p_y I[p_x p_y]}{\int d^3r d^3p p_x^2 p_y^2 f^0(1 - f^0)} \tag{9}$$

where $I[p_x p_y]$ is the collision integral in the Boltzmann equation weighted by the momentum function $p_x p_y$ [8, 11]. It is in the collision integral, that the scattering matrix enters. The collision rate (9) is closely related to the viscosity of the gas and it is therefore sometimes called the viscous relaxation rate [14].

When the atoms are strongly interacting, there are significant pair correlations even in the normal phase. The correlations depend strongly on temperature and interaction strength which is parametrized by the scattering length a in (6). Correlations and their dependence on a and T enter the theory for collective modes through (9). In Fig. 2, we plot the scattering rate $1/\tau$ as a function of T for: (a) strong coupling right at a Feshbach resonance $|a| \to \infty$, and (b) in the weak coupling regime $k_F a = -0.06$. To clearly identify the importance of medium effects on the scattering matrix, the rate is calculated using three different approximations. The dashed curves are a classical approximation where Pauli blocking effects are neglected and the two-body scattering matrix is used. The dash-dotted lines include Pauli blocking in the collision integral $I[p_x p_y]$ while the two-body scattering matrix is still used. We see that Pauli blocking reduces the scattering rate as compared to the classical result as expected; the classical rate scales as T^{-2} whereas $\tau^{-1} \propto T^2$ for $T \to 0$ due to Pauli blocking. Finally, the solid lines use the many-body scattering matrix (7) in addition to including Pauli blocking effects in the collision integral. Medium effects in the scattering matrix

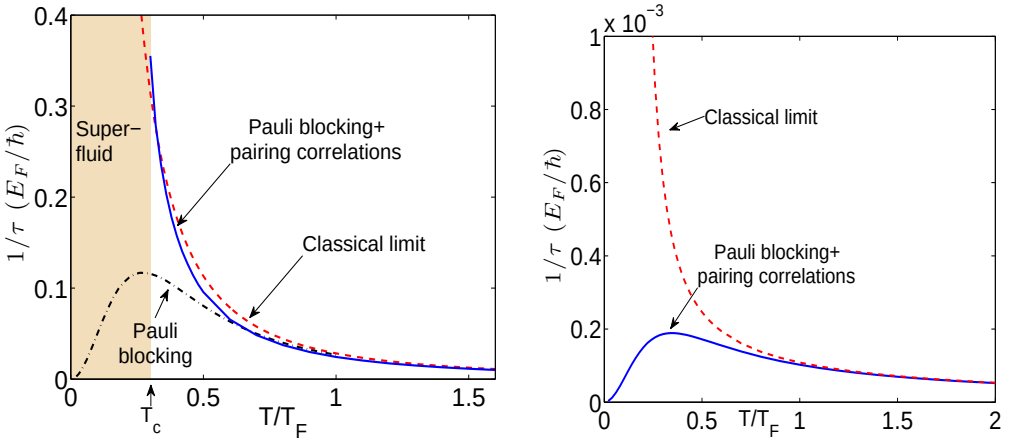

Figure 2. The viscous relaxation rate rate $1/\tau$ for a gas in the unitarity limit (a) (From [8]) and in the weak coupling limit (b). The superfluid region is indicated in (a) whereas it is not visible in (b) due to the smallness of T_c. The dashed lines show the classical limit, the dash-dotted lines include Fermi blocking, and the solid lines include medium effects in the cross section.

are included through the pair propagator $\Pi_0(\omega, \boldsymbol{K})$ in (7). As seen by comparing the solid and the dash-dotted lines in Fig. 2 (a), medium effects significantly increase the scattering rate over a wide range of temperatures above T_c for the strong coupling case. This is due to pair correlations. It is the same physics which gives rise to a divergence in the $\boldsymbol{K} = 0$ scattering matrix at T_c signaling the onset of Cooper pairing. From Fig. 2 (a), we see that the scattering rate calculated including both pair correlations and Pauli blocking effects is almost the same as the classical rate which neglects both effects. Thus, pair correlations nearly cancel the reduction of the scattering rate due to Pauli blocking in the normal phase. These strong pair correlations are often referred to as the pseudogap effect. So we have demonstrated that it is essential to include medium effects in the scattering matrix (7) when one considers strong coupling Fermi gases; a simple two-body scattering matrix strongly underestimates the correlations. In contrast, there are no observable medium effects on the scattering matrix in the weak coupling regime depicted in Fig. 2 (b). Here the curves using a two-body and a many-body T_{oo} are essentially indistinguishable.

Once we know the scattering rate $1/\tau$, we can calculate the collective mode frequencies as discussed above. In Fig. 3, we plot the scissors mode frequency ω_S and damping Γ_S obtained from the real and imaginary parts of the solution of (8), i.e. $\omega = \omega_S - i\Gamma_S$. The scattering rate is obtained from (9) using the many-body scattering matrix (7). The gas is strongly interacting with $|a| \to \infty$ and we compare with the experimental data in Ref. [8]. Taking into account the experimental uncertainties and the fact that there are *no fitting parameters* in the theory, the agreement between theory and experiment is good. This indicates that the expressions (7) and (9) account for most of the correlation effects even for strongly correlated Fermi gases. Since the medium effects increase the scattering rate significantly, they make the modes more hydrodynamic. We conclude that

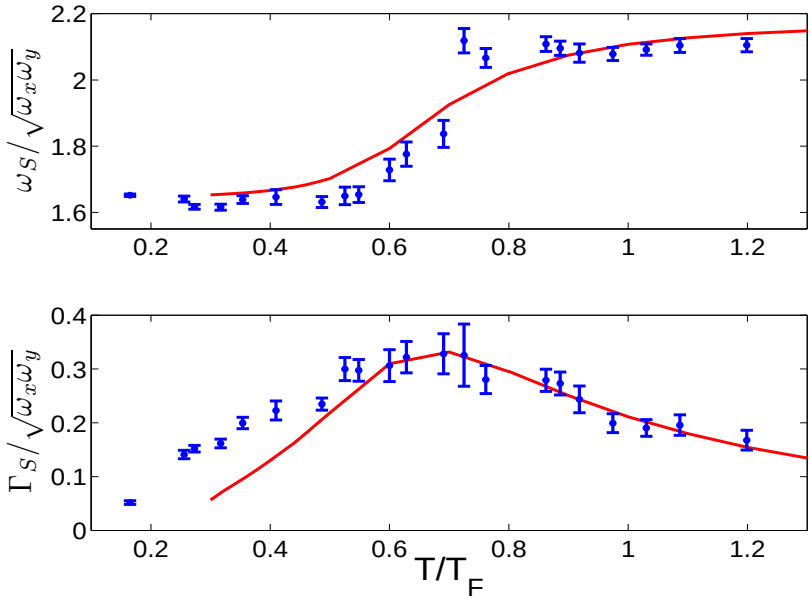

Figure 3. Sketch of the compression mode, the quadrupole mode and the scissors mode (from left to right) in the plane perpendicular to the long axis of the cloud [8].

the observation of well defined hydrodynamic modes above T_c (See Fig. 3 and Ref. [8]) is a signature of many-body effects on the scattering.

4 Conclusion

We developed an effective theory for multi-channel Feshbach scattering in cold alkali atom gases. The theory expresses the scattering in terms of physical observables only. It allows for the inclusion of many-body effects in all channels and provides a precise link between microscopic two-body multi-channel calculations and effective many-body theories. Many-body effects significantly increase the scattering rate over wide range of temperatures. We showed how this can be detected on the frequency and damping of collective modes. Our results were finally compared to experimental data obtaining good agreement.

References

1. Pethick CJ, Smith H (2002) Bose-Einstein Condensation in Dilute Gases. Cambridge University Press, Cambridge
2. Giorgini S, Pitaevskii LP, Stringari S (2008) Rev Mod Phys 80:1215
3. Köhler T, Góral K, Julienne PS (2006) Rev Mod Phys 78:1311
4. Perali A, Pieri P, Strinati GC (2004) Phys Rev Lett 93:100404
5. Holland MJ, Kokkelmans SJ, Chiofalo ML, Walser R (2001) Phys Rev Lett 87:120406; Kokkelmans SJ, Milstein JN, Chiofalo ML, Walser R, Holland MJ (2003) Phys Rev A 65:053617

6. Kinast J, Turlapov A, Thomas JE (2005) Phys Rev Lett 94:170404
7. Wright MJ, *et al.* (2007) Phys Rev Lett 99:150403
8. Riedl S, *et al.* (2008) Phys Rev A 78:053609
9. Bruun GM, Jackson AD, Kolomeitsev EE (2005) Phys Rev A 71:052713
10. Bruun GM, Pethick CJ (2004) Phys Rev Lett 92:140404
11. Massignan P, Bruun GM, Smith H (2005) Phys Rev A 71:033607
12. Bruun GM, Smith H (2007) Phys Rev A 76:045602
13. Guéry-Odelin D, Stringari S (1999) Phys Rev Lett 83:4452
14. Bruun GM, Smith H (2005) Phys Rev A 72:043605

Few-Body Systems 0, 1–4 (2009)

Few-Body Systems

Using a Jacobi-Davidson "nuclear orbital" method for small doped ^{3}He clusters*

M. P. de Lara-Castells** [1], A. O. Mitrushchenkov[2], G. Delgado-Barrio[1], and P. Villarreal[1]

[1] Instituto de Física Fundamental (C.S.I.C), Serrano 123, E-28006 Madrid, Spain
[2] Université Paris-Est, Laboratoire Modélisation et Simulation Multi Echelle, MSME FRE 3160 CNRS, 77454 Marne-la-Vallée, Cedex 2, France

Abstract. An efficient full configuration-interaction (CI) treatment has been recently developed as a benchmark quantum chemistry (QC) method to study doped ^3He_N clusters [J. Chem. Phys. **125**, 221101 (2006)]. The method, which uses an iterative Jacobi-Davidson diagonalization algorithm, is applied here to small clusters ($N \leq 4$) containing Cl_2 as dopant.

1 Introduction

Infrared (IR) spectra of the carbonyl sulfide (OCS) molecule inside He nanodroplets have provided the first experimental evidence for the onset of microscopic superfluidity [1] motivating numerous spectroscopic studies of small doped He clusters [2, 3]. It has also given rise to renewed impetus for theoretical studies in which, due to the non-classical nature of the particles involved, it is crucial the use of quantum treatments. Thus, diffusion and path-integral Monte Carlo methods have been applied to describe the structure and energy levels of such species [4-6]. Alternatively, (QC)-like approaches, which consider [7] the He atoms as "electrons" and the dopant as "nuclei", provide also wave functions and therefore allow, through spectral simulations, a proper comparison with the experiment. Within this framework, Hartree/Hartree-Fock (H/HF) methods have been implemented [8-13] for simulating Raman and infrared spectra of diatomic molecules in bosonic/fermionic He environments. These simulations have stressed the key role of the spin quantum statistics effects in the different spectra experimentally observed depending on the helium isotope considered [1]. The main approximations involved in QC-like approaches (*i.e*, adiabaticity of the diatomic stretch and decoupling of the diatomic rotation from the He-atoms orbital angular momentum) have been recently assessed for heavy as well as light dopant molecules [14, 15].

Major difficulties in developing these QC treatments are caused by the very repulsive He-He short distance interaction. Thus, truncated He-He potentials are

*Article based on the presentation by P. Villareal at the Fifth Workshop on Critical Stability, Erice, Sicily, Received November 21, 2008; Accepted January 16, 2008
** *E-mail address:* delara@imaff.cfmac.csic.es

used, for example, in density-functional-theory approaches [16], a recent full CI treatment [17], and H/HF implementations for doped helium clusters [10]. As a benchmark method, we have developed a full CI treatment [18] where it has been possible to treat the bare He-He potential by replacing the commonly used Davidson (D) algorithm of diagonalization [19] by a Jacobi-Davidson (JD) one [20]. The treatment, applied to $(^3\mathrm{He})_N$-Br_2 clusters, is extended here to the study of Cl_2-doped fermionic helium clusters.

2 Application of the full CI method to $(^3\mathrm{He})_N$-Cl_2 clusters

The $(^3\mathrm{He})_N$-Cl_2 potential energy surface (PES) is described by the sum of pairwise Morse-type He-Cl [21] and semiempirical He-He [22] interactions. The Cl_2 bond length is fixed to its equilibrium value [21]. The basis sets are composed by products of n_{max} numerical radial functions and spherical harmonics $Y_{\ell m}$ with different ℓ_{max} and m_{max} values, and the states are classified according to the D_{2h} point group.

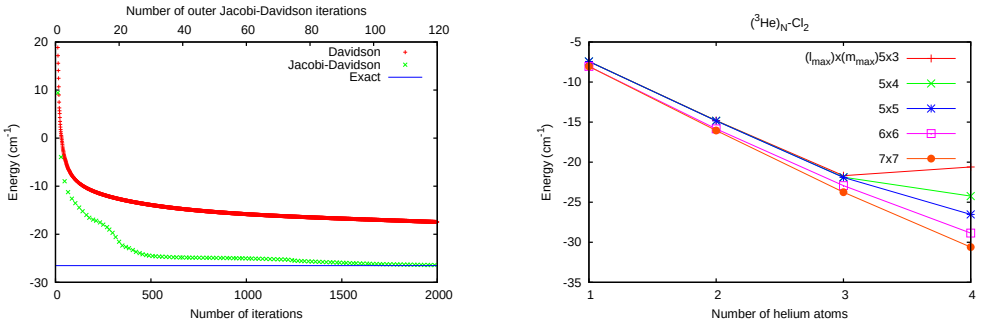

Figure 1. a) Left panel, energy (N=4, S = 0, n_{max}=4, ℓ_{max}=m_{max}=5 state) for JD and D procedures as a function of the number of iterations. The converged, "exact", energy is also shown. b) Right panel, ground-state energies (cm^{-1}) of $(^3\mathrm{He})_N$-Cl_2 clusters as a function of the cluster size for different ℓ_{max} and m_{max} values.

In Fig. 1(a), we first compare the convergence rate of D and JD procedures to the $(^3\mathrm{He})_4$-Cl_2 ground state energy. Each outer JD iterative solver used about 14 internal JD iterations, thus one JD result is presented at each 14 D iterations. Note the fast convergence of the JD procedure as compared to the standard D one. At the 335th outer JD iteration, the energy difference $E^{(i)} - E^{(i-1)}$ has converged to the desired accuracy (10^{-10} cm^{-1}), the norm of the residual vector [18] being only 4×10^{-4} cm^{-1}. The total required number of Hamiltonian applications is about 5000. In contrast, after 5000 D iterations, the energy is still 2.7 cm^{-1} above the "exact" energy, the norm of the residual being very large (13 cm^{-1}). In fact, it was not possible to lower that value to less than 1 cm^{-1} through further 30000 D iterations.

Full CI energies of the different sized complexes are displayed in Table 1(a). The high degree of degeneracy for the lowest-energy states of each spin multiplicity is reminiscent to that found for $(^3\mathrm{He})_N$-Br_2 clusters. Thus, for any size, the energy differences among these states are less than 1 cm^{-1}. However, in con-

trast to the bromine case, the rather linear behavior of ground state energies with N is not broken at N=4. In order to analyse this behavior, we have calculated ground state energies using different basis sets. The results are displayed in Fig. 1(b). Note that the larger ℓ_{max} and m_{max} values, the clearer a linear behavior of the energies with N. At N=4, also note that for ℓ_{max}=5 quite large m_{max} values ($\geq$ 4) are necessary to make the cluster bound, *i.e* to properly describe the short-range He-He repulsion.

Table 1. Energies (cm^{-1}) of N-sized clusters using ℓ_{max}=m_{max}=6. The states are classified according to the total spin (S), and the symmetry within the D_{2h} point group. Values in boldface correspond to the lowest energy states within a given (N, S) manifold. (b) NO occupation numbers larger than 0.05 for the lowest-energy states at each (N, S) manifold. Second column indicates the symmetries of the NOs within the D_{2h} point group whereas the corresponding $D_{\infty h}$ symmetries are specified in the first column.

				(N, S)				
a)	(1,1/2)	(2,0)	(2,1)	(3,1/2)	(3,3/2)	(4,0)	(4,1)	(4,2)
A_g	**-8.05**	**-15.85**	-14.38	-22.47	-20.58	**-28.70**	-26.70	-28.06
B_{3u}/B_{2u}	-7.43	-14.93	**-15.48**	**-22.93**	-21.75	-25.40	-28.57	-24.99
B_{1g}	-6.43	-14.80	-14.88	-22.47	**-22.90**	-28.41	**-28.85**	**-28.09**
B_{1u}	-3.14	-11.10	-10.95	-18.41	-19.76	-24.21	-24.27	-23.61
B_{2g}/B_{3g}	-2.93	-10.80	-10.87	-18.36	-18.13	-24.23	-24.58	-24.07
A_u	-1.39	-10.41	-10.35	-18.31	-18.36	-24.84	-24.37	-24.63
b)	η (NO occupation numbers)							
$1\sigma_g^+$	$1a_g$	1.54	0.99	1.24	0.97	0.98	1.08	0.95
$1\pi_u$	$1b_{2u}$+$1b_{3u}$	0.37	0.99	1.33	1.83	1.81	1.69	1.83
$1\delta_g$	$2a_g$+$1b_{1g}$	0.08		0.38	0.13	0.87	0.84	0.98
$1\phi_u$	$2b_{3u}$+$2b_{2u}$				0.06	0.24	0.29	0.15
$1\gamma_g$	$3a_g$+$2b_{1g}$					0.07	0.06	0.06

Single-particle wavefunctions diagonalizing the first-order density matrix define the "nuclear" natural orbitals (NO). Table 1(b) lists their relevant η occupation numbers at $N \geq 2$. The first He populates the lowest energy $1\sigma_g^+$ orbital. For N=2, significant mixing between $(1\sigma_g^+)^2$, $(1\sigma_g^+)$ $(1\pi_u)$, and $(1\sigma_g^+)$ $(1\delta_g)$ configurations is found for the lowest-energy singlet state whereas the triplet one is well described by a $(1\sigma_g^+)$ $(1\pi_u)$ single-reference state. Aside from the highest spin states, the full CI wavefunctions for $N \geq 3$ have not a clear dominant configuration. For N=3, the quadruplet lowest-energy state is approximately described by a $(1\sigma_g^+)$ $(1\pi_u)$ $(1\pi_u)$ reference although there is also substantial configurational mixing with $1\delta_g$ and $1\phi_u$ NOs. For N=4, the lowest-energy quintuplet state is dominated by a $(1\sigma_g^+)$ $(1\pi_u)$ $(1\pi_u)$ $(1\delta_g)$ configuration even though the configurational mixing with $1\phi_u$ and $1\gamma_g$ NOs is also considerable. For any cluster size, the listed η values sum to at least 99% of N, while the remaining 1% is distributed among more than 189 orbitals. Overall, this result points out the robustness of the helium "nuclear orbital" approach already tested for $(^3He)_N$-Br_2 complexes.

3 Conclusions

In agreement to previous results, our full CI study of small $(^3He)_N$-Cl_2 aggregates indicates (1) the efficiency of the JD procedure; (2) the adequacy of the "nuclear orbital" approach, and (3) the high degree of degeneracy for the lowest energy spin states. It should be stressed that along with the corresponding selection rules this high degeneracy is found to be the main responsible [8] for the broad unstructured spectra exhibited by molecules inside fermionic nanodroplets [1]. Extensions to ^{4}He and mixed ^{4}He/^{3}He doped clusters is now in progress.

Acknowledgement. This work has been supported by the CICYT and MICINN-CSIC Spanish Grants Nos. FIS2007-62006 and 2007501004. The Centro de Supercomputación de Galicia (CESGA) and the Red Española de Supercomputación (MareNostrum at BSC) are acknowledged for the use of their resources.

References

1. Grebenev S., Toennies J. P., Vilesov A. F (1998) Science 279:2083.
2. Tang J., Y. Xu, A. R. W McKellar, W. Jäger (2002) Science 297:2030.
3. Tang J, McKellar A. R. W., Mezzacapo F., S. Moroni (2004) Phys Rev Lett 92:145503.
4. Di Paola C., Gianturco F. A., López-Durán D., de Lara-Castells M. P., Delgado-Barrio G., Villarreal P., Jellinek J. (2005) ChemPhysChem 6:1348.
5. Paesani F., Viel A., Gianturco F. A., Whaley K. B. (2003) Phys Rev Lett 90:073401.
6. Li Z., Wang L., Ran H., Xie D., Blinov N., Roy P. -N., Guo H. (2008) J Chem Phys 128:22513.
7. Jungwirth P. and Krylov A. (2001) J Chem Phys 115:10214.
8. López-Durán D., de Lara-Castells M. P., Delgado-Barrio G., Villarreal P., Paola C. D., Gianturco F. A., Jellinek J. (2004) Phys Rev Lett 93:053401.
9. López-Durán D., de Lara-Castells M. P., Delgado-Barrio G., Villarreal P., Paola C. D., Gianturco F. A., Jellinek J. (2004) J Chem Phys 121:2975.
10. de Lara-Castells M. P., López-Durán D., Delgado-Barrio G., Villarreal P., Paola C. D., Gianturco F. A., Jellinek J. (2005) Phys Rev A 71:033203.
11. de Lara-Castells M. P., Prosmiti R., López-Durán D., Delgado-Barrio G., Villarreal P. (2006) Phys Rev A 74:053201.
12. Villarreal P., de Lara-Castells M. P., Prosmiti R., Delgado-Barrio G., Villarreal P., Di Paola C., Gianturco F. A., Jellinek J. (2007) Phys Scr 76:C96.
13. de Lara-Castells M. P., Prosmiti R., López-Durán D., Delgado-Barrio G., Villarreal P., Gianturco F. A., Jellinek J. (2007) Int J Quantum Chem 107:2902.
14. Roncero O., Pérez-Tudela R., de Lara-Castells M. P., Prosmiti R., Delgado-Barrio G., Villarreal P. (2007) Int J Quantum Chem 107:2756.
15. Roncero O., de Lara-Castells M. P., Delgado-Barrio G., Villarreal P., Stoecklin T., Voronin A., Rayez J. C. (2008) J Chem Phys 128:164313.
16. Barranco M., Guardiola R., Hernández S., Mayol R., Navarro J., Pí M. (2006) J Low Temp Phys 142:1.
17. Felker P. M., (2006) J Chem Phys 125:184313.
18. de Lara-Castells M. P., Delgado-Barrio G., Villarreal P., Mitrushchenkov A. O. (2006) J Chem Phys 125:221101.
19. Davidson E. R. (1975) J. Comput. Phys. 17:87.
20. G. L. Sleijpen and H. A. Van der Vorst (1996) SIAM J. Matrix Anal. Appl. 17(2):401.
21. Bacić Z., Kennedy-Mandzink M., Moskowitz J. W. (1992) J Chem Phys 97:6471.
22. Aziz R. A., M. J. Slaman M. J. (1991) J Chem Phys 94:8047.

Few-Body Systems 0, 1–4 (2009)

Few-Body Systems

A study of the Ar_3 system at low temperature *

R. Pérez de Tudela, M. Márquez-Mijares**, T. González-Lezana***, O. Roncero, S. Miret-Artés, G. Delgado-Barrio and P. Villarreal

Instituto de Física Fundamental, CSIC, Serrano 123, 28006 Madrid, Spain

Abstract. The energy of the Ar trimer has been investigated in terms of the temperature for $T \leq 1\,K$, by means of a path-integral Monte Carlo calculation and a variational approximate method based on the use of the interparticle distances. The comparison reveals that the values of the energy obtained via both methods are in a fairly good agreement.

1 Introduction

Molecular clusters formed by rare gas atoms has attracted the attention of a large series of investigations in the past. Their unique properties convert them in an ideal scenario in between few body molecular aggregates and continuum media. Transition properties between solid-like and liquid-like forms for Ar_N with $N \geq 3$ clusters have been analysed via different approaches such as, for example, Monte Carlo methods [1, 2, 3]. The molecular Ar trimer, in particular, has been the subject of numerous studies devoted to describe the energy levels and geometries of the corresponding bound states for the case of a zero total angular momentum, $J = 0$ (see Refs. [4, 5] for the most recent examples). Recently, the analysis of the Ar_3 system has been extended to the calculation of the rovibrational spectra for $J \leq 6$ [6, 7].

In this work we have studied the average binding energy of the Ar trimer in terms of the temperature by means of a path-integral Monte Carlo (PIMC) method. For comparison, an extension of the variational approximate approach based on the use of distributed Gaussian functions (DGF) to describe the interparticle distances reported in Refs. [6, 8] have been used. The actual dependence of the energy as a function of the temperature is obtained by means of a Boltzmann average of the corresponding rovibrational spectra for different values of J.

*Article based on the presentation by T. González-Lezana at the Fifth Workshop on Critical Stability, Erice, Sicily, Received November 14 2008; Accepted January 15, 2009

** *Alternative address:* Instituto Superior de Tecnologías y Ciencias Aplicadas, Avda. Salvador Allende y Luaces, Quinta de Los Molinos, Plaza, La Habana 10600, Cuba

*** *E-mail address:* tglezana@imaff.cfmac.csic.es

The temperature range considered covers up to 1 K and the Ar-Ar interaction is described by means of a Morse potential with the following values for the corresponding parameters: $D = 99\,\mathrm{cm}^{-1}(1\,\mathrm{cm}^{-1} = 1.23984\times10^{-4}\,\mathrm{eV})$, $\alpha = 1.717\,\mathrm{\AA}^{-1}$ and $r_0 = 3.757\,\mathrm{\AA}$ [9].

2 Theory

2.1 Path-integral Monte Carlo method

The PIMC approach employed here has been described elsewhere [10, 11]. Briefly, the three-body density matrix at a temperature T is replaced by the product of M density matrices at MT:

$$\rho(R_1, R_{M+1}; \beta) = \int dR_2 \ldots dR_M \prod_{\alpha=1}^{M} \rho(R_\alpha, R_{\alpha+1}; \tau), \tag{1}$$

where R_α represents the $3N$ positions of the N particles: $R_\alpha \equiv \{\mathbf{r}_1^\alpha, \ldots, \mathbf{r}_N^\alpha\}$, being the $\mathbf{r}_i^\alpha$ vectors, those which determines the position of the ith Ar atom in the R_α set, $\beta = 1/k_B T$ and $\tau = \beta/M$. M is defined, in the case of the Ar_3 system, as $M = 80/T$ [12]. The energy $E(T)$ can be obtained as the thermal average of the Hamiltonian H as:

$$E(T) = Z^{-1} \int dR_1 \int dR_{M+1} \, \langle R_{M+1} \,|\, \hat{H} \,|\, R_1 \rangle \, \rho(R_1, R_{M+1}; \beta) \tag{2}$$

where $Z = \int dR \, \rho(R, R; \beta)$ is the partition function. Eq. (2) can be expressed, by using the energy estimators proposed in Refs. [13, 14] as:

$$E(T) = \left\langle \frac{3(N-1)}{2} k_B T + \frac{1}{2M} \sum_{\alpha=1}^{M} \sum_{i=1}^{N} (\mathrm{r}_i^\alpha - \mathrm{r}_i^M) \frac{\partial V(\mathrm{r}_i^\alpha)}{\partial \mathrm{r}_i^\alpha} + \frac{1}{M} \sum_{\alpha=1}^{M} \sum_{i<j}^{N} V(\mathrm{r}_{ij}^\alpha) \right\rangle, \tag{3}$$

where $\mathrm{r}_i^M = M^{-1} \sum_{\alpha=1}^{M} \mathrm{r}_i^\alpha$ and $\mathrm{r}_{ij}^\alpha = \mid \mathbf{r}_i^\alpha - \mathbf{r}_j^\alpha \mid$. The first two terms in Eq. (3) correspond to the classical kinetic energy and a quantum correction. Finally, the integration is effectively evaluated via a Metropolis Monte Carlo algorithm, as an average over a number of paths $\{R_1, R_2, \ldots, R_M, R_{M+1}\}$ sampled according to a probability density proportional to the factorised product of M density matrices of Eq. (1).

2.2 Distributed Gaussian functions method

A DGF method [6] has been applied to calculate the rovibrational spectra for the Ar_3 system at different values of the total angular momentum, J. Bound state energies for the $J > 0$ problem are obtained via the diagonalization of the rotational Hamiltonian expressed on a basis formed by the eigenfunctions, labelled with k, of the purely vibrational problem, $J = 0$, and standard rotational functions in terms of J and its projection on the space- and body-fixed frames. The latter projection, Ω, is employed, besides the vibrational quantum number ℓ, to classify the rovibrational states in the different irreducible representations [6].

The corresponding rovibrational spectra, $E^J_{k\Omega}$, formed with those levels from the physically acceptable representations A'_1 and A''_1, are then used in the following Boltzmann average to obtain the energy in terms of T:

$$E(T) = \left[\sum_{J=0}^{J_{max}} \sum_i E_i^J \, e^{-E_i^J/k_BT}\right] \cdot \left[\sum_{J=0}^{J_{max}} \sum_i e^{-E_i^J/k_BT}\right]^{-1} \quad (4)$$

where the i stands for the k, Ω indexes for those rovibrational states belonging, for each value of J, to the A'_1 and A''_1 representations. In order to converge the results at $T = 1\,\mathrm{K}$, calculations with $J_{max} = 10$ and 12 vibrational states were necessary.

3 Results

The values of the average energy obtained via the two methods employed in this work are shown in Figure 1. Although the PIMC predictions are below the DGF results, both sets of energies are in a quite good agreement, with differences which do not exceed $2\,\mathrm{cm}^{-1}$ for the $T \leq 1\,\mathrm{K}$ case studied here. According to Eq. (3), the values of $E(T)$ calculated via the Monte Carlo approach are the result of a classical contribution and some quantum mechanical correction. Results from Fig. 1 indicate that at $T \approx 0\,\mathrm{K}$, the PIMC calculation seems to take into account most of the possible quantum effects which correct the classical estimation of $3 \times D = -297\,\mathrm{cm}^{-1}$.

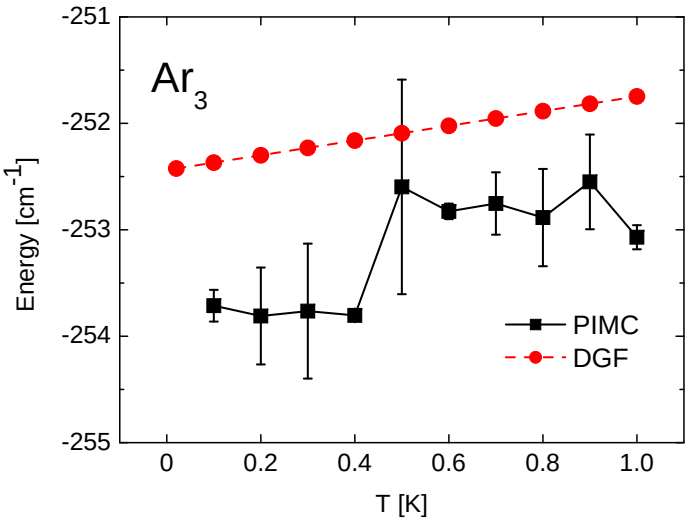

Figure 1. Energy for the Ar_3 system in terms of the temperature for $T \leq 1$ K: DGF results are in red circles and dashed line and PIMC energies are in squares and black line.

The observed trend suggests a progressive improvement in the actual comparison between the DGF and PIMC results as T increases. It would be of interest to test the behaviour of the average energy at a higher temperature regime where

the quantum contribution is expected to decrease and possible phase transition effects are likely to appear. That requires the inclusion of the rovibrational spectra of a larger number of total angular momentum in the DGF calculation. Work in this direction is currently in progress.

Acknowledgement. Support from the Spanish MEC under Grants FIS2007-62006, CTQ2007-62898 and from CSIC under Grant 200650I134 are acknowledged.

References

1. Etters RD, Kaelberer J (1977) J Chem Phys 66:5112
2. Franke G, Hilf ER, Borrmann P (1993) J Chem Phys 98:3496
3. Beck TL, Doll JD, Freeman DL (1989) J Chem Phys 90:5651
4. Roy PN (2003) J Chem Phys 119:5437
5. Baccarelli I, Gianturco FA, González-Lezana T, Delgado-Barrio G, Miret-Artés S, Villarreal P (2005) J Chem Phys 122:144319
6. Márquez-Mijares M, González-Lezana T, Roncero O, Miret-Artés S, Delgado-Barrio G, Villarreal P (2008) Chem Phys Lett 460:417
7. Karlický F, Lepetit B, Kalus R, Gadea FX (2007) J Chem Phys 126:74305
8. Baccarelli I, Gianturco FA, González-Lezana T, Delgado-Barrio G, Miret-Artés S, Villarreal P (2007) Phys Rep 452:1
9. González-Lezana T, Rubayo-Soneira J, Miret-Artés S, Gianturco FA, Delgado-Barrio G, Villarreal P (1999) J Chem Phys 110:9000
10. Ceperley DM (1995) Rev Mod Phys 67:279
11. Kwon Y, Ceperley DM, Whaley KB (1996) J Chem Phys 104:2341
12. Borrmann P (1994) Comp Mat Science 2:593
13. Herman MF, Bruskin EJ, Berne BJ (1982) J Chem Phys 76:5150
14. Glaesemann KR, Fried LE (2002) J Chem Phys 116:5951.

Few-Body Systems 0, 1–4 (2009)

Few-Body Systems

A Quantum Mechanical Study of Ozone Isotope Effect*

S. Yu. Grebenshchikov**

Max-Planck-Institut für Dynamik und Selbstorganisation, 37073 Göttingen, Germany

Abstract. The rate of ozone recombination, $O_2+O+M \rightarrow O_3+M$, is strongly sensitive to the masses of the participating oxygen isotopes – the effect ultimately leading to the unconventional fractionations of ozone isotopomers in the Earth atmosphere. The mass dependence for asymmetric molecules is reconstructed, within the strong collision approximation, from the partial widths of narrow resonances of O_3 and demonstrated to stem from the contributions of highly rotationally excited ozones.

1 Introduction

Ozone in the stratosphere is formed primarily in the Chapman cycle, i.e. via collisional recombination of the atomic and molecular oxygen:

$$\begin{aligned} O(\alpha) + O_2(\alpha) &\rightarrow O_3^\star & (1)\\ O_3^\star + M &\rightarrow O_3 + M\,. & (2) \end{aligned}$$

In (1), ozone above dissociation threshold, $O_3^\star$, forms from a given arrangement (or isotope-specific) channel α. It can dissociate again unless stabilized in (2) by a collision with the buffer gas M. The incoming oxygen atom in (1) always becomes one of the end atoms of O_3 (never the central atom). Likewise, the dissociating $O_3^\star$ has only two accessible arrangement channels in which one of the end atoms is removed.

An intriguing isotopic fractionation effect in O_3 [1] was traced down to the strong sensitivity of the recombination rates in (1-2) to the masses of oxygen isotopes (^{16}O, ^{17}O, or ^{18}O, abbreviated as 6, 7, or 8, respectively). Figure 1(a) shows the room-temperature recombination rates, $k_{\rm rec}(k_BT, \alpha)$, measured in various isotope-specific channels α. For the 668 molecule, for example, two such channels are:

$$8 + 66(\mathrm{ZPE}_\alpha) \leftrightharpoons 866^{(\star)} \leftrightharpoons 86(\mathrm{ZPE}_\beta) + 6 \qquad (3)$$

*Article based on the presentation by S. Yu. Grebenshchikov at the Fifth Workshop on Critical Stability, Erice, Sicily, Received January 16, 2009; Accepted February 10, 2009.

** *E-mail address:* sgreben@gwdg.de

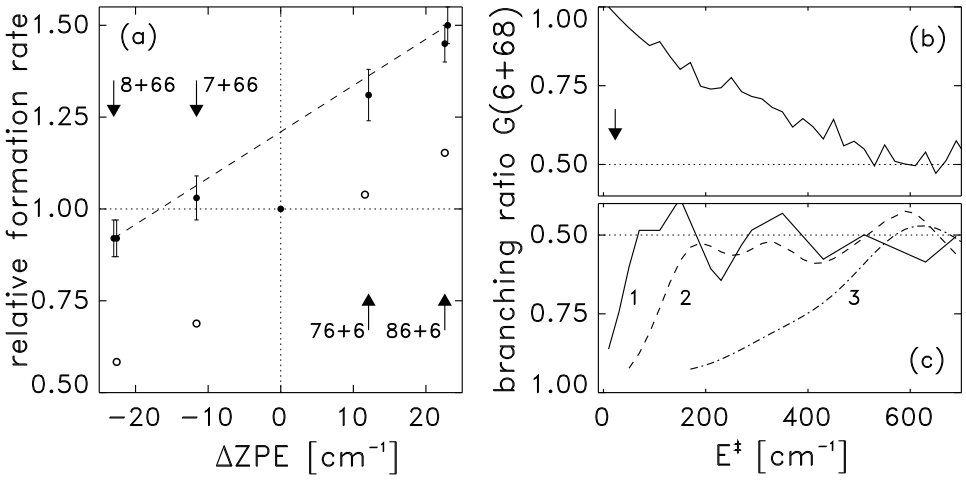

Figure 1. (a) Relative recombination rates versus ZPE difference between the outgoing and the incoming diatomic oxygen molecules, $\Delta\,\mathrm{ZPE}$. Solid symbols are experimental rates [2] for the following reactions (with respective $\Delta\,\mathrm{ZPE}$ in cm^{-1}): $8+66$ and $68+8$ (-23); $7+66$ (-12); $88+7$ $(+12)$; $86+6$ and $6+88$ $(+23)$; Open symbols – calculations with Eq. (4). Arrows relate $\Delta\,\mathrm{ZPE}$ values to the calculated isotope-specific channels; (b,c) Branching ratio in the 6+68 channel for resonance states in the 668 ozone plotted against energy in excess of the lowest (6+68) dissociation threshold, $\mathrm{E}^{\ddagger}$. In (b): Averaging over all $J \leq 40$. In (c): Averaging for fixed $J = 0$ (1), $J = 20$ (2), $J = 40$ (3). Arrow marks the position of threshold for 8+66.

The rates in these channels (relative to the 'standard' rate of $6 + 66 \to 666$) are substantially different: 0.92 in the left channel vs. 1.45 in the right one [Fig. 1(a)]. The measured rates correlate with the asymmetry between the thresholds of the two channels, i.e. with the difference of the vibrational zero-point energies (ZPEs) of the outgoing and incoming diatoms. In the 668 case, the ZPE_α of the lighter 66 diatom exceeds the ZPE_β of the heavier 68 diatom. The recombination from the 'heavier' channel in Eq. (3), where $\Delta\,\mathrm{ZPE} = \mathrm{ZPE}_\alpha - \mathrm{ZPE}_\beta > 0$, is faster than the 'standard' (for which $\Delta\,\mathrm{ZPE} = 0$). Conversely, channels with lighter diatoms ($\Delta\,\mathrm{ZPE} < 0$) generally lead to slower recombinations. This almost linear dependence of $k_{\mathrm{rec}}(\alpha)$ on $\Delta\,\mathrm{ZPE}$ is surprisingly steep and significantly exceeds the expected ratio of $\exp(\Delta\,\mathrm{ZPE}/k_B T) \sim 1.1$ (the threshold asymmetry, $\Delta\,\mathrm{ZPE} \lesssim 23\,\mathrm{cm}^{-1}$, is much smaller than both $k_B T \approx 200\,\mathrm{cm}^{-1}$ or the depth of the ozone well, $V_0 \approx 9000\,\mathrm{cm}^{-1}$) [3].

The $\Delta\,\mathrm{ZPE}$-dependence has been extensively investigated using statistical models [4] and classical mechanics [5]. Quantum scattering calculations performed for a non-rotating ozone (see, e.g., Refs. [5, 6]) did not provide a consistent explanation of the observed rates. The aim of this communication is to demonstrate that the treatment of the association step (1) in terms of resonances in rotationally excited O_3 is capable of reproducing the experiment.

2 Resonance Recombination in the Strong Collision Approximation

The full quantum treatment of the reactions (1-2) is still beyond the power of present-day computers. The problem is made tractable by first introducing the strong collision approximation (SCA) [7] and replacing the step (2) with a model stabilization probability. Next, the step (1) is assumed to be dominated by isolated narrow resonances, the only stabilizable states above threshold. The absolute thermal rate constant $k_{\rm rec}(k_BT,\alpha)$ becomes a sum over individual contributions of resonance states, $[E_n(J),\Gamma_n(J)]$, calculated for a fixed total angular momentum J of O_3 [7]:

$$Q_r(\alpha)k_{\rm rec}(k_BT,\alpha)=\sum_J(2J+1)\sum_n\Gamma_n(\alpha;J)\frac{\omega}{\omega+\Gamma_n(J)}\exp(-E_n(J)/k_BT) \quad (4)$$

Here $Q_r(\alpha)$ is the O/O_2 partition function, $\Gamma_n(\alpha;J)$ is the partial resonance width in channel α, and ω is the frequency of 'strong collisions' with M. The problem (1-2) reduces to calculation of near-threshold resonance states in the isolated rotating O_3. In the experimentally relevant low-pressure limit, $k_{\rm rec}\sim\omega$, and the relative rates are independent of the SCA parameter ω.

Dynamics calculations are performed using a modified version of the accurate three-dimensional ozone potential [5] supporting ~ 250 bound states. Shallow van der Waals wells in the asymptotic channels are eliminated and only one permutation is considered. The molecular Hamiltonian in Jacobi coordinates is set in the discrete variable representation and made complex symmetric using an optical potential in each channel α. The time-dependent Schrödinger equation is solved and the complex eigenvalues are retrieved with filter diagonalization [8]. Only narrow states with $\Gamma_n\lesssim 1\,{\rm cm}^{-1}\ll\Delta\,{\rm ZPE}$ are considered. Two additional calculations for each J are performed to estimate the partial widths $\Gamma_n(\alpha)$ and $\Gamma_n(\beta)=\Gamma_n-\Gamma_n(\alpha)$ from perturbation theory. The coupling to products in the optical Hamiltonian is slightly rescaled either in one (α) or in the other (β) arrangement channel, and $\Gamma_n(\alpha)$ is evaluated from the variations, $\delta^{(\alpha,\beta)}\Gamma_n$, of the imaginary parts of the eigenvalues: $\Gamma_n(\alpha)/\Gamma_n=\delta^{(\alpha)}\Gamma_n/(\delta^{(\alpha)}\Gamma_n+\delta^{(\beta)}\Gamma_n)$.

3 Results and Discussion

Resonance spectra for $J\le 40$ are calculated for three isotopomers: 666, 668 and 667. About 6000 resonances are calculated for each molecule. The model is trustworthy and the relative rates based on Eq. (4) [Fig. 1(a)] agree with experiment to within 80%. The ΔZPE-dependence is reproduced remarkably well: The recombination from the 'lighter' channels ($\Delta\,{\rm ZPE}>0$) is significantly faster than from the 'heavier' channels ($\Delta\,{\rm ZPE}<0$).

The explanation of the strong impact which tiny ΔZPE asymmetries have on $k_{\rm rec}(k_BT;\alpha)$ is provided by Fig. 1(b,c) showing – for 668 – the branching ratio in the lowest channel, $G(6+68)=\langle\Gamma(6+68)/\Gamma\rangle$, versus energy in excess of the 6+68 threshold; $G(6+68)$ in Fig. 1(b) is averaged over narrow energy windows containing many resonances with all $J\le 40$. The lowest channel is preferentially populated near threshold, $G(6+68)\sim 1$. As energy increases, $G(6+68)$ slowly decreases and reaches the value of 0.5 – both arrangement channels become

statistically equivalent. The statistical limit is reached, however, only $500\,\mathrm{cm}^{-1}$ above threshold, high above $\Delta\,\mathrm{ZPE}$: The asymmetry 'spreads' across a broad energy range. The effect is markedly J-dependent, as illustrated by $G(6+68)$ plotted for selected J values in Fig. 1(c). The higher J, the higher the energy, at which the two channels equilibrate. The reason are the centrifugal barriers building up in both arrangement channels and reaching deep into continuum. Their heights, which mark the effective thresholds, remain separated by $\sim\Delta\,\mathrm{ZPE}$.

Acknowledgement. I would like to thank Reinhard Schinke for many insightful discussions of the ozone isotope effect. The financial support of the Deutsche Forschungsgemeinschaft is gratefully acknowledged.

References

1. Mauersberger, K., et al.: Adv. At. Mol. Opt. Phys. **50**, 1 (2005), and references therein
2. Janssen, C., et al.: PCCP **3**, 4718 (2001)
3. There is a second isotope effect in Fig. 1(a). All molecules with identical end atoms ('symmetric' 666, 686, 868 etc.) – for which $\Delta\,\mathrm{ZPE} = 0$ – fall out of the linear $\Delta\,\mathrm{ZPE}$-dependence. Their recombination is apparently less efficient (by about 15%) than for asymmetric isotopomers. This 'symmetry' or 'mass-independent' effect is not considered in this work
4. Gao, Y. Q., Marcus, R. A.: Science **293**, 259 (2001)
5. Schinke, R., et al.: Annu. Rev. Phys. Chem. **57** 625 (2006), and references therein
6. Babikov, D., et al.: J. Chem. Phys. **119**, 2577 (2003)
7. Germann, T. C., Miller, W. H.: J. Phys. Chem. **A101**, 6358 (1997)
8. Mandelshtam, V. A.: Prog. in Nucl. Magn. Reson. Spec. **38**, 159 (2001)